A human tissue-specific *ex vivo* model of biological scaffold integration: Understanding the interface

Samuel James Bullers

Thesis submitted in fulfillment of the requirements for the degree of Doctor of Philosophy

Department of Biology

University of York

September 2012

‘I'm playing all the right notes - but not necessarily in the right order.’

Eric Morecambe, 1971

Abstract

Tissue-derived decellularised biological scaffolds have application in regenerative medicine as biomaterials, with the aim of restoring tissue function lost due to damage or disease. Following surgical intervention, it is axiomatic that cells of the immune system respond to the implantation. *In vivo* animal implantation studies have highlighted that macrophages can surround biomaterials during an encapsulation-type response and infiltrate into biological scaffolds during an integration-type response. Despite the clinical application of tissue-derived biological scaffolds, little is known about the human tissue response to these biomaterials. The aim of this study was to develop and examine an *ex vivo* biomaterial-human tissue interface in order to identify potential factors and immune mechanisms that govern the tissue response to a biological scaffold, with focus on the macrophage phenotype at the *ex vivo* interface.

An organotypic culture model was established in which human urinary tract tissue was maintained in close apposition with a porcine urinary bladder-derived decellularised biological scaffold. Immunolabelling of histological sections from the tissue constructs using a panel of functional markers identified a striking and significant up-regulation of the macrophage-associated marker, CD163. Mechanistic investigations into CD163 expression in human peripheral blood-monocyte-derived macrophages identified that a subpopulation of monocyte-derived macrophages had a greater propensity towards expression of CD163 and the population of CD163+ macrophages could be increased following activation of the nuclear receptor, PPARγ. Pharmacological inhibition of PPARγ abated the CD163+ subpopulation and inhibited the glucocorticoid-dependent induction of CD163, indicating that CD163 expression was dependent on PPARγ function. Immunolabelling of PPARγ in the biomaterial-tissue constructs showed intense nuclear localisation of the PPARγ in cells at the biomaterial-tissue interface and in cells, with a macrophage-like morphology, present within the biological scaffold.

CD163 expression and PPARγ function are associated with the resolution phase of inflammation. It is proposed that factors that govern inflammation resolution are involved in determining the phenotype of macrophages at a biomaterial-tissue interface.

Contents

List of figures

List of tables

Acknowledgements

I wish to thanks my supervisors Professor Jenny Southgate and Professor Eileen Ingham for their patience, support, encouragement and help over the last four years.

I would like to thank Simon Baker and Jenny Hinley for their friendship and advice over the last five years; I could not have done this without them. I am also grateful to all members of the Jack Birch Unit, University of York, past and present and members of the Institute for Medical and Biological Engineering, University of Leeds for their assistance, advice and friendship.

Thank you to Helen Berry and everyone at Tissue Regenix Group for supporting the study and myself.

I also wish to thank members of the Center for Immunology and Infections, University of York, for providing stimulating conversation about immunology.

I am eternally grateful to the Hull York Medical School Experimental Medicine Unit, in particular Carol Taylor, David Thompson, Nicola Marshall and Nelisa Poshai, for recruiting volunteers, taking informed consent and collecting blood samples and for the help they provided with the IRAS ethics application to obtain human blood for this study.

Thank you to the clinicians for the supply of surgical specimens used in this study and to the volunteers for donating blood to the study and surgical specimens for research.

I am grateful to the BBSRC for funding this work and Tissue Regenix Group for their extra funding.

I would like to thank Richard Berks and Toby Hodges for their friendship and support.

A huge thank you to Mum, Dad and Claire for their love and support and to Jennifer, for her love, endless patience, understanding and faith in my ability to achieve this.

Authors declaration

The candidate confirms that all work submitted is his own and that appropriate credit has been given where reference has been made to the work of others.

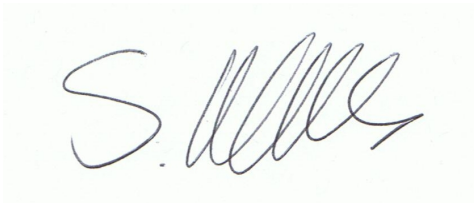

S. Bullers

September 2012

1.0 Introduction

1.1 The immune system

The immune system primarily serves to protect the host from exogenous pathogens. A variety of cell types, known collectively as leukocytes have evolved to aid in this process. Cells of the innate immune system are capable of a variety of cellular functions such as release of inflammatory cytokines, the process of phagocytosis and production of reactive oxygen species. Together these combine to generate a plethora of mechanisms designed to contain and eliminate foreign pathogens. Cells of the innate immune system are responsible for the immediate recognition and response to infectious agents. The cells employ broadly specific effector mechanisms to remove the infectious agent and comprise; granulocytes, such as basophils, eosinophils, mast cells and neutrophils and mononuclear phagocytes, such as macrophages and dendritic cells, which can ingest foreign material and stimulate the adaptive immune system (reviewed in (Janeway and Medzhitov, 2002)). The adaptive immune system conducts later stage immune responses and provides a more specific immune response through clonal expansion of T-lymphocytes and B-lymphocytes and the generation of antibodies by terminally differentiated B-lymphocytes (plasma cells). Together these systems perpetuate the specific immune response to the infectious agent. Over the last four decades, understanding of the roles of the immune system has expanded and the role of leukocytes is no longer restricted to raising inflammatory responses to pathogens. In addition, extensive work in the field of mucosal immunology has shown that the immune system can be highly tolerant and research into autoimmune diseases has highlighted the importance of tight immune-regulatory mechanisms.

In this introduction key processes involved in the generation and execution of innate immunity by mononuclear phagocytes and how this aspect of the immune system impacts on our current understanding of the integration of medical grade biomaterials used in regenerative medicine is reviewed, drawing upon current understanding of both murine and human systems.

1.2 Macrophages

Macrophages are the sentinels of the immune system. They are large, phagocytic cells, which contribute to host defense by responding to, engulfing and eliminating pathogens, making them essential for host defense. Mature macrophages are resident in nearly all tissues within the body (Galli and Tsai, 2010) and the nomenclature of different macrophage populations is based on anatomical location (reviewed in (Mosser and Edwards, 2008). Macrophages can be identified histologically by their kidney-shaped nuclei and large volume of cytoplasm and, along with other cells, may be functionally characterised by expression of cluster of differentiation (CD) markers (classified in (Bernard and Boumsell, 1984; Boumsell, 1996; Zola et al., 2007)) and cytokine profile, as well as the expression of metabolic enzymes, chemokines and other receptors.

1.2.1 The innate immune responses of macrophages

Macrophages are equipped with a broad range of pattern recognition receptors (PRRs), which recognise pathogen-associated molecular patterns (PAMPs). Toll-like receptors (TLR) are highly conserved PRRs found on mammalian innate leukocytes which recognise a range of PAMPs (reviewed in (Takeuchi and Akira, 2010)). The prototypic TLR signaling pathway is the ligation of TLR-4 with bacterial lipopolysaccharide (LPS), which leads to production of the pro-inflammatory cytokines tumour necrosis factor alpha (TNFα), interleukin (IL)-12p40, IL-1β and IL-6 by macrophages. This enhances antimicrobial and tumouricidal capacity (reviewed in (Mosser, 2003)). LPS combined with the pro-inflammatory cytokine, interferon-γ (IFNγ) up-regulates inducible nitric oxide synthetase (iNOS; *NOS2*) (Xie et al., 1993) via the adaptor protein myeloid differentiation primary response gene 88 (MyD88) and the transcription factor, nuclear factor κ B (NFκB), enhancing inflammatory cytokine production (reviewed in (Zhang and Ghosh, 2001). iNOS converts L-arginine to N^G-hydroxyl-L-arginine (NOHA) which produces L-citrulline and nitric oxide (NO), a toxic oxygen species, as well as other reactive oxygen species such as H_2O_2 (reviewed by (Bronte and Zanovello, 2005)) which kills most microbes. NO has been shown to inhibit viral replication (Karupiah et al., 1993) as well as kill bacteria. While it is well documented that murine macrophages kill bacteria using NO produced by iNOS, it has been shown that human alveolar macrophages exerted antimicrobial effects independent of NO production (Thoma-Uszynski et al., 2001). This species difference was also observation in human peripheral blood monocytes and peritoneal macrophages, which showed negligible iNOS activity in

response to LPS and LPS+IFNγ compared to the murine macrophage cell line, J774 (Weinberg et al., 1995). Based on the observation that murine and human macrophages may execute different antimicrobial pathways in response to TLR activation, Kapetanovic et al recently proposed porcine bone marrow-derived macrophages as a superior model for investigation of human macrophage biology due to similar characteristics in NO production compared to human macrophages in response to LPS and comparative regulation of other metabolic pathways (Kapetanovic et al., 2012).

Bacteria are engulfed and eliminated by macrophages in the process of phagocytosis. Phagocytosis of bacteria can induce signals for production and release of pro-inflammatory cytokines such as IL-1β and IL-6, perpetuating inflammation (reviewed in (Underhill and Goodridge, 2012)). Macrophages also employ phagocytosis to remove other particulates including cell debris however, phagocytosis is limited by the amount of membrane available and beyond this limit the macrophage undergoes 'frustrated phagocytosis' (Cannon and Swanson, 1992) in which it cannot engulf the foreign material. During 'frustrated phagocytosis', macrophages fuse to form foreign body giant cells (FBGC) which encapsulate the foreign body, creating a barrier between the foreign material and the host, a process common in the host response to implanted synthetic medical devices ((Hu et al., 2001), reviewed in (Anderson et al., 2008)).

1.2.2 Bridging innate and adaptive immunity

Macrophages are professional antigen presenting cells, which present antigen to lymphocytes. The precise mechanisms involved in the processing and presentation of peptide epitopes to T cells is beyond the scope of this introduction but are reviewed in (Guermonprez et al., 2002). Exogenous phagocytosed material is digested in the phagolysosome and the resulting peptides transported to the endosome. The exogenous-derived peptides are loaded onto major histocompatibility complex (MHC) class II molecules and presented to CD4+ T-helper (Th) cells (figure 1-1). Endogenous antigens, such as viral antigens, are targeted to the proteasome for degradation and the resulting peptides are loaded onto MHC class I molecules and presented to CD8+ cytotoxic (CTL) T cells (reviewed in (Vyas et al., 2008)). Exogenous phagocytosed material can also be presented to CD8+ cytotoxic T cells via MHC class I through antigen cross-presentation (reviewed in (Kaufmann and Schaible, 2005)). To stimulate an effective immune response T cells also require stimulation from the antigen presenting cell co-stimulatory molecules CD80 or CD86 via the T cell co-stimulatory molecule, CD28 (figure 1-1). Macrophages up-

regulate functional proteins associated with enhancement of adaptive immune responses in response to inflammatory stimuli. For example, MHC class II is up-regulated in human peripheral blood monocytes in response to IFNγ (Sztein et al., 1984). Furthermore, the co-stimulatory molecule, CD80 has been shown to be up-regulated by human monocyte-derived macrophages in response to IFNγ and TNFα (Ambarus et al., 2012). Recognition of antigens by naïve T cells with the cognate T cell receptor (TCR) induces IL-2 cytokine release by the T cells and results in T cell clonal expansion and maturation into effector T cells. Activation of the co-stimulatory molecules results in secretion of IL-12 by macrophages and stimulates IFNγ secretion by CD4+ T cells, which feeds back to the macrophages (figure 1-1). This exchange of cytokines further enhances the T cell response and directs the development of the immune response through the recruitment and activation of other leukocytes (reviewed in (Zhu and Paul, 2008)).

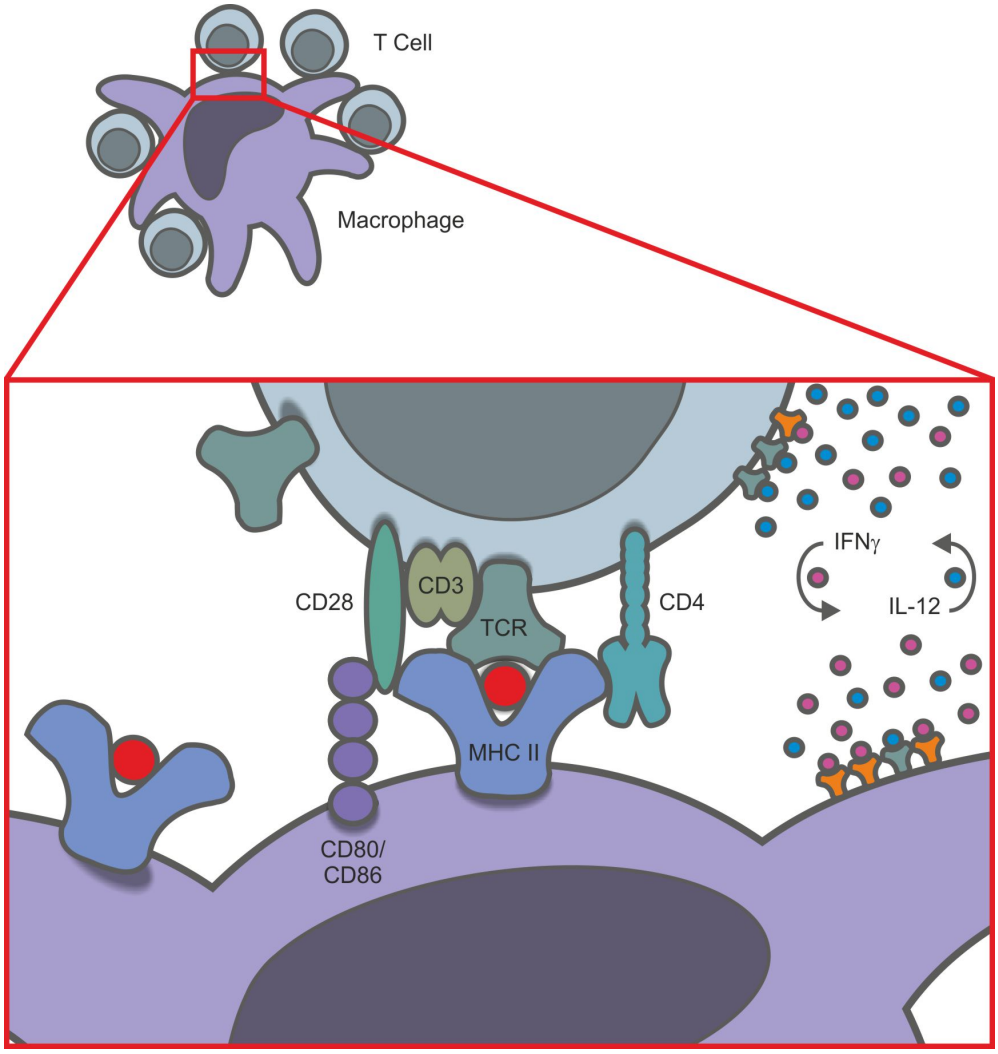

Figure 1-1. Schematic representation of the basic mechanisms involved in antigen presentation to CD4+ T cells by macrophages. Processed antigen (red circle) is loaded onto MHC class II and presented to the CD4+ T cells. The co-stimulatory molecules CD80/CD86 are up-regulated to enhance the response to the antigen. IL-2 secretion by the stimulated T cell induces clonal expansion of the T cells. IFNγ secretion by the activated T cell further stimulates the antigen presenting cells to up-regulate expression of MHC class II and CD80 and enhances IL-12 secretion.

1.2.2.1 CD4+ T-helper cell heterogeneity

Mosmann and Coffman first identified two subsets of murine CD4+ T cells which showed polarised functions depending on the environmental signals (Mosmann et al., 1986). Since this description, the field of CD4+ T cell heterogeneity has expanded and to date, four distinct CD4+ T cell lineages have been characterised. These CD4+ T cell fates are

determined by the pattern of signals received by the CD4+ T cell following presentation of antigen. The precise characteristics and functions of CD4+ T cell subsets in homeostasis, infection and disease are beyond the scope of this introduction. Currently recognised CD4+ T cell populations and the cytokine environment associated with the differentiation of the cell lineages are presented in table 1-1 (reviewed in (Zhu and Paul, 2010)).

Table 1-1. Cytokines associated with CD4+ T cell lineages

CD4+ T cell	Associated cytokines
Th1	**IFNγ, IL-12,** IL-2, TNFα
Th2	**IL-2, IL-4**, IL-5, IL-10, IL-13, IL-25
Th17	**IL-6**, IL-17a, IL-17f, **IL-21**, IL-22**, IL-23**, **transforming growth factor (TGF)-β**
Tregs	**IL-2,** IL-10, IL-35, **TGF-β**

Bold – required for induction of CD4+ T cell lineage. Derived from (Zhu and Paul, 2008). Not bold – cytokines produced by differentiated CD4+ T cells.

1.2.3 Macrophage heterogeneity

Macrophages also show heterogeneity. Heterogeneity in macrophage function arises from lineage and monocyte diversity and context dependent phenotypic plasticity (figure 1-2). Evidence for this diversity and plasticity will be discussed further and applied to current knowledge of medical device integration.

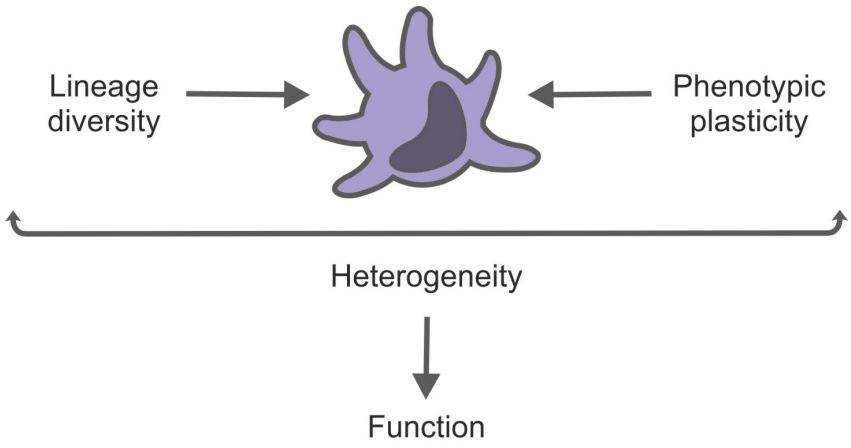

Figure 1-2. Diversity in macrophage function results from the heterogeneity in macrophages, which arises from lineage diversity and phenotypic plasticity.

1.3 Lineage diversity

1.3.1 Haematopoiesis as a source of leukocyte diversity

Haematopoiesis is a hierarchical developmental process in which haematopoietic cells are generated from a haematopoietic stem cell and common progenitor cells. A basic representative diagram of the 'classical model' of haematopoiesis is shown in figure 1-3. The classic model of haematopoiesis was mainly elucidated using murine systems. The diagram shown in figure 1-3 is designed to highlight the basic lineage of leukocytes within the circulating blood however, it is an over simplification of a very complex process. Multipotent stem cells undergo asymmetric cell division within the bone marrow to give rise to haematopoietic stems (HSC) cells. These haematopoietic stems cells commit to an early fate of either lymphoid or myeloid lineages by differentiating into either a common

lymphoid progenitor (CLP) or a common myeloid progenitor (CMP) (figure 1-3). Common lymphoid progenitors differentiate into lymphocytes such as B cells, T cells and natural killer (NK) cells. Common myeloid progenitors differentiate into granulocyte/macrophage progenitor cells, which can give rise to monocytes and granulocytes such as neutrophils, eosinophils and basophils (figure 1-3). Although not commonly found in circulating blood and not depicted in figure 1-3, mast cells are also granulocytes derived from hematopoietic stem cells. Mast cells are derived from the common myeloid progenitor however, a mast cell progenitor (MCP) has been reported to be the precursor to mast cells, independent of the granulocyte/macrophage progenitor (Chen et al., 2005), indicating a different lineage of these cells compared to other granulocytes. Lack of consensus within the field of haematopoiesis research has resulted in multiple complex models of haematopoiesis (reviewed in (Ceredig et al., 2009)).

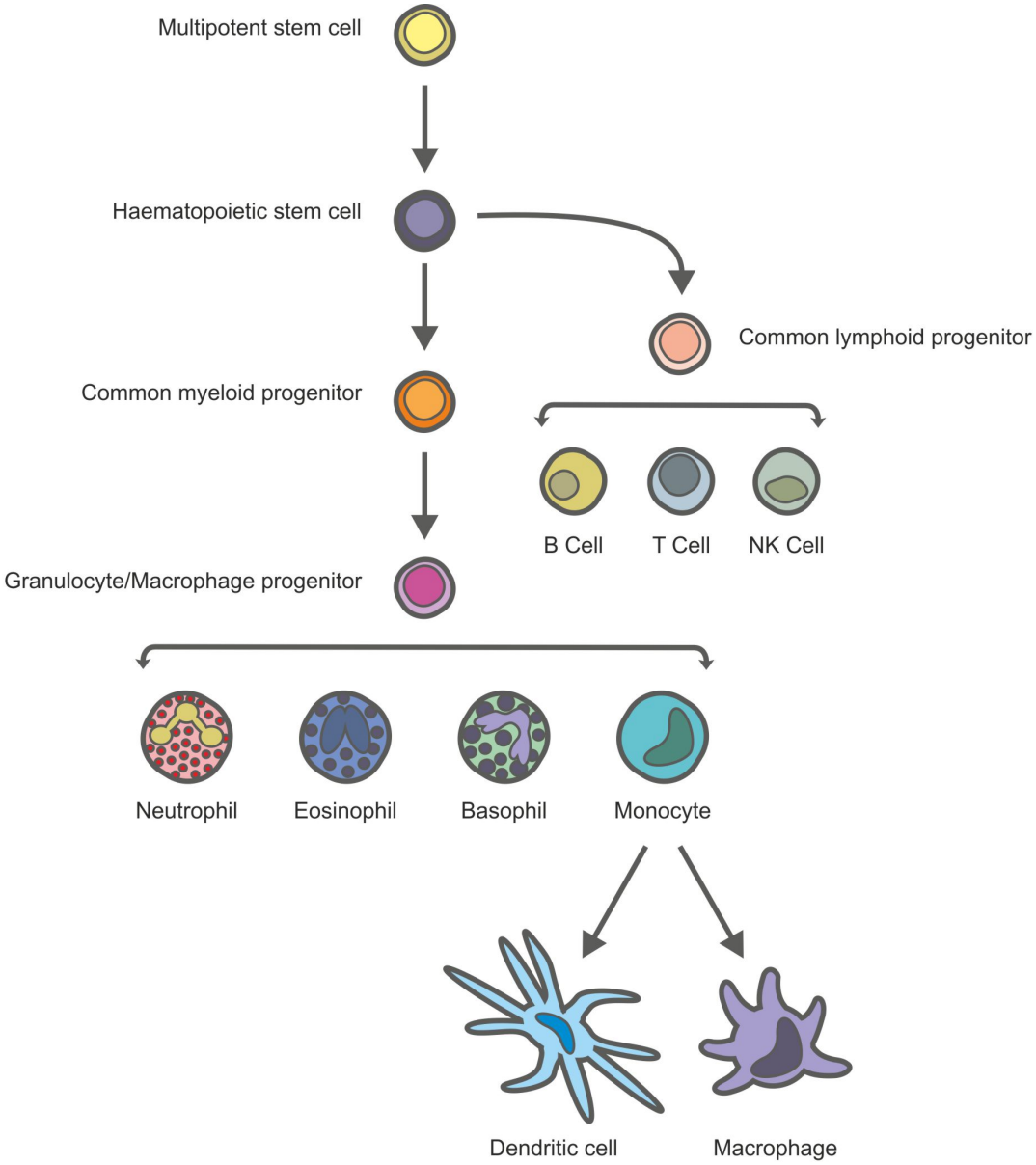

Figure 1-3. Classic model of haematopoiesis highlighting the generation of lymphocytes, granulocytes and monocytes.

1.3.2 Lineages of the mononuclear phagocyte system

Macrophages and dendritic cells (DC), along with their monocytes precursors, make up the mononuclear-phagocyte system (MPS) (Hume et al., 2002). Monocytes differentiate from granulocyte/macrophage progenitors via monoblast and promonocyte precursors (Ma et al., 2003). In mice it has been shown that granulocyte/macrophage progenitors give rise to more specialised macrophage/DC progenitors (Fogg et al., 2006). The macrophage/DC progenitors were reported to have lost the ability to differentiate into granulocytes but were able to generate monocytes and a common DC progenitor (CDP) (Fogg et al., 2006) which had the ability to generate conventional or plasmacytoid DC subsets ((Naik et al., 2007; Auffray et al., 2009a); figure 1-4). Central to the 'classic model' of haematopoiesis is the dogma that cell lineage fate is determined early on in haematopoiesis and restricted to either a myeloid or lymphoid lineage. However, in mice it has been established that lymphoid progenitors can generate DCs (Manz et al., 2001), depicted through generation of a common DC precursor from a lymphoid progenitor ((Geissmann et al., 2010; Takizawa et al., 2012); figure 1-4). Doulatov et al recently challenged the lineage restriction dogma using human neonatal cord blood and human bone marrow (Doulatov et al., 2010). Multi-lymphoid progenitor cells were shown to have the potential to generate all lymphoid cell types as well as monocytes, macrophages and DCs *in vitro* while the myeloid lineage commitment adhered to the 'classic model' ((Doulatov et al., 2010); figure 1-4). A common macrophage/DC progenitor has not been reported in humans to date (Doulatov et al., 2012) therefore it is unclear whether the generation of monocytes, macrophages and DCs from a lymphoid progenitor is derived via a macrophage/DC progenitor (figure 1-4 – red arrow). In addition, although precursors of DCs have been generated from human CD34+ haematopoietic stem cells (Blom et al., 2000), a 'common DC precursor', such as that described in the mouse, has not been described in humans (Collin et al., 2011). Therefore, while in mice, plasticity in the lymphoid lineage permits DC generation via a common precursor of the myeloid lineage; in humans, monocytes, macrophages and DCs are described as being generated only from the granulocyte/macrophage progenitor or the multi-lymphoid progenitor in what appears, so far, to be separate lineages with common cell fates. However, more in-depth analysis may determine if the human lymphoid lineage does crossover into the myeloid lineage via a common precursor (Doulatov et al., 2012).

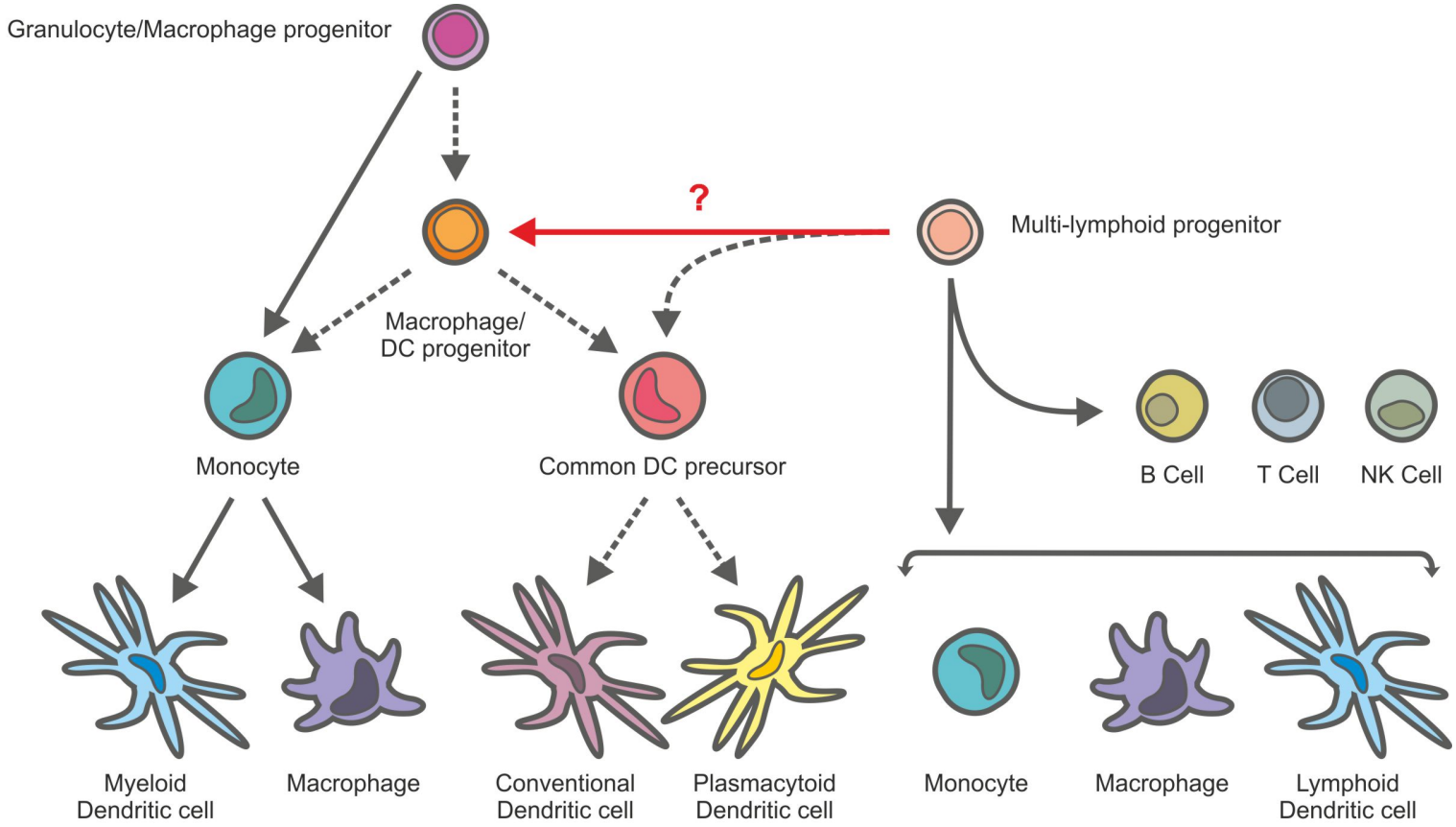

Figure 1-4. Generation of the mononuclear phagocyte system. Solid lines represent described human pathways. Broken lines represent other known murine pathways. Red line indicates hypothetical generation of macrophage/DC progenitors from multi-lymphoid progenitors.

1.3.2.1 Generation of mononuclear phagocytes independent of haematopoiesis

Shultz et al addressed the observation that bone marrow transplantation in mice was relatively ineffective at replacing tissue macrophages. It was postulated that a pool of myeloid cells persisted in tissues independent of the haematopoietic system and that these were initially deposited from the fetal yolk sac (Schulz et al., 2012). Macrophages harvested from a variety of tissues of embryonic mice were clustered, based on transcriptional profiling, to yolk sac macrophages or haematopoietic stem cell-derived macrophages. Tissue yolk sac-like macrophages were also independent of the transcription factor, Myb, in contrast to haematopoietic stem cell-derived macrophages. Myb knockout mice showed a persistence of tissue macrophages with characteristics similar to yolk-sac macrophages in a panel of tissues (Schulz et al., 2012). In addition, analysis of CD45.2 host mice transplanted with CD45.1 donor mouse bone marrow three months post transplantation, showed maintenance of host yolk-sac-derived macrophages in their tissues. The tissues were devoid of CD45.2 host haematopoietic stem cell-derived macrophages and the majority of haematopoietic stem cell-derived macrophages were of donor origin (Schulz et al., 2012). This was most striking in the epidermis where 100% of the murine macrophages, defined as CD11b+ F4/80+, were of CD45.2 host origin and resembled yolk sac macrophages (Schulz et al., 2012). This study also suggested that Langerhans cells, which are epidermal DCs, are solely derived from the yolk sac. Although Langerhans cell precursors are resident in the epidermis before birth (Chang-Rodriguez et al., 2005), the origin of the precursor is unknown. Recently, it was determined that yolk sac macrophages deposited in the embryo contributed little to the persistence of Langerhans cells and although yolk sac-derived precursors remained in the skin, the majority of cells were replaced later in embryogenesis by fetal liver monocytes which provided the pool of Langerhans cells (Hoeffel et al., 2012). The significance of haematopoietic system-independent myeloid cells, in human myeloid cell development is yet to be determined.

1.3.3 Monocyte diversity

As discussed in section 1.3.2, monocytes are generated from progenitor cells in the bone marrow in a macrophage colony stimulating factor (M-CSF) dependent manner. Mice deficient in the M-CSF receptor, CD115 were shown to have reduced levels of mononuclear phagocytes in the peripheral blood, peritoneal cavity, pleural cavity as well as in the liver, skin and kidney (Dai et al., 2002). Monocytes circulate in the peripheral blood, characterised by their 'kidney-' or 'horse shoe'-shaped nuclei and are able to extravasate into tissues and further differentiate into macrophages and some DC subsets, therefore

acting as a motile reservoir for tissue macrophage and DC renewal. In addition to contributing to the macrophage pool as part of tissue homeostasis and during inflammation, monocytes express many other functional capabilities. Monocytes are able to take up foreign material, self cells and cell debris through phagocytosis as well as remove exogenous toxic molecules via scavenger receptors. In addition, human peripheral blood monocytes have been shown to produce the inflammatory cytokines IFNγ, TNFα, IL-1β and IL-12p70 and the chemokine, IL-8 in response to bacteria, such as *Neisseria meningitides* (Webster et al., 2010) (for a complete review on monocytes see (Auffray et al., 2009b))

1.3.3.1 Monocyte subsets

In addition to the complexity of haematopoiesis, in which monocytes may develop from myeloid and lymphoid progenitors, monocytes circulating in peripheral blood have also been shown to be heterogeneous. The identification of multiple subpopulations of human peripheral blood monocytes was initially described by Passlick et al using flow cytometric analysis of peripheral blood monocytes labelled with anti-CD14 and anti-CD16 antibodies (Passlick et al., 1989). Human peripheral blood monocytes are broadly classed into two subsets, $CD14^{hi}$CD16- which are referred to a 'classical monocytes' and $CD14^{hi}$CD16+ which are referred to as 'non-classical' monocytes (reviewed in (Gordon and Taylor, 2005)). In mice, monocyte subsets have been reported to have distinct fates and functions. Common macrophage/DC progenitor cells can differentiate into two distinct monocyte subsets: those that are Gr1+$Ly6C^{hi}$ and those that are Gr1-$Ly6C^{lo}$. Gr1+$LyC6^{hi}$ monocytes have been described as 'inflammatory' monocytes, which are recruited to sites of inflammation and differentiate into macrophages with a more 'inflammatory' phenotype. Gr1-$LyC6^{lo}$ monocytes are described as 'patrolling' or 'resident' monocytes, which may be involved in tissue repair and re-population of tissues with macrophages during normal tissue homeostasis ((Geissmann et al., 2003; Auffray et al., 2007), reviewed in (Geissmann et al., 2010)). In agreement with this paradigm, $Ly6C^{hi}$ monocytes were shown to be recruited to the site of injury during the inflammatory phase in a murine model of myocardial infarction (MI) (Nahrendorf et al., 2007). The $Ly6C^{hi}$ monocytes were found to secrete significantly more matrix-metalloproteases (MMPs) and the pro-inflammatory cytokine, TNFα than $Ly6C^{lo}$ monocytes. The 'healing phase' post MI was dominated by $Ly6C^{lo}$ monocytes which secreted less TNFα and promoted angiogenesis through secretion of the pro-angiogenic factor, vascular endothelial growth factor (VEGF) (Nahrendorf et al., 2007). Gr1-$LyC6^{lo}$ monocytes expressed high levels of the chemokine receptor, CX_3CR1. Conversely, the

monocyte subset defined by Gr1+LyC6^{hi} expressed low levels of CX_3CR1. Human peripheral blood monocytes have also been shown to display similar heterogeneity in CX_3CR1 expression, exhibiting CD14^{hi}CD16- CX_3CR1^{lo} or CD14^{hi}CD16+CX_3CR1^{hi} (Geissmann et al., 2003). Based on these observations, it has been suggested that the murine Gr1+Ly6C^{hi} monocytes are functionally equivalent to human CD14^{hi}CD16- 'classical' monocytes, while Gr1-Ly6C^{lo} monocytes are similar to CD14^{hi}CD16+ 'non-classical' monocytes (Geissmann et al., 2003; Gordon and Taylor, 2005). More recently, another subset of human CD16+ monocytes has been classified (Ziegler-Heitbrock et al., 2010). These CD14$^{dim/lo}$CD16+ were shown to express lower levels of other CD14^{hi} monocyte-associated markers such as CD11b and CD163 and were shown to have an important role in sensing nucleic acids and viruses through TLR7 and TLR8 (Cros et al., 2010).

1.3.3.2 Sources of monocytes during inflammation

As already discussed, monocytes are bone marrow-derived myeloid cells which originate from precursor cells within the bone marrow. The chemokine receptor, CCR2 is key in mediating monocyte egress from the bone marrow into the blood vessels and CCR2 deficient mice have been shown to have a marked reduction in the recruitment of macrophages to the site of thioglycollate-induced peritoneal inflammation (Kurihara et al., 1997; Kuziel et al., 1997) and greater susceptibility to infection by bacteria, such as *Listeria monocytogenes* (Kurihara et al., 1997). In the blood, monocytes circulate freely until recruited to a site of inflammation or injury (reviewed in (Shi and Pamer, 2011)). In order to access inflamed tissue or a site of infection, monocytes leave the blood circulation by adhering to and rolling along the blood vessel wall via L-selectins and E- selectins and P-selectins, expressed on inflamed blood vessel endothelial cells. Monocyte integrin interactions with cell adhesion molecules (CAM) on endothelial cells, for example, the integrin β_1- very late antigen (VLA) 4 interaction with vascular CAM (VCAM) 1, arrests leukocyte rolling and stabilises monocyte adherence to the vessel wall. Monocyte are then able to spread and crawl along the vessel wall before exiting the vasculature via extravasation (reviewed by (Ley et al., 2007)). Recently, the paradigm that monocytes circulating in the blood and patrolling the blood vessels are the only monocytes poised to respond to inflammatory stimuli has been challenged. Swirski et al described a reservoir of monocytes within the subcapsular red pulp of the murine spleen which were found to be 'deployed' following ischemic MI (Swirski et al., 2009). Populations of both Ly6C^{hi} and Ly6C^{lo} monocytes were shown to be present in the spleen however, of the monocytes deployed

from the spleen, it was only Ly6C^{hi} monocytes which accumulated at the site of injured tissue (Swirski et al., 2009).

1.4 Macrophage plasticity – evolving paradigms of macrophage activation

Historically, macrophages were regarded to be inflammatory cells characterised by the release of inflammatory cytokines in response to microorganisms, as described above. Extensive research into macrophage biology over the last 20 years has however, highlighted macrophage plasticity, which enables macrophages to perform a wide range of functions through phenotypic diversity. The different roles of macrophages, in addition to their role in eliminating foreign material, and the evolution of the models of macrophage activation is discussed further in the following sections.

1.4.1 Alternative activation of macrophages

Stein et al first reported upon the 'alternative activation' of macrophages through studies of the macrophage mannose receptor, CD206 (Stein et al., 1992). The Th1 cytokine, IFNγ had previously been shown to down-regulate the activity of CD206 in macrophages from BALB/c mice, as measured by degradation of ^{125}I-Mannose-bovine serum albumin (BSA) (Mokoena and Gordon, 1985). The Th2 cytokine IL-4 rapidly up-regulated CD206 mRNA expression and enhanced the mannose binding and internalisation activity of the mannose receptor of bone marrow-derived macrophages from BALB/c mice as measured by degradation of ^{125}I-Mannose-BSA (Stein et al., 1992). This report suggested that macrophage activation was not limited to inflammatory stimuli and inflammatory responses. Since the report by Stein et al, the function of alternatively-activated macrophages has been extensively studied (reviewed in (Goerdt and Orfanos, 1999; Gordon, 2003; Varin and Gordon, 2009; Gordon and Martinez, 2010); figure 1-5). IL-4 was shown to suppress IFNγ-induced NO production by primary murine peritoneal macrophages (Bogdan et al., 1994) and another Th2 cytokine, IL-13, was also found to up-regulate the murine macrophage mannose receptor (Doyle et al., 1994). IL-4 and IL-13 both stimulate arginase 1 protein expression and activity in murine macrophages. Arginase 1 converts L-arginine to L-ornithine and urea. L-ornithine is then either converted to proline by ornithine aminotransferase for collagen synthesis, or putrescine by ornithine decarboxylase for use in cell division, indicating a central role for arginase 1 in tissue repair (reviewed by (Bronte and Zanovello, 2005; Munder, 2009)). The inhibition of the arginase 1-dependent pathway by the NOS2-dependent pathway and the differential use of L-

arginine has resulted in arginase 1 and iNOS expression becoming a hallmark for the dichotomy of classical- versus alternative-activation in murine macrophages. However, studies have suggested that arginase 1 protein expression is not detected in human mononuclear cells and was instead restricted to human granulocytes (Munder et al., 2005). Furthermore, by contrast to murine macrophages, it has been shown that IL-4 does not up-regulate arginase 1 expression by human monocyte-derived macrophages (Munder et al., 2005). This, coupled with the disparity in iNOS induction in response to microbial products by human macrophages, discussed previously (section 1.2.1), emphasises differences between the mechanisms used by human and murine macrophages in host defense and homeostasis.

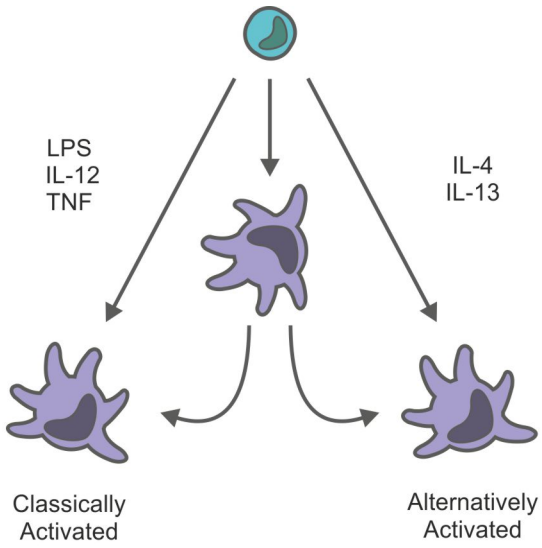

Figure 1-5. The dichotomy of macrophage activation.

As further functions of alternatively-activated macrophages were investigated, it emerged that the alternative-activation of macrophages was not beneficial in all circumstances and some functions associated with Th2 cytokines and the non-classically activated macrophage phenotype were coupled with many disease pathologies. For example, IL-13 signalling through the IL-13 receptor α_2 has been shown to induce TGF-β_1 expression in the human monocytic cell line, THP-1 when cultured in the presence of the pro-inflammatory cytokine, TNFα highlighting a synergy between the Th1 and Th2 signals (Fichtner-Feigl et al., 2006). Furthermore, in a murine bleomycin-induced model of lung fibrosis, siRNA knockdown of IL-13Rα_2 and the blockage of IL-13Rα_2 signalling using decoy

oligonucleotides resulted in reduced bleomycin-induced collagen deposition in the lung and reduced pulmonary fibrosis indicating a role for IL-13 signalling in lung fibrosis (Fichtner-Feigl et al., 2006).

ECF-L (Ym-1) and Relmα (FIZZ1) are well characterised markers of murine alternatively-activated macrophages (Raes et al., 2002a; b) and up-regulation of Relmα by alternatively-activated macrophages derived from a murine nematode infection model was found to be dependent on IL-4 (Loke et al., 2002). ECF-L expression has also been observed at sites of granuloma formation in murine models of schistosomiasis (figure 1-6). Furthermore, arginase 1 mRNA expression and arginase 1 activity was induced in the lung tissue of mice infected with *Schistosoma mansoni* and was significantly reduced in IL-4 knockout mice infected with *S.mansoni* (Hesse et al., 2001). Infected IL-4/IL-13 knockout mice showed significantly reduced lung granuloma formation compared to wild-type mice infected with *S.mansoni*, indicating that IL-4 and IL-13 contribute to the lung pathology of *S. mansoni* infections (Hesse et al., 2001).

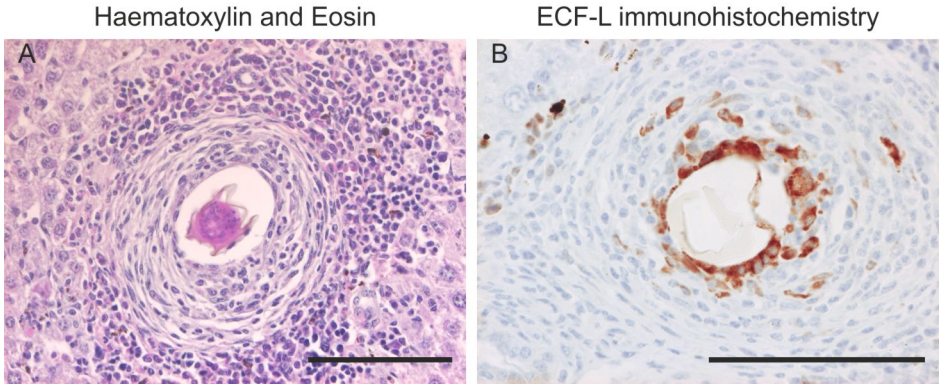

Figure 1-6. Granuloma formation around *S.mansoni* eggs in mouse liver and the presence of ECF-L+ cells. Tissue blocks courtesy of A.Mounford. Scale bars represent 100 microns.

Granulomas are made up from a combination of host cells including FBGC. *In vitro* foreign body-type multinucleated giant cells have been shown to be induced in human monocyte-derived (McNally and Anderson, 1995) or murine bone marrow-derived (MacLauchlan et al., 2009) macrophages cultured in the presence of IL-4. Granuloma formation and multinucleated giant cell formation is central to the pathology of tuberculosis and triggered by the macrophage inflammatory response to *M. tuberculosis*. Bacterial products

from mycobacteria have been shown to induce granuloma formation and multinucleated giant cells using a human *in vitro* model of granuloma formation (Puissegur et al., 2007), indicating that IL-4 is not the only driver of granuloma and multinucleated giant cell formation. The collaboration between the inflammatory cytokines TNFα and IL-13 in murine macrophage-mediated lung fibrosis and the observation that inflammatory bacterial components and the anti-inflammatory cytokine, IL-4 have a role in different models of granuloma and FBGC formation implies that macrophage activation can not be split into a simple dichotomy.

1.4.2 Continuum of macrophage activation

Despite emerging evidence for the effects of other non-inflammatory cytokines, such as IL-10 and TGF-β_1, which were shown to further modulate a non-inflammatory macrophage phenotype, it was proposed that the term 'alternative activation' should be limited to the effects of IL-4 and IL-13 on macrophages (Gordon, 2003) and other macrophage functions should be defined separately. Expansion of the non-inflammatory functions of macrophages and restriction of the term 'alternatively –activated' to macrophages stimulated with IL-4/IL-13 only, resulted in other models of macrophage activation being proposed. The observation that macrophages followed a similar dichotomy to that of the Th1/Th2 paradigm of CD4+ T-cell spawned the concept of M1/M2 macrophages, which respond to IFNγ and IL-4/IL-13 stimuli with expression of iNOS or arginase 1 respectively. M1/M2 macrophages not only have distinct functional phenotypes, but the cells also influence CD4+ T-cell proliferation and activity in different ways (Mills et al., 2000). It was however, also recognised that a continuum of activation states may exist between the M1 and M2 macrophage phenotypes indicating a high degree of plasticity or adaptability in macrophage function (Mills et al., 2000).

The description of 'type II-activated' macrophages, coined by Anderson et al (Anderson and Mosser, 2002), was based on an observation by Sutterwala et al in which ligation of FcγRs on LPS-activated murine bone marrow-derived macrophages suppressed IL-12 synthesis and induced secretion of IL-10. However, in the absence of LPS, FcγR ligation was not enough to enhance IL-10 production alone and FcγR I, II or III knockout mice showed reduced LPS-induced IL-10 production, indicting that both signals were required (Sutterwala et al., 1998). In addition, passive transfer of 'type II-activated' macrophages into mice was able to reverse Th1 dominated responses mediated by IFNγ + LPS-activated macrophages and favor IL-4 production by T-cells indicating a biasing towards a Th2-like

response (Anderson and Mosser, 2002). These studies illustrated that other signals induced non-inflammatory macrophage functions and contributed to the understanding of macrophage heterogeneity.

The M1/M2 paradigm highlighted the synergy between macrophages and CD4+ T-cells during a polarised immune response however, the model was still believed to be an oversimplification, which did not consider the many emerging roles of non-classically activated macrophages. Mantovani et al reviewed the role of chemokines in macrophage polarisation and proposed M2 macrophages to be further separated into M2a, M2b and M2c to reflect other functions of non-classically activated macrophages (Mantovani et al., 2004). M2a macrophages were described as 'alternatively activated' as previously illustrated by Stein et al and were associated with granuloma formation, encapsulation of parasites and allergy, mediated by IL-4/IL-13. M2b macrophages underwent 'type II' activation associated with Th2 activation and immunoregulation due to secretion of high levels of IL-10 as previously described (Sutterwala et al., 1998; Anderson and Mosser, 2002) but were also shown to secrete high levels of the pro-inflammatory cytokines TNFα, IL-1 and IL-6 and express the co-stimulatory receptor CD86. M2c macrophages were described as 'deactivated', due to induction by IL-10 and glucocorticoids and characterised by secretion of IL-10 and TGF-β. M2c were described as having roles in matrix deposition and tissue remodelling ((Mantovani et al., 2004); figure1-7).

Figure 1-7. The continuum of macrophage activation and specialised 'M2' macrophages.

1.4.3 Spectrum of macrophage activation

The models described above attempted to 'pigeon-hole' macrophage phenotypes and are currently limited by the methods of analysis. It is likely that macrophage phenotype is a dynamic process governed by constantly fluctuating environmental cues. More recently, Mosser and Edwards proposed a spectrum of macrophage activation. This model gave

greater focus on the homeostatic roles of macrophages, as well as the role of macrophages as immune effector cells (Mosser and Edwards, 2008). Classically-activated macrophages were illustrated as previously described due their role in pathogen killing and production of inflammatory cytokines. Macrophages that were activated in response to IL-4 were characterised as 'wound-healing' macrophages rather than 'alternatively-activated', in order to incorporate the central role of macrophages in tissue repair and also in tissue fibrosis. Previously described 'type II' macrophages, induced by LPS and immune complexes, IL-10 or glucocorticoids were renamed as 'regulatory macrophages', based on their capacity to secrete high amounts of IL-10 and dampen immune responses ((Mosser and Edwards, 2008); figure 1-8).

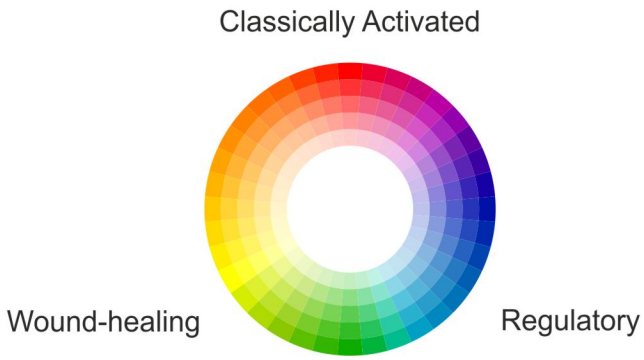

Figure 1-8. The spectrum of macrophage activation.

This spectrum of macrophage activation is still challenged by the M1/M2 paradigm (Biswas and Mantovani, 2010; Galli et al., 2011; Sica and Mantovani, 2012), resulting in confusion in macrophage nomenclature. The attraction of the 'spectrum of macrophage activation' model is the overlap between the major macrophage phenotypes. It permits description of an infinite number of macrophage phenotypes, which, while making targeting of macrophage for disease therapy challenging, may best reflect macrophage heterogeneity.

1.5 The role of macrophages in wound healing

Macrophages have been identified as the key inflammatory cells at a site of tissue injury (Ross and Odland, 1968), which promote wound healing through sensing and responding to tissue damage, stimulating angiogenesis and inducing collagen synthesis (Hunt et al., 1984). Application of murine peritoneal macrophages to a cutaneous wound site on the ventral

region was shown to accelerate wound closure in mice. In addition, isolation and transfer of murine peritoneal macrophages from 'young' (5-8 months) to 'old' mice (24-27 months) accelerated cutaneous wound healing to a rate comparable to that of young mice (Danon et al., 1989) indicating that macrophages play an orchestrating role in wound healing events.

1.5.1 Sensing and responding to damage

Tissue injury shows the hallmarks of acute inflammation characterised by five main processes, rubour (redness), tumour (swelling), calor (heat), dolor (pain) and functio laesio (loss of function) (Bannenberg et al., 2007). The damage caused by a wound event results in a cascade of leukocytes being recruited to the site of injury (reviewed in (Martin and Leibovich, 2005)). A recent, elegant study using Zebrafish larvae identified that immediately following tissue damage a sustained concentration of hydrogen peroxide (H_2O_2) was detectable at the wound margin. The release of H_2O_2 was maintained at the wound margin for the time sampled (1.5 hours) and formed a gradient from the wound margin into the surrounding tissue (Niethammer et al., 2009). H_2O_2 was found not to be of leukocyte origin but provided a signal to recruit leukocytes to the wound margin. This was shown by inhibition and knockdown of the Nox enzyme, dual oxidase (Doux), which attenuated H_2O_2 production and leukocyte recruitment to the wound margin (Niethammer et al., 2009). Upon tissue injury, cell content can be released from damaged cells into the surrounding tissue environment. Released endogenous ligands have been shown to activate cell of the innate immune system through TLRs (reviewed in (Tsan and Gao, 2004) indicating that these receptors play a role in both sensing damage and pathogens. The inflammatory cytokines IL-1β and TNFα up-regulate NFκB-dependent expression of cyclooxygenase 2 (COX2) which generates prostaglandin E_2 (PGE_2) from arachidonic acid (reviewed in (Lawrence et al., 2002)). Release of PGE_2 mediates vasodilation of blood vessels, while bradykinin and histamine mediate vascular permeability (Williams and Peck, 1977) promoting diapedesis of leukocytes from the vasculature into the tissue. Leukotrienes stimulate adhesion and chemotactic movement of leukocytes and the generation of superoxides by neutrophils (reviewed in (Samuelsson, 1983)). Leukotriene B_4 (LTB_4) is also generated from arachidonic acid via the 5-lipooxygenase (5-LOX) pathway (reviewed in (Serhan and Savill, 2005)) highlighting that derivatives of the polyunsaturated omega-6 fatty acid, arachidonic acid are central to perpetuating the inflammatory response.

Damage-associated molecular patterns (DAMPs) have also been shown to induce inflammatory responses by innate leukocytes. DAMPs are usually sequestered intracellularly and are concealed from recognition by the immune system. Necrosis or tissue damage results in the release of the DAMPs for recognition by innate immune cells which, in the absence of microorganisms, generates 'sterile inflammation' (reviewed in (Chen and Nuñez, 2010)). For example, the chromatin-associated protein, high mobility group box 1 (HMGB1) is a DAMP. Application of HMGB1 to human peripheral blood monocyte-derived dendritic cells up-regulated CD80, CD86 and MHC II protein expression, enhanced the production of the pro-inflammatory cytokines, TNFα, IL-12p70 and IL-6 and promoted dendritic cell migration (Yang et al., 2007).

Uric acid has been identified as a danger signal released by 'injured cells' which promotes the expression of CD80 and CD86 by murine dendritic cells and enhances the generation of a CD8+ T-cell response (Shi et al., 2003). Uric acid has also been shown to induce IL-1β and IL-18 production by the monocytic cell line, THP-1 (Martinon et al., 2006). The generation of these inflammatory cytokines was found to be through the PRR, NACHT, LRR and PYD domains containing protein 3 (NALP3) inflammasome in a knockout mouse model (Martinon et al., 2006).

1.5.2 Macrophage function in wound healing

Inflammatory cells such as neutrophils and macrophages are initially recruited to the site of a wound in order to eliminate potential pathogens at the site of injury. The rapid process of microbial clearance and tissue remodelling leads to disorganised deposition of matrix, fibrotic granulation and scar tissue formation (summarised in (Stramer et al., 2007)). Early studies to determine the specific roles of macrophages in wound healing used a guinea pig model of wound repair and depleted macrophages using hydrocortisone acetate. Evaluation of the macrophage-depleted wound sites indicated a lack of clearance of wound debris and a delay in fibrosis in scar tissue formation (Leibovich and Ross, 1975). Macrophages are central in the clearance of apoptotic cells (reviewed by (Erwig and Henson, 2008)) and have been reported to secrete TGF-β at the site of tissue injury (Rappolee et al., 1988) which has been shown to enhance the formation of granulation tissue and increase angiogenesis following subcutaneous injection in newborn mice (Roberts et al., 1986). In agreement with this observation, TGF-β_1 null mice showed a reduction in granulation of wound tissue and increased epithelialisation compared to wounds in control mice, however, the authors reported no impairment in wound healing

(Koch et al., 2000). Using a genetic approach to knock out the transcription factor essential for the differentiation of macrophages and mature neutrophils, PU.1, Martin et al showed that incision into the dorsal forepaw of PU.1 null mice showed an absence of macrophages recruitment, defined by F4/80 expression, to the incision site and reduced mRNA expression of TGF-β_1 compared to the wild type control mice (Martin et al., 2003). However, the incision site in the PU.1 null mice healed at the same rate as the incision made in the wild type mice. Based on this targeted approach, the authors argued that the presence of PU.1+ inflammatory cells was not required for efficient wound healing, (Martin et al., 2003) however, other redundant mechanisms which may contribute to wound-healing were not discussed.

1.5.2.1 Macrophage induction of neo-vascularisation

A central process in wound healing is the production of new vasculature, which provides nutrients to the healing tissue site and newly formed tissue. It is well established that macrophages play a coordinating role in the promotion of vascularisation. Early studies showed that injection of macrophages, activated *in vitro* using latex ingestion, into the corneal stroma of guinea pigs induced vascularisation (Polverini et al., 1977). *In vitro* the macrophage cell line U937 and primary rat peritoneal macrophages have been reported to produce the pro-angiogenic factor, VEGF in response to H_2O_2 highlighting a further role for H_2O_2 in wound healing (Cho et al., 2001). VEGF has also been shown to be secreted by human monocyte-derived macrophages activated with 10ng.mL^{-1} LPS indicating that inflammatory stimuli present in a wound environment and NF-κB activation can also stimulate angiogenesis (Kiriakidis et al., 2003). Yolk sac-derived early tissue macrophages have also been shown to associate with the sprouting blood vessel tips and act as 'cellular chaperones' to aid tip cell fusion down-stream of tip induction during neo-vascularisation in the mouse (Fantin et al., 2010), a process which may also occur during wound-healing.

1.5.3 The resolution of inflammation following damage

Inflammation is a key process in the orchestration of tissue repair following injury and is critical for eliminating microbes however, a failure to down-regulate inflammatory signals can lead to chronic inflammation, fibrosis and tissue destruction (reviewed in (Maderna and Godson, 2009)). The dampening of this inflammatory response is not due to a passive loss of inflammatory signals but an active process and it is now recognised that tight regulatory mechanisms have evolved to dampen the inflammatory response to restore tissue homeostasis – a process referred to as 'inflammation resolution'. Inflammation

resolution is not only defined as the generation of anti-inflammatory signals, which are able to regulate inflammation, but the clearance of the inflammatory signals at a site of inflammation. For example, in addition to binding and clearing toxic haem, the macrophage haemoglobin scavenger receptor, CD163 is able to bind the TNF superfamily member, TNF-like weak inducer of apoptosis (TWEAK) (Bover et al., 2007), permitting CD163+ macrophages to clear soluble TWEAK, which has been suggested to have implications in inflammatory diseases such as atherosclerosis (Moreno et al., 2009). Therefore, 'anti-inflammatory' can be defined as the processes involved in arresting the generation of inflammation, while resolution involves clearing the inflammatory signals that are already present at a site of inflammation. An illustrated example of this process is that anti-inflammatory signals stop the recruitment of neutrophils to a site of inflammation, while pro-resolving signals enhance the clearance of these pro-inflammatory cells by phagocytes (Serhan, 2010). The two mechanisms are not mutually exclusive and pro-resolving signals may encompass and promote anti-inflammatory signals and vice versa. The current paradigm of inflammation dynamics indicates that inflammation resolution signals are induced at a later phase of inflammation (box at the asymptote of the inflammatory curve, figure 1-9), which function to restore tissue homeostasis (Maderna and Godson, 2009). Failure to resolve leads to chronic inflammation (purple line, figure 1-9).

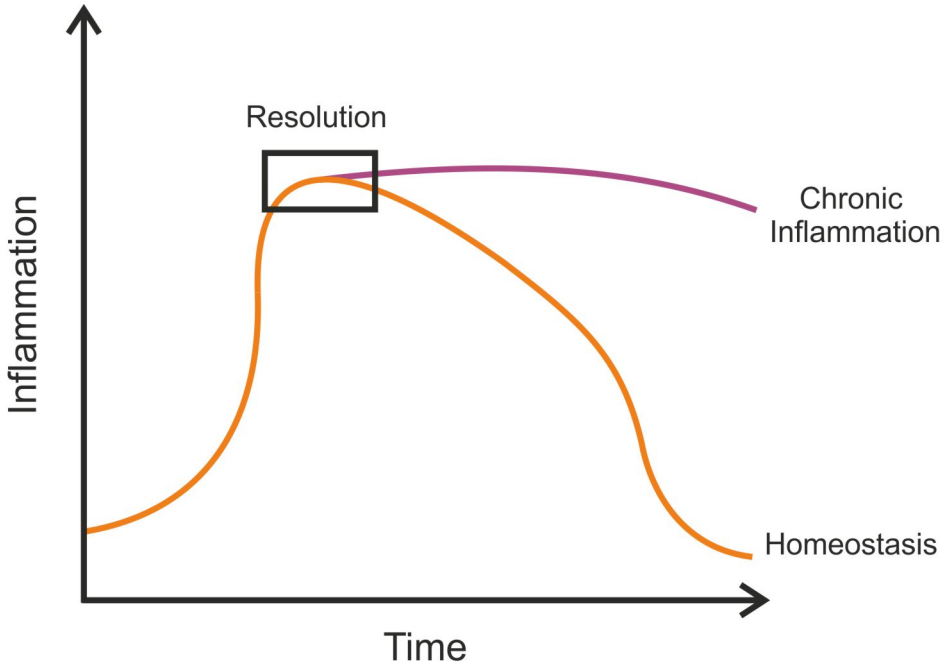

Figure 1-9. The curve of inflammation. Tissue injury results in a rapid influx of inflammatory leukocytes. This inflammation is 'self-limiting' and the generation of anti-inflammatory and pro-resolving signals dampens inflammation and restores tissue homeostasis by removal of inflammatory mediators. Failure to resolve inflammation leads to sustained inflammatory signals and chronic inflammation.

The current paradigm of acute resolving inflammation, in which genes implicated in resolution are expressed at a later phase of inflammation, was recently challenged. Transcriptome analysis of blood leukocytes from patients admitted with severe blunt trauma, isolated immediately post injury, showed striking changes in genes involved in inflammatory and 'compensatory' anti-inflammatory response (Xiao et al., 2011). Although this analysis was systemic and not site-specific, the authors highlighted that expression of pro-inflammatory genes, such as members of TLR signaling pathways and anti-inflammatory genes, such as IL-10, was simultaneous, indicating that during inflammation, genes involved in the resolution phase of inflammation are also expressed (Xiao et al., 2011). Transcriptome analysis of pooled blood leukocytes was suggestive of concurrent expression of inflammatory and anti-inflammatory genes by all leukocytes however, the method of analysis failed to indicate if there was heterogeneity in gene expression within

subsets of leukocytes, in particular if there was a subset of human blood monocytes that specifically expressed anti-inflammatory genes during an inflammatory response.

1.5.3.1 Induction of inflammation resolution

There is increasing interest in whether, during an inflammatory response, there is a phenotypic switch in macrophage function from inflammatory to anti-inflammatory bringing about the resolution of inflammation or if there are dedicated, predetermined macrophages subsets which function to resolve inflammation, potentially based on the lineage from which they are derived. The former is supported by the observation that culture of human PBMC with ultraviolet-irradiated autologous apoptotic peripheral blood lymphocytes reduced LPS-induced TNFα and IL-1β secretion and enhanced IL-10 secretion compared to a medium only control (Voll et al., 1997). Extensive research has demonstrated that phagocytosis of apoptotic cells by macrophages inhibits iNOS generation and enhances TGF-β generation and the release of arachidonic acid (reviewed in (Erwig and Henson, 2007), initiating the resolution phase of inflammation. Investigation into arachidonic acid and other lipid mediators of inflammation has provided insight into the dynamics of inflammation resolution and has supported the hypothesis that the early phase of inflammation programs the resolution phase of inflammation (Serhan and Savill, 2005). Levy et al showed that application of TNFα to a murine dorsal air pouch showed rapid and transient production of PGE_2 and LTB_4 in exudates taken from the pouch. This rise in PGE_2 and LTB_4 was concomitant with neutrophil infiltration and peaked at approximately two hours post TNFα administration, but was absent eight hours post TNFα administration (Levy et al., 2001). The authors also reported the generation of lipoxin A_4 in the exudates, which peaked at four hours post administration of TNFα was sustained for the rest of the sample period (eight hours) (Levy et al., 2001). Lipoxin A_4 is also generated from arachidonic acid, via the 15-lipooxygenase (15-LOX) pathway (Maderna and Godson, 2009) however, lipoxin A_4 is strongly associated with anti-inflammatory and 'pro-resolving' actions (reviewed in (Serhan et al., 2008)) indicating that during inflammation there is a switch in lipoxygenase pathways resulting in differential utility of arachidonic acid and fatty acid inflammatory signals (Levy et al., 2001). Lipoxin A_4 is a potent chemoattractant for human monocytes and increases monocyte adhesion to laminin-coated plastic *in vitro* (Maddox and Serhan, 1996). Lipoxin A_4 has also been shown to rapidly induce phagocytosis of human neutrophils by human monocyte-derived macrophages (Godson et al., 2000), furthermore, 15-LOX expression by primary human monocytes has been shown to be up-regulated by IL-13 (Nassar et al., 1994) in line with the anti-inflammatory activities of this

cytokine. Interestingly, PGE_2 has also been shown to up-regulate 15-LOX mRNA expression and lipoxin A_4 production by human polymorphonuclear cells (Levy et al., 2001) supporting evidence that inflammatory signals can program the resolution of inflammation.

1.5.3.2 Resolution signals and tissue regeneration

Investigation into tissue regeneration in a murine cornea wound healing model reported that C57BL/6J mice deficient in 'leukocyte-type' 12/15 LOX (Jax®Gemm®strain) showed reduced biosynthesis of lipoxin A_4 and impaired wound healing following corneal epithelial removal. Furthermore, topical application of lipoxin A_4 to the eye accelerated re-epithelialisation indicating a potential role for lipoxin A_4 in wound healing (Gronert et al., 2005). Protectins and D-series resolvins are docosahexaenoic acid (DHA) derivatives (reviewed in (Serhan, 2010) and also were identified in the resolving phase of a murine peritonitis models of self-resolving inflammation (Bannenberg et al., 2005). Resolvins and protectins were reported to actively promote mechanisms involved in the resolution of inflammation and potentially wound-healing, as indicated by TGF-β production detected during the resolution phase (Bannenberg et al., 2005). More recently, the macrophage-specific DHA derivative, macrophage mediator of resolving inflammation (maresin), has indicated DHA derivatives have a specific role in tissue regeneration. Application of maresin 1 at 100nM to a planaria model of tissue regeneration showed enhanced rate of anterior region re-growth following surgical removal when compared to the vehicle control (Serhan et al., 2012). Planaria tissue regeneration correlated with maresin 1 concentration and LOX inhibition with baicalein blocked maresin 1 biosynthesis and reduced the rate of maresin 1-enhanced tissue regeneration of the planaria anterior region (Serhan et al., 2012).

1.5.4 Macrophage paradigms and wound healing

The advent of different models of macrophage activation has generated interest in the precise phenotype of macrophages during wound healing. CD14+ human umbilical cord blood-derived monocytes injected into the murine eye in a model of oxygen-induced retinopathy (OIR) were reported to differentiate into M2 macrophages, which induced angiogenesis and tissue repair and reduced apoptosis and oxidative stress (Marchetti et al., 2011). Wound-healing macrophages described by Mosser and Edwards were characterised based on the bias of IL-4 towards arginase 1 expression and collagen production over induction of iNOS in the mouse. However, the presence of inflammatory macrophages, which clear microbes and debris, and the observation that inflammatory mediators provide initial signals to promote wound healing (Niethammer et al., 2009); the role of TGF-β in

matrix deposition and fibrosis (Roberts et al., 1986; Fichtner-Feigl et al., 2006); the induction of macrophage VEGF by ROS (Cho et al., 2001) and LPS (Wu et al., 2010) and the maintenance of hypoxia-induced VEGF secretion by murine bone-marrow derived macrophages in the presence of the regulatory cytokine, IL-10 (Wu et al., 2010); indicates that the wound-healing macrophage phenotype is not only mediated by IL-4 and the role of the macrophage in wound healing is strongly governed by many other environmental cues. Additionally, these paradigms have not focused on the lipid class switch, which brings about the resolution of inflammatory responses and appears to be a key process in the orchestration of wound healing.

1.6 Macrophage response to medical devices

As macrophages have been associated with sensing damage, tissue repair, neo-vascularisation and tissue remodelling; and with fibrosis and foreign-body encapsulation, it is axiomatic that macrophages play a role in the host response to implanted medical devices and there has been considerable interest in dissecting the immune response to implanted medical grade materials (biomaterials) used in regenerative medicine.

1.6.1 Biomaterials

A biomaterial can be defined as any material, natural or synthetic, which can be used *in vivo* or *in vitro* to restore, replace or represent a biological system. Biomaterials are being developed for use in both tissue engineering strategies and regenerative medicine. In tissue engineering strategies, biomaterials provide a three-dimensional (3D) scaffold that is compatible with cell growth and differentiation, facilitating the formation of an *in vitro* tissue construct. In regenerative medicine, scaffolds may be implanted *in vivo* to aid restoration of tissue or restore tissue function lost through damage or disease. Biomaterials used in either approach are not mutually exclusive and biomaterials used in regenerative medicine and tissue engineering can provide iterative feedback into biomaterial function, design and development (Figure 1-10).

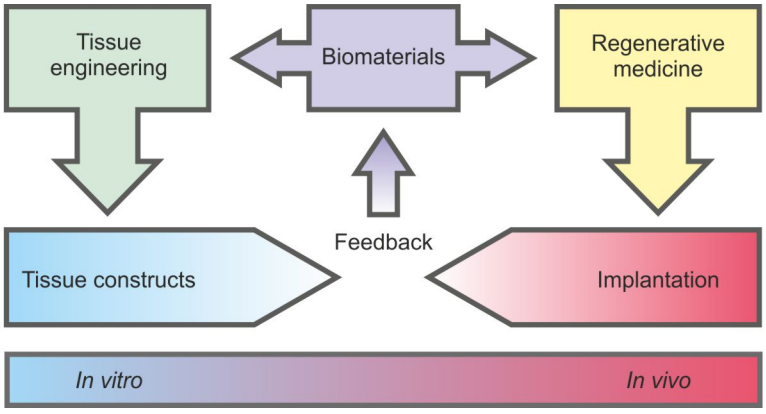

Figure 1-10. The relationship between tissue engineering and regenerative medicine.

1.6.1.1 Biological scaffolds as biomaterials

The extracellular matrix (ECM) is a 3D scaffold composed of molecules secreted by the cells of a given tissue or organ during development and is a dynamic structure, consisting of structural proteins such as collagens and fibronectin (reviewed in (McDonald, 1988)) and is constantly degraded and remodelled (reviewed in (Birkedal-Hansen, 1995)). The ECM can be harvested, maintaining its 3D structure from a diverse range of tissues and organs using a variety of methodologies. These methods range from application of mechanical force to use of detergents, all of which aim to remove the tissue-derived cells to produce a 'biological scaffold'. Examples of tissues which have been successfully decellularised include: porcine urinary bladder (Bolland et al., 2007), porcine pericardium (Mirsadraee et al., 2006) and human amniotic membrane (Wilshaw et al., 2006), all decellularised using a detergent-based protocol followed by treatment with nucleases and terminal disinfection with 0.1% (v/v) peracetic acid; porcine small intestinal submucosa (SIS) prepared by mechanically delaminating the porcine jejunum and removal of the serosa and the tunica muscularis followed by disinfection in 0.1% (v/v) peracetic acid (Badylak et al., 1989) and porcine liver, decellularised using 0.02% (w/v) trypsin/0.05% (w/v) Ethylenediaminetetraacetic acid (EDTA) followed by treatment with 3% (v/v) Triton X-100 for one hour and 4% sodium deoxycholic acid for a further hour (Lin et al., 2004; Brown et al., 2010). These biological scaffolds have application in both tissue engineering and regenerative medicine, however focus has turned to the therapeutic applications of these materials in the clinic. As such, the use of biological scaffolds in regenerative medicine has been extensively reviewed (Badylak, 2002; 2004; 2007; Badylak et al., 2009). Applications of porcine SIS in *in vivo* models described in the early literature included use as a vascular graft repair of a defect in the infrarenal aorta in a canine model (Badylak et al., 1989); as a biological scaffold to repair a partial defect in the small bowel of canines (Chen and Badylak, 2001); a patch repair in urinary bladder augmentation following partial cystectomy in Sprague-Dawley rats (Kropp et al., 1995); repair of a segmental defect of the Achilles tendon in canines (Badylak et al., 1995); and repair of a circumferential segment defect in canine oesophagus (Badylak et al., 2000). These studies highlight the versatility of harvested ECM for use as a biological scaffold in regenerative medicine. The therapeutic application of some commercially available biological scaffolds is summarised in Table 1-2 (reviewed in (Badylak, 2007)).

Table 1-2. Commercially available biological scaffold used in regenerative medicine

Product	Material	Chemical modification	Application	Company
Oasis®	Porcine SIS	None	Partial and full thickness wounds	Healthpoint Ltd.
Alloderm®	Human skin	Cross-linked	Abdominal wall repair and breast reconstruction	Lifecell™
dCell®	Porcine pericardium	None	Vascular repair	Tissue Regenix Group Plc.
TissueMend®	Fetal bovine dermis	None	Tendon repair and reinforcement of the rotary cuff	TEI biosciences Inc.
Biodesign™	Porcine SIS	None	Hernia and abdominal wall repair	Cook Biotech Inc.
Veritas®	Bovine pericardium	None	Vascular repair	Synovis®
Permacol™	Porcine dermis	Cross-linked	Hernia and abdominal wall repair	Covidien
Collamend™	Porcine dermis	Cross-linked	Hernia and abdominal wall repair	Bard Inc.

1.6.2 The biocompatibility and integration of biological scaffolds

In vivo implantation studies in either animal defect models or subcutaneous implantation studies have been employed to determine the application and biocompatibility of biological scaffolds. Many studies in which biological scaffolds have been implanted into animal models have used histological analysis to determine leukocyte infiltration as a measure of the inflammatory response. Evaluation of Veritas®, a commercially available decellularised bovine pericardium in a rabbit hysterectomy model, in which Veritas® acted as an 'anti-adhesion barrier' for up to 29 days before harvesting and staining of histological sections with haematoxylin and eosin showed infiltration of host cells into the biological scaffold at day 29 (Connolly, 2006). The authors reported limited infiltration of cells with polymorphic nuclei and mononuclear cells indicating a relatively small inflammatory response, however, immunohistochemistry was not used to identify these cells (Connolly,

2006). The biocompatibility of decellularised human pericardium was assessed by subcutaneous implantation into Mf-1 hairless mice for three months and compared to subcutaneous implantation of fresh/frozen (non-viable) human pericardium and glutaraldehyde-fixed pericardium. Upon harvesting, the fresh/frozen and glutaraldehyde-fixed implants were shown to be encapsulated with a fibrous membrane indicative of a foreign body type response (Mirsadraee et al., 2007). Immunohistochemical analysis of the fresh/frozen implants revealed that >70% of the cells within the capsule and infiltrating into the implant were CD11b+, and were suggested by the authors to be macrophages, however murine neutrophils also express CD11b (Jaeschke et al., 1991) and other cells with polymorphic nuclei were also observed (Mirsadraee et al., 2007). CD11b+ cells were also observed in the decellularised human pericardium implant accompanied by CD34+ cells, suggested by the authors to be indicative of a wound-healing response. The decellularised human pericardium implant also showed a reduced presence of CD3+ and CD4+ cells compared to the fresh/frozen human pericardium implant, indicating a lower T cell infiltration (Mirsadraee et al., 2007). Subcutaneous implantation of fresh/frozen human amniotic membrane, fresh glutaraldehyde-fixed human amniotic membrane and decellularised human amniotic membrane into Mf-1 mice for three months also showed fibrotic encapsulation of fresh/frozen and the glutaraldehyde-fixed human amniotic membrane accompanied by the presence of mononuclear and polymorphic nuclear cells and areas of calcification (Wilshaw et al., 2008). Conversely, the harvested decellularised amniotic implant showed dense infiltration of host cells with mononuclear and fibroblastic morphology. In addition, neo-vascularisation of the implanted decellularised human amniotic membrane was also reported (Wilshaw et al., 2008). Immunohistochemical evaluation of the implants showed a consistent presence of F4/80+ macrophages in all three implant types. F4/80+ cells were located within the dense fibrous capsule surrounding the fresh/frozen and glutaraldehyde-fixed human amniotic membrane. The F4/80+ cells identified in the implantation of the decellularised human amniotic membrane were located within a thin capsule that surrounded the implant (Wilshaw et al., 2008). An example of encapsulation of fresh/frozen porcine bladder material mediated by F4/80+ cells following subcutaneous implantation into a mouse for three months before harvesting the explants is shown in figure 1-11. Implantation of decellularised porcine bladder matrix did not shown signs of fibrosis or encapsulation. Instead, F4/80+ cells were observed infiltrating the decellularised porcine bladder implant (figure 1-11).

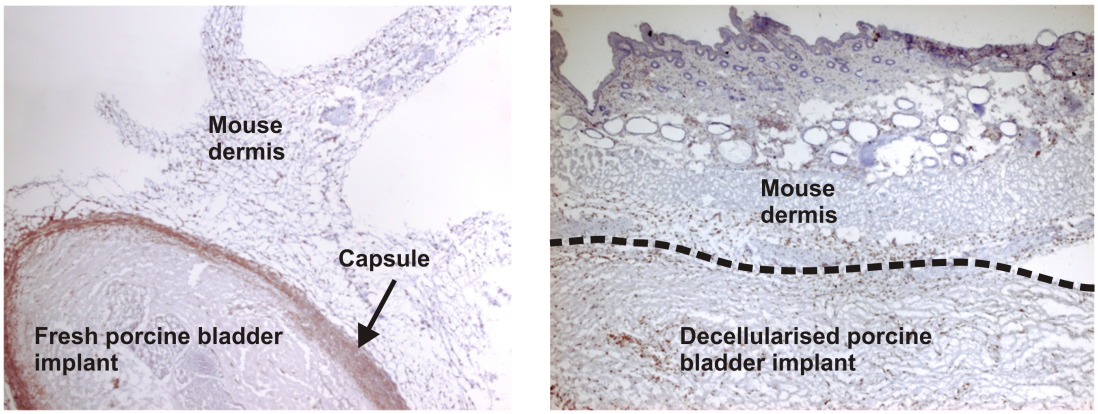

Figure 1-11. The presence of murine macrophages following subcutaneous implantation of fresh, frozen porcine bladder or decellularised porcine bladder tissue into mice. The materials were harvested three months post implantation and immunolabelled for the expression of the murine macrophage marker, F4/80. Images courtesy of J. Southgate.

It was previously shown that during the integration of mechanically-isolated ^{14}C-labelled porcine tunica submucosa, generated by intravenous injection of ^{14}C-proline into the pigs for 26 weeks, into a canine model of augmentation cystoplasty that the biological scaffold was rapidly degraded (Record et al., 2001). Liang and colleagues illustrated that increased cross-linking of a decellularised bovine pericardium using increasing concentrations of aqueous genipin decreased the capacity of the scaffold to be degraded following subcutaneous implantation into Wistar rats (Liang et al., 2004). Degradation of the decellularised pericardium was accompanied by infiltration of inflammatory cells such as macrophages and histological evaluation of the biological scaffolds harvested three days post implantation showed decreased inflammatory cell infiltration with increased cross-linking (Liang et al., 2004). Subcutaneous implantation of mechanically-isolated porcine tunica submucosa labelled with ^{14}C, generated as described above, into Sprague-Dawley rat model of abdominal wall defect showed the presence of CD68+ macrophages at the site of implantation (Valentin et al., 2009). Administration of clodronate liposomes to ablate phagocytic cells showed a marked reduction in CD68+ cells at the site of implantation compared to rats that received saline or PBS liposome controls. The observed reduction in CD68+ cells correlated with a significant reduction in the degradation of the biological scaffold compared to rats that received saline or PBS liposome controls, as measured by liquid scintillation counts of ^{14}C at the graft sites (Valentin et al., 2009), indicating that

macrophages are required for the degradation and early remodelling events of biological scaffolds at least in rodents.

1.6.3 Macrophage phenotype in response to biological scaffolds

The presence of macrophages both during a fibrotic encapsulation response and the realisation that macrophages are key cells in the degradation and integration of biological scaffolds, coupled with the description of macrophage heterogeneity prompted focus on the macrophage phenotype in response to biological scaffolds. The macrophage phenotype in response to biomaterials has been recently reviewed (Badylak and Gilbert, 2008; Brown et al., 2012a). Key characterisation studies of the macrophage phenotype during the *in vivo* response to biological scaffolds will be discussed briefly.

Repair of a defect in the ventrolateral abdominal wall musculature of Sprague-Dawley rats with either allogeneic rat body wall ECM or xenogeneic porcine urinary bladder wall ECM followed by harvesting at either 3, 7, 14 or 28 days post surgery and histological analysis indicated a bias of CD163+ cells, used as marker of M2 macrophages, over CCR7+ cells, used as a marker of M1 macrophages. Conversely, implantation of autologous body wall tissue or xenogeneic porcine urinary bladder tissue to repair the defect showed a higher ratio of CCR7+ cells to CD163+ cells across the 28 day time course (Brown et al., 2009). Furthermore, gene expression analysis indicated that both the acellular allograft and the acellular xenograft showed a higher ratio of arginase 1 gene expression to iNOS gene expression however, the cellular allograft and xenograft did not show a marked increase in the ratio of iNOS:arginase 1 gene expression (Brown et al., 2009). From this, the authors concluded that the presence of a cells in the graft skewed the macrophage phenotype towards an M1 type phenotype while the absence of cells in the decellularised matrix polarised the macrophages towards an M2 phenotype which were central in the constructive remodelling of the biological scaffold (Brown et al., 2009). In a similar study, repair of a ventrolateral abdominal wall defect in Sprague-Dawley rats using either porcine-derived SIS or a carbodiimide cross-linked form of SIS and histological evaluation at 1, 2, 4 or 16 weeks post surgery again showed an increase in CD68+ immunopositive cells at the implantation site over the first four weeks which decreased by week 16 (Badylak et al., 2008). Immunolabelling for CD163, used as a marker of M2 macrophages and CD80, used as a marker of M1 macrophages indicated that repair of the defect using porcine-derived SIS showed a predominantly M2 macrophages response at all time points. Conversely, repair of the defect with carbodiimide cross-linked form of SIS showed constant and

greater presence of CD80+ cells over the all time points compared to the SIS implant and reduction in the percentage of CD163+ cells at weeks four and 16, which gave an increased ratio of CD80:CD163 (Badylak et al., 2008). Brown et al discussed the potential for using macrophage phenotype as a predictor of constructive remodelling of implanted biomaterials (Brown et al., 2012b). In a screening of 14 commercially available, FDA approved biological scaffolds implanted into the abdominal wall of Sprague-Dawley rats for 14 days, a significant correlation between a higher ratio of M2:M1 macrophages, defined by expression of CD206 and CCR7 respectively, and constructive remodelling of the implant was observed. Furthermore, the ratio of M2:M1 macrophages at day 14 was also reported to correlate with constructive remodelling of implants harvested at a later day 35 time point (Brown et al., 2012b).

1.7 Summary

Animal models of immunological processes and *in vivo* implantation studies are currently the gold standard in understanding immune mechanisms and material biocompatibility, respectively. Animal models have provided invaluable tools to interrogate the properties of biomaterials and explore the potential applications of biological scaffolds in regenerative medicine, as such there has been little use of *in vitro* approaches in these types of studies. However, biological scaffolds employed in regenerative medicine are ultimately designed for use in man, and disparity between mouse and human immune functions, which are not considered when using these models to infer the host immune response to various materials with therapeutic application, may lead to a lack of mechanistic understanding of biomaterial-tissue interactions. This observation, coupled with the need to reduce, refine and replace animal studies, highlights the necessity to develop better *in vitro* models in regenerative medicine. *In vivo* implantation studies used to determine the macrophage phenotype in response to biological scaffolds remain limited to the M1 and M2 activation paradigm and few *in vivo* studies have interrogated the functional significance of the markers observed, resulting in the oversimplification of a complex and dynamic process. A clear illustration of this is in the use of histopathological markers of M2 macrophages as an indicative marker of a regenerative tissue response. However, M2 markers are also observed during encapsulation responses and M2 macrophages play a key role in tissue fibrosis, highlighting that care is required when defining the macrophage response to biomaterials. Finally, implantation of biological scaffolds also represents a unique environment to the immune system and is not considered in any models of macrophage activation therefore, it has been speculated that the macrophage phenotypic function during the integration of biological scaffolds is as unique as the environment (Baker et al., 2011; Jones et al., 2007).

1.8 Thesis aims and objectives

The overall aim of this research project was to build on understanding from rodent biomaterial implantation studies by gaining insight into the human tissue response to a decellularised biomaterial. The specific aims of this project were to investigate the cells that colonise a biological scaffold by examining an *ex vivo* biomaterial-tissue interface and to identify potential factors and immune mechanisms that govern the tissue response to a biological scaffold, with particular focus on the phenotype of macrophages at the *ex vivo* interface. The aims of this thesis were achieved through meeting the following objectives:

a) Assemble and characterise an 'antibody tool kit' to examine the expression of a range of functional cell markers on a panel of tissues and cells (Chapter 3).
b) Develop an organotypic culture model of an *ex vivo* biomaterial-tissue interface using porcine urinary tract tissue and human urinary tract tissue (Chapter 4).
c) Identify objective markers of macrophage phenotype expressed at the *ex vivo* biomaterial-tissue interface and potential cell signalling mechanisms that are active at the *ex vivo* interface (Chapter 4).
d) Examine how these signalling mechanisms govern functional marker expression by macrophages and therefore infer macrophage phenotype, using *in vitro* cell culture (Chapter 5).

2.0 Materials and methods

2.1 General methods

All work was performed in the Jack Birch Unit for Molecular Carcinogenesis in the Department of Biology at the University of York. Manufacturers and suppliers are listed within the text with a complete list given in appendix I-I. All stock solutions were prepared using de-ionised water centrally fed from a fully customised Lubron water system. The de-ionised water was further purified to 18.2 Megohms using a Purelab Ultra water purifier (Elga LabWater) unless otherwise stated. Where required, heat stable solutions, plasticware, glassware and surgical instruments were sterilised by autoclaving at 121 degrees Celsius (°C) at a pressure of 1 bar for 15 minutes.

2.2 Collection of tissue specimens

2.2.1 Statement of ethics

Ethical permission was in place to take human ureter, bladder and renal pelvis tissue from adult and paediatric non-urothelial cancer patients with no history of urothelial cancer undergoing urological operations.

Ethical permission was obtained for this study to take human peripheral blood from healthy volunteers at two separate sites:

- University of Leeds – Ethics code R0109.
- Hull York Medical School Experimental Medicine Unit (HYMS EMU) based at York hospital – Leeds Central Research Ethics Committee code 10/H1313/93.

All tissue was obtained from anonymised patients and volunteers following written informed consent.

2.2.2 Porcine bladder tissue

Porcine bladder tissue was collected from the local abattoir (Traves of Escrick) and transported back to the Jack Birch Unit at ambient temperature in 1x Hank's balanced salt solution (HBSS) $+Ca^{2+}$ $+Mg^{2+}$ supplemented with 20 $KIU.mL^{-1}$ Trasylol® (Bayer Healthcare Pharmaceuticals), 10mM 4-(2-hydroxyethyl)-1-piperazineethanesulphonic acid (HEPES; Life Technologies), 20 $U.mL^{-1}$ penicillin (Life technologies) and 20$\mu g.mL^{-1}$ streptomycin (Life Technologies), hereon referred to 'complete porcine transport medium'.

2.2.3 Human ureteric and bladder tissue

Ureteric and bladder tissue samples were kindly provided by surgeons at York Hospital, York; St James's University Hospital, Leeds; Castle Hill Hospital, Cottingham and the Leeds General Infirmary, Leeds following one of two main procedures:

- Samples of normal human ureter obtained from open nephrectomy procedures.
- Samples of renal pelvis obtained by laparoscopic pyeloplasty.

Samples were transported back to the Jack Birch Unit at ambient temperature in 1x HBSS $+Ca^{2+}$ $+Mg^{2+}$ supplemented with 20 $KIU.mL^{-1}$ Trasylol® and 10mM HEPES, hereon referred to as 'complete transport medium'.

2.2.4 Human peripheral blood

Human peripheral blood was obtained via venipuncture from healthy volunteers using the Monovette® blood collection system (Sarstedt). Blood was collected by trained phlebotomists, into 7.5mL aspiration tubes containing lithium-heparin coated beads and transported to the Jack Birch Unit at ambient temperature.

2.3 Cytokines, Agonists and Inhibitors

A complete list of cytokines, agonists and inhibitors is shown in Table 2-1. All cytokines, agonists and inhibitors were made up according to the manufacturer's instructions, aliquoted and stored at -80°C. In all experiments in which cytokines, agonists and inhibitors were used a vehicle control was included and the concentration of the vehicle was kept to less than 0.1% (v/v).

Table 2-1. Cytokines, agonists and inhibitors suppliers and vehicle

Compound name	Type	Supplier	Catalogue number	Vehicle
Dexamethasone	Agonist	Tocris	1126	Dimethyl Sulfoxide (DMSO)
Dexamethasone	Agonist	Sigma-Aldrich	D4902	100% Ethanol
Interleukin 10 (IL-10)	Cytokine	R&D Systems	217-IL	PBS containing 0.1% (w/v) BSA
Phorbol 12-myristate 13-acetate	Agonist			Chloroform
T0070907	Inhibitor	Tocris	2301	DMSO
Troglitazone	Agonist	GlaxoSmithKline		DMSO
Troglitazone	Agonist	Sigma-Aldrich	T2573	DMSO

*Phosphate buffered saline (PBS; see appendix I-II) containing 0.1% (w/v) BSA.

2.4 Organ culture

All organ culture procedures were performed following standard aseptic techniques in a class II laminar air flow cell culture safety cabinet with high efficiency particulate air (HEPA) filters (Medical Air Technology). Tissue and tissue constructs were incubated in a humidified atmosphere of 37°C and 5% (v/v) carbon dioxide (CO_2) in air in a Heraeus HERAcell® 240 incubator (Thermo Electron Corporation) unless otherwise stated.

2.4.1 Preparation of porcine bladder tissue for organ culture

Porcine bladder tissue was removed from the complete porcine transport medium and placed in a 145 millimeter (mm) cell culture dish (Greiner Bio-one) using sterilised forceps. Excess fatty tissue was removed from the exterior of the bladder using a sterile scalpel and sterile scissors. The porcine bladder epithelium was exposed by cutting the porcine bladder from the neck of bladder to the dome as shown in figure 2-1.

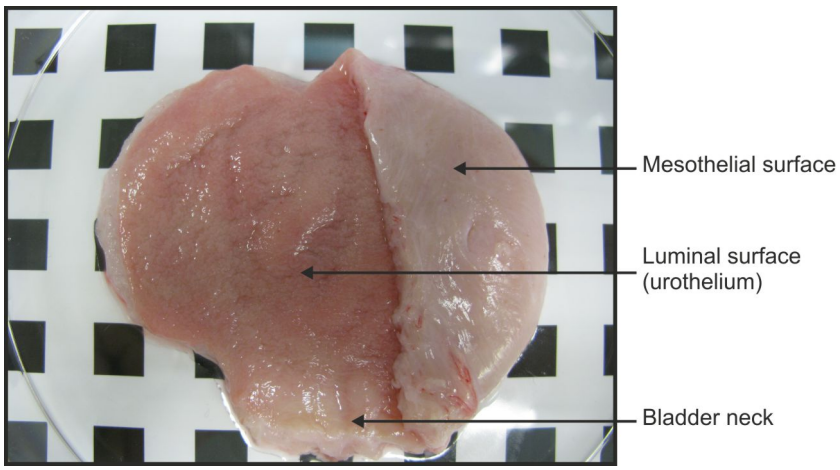

Figure 2-1. Macroscopic image of a dissected porcine bladder highlighting the internal luminal surface and external mesothelial surface. One centimeter square checked-pattern background indicates scale.

Split-thickness bladder tissue was created by cutting horizontally through the muscle of the porcine bladder. The lumen-facing split thickness tissue was cut into approximately half centimeter square (cm^2) pieces and maintained in fresh porcine bladder transport medium until use.

2.4.2 Preparation of human ureteric tissue for organ culture

During the course of the study, human ureteric tissue from five donors was used (Table 2-2). Human ureteric tissue was removed from the complete transport medium and placed in a 90mm Petri dish (Sterilin) using sterilised forceps. The urothelium of the human ureteric tissue was exposed by inserting a blade of a pair of sterilised scissor into the lumen of the ureter and cutting along the length of the tissue. The tissue was cut into approximately half centimeter square pieces and maintained in complete transport medium until use.

2.4.3 Maintenance of organ culture constructs

Organ culture constructs were cultured on the membrane of a cell culture well insert with three micrometer (μm) pores (BD Falcon™, catalogue number 734-0034) in a six well plate (Corning® Costar®). One millilitre (mL) of Waymouth's medium (Life Technologies) supplemented with 10% (v/v) foetal bovine serum (FBS, Sera Laboratories International, Lot 110006), 300μg.mL^{-1} L-ascorbic acid (Sigma-Aldrich), 2μg.mL^{-1} hydrocortisone hemisuccinate (Sigma-Aldrich) and 450ng.mL^{-1} ferrous sulphate (Fisons) was added to the well of the six well plate ensuring the area between the base of the well and the membrane of the cell culture well insert was completely flooded. Sterile de-ionised water was added to the central area of the six well plate to ensure a humidified environment. The organ culture medium was changed every two days.

Table 2-2. Human tissue used in organ culture experiments

Organ culture line	Tissue	Procedure	Age of patient at the time of procedure	Gender
Y1050	Ureter	Nephrectomy	60	Female
Y1083	Ureter	Nephrectomy	51	Female
Y1129	Ureter	Nephrectomy	61	ND
Y1132	Ureter	Nephrectomy	65	ND
Y1193	Ureter	Nephrectomy	73	Female

ND-No data

2.5 Cell culture

All cell culture procedures were conducted using standard aseptic techniques within a class II laminar airflow cell culture safety cabinet with HEPA filters. Cells cultures were incubated in a humidified atmosphere at 37°C and 5% (v/v) CO_2 in air in a Heraeus HERAcell® 240 incubator unless otherwise stated.

2.5.1 Peripheral blood mononuclear cell culture

2.5.1.1 Peripheral blood mononuclear cell medium

Peripheral blood mononuclear cells (PBMC) were cultured in Roswell Park Memorial Institute (RPMI; Life Technologies) 1640 supplemented with 10% (v/v) FBS (Sera Laboratories International, Lot 110006) heat inactivated at 56°C for 30 minutes and 2mM L-glutamine (Sigma-Aldrich); referred to as 'complete PBMC medium'.

2.5.1.2 Isolation of PBMC

Human PBMC were isolated using density centrifugation over the polysaccharide solution, Lymphoprep™ (Axis-Shields). Single donor blood was diluted 1:1 with RPMI 1640 medium containing 20mM HEPES hereon referred to as 'RPMI transport medium'. Seven millilitres of dilute blood was carefully layered over 3mL of Lymphoprep™ in a sterile round bottom centrifuge tube (Sterilin). The preparation was centrifuged at 800g for 30 minutes at 20°C with the centrifuge brakes turned off to ensure a clean separation of the PBMC within the 'buffy coat' (figure 2-2).

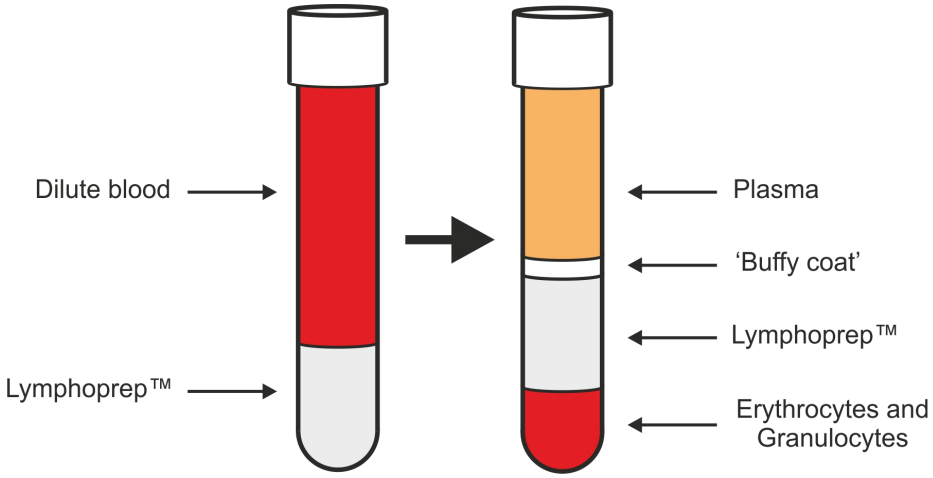

Figure 2-2. Schematic diagram of the separation of PBMC from whole blood using density centrifugation. Seven millilitres of dilute whole blood was carefully layered over three millilitres of Lymphoprep™ within a round-bottom tube. Centrifugation at 800g for 30 minutes separated the dilute blood into four distinct layers. The buffy coat contained the PBMC, which were carefully aspirated from the other layers.

The 'buffy coat' was removed using a sterile glass Pasteur pipette and plastic bulb and transferred into a sterile round-bottom test tube. RPMI transport medium was added to the PBMCs up to a volume of approximately 10mL per sterile round-bottom tube. The cells were then centrifuged at 400g for 15 minutes at 20°C. The supernatant was decanted and the pellet resuspended by flicking. The cells were resuspended in 10mL RPMI transport medium and centrifuged at 400g for 15 minutes at 20°C. This washing process was performed a total of three times.

2.5.1.3 PBMC enumeration

Isolated PBMC were resuspended in an appropriate volume of complete PBMC medium dependent on the visual size of the pellet. An aliquot of the PBMC single cell suspension was diluted 1:10 (v/v) with 0.4% (w/v) Trypan blue solution (Sigma-Aldrich) and used to fill a ruled haemocytometer by capillary action before counting the cells in a 4x4 grid in a total volume of 0.0001cm^3. The total number of peripheral blood mononuclear cells was calculated.

2.5.1.4 Latex bead ingestion assay

In order to enumerate the number of monocytes in the PBMC suspension, the percentage of phagocytic PBMC was determined using a latex bead ingestion assay. The PBMC suspension (100µL) in complete PBMC medium was added to 15µL heat inactivated FBS and 50µL of 1% (w/v) polystyrene latex beads with an average diameter of 1.1µm (Sigma-Aldrich, catalogue number LB-11). The preparation was incubated at 37°C for 30 minutes. Following incubation, 100µL heat inactivated FBS was layered under the preparation before centrifuging at 100g for one minute at ambient temperature to separate out the uningested beads. The supernatant was removed and the pellet was resuspended by flicking. Complete PBMC medium (100µL) was added and the preparation centrifuged at 100g for one minute. The supernatant was removed and the pellet resuspended by flicking before adding 100µL complete PBMC medium. Ten microlitres of the preparation was pipetted onto a Super Frost plus glass microscope slide (Thermo Fisher). The percentage of phagocytic mononuclear cells was enumerated by counting over 100 cells across multiple fields of view (Figure 2-3). A three-step calculation was followed to determine the number of phagocytic mononuclear cells per millilitre of cell suspension using the latex bead ingestion assay:

1) Percentage of phagocytic mononuclear cells:

$$\frac{Total\ number\ of\ \ phagocytic\ mononuclear\ cells\ per\ \ field\ of\ \ view}{Total\ number\ of\ mononuclear\ cells\ per\ \ field\ of\ \ view} \times 100$$

2) Total number of phagocytic mononuclear cells obtained in suspension:

$$Total\, number\ of\ mononuclear\ cells \times \left(\frac{Percent\ of\ \ phagocytic\ \ mononuclear\ cells}{100} \right)$$

3) Number of phagocytic mononuclear cells obtained per millilitre of cell suspension:

$$\frac{Total\, number\ of\ \ phagocytic\, mononuclear\ cells\, in\ suspension}{Total\, volume\, of\ cell\, suspension\, (mL)}$$

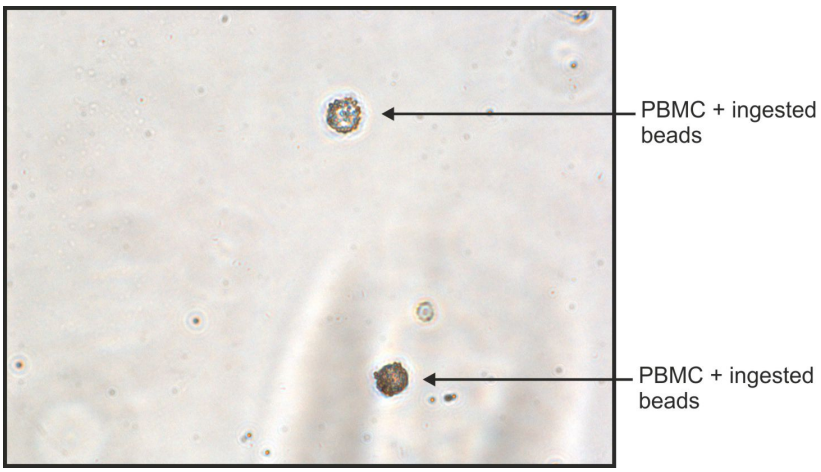

Figure 2-3. Phase contrast image of phagocytic mononuclear cells that have ingested latex beads.

During the course of this study, PBMC were isolated from the blood of 32 donors in total. The details of blood samples collected are shown in Table 2-3.

Table 2-3. Blood samples collected throughout the study

Ethics code	Donor ID	Sample ID	Volume of blood obtained (mL)
R0109	R0109-005	R0109-005-001	ND
	R0109-003	R0109-003-003	ND
10/H1313/93	10/H1313/93-001	10/H1313/93-001-001	36
	10/H1313/93-002	10/H1313/93-002-001	32
	10/H1313/93-003	10/H1313/93-003-001	31
	10/H1313/93-004	10/H1313/93-004-001	30
	10/H1313/93-005	10/H1313/93-005-001	28
	10/H1313/93-006	10/H1313/93-006-001	26
	10/H1313/93-007	10/H1313/93-007-001	17.2
	10/H1313/93-008	10/H1313/93-008-001	21
	10/H1313/93-009	10/H1313/93-009-001	29
	10/H1313/93-010	10/H1313/93-010-001	29.5
	10/H1313/93-001	10/H1313/93-001-002	21
	10/H1313/93-002	10/H1313/93-002-002	30.2
	10/H1313/93-003	10/H1313/93-003-002	32
	10/H1313/93-011	10/H1313/93-011-001	29
	10/H1313/93-008	10/H1313/93-008-002	30
	10/H1313/93-005	10/H1313/93-005-002	31
	10/H1313/93-012	10/H1313/93-012-001	31
	10/H1313/93-013	10/H1313/93-013-001	30
	10/H1313/93-014	10/H1313/93-014-001	29.5
	10/H1313/93-015	10/H1313/93-015-001	30.5
	10/H1313/93-016	10/H1313/93-016-001	30.5
	10/H1313/93-003	10/H1313/93-003-003	32
	10/H1313/93-017	10/H1313/93-017-001	30
	10/H1313/93-012	10/H1313/93-012-002	32
	10/H1313/93-001	10/H1313/93-001-003	29.5
	10/H1313/93-005	10/H1313/93-005-003	30.5
	10/H1313/93-015	10/H1313/93-015-002	29.5
	10/H1313/93-014	10/H1313/93-014-002	30
	10/H1313/93-018	10/H1313/93-018-001	30
	10/H1313/93-016	10/H1313/93-016-002	32

10/H1313/93-019	10/H1313/93-019-001	28.4
10/H1313/93-020	10/H1313/93-020-001	32
10/H1313/93-021	10/H1313/93-021-001	30
10/H1313/93-013	10/H1313/93-013-002	32
10/H1313/93-022	10/H1313/93-022-001	32
10/H1313/93-023	10/H1313/93-023-001	32.5
10/H1313/93-024	10/H1313/93-024-001	32
10/H1313/93-025	10/H1313/93-025-001	32
10/H1313/93-008	10/H1313/93-008-003	32
10/H1313/93-004	10/H1313/93-004-002	31
10/H1313/93-006	10/H1313/93-006-002	32
10/H1313/93-017	10/H1313/93-017-002	22
10/H1313/93-026	10/H1313/93-026-001	32
10/H1313/93-024	10/H1313/93-024-002	33
10/H1313/93-022	10/H1313/93-022-002	33
10/H1313/93-021	10/H1313/93-021-002	33
10/H1313/93-027	10/H1313/93-027-001	32
10/H1313/93-012	10/H1313/93-012-003	33
10/H1313/93-028	10/H1313/93-028-001	33
10/H1313/93-002	10/H1313/93-002-003	32
10/H1313/93-023	10/H1313/93-023-002	30
10/H1313/93-014	10/H1313/93-014-003	32
10/H1313/93-020	10/H1313/93-020-002	32
10/H1313/93-018	10/H1313/93-018-002	33
10/H1313/93-016	10/H1313/93-016-003	32
10/H1313/93-029	10/H1313/93-029-001	32
10/H1313/93-009	10/H1313/93-009-002	32
10/H1313/93-030	10/H1313/93-030-001	32
10/H1313/93-006	10/H1313/93-006-003	31.5
10/H1313/93-021	10/H1313/93-021-003	32
10/H1313/93-017	10/H1313/93-017-003	32
10/H1313/93-024	10/H1313/93-024-003	32

ND – No data

2.5.2 Seeding of PBMCs onto multiwell slides

Glass multiwell slides (CA Hendley, catalogue number PH-057) were cleaned with 70% (v/v) ethanol in dH_2O water before autoclaving. Slides were transferred aseptically to a flat bottom 4 well dish (Nunc). PBMC suspension (50μL) at $1.52x10^6$ phagocytic mononuclear cells per millilitre was added to each well of the multiwell slide producing a final seeding density of $2x10^5$ phagocytic mononuclear cells per cm^2. Slides were incubated for three hours in a humidified environment at 37°C and 5% (v/v) CO_2 to allow attachment.

Following incubation, each slide was vigorously washed twice with 5mL 1x HBSS $+Ca^{2+}$ $+Mg^{2+}$ followed by flooding the slide with 5mL complete PBMC medium +/- agonist, inhibitor, cytokine or vehicle control treatment before returning to the incubator.

2.5.2.1 Fixation of cells seeded onto multiwell slides

Medium was aspirated from each slide before washing twice with 5mL PBS. Excess PBS was removed by tapping the slide on paper towel before fixing the slides in 1:1 (v/v) methanol and acetone (methanol:acetone) for 30 seconds at ambient temperature and allowing to air dry. Slides were labelled appropriately using a glass etching pen and wrapped back-to-back in cling film. The slides were then stored at -20°C in the presence of desiccated silica gel crystals.

2.5.3 Seeding of PBMCs onto glass Petri dishes

Glass Petri dishes (Pyrex) with a diameter of nine centimeters (cm) were washed with 70% (v/v) ethanol in dH_2O water before sending to central glass washing services for washing with an acid rinse cycle. The Petri dishes were immersed in dH_2O water for >24 hours before autoclaving at 121°C (1 bar) for 15 minutes.

All remaining PBMC suspension from each donor was added to the sterilised glass Petri dish to ensure the maximum number of adherent cells could be harvested for analysis. Complete PBMC medium was added to the seeded PBMC suspension up to a total volume of 10mL. The cells were then incubated for three hours in a humidified environment at 37°C and 5% (v/v) CO_2 in air to allow for attachment.

Following incubation the cells were vigorously washed twice with 10mL 1x HBSS $+Ca^{2+}$ $+Mg^{2+}$ followed by flooding the glass Petri dish with 10mL complete PBMC medium +/- agonist, inhibitor, cytokine or vehicle control treatment before returning to the incubator.

2.5.4 Seeding of biological scaffolds

Biomaterial was cut to approximately 1cm^2 and pre-conditioned in complete PBMC medium for 24 hours. Sterile metal seeding rings with a seeding area of 0.5cm^2, stored in sterile PBS, were dried on sterile autoclaved filter paper (Whatman) and place into the centre of a well of a six well plate (Corning Incorporated) using sterile forceps. Preconditioned biomaterial was drained of liquid on sterile filter paper before placing it on top of the seeding ring. A sterile metal seeding ring was dried on autoclave paper and placed on top of the dehydrated biomaterial. PBMC suspension (100μL) at 1x10^6 phagocytic mononuclear cells per mL was seeded on top the biomaterial as indicated in figure 2-4, to produce a final seeding density of 2x10^5 phagocytic mononuclear cells per cm^2. The biomaterial-cell constructs were then incubated for three hours in a humidified atmosphere at 37°C and 5% (v/v) CO_2 in air to allow for attachment.

Following incubation, the biomaterial was removed from between the seeding rings and gently dipped into 10mL 1x HBSS +Ca^{2+} +Mg^{2+} within a sterile 30mL Universal tube (Sterilin). The seeded biomaterial was returned the well of the six well plate and the well flooded with 4mL of complete PBMC medium before returning to the incubator.

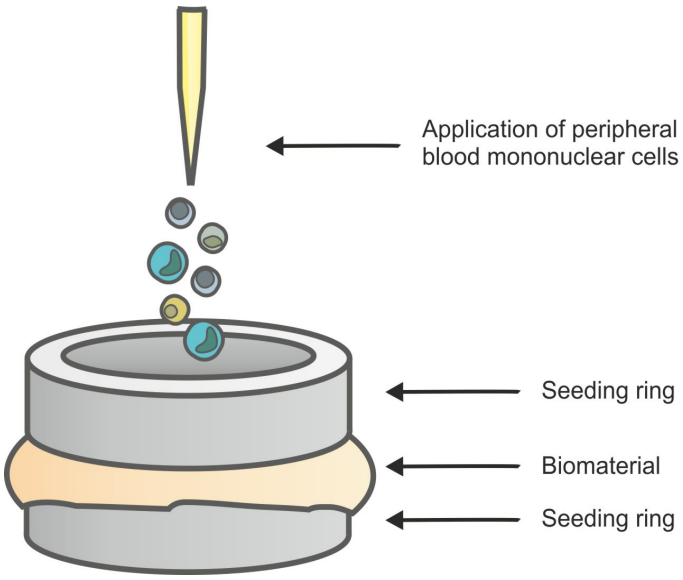

Figure 2-4. Schematic diagram of the seeding of a biomaterial with PBMC. Biological scaffolds were dehydrated on sterile filter paper and sandwiched between two sterile seeding rings. PBMC were seeded on to the apical surface of the biomaterial by applying diluted cell suspension into the upper seeding ring.

2.5.5 THP-1 cell culture

2.5.5.1 THP-1 cell medium

THP-1 cells were cultured in RPMI 1640 supplemented with 10% (v/v) heat inactivated FBS (Lot 110006), 2mM L-glutamine and 0.05mM β-mercaptoethanol (Sigma-Aldrich); referred to as 'complete THP-1 medium'.

2.5.5.2 THP-1 cell propagation

The human monocytic cell line, THP-1 (ATCC® Number TIB-202™) was a kind gift from Dr Nathalie Signoret (University of York). THP-1 cells were propagated in a 75cm^2 vented cell culture flask (Iwaki) in complete THP-1 medium. The THP-1 cells were cultured in suspension in a humidified atmosphere at 37°C and 5% (v/v) CO_2 in air and maintained between 1x10^5 and 1x10^{6}cells.mL^{-1} by passaging every three to four days.

2.5.5.3 THP-1 cell passage

The flask was agitated to resuspend the THP-1 cells. An aliquot of THP-1 cells was removed from the flask into a bijou and the THP-1 cells enumerated by loading 10μL of THP-1 cell suspension onto a ruled haemocytometer by capillary action and the THP-1 cells counted in a 4x4 grid. Cells were adjusted to 1x10^{5}cells.mL^{-1} by adding the appropriate volume of cell suspension to an appropriate volume of complete THP-1 medium in a 75cm^2 vented cell culture flask.

2.5.5.4 Seeding of THP-1 cells onto cell culture dishes

THP-1 cells were transferred to a sterile 30mL Universal tube and centrifuged at 300g for five minutes. The supernatant was discarded and the THP-1 cell pellet was resuspended in an appropriate volume of complete THP-1 medium. An aliquot of THP-1 cell suspension was diluted 1:10 (v/v) with 0.4% (w/v) Trypan blue solution and the dilute single cell suspension enumerated using a ruled haemocytometer as previously described. The THP-1 cells were adjusted to 1x10^{6}cells.mL^{-1} and 5mL of dilute cell suspension added to a 100mm sterile cell culture dish (BD Falcon™) in combination with 5mL of medium containing the vehicle control or treatment at double the desired final concentration.

2.5.6 Ureteric and bladder stromal cell culture

2.5.6.1 Stromal cell medium

Stromal cells were cultured in Dulbecco's modified Eagles medium (DMEM, Life Technologies) supplemented with 5% (v/v) FBS (Lot 110006) and 2mM L-glutamine; referred to as 'complete stromal cell medium'.

2.5.6.2 Stromal cell isolation

Human stromal cells were established from fresh surgically excised human ureter as previously described by Kimuli et al (Kimuli et al., 2004). Two human stromal cell lines were used in this study as shown in Table 2-4. Following removal of the urothelium, the stromal tissue was finely homogenised with a sterile scissors. The homogenates were aspirated with a sterile Pasteur pipette and transferred to a 30mL Universal tube and centrifuged at 300g for five minutes. Following centrifugation, the remaining transport medium was aspirated from the homogenates. The suspended homogenates were immersed in an appropriate volume of collagenase IV (Sigma), dependent on the amount of material, for two hours with agitation at 37°C. Following incubation, the homogenates were centrifuged as described above and the collagenase IV aspirated. The homogenates were washed once with 5mL of complete stromal cell medium, centrifuged as described above and the medium aspirated. The homogenised explants were resuspended in an appropriate volume of complete stromal medium allowing for approximately 100µL per 25cm^2 vented cell culture flask (Iwaki) to be seeded and the homogenised explants transferred to 25cm^2 vented cell culture flasks. Stromal cells were incubated in a humidified atmosphere at 37°C and 10% (v/v) CO_2 in air for 48 hours to allow for attachment before the complete stromal cell medium was replenished.

2.5.6.3 Stromal cell propagation

Stromal cells were propagated in a 75cm^2 vented cell culture flask (Iwaki) in 15mL of complete stromal cell medium. Stromal cells were maintained in a humidified atmosphere at 37°C and 10% (v/v) CO_2 in air. Cells were passaged once they reached approximately 80% confluency.

2.5.6.4 Stromal cell passaging

At confluency, the complete stromal cell medium was aspirated from the flask and 5mL of pre-warmed 0.1% (w/v) EDTA added to the flask. The flask was incubated at 37°C for approximately five minutes until the cells had begun to round up. The 0.1% (w/v) EDTA

solution was aspirated from the flask and 500µL pre-warmed Trypsin-Versene (Sigma-Aldrich - see appendix I-II) added to the flask and the flask incubated at 37°C until the cells had begun to detach from the culture surface. The flasks were tapped vigorously to detach the cells, which were resuspended in 10mL complete stromal cell medium and centrifuged at 300g for five minutes. Following centrifugation the supernatant was removed and the stromal cell pellet agitated. The cells were resuspended in an appropriate volume of complete stromal cell medium. Stromal cells in single cell suspension were equally distributed into multiple 75cm^2 vented cell culture flasks and each flask made up to a total volume of 15mL complete stromal cell medium.

Table 2-4. Stromal cell lines established and used for experiments in this study

Stromal cell line	Tissue	Procedure	Age of patient at the time of procedure	Gender
Y863	Ureter	Cystectomy	67	Male
Y886	Bladder	Transurethral resection of prostate (TURP)	68	Male

2.6 General histology

2.6.1 Fixation

Harvested primary tissue, tissue constructs and biological scaffolds were fixed by immersing in either 10% (v/v) formalin in PBS plus calcium (PBSc) (Appendix I-III) or zinc salt fixative (Appendix I-III) for at least 24 hours at ambient temperature. Following fixation the tissue, tissue constructs and biological scaffolds were immersed in 70% (v/v) ethanol in dH_2O until processed.

2.6.2 Embedding in paraffin wax

Fixed tissue was cut to size using a sterile scalpel and placed into a labelled embedding cassette (Thermo Scientific - RA Lamb). All initial steps were performed on a shaker platform at ambient temperature. Tissue was dehydrated by immersion in 90% (v/v) ethanol in dH_2O for two hours followed by immersion in 100% ethanol for two hours. The cassettes were then immersed in 100% xylene for two hours followed by immersion for a

further two hours in fresh xylene. The embedding cassettes were then immersed in molten Shandon Histoplast paraffin wax (Thermo Scientific) and incubated at 60°C overnight. The samples were removed from the embedding cassettes and orientated on a heat block within a metal mold before immersing in molten Shandon Histoplast paraffin wax. The blocks were cooled at -12°C on a cold block to allow the blocks to set and removed from the metal molds.

2.6.3 Sectioning of embedded tissue

Tissue blocks were cooled for ≥1 hour at -12°C on a cold block and five microns thick tissue sections cut using a Leica RM2135 microtome. Tissue sections were floated on 40°C water in a water bath (Thermo Scientific - RA Lamb) before being lifted onto Superfrost plus or Superfrost Ultra glass microscope slides (Thermo Scientific). The tissue sections were dried on a drying rack at 40°C (Thermo Scientific - RA Lamb) or at ambient temperature. The tissue sections were baked before use by placing directly onto the drying rack heated surface at 40°C for between one and six hours.

2.6.4 Staining of tissue sections

2.6.4.1 Haematoxylin and eosin (H&E) staining

Recipes for stains can be found in appendix I-III. Tissue sections were dewaxed in two changes of xylene for 10 minutes followed by two changes in xylene for one minute and rehydrated through a graded series of ethanols from 100% (v/v) to water for one minute for each change. Tissue sections were stained in Mayer's haematoxylin for 30 seconds to one minute and washed immediately in running water to remove all residual stain. The slides were then immersed in Scott's tap water for one minute before washing under running tap water for a further minute. Slides were then stained with aqueous 1% (w/v) eosin (Thermo Scientific – RA Lamb) for 30 seconds and washed immediately in running water to remove all residual stain. The tissue sections were dehydrated from water through a graded series of ethanol to 100% (v/v) ethanol for one minute for each change, followed by two, one minute changes in xylene, before finally immersing in Histoclear (Fisher Scientific). The tissue sections were then mounted with 22x22 millimeter (mm) number 1.5 coverslips (Scientific Laboratory Supplies) using DPX mounting fluid (CellPath).

2.6.4.2 Hoechst 33258 nuclear staining

Tissue sections were dewaxed in two changes of xylene for 10 minutes followed by two changes in xylene for one minute and rehydrated through a graded series of ethanol from

100% (v/v) for one minute for each change to water. Sections were incubated in PBS containing 0.5% (w/v) Triton-X (Sigma) on a shaking platform for 15 minutes at ambient temperature. The slides were washed by immersing them in 5mL of PBS and incubated on a shaking platform for five minutes at ambient temperature. Five milliliters of Hoechst 33258 (Sigma-Aldrich; catalogue number 861406) at 0.1µg.mL^{-1} was added to each slide. The slides were then incubated on a shaking platform for 10 minutes at ambient temperature, followed by washing 3x15 minutes with 5mL per slide of PBS. The sections were mounted in 0.1% (w/v) p-Phenylendiaminodihydrochloride (Sigma-Aldrich) in 90% (w/v) glycerol in PBS at pH8 (Appendix I-IV); referred to as 'IF anti-fade mountant', 22x22 mm number 1.5 coverslips were applied to the mountant and the slides sealed with clear nail varnish. The slides were protected from light and kept at 4°C.

2.7 Tissue decellularisation

Porcine bladders were decellularised following the procedure described by Bolland et al (Bolland et al., 2007). Handling of the porcine bladder was performed aseptically in a class II cell culture safety cabinet.

2.7.1 Stock solutions

Components of all stock solutions can be found in Table 2-5.

Table 2-5. Stock solutions for porcine bladder decellularisation

Stock solutions
10% (w/v) EDTA in dH_2O
2M Tris-hydrochloric acid (HCL) pH 8.0 in dH_2O
10% (w/v) Sodium dodecyl sulphate (SDS) in dH_2O
2M Tris-HCL pH 7.5 in dH_2O
1M Magnesium chloride ($MgCl_2$) in dH_2O
100U.mL^{-1} RNAse A (Sigma 83833) in dH_2O
10,000U.mL^{-1} DNAse I (Sigma DN25) in 1:1 (v/v) glycerol/ 5mM sodium acetate, 1mM $CaCl_2$

2.7.2 Decellularisation buffers

One litre of each decellularisation buffer was prepared per bladder and autoclaved prior to use. SDS, BSA, RNAse A, DNAse I and Trasylol® were not autoclaved and, where appropriate, were syringe filter sterilised on the day of use (Table 2-6).

Table 2-6. Components of porcine bladder decellularisation buffers

Decellularisation buffer	Components
Wash buffer	10 KIU.mL^{-1} Trasylol®*; 0.1% (w/v) EDTA in PBS.
Hypotonic buffer	10 KIU.mL^{-1} Trasylol®*; 10mM Tris-HCL pH 8.0 and 0.1% (w/v) EDTA in dH_2O.
SDS buffer	10 KIU.mL^{-1} Trasylol®*; 10mM Tris-HCL pH 8.0; 0.1% (w/v) EDTA; 0.1% (w/v) SDS* in dH_2O.
Wash buffer (no EDTA)	10 KIU.mL^{-1} Trasylol®* in PBS
Nuclease solution	50mM Tris-HCL pH 7.5; 10mM $MgCl_2$; 0.005% (w/v) BSA*; 1000U RNAse A*, 50,000U DNAse I* in dH_2O.
Hypertonic buffer	1.5M NaCl; 0.05 Tris-HCL pH 7.6 in dH_2O.
Disinfection buffer	0.1% (v/v) Peracetic acid (PAA – Sigma 77240) pH 7.2 in dH_2O.

*Syringe filter sterilised if required and added at time of use.

2.7.3 Decellularisation of porcine bladders

Intact bladders were trimmed of excess fatty tissue before being washed in complete wash buffer. The bladders were transferred to a sterile one litre tub and distended by filling with approximately 500mL hypotonic buffer using a sterile 50mL syringe (Becton, Dickinson and Company) inserted into the neck of the bladder. The bladder neck was clamped shut using a pair of Spencer Wells forceps and the expanded bladder immersed in approximately 500mL of hypotonic solution within the sterile one litre tub. The distended and immersed bladder was incubated for 24 hours at 4°C.

The bladders were removed from the buffer by unclamping the neck and gently elevating the bladders from the dome allowing the buffer to drain from the neck. The waste buffer

was discarded and the bladders distended by filling with approximately 500mL SDS buffer using a sterile funnel inserted into the neck of the bladder. The bladder neck was clamped shut using Spencer Wells forceps and the expanded bladder immersed in approximately 500mL SDS buffer. The bladders were incubated on a shaking platform for 24 hours at ambient temperature.

Following incubation, the SDS buffer was discarded and the bladders were distended and immersed in the wash buffer (no EDTA) as described above. The bladders were incubated on an shaking platform for a minimum of 24 hours at 37°C. Following incubation the wash buffer was discarded and the bladders transferred to a new sterile one litre tub. The bladders were distended and immersed in nuclease buffer and incubated on a shaking platform with gentle agitation for 24 hours at 37°C.

The nuclease buffer was discarded and replaced with wash buffer. The bladders were incubated on a shaking platform for 24 hours at 37°C. Following incubation, the wash buffer was discarded and the bladders distended and immersed in hypertonic buffer. The bladders were incubated on an shaking platform for 24 hours at 37°C. Following incubation the hypertonic buffer was discarded and replaced with wash buffer and incubated as described previously.

The bladders were distended and immersed in disinfection buffer and incubated on an orbital shaker for a minimum of three hours at ambient temperature. The disinfection buffer was discarded and the bladders placed into a sterile Petri dish. The bladder neck was removed and the bladders were dissected into a flattened sheet by incising from the bladder neck to the bladder dome using sterile scissors. The flattened sheet was then washed by immersing in fresh sterile PBS for 1 hour and incubating on a shaking platform at ambient temperature. This wash process was repeated three times, transferring to a fresh 150mL pot (Sterilin) with each wash. The flattened bladder sheet was then incubated in fresh sterile PBS for 24 hours at 4°C before being transferred and stored in a 150mL Sterilin pot in fresh sterile PBS at 4°C.

2.7.4 Confirmation of tissue decellularisation

Approximately 1cm^2 biopsies were cut from the dome and walls of the decellularised porcine bladder biomaterial. The biopsies were immersed in 10% (v/v) formalin and processed for histological examination as described in Section 2.6. Sections were dewaxed and hydrated to water as described in Section 2.6.4.1 and either stained with haematoxylin

and eosin as described in section 2.6.4.1 or Hoechst 33258 as described in Section 2.6.4.2 to confirm removal of cellular components and nuclear material respectively.

2.7.5 Contact cytotoxicity assay

Six biopsies approximately 0.5cm^2 were taken from the dome and walls of each decellularised porcine bladder. Three biopsies were immersed in 5mL of PBS overnight. The remaining three samples were immersed 5mL of 10% (w/v) SDS as a positive control for cytotoxicity. The samples were incubated overnight at ambient temperature.

Following incubation, each sample was anchored to the bottom of the well of a six well plate using approximately two centimeters of Nexcare™ Steri-Strip™ (3M). Negative control wells were set up using Steri-Strip™ only. The human stromal cells cultures were detached from the cell culture flask into single cell suspension as described in Section 2.5.6.4. Dilute stromal cell suspension were then counted using a haemocytometer. The stromal cell density was adjusted in complete stromal cell medium and the stromal cells seeded into the six well plate at a final seeding density of $4.2x10^3$ $cells.cm^{2-1}$ in a total volume of 3mL of complete stromal cell medium per well. The cell culture plates were incubated in a humidified environment at 37°C and 10% (v/v) CO_2 in air for 48 hours.

Following incubation, phase contrast images of the cells at the interface between the negative control, positive control and test material were captured to determine cytotoxicity.

2.8 Immunolabelling

2.8.1 Antibodies

A complete list of antibodies and their optimum concentration for each application can be found in table 2-7. Mouse IgG isotype control antibody (Dako, catalogue number X0931), at a concentration equal to the highest primary antibody concentration in each experiment, was included in all cytometry and histological immunolabelling experiments as a negative control for antibody labelling. Allophycocyanin-conjugated mouse IgG (R&D Systems, catalogue number IC0041A), fluorescein isothiocyanate-conjugated mouse IgG (AbD Serotec, catalogue number MCA928F) or phycoerythrin-conjugated mouse IgG (Miltenyi Biotech, catalogue number 130-092-212) isotype control antibodies were used at a concentration equal to the relevant primary antibody concentration in all flow cytometric analysis as a negative control for immunolabelling.

Table 2-7. Primary and secondary antibodies used

Key:

IB – Immunoblotting

IHC – Immunohistochemistry

IF – Immunofluorescence

FC – Flow cytometry

APC – Allophycocyanin

FITC - Fluorescein isothiocyanate

PE – Phycoerythrin

ND – No data

Antibody	Supplier	Host	Type	Clone	Isotype	Application	Catalogue number	Conjugation	IgG Concentration ($\mu g.mL^{-1}$)	Dilution
Anti-human Arginase 1	ProteinTech	Rabbit	Polyclonal	NA	IgG	IB	16001-1-AP		0.352	1/700
						Tissue IHC/IF			2.465	1/100
Anti-human CD11b	R&D Systems	Mouse	Monoclonal	238446	IgG_{2B}	Cell IF	MAB16991		10	1/10
						FC	FAB16991A	APC	10	Neat
Anti-human CD14	Miltenyi Biotec	Mouse	Monoclonal	TÜK4	IgG_2a	FC	130-091-242	PE	1	1/11
Anti-human CD3	Novocastra	Mouse	Monoclonal	PS1	IgG_2a	Tissue IHC/IF	NCL-L-CD3-PS1		4	1/50
						Cell IF			2	1/100
Anti-human CD34	Novocastra	Mouse	Monoclonal	QBEND/10	IgG_1	Tissue IHC/IF	NCL-L-END		ND	1/50
Anti-human CD36	Atlas Antibodies	Rabbit	Polyclonal	NA	IgG	Tissue IHC	HPA002018		3	1/20
						Tissue IF			6	1/10
Anti-human CD68	Dako	Mouse	Monoclonal	PG-M1	$IgG_3\kappa$	Tissue IHC/IF	M0876		0.8	1/50
						Cell IF			0.2	1/200
	R&D Systems	Mouse	Monoclonal	298807	IgG_{2B}	FC	IC20401A	APC	10	Neat

Antibody	Supplier	Host	Type	Clone	Isotype	Application	Catalogue number	Conjugation	IgG Concentration ($\mu g.mL^{-1}$)	Dilution
Anti-human CD80	R&D Systems	Mouse	Monoclonal	37711	IgG_1	Tissue IHC/IF	MAB140		10	1/50
						Cell IF			50	1/10
Anti-human CD117	Dako	Rabbit	Polyclonal	NA	IgG	Tissue IHC/IF	A4502		23.8	1/600
Anti-human CD163	AbD Serotec	Mouse	Monoclonal	EDhu-1	IgG_1	IB	MCA1853		1	1/500
						Tissue IHC/IF			5	1/100
						Cell IF			2.5	1/200
						FC	MCA1853F	FITC	9.1	1/11
Anti-human GR	Novocastra	Mouse	Monoclonal	4H2	IgG_2a	IB	NCL-GCR		1.22	1/100
						Tissue IHC/IF			1.22	1/100
						Cell IF			6.1	1/20
Anti-human HLA-DR	Dako	Mouse	Monoclonal	TAL.1B5	$IgG_1\kappa$	Tissue IHC/IF	M0746		0.6	1/100

Antibody	Supplier	Host	Type	Clone	Isotype	Application	Catalogue number	Conjugation	IgG Concentration ($\mu g.mL^{-1}$)	Dilution
Anti-human Ki67	Novocastra	Mouse	Monoclonal	MM1	IgG_1	Tissue IHC	NCL-L-KI67		0.56	1/100
						Cell IF			0.14	1/400
Anti-human macrophage	AbD Serotec	Mouse	Monoclonal	MAC387	IgG_1	Tissue IHC/IF	MCA874G		10	1/100
Anti-human PPARγ	Santa Cruz	Mouse	Monoclonal	E-8	IgG_1	IB	SC-7273		0.4	1/500
						Tissue IHC/IF			0.05	1/4000
	GSK	Mouse	Monoclonal			Cell IF	Gift			1/400
Anti-human αSMA	Sigma-Aldrich	Mouse	Monoclonal	1A4	IgG_2a	Tissue IHC/IF	A2547		Ascites fluid	1/4000
Anti-porcine CD107a	AbD Serotec	Mouse	Monoclonal	4E9/11	IgG_1	Tissue IHC/IF	MCA2315		5	1/200

Antibody	Supplier	Host	Type	Clone	Isotype	Application	Catalogue number	Conjugation	Ig Concentration ($\mu g.mL^{-1}$)	Dilution
Anti-mouse IgG	Molecular Probes	Goat	Polyclonal			Tissue/Cell IF	A11001	Alexa Fluor® 488	4	1/500
							A11005	Alexa Fluor® 594	2.9	1/700
Anti-rabbit IgG	Molecular Probes	Goat	Polyclonal			Tissue/Cell IF	A11008	Alexa Fluor® 488	4	1/500
							A11012	Alexa Fluor® 594	5	1/400
Anti-mouse IgG	Dako	Rabbit	Polyclonal			Tissue IHC	E0354	Biotin	6.5	1/200
Anti-rabbit IgG	Dako	Goat	Polyclonal			Tissue IHC	E0432	Biotin	1.27	1/600
Anti-mouse IgG	Molecular Probes	Goat	Polyclonal			IB	A21057	Alexa Fluor® 680	0.2	1/10000
Anti-rabbit IgG	Rockland	Goat	Polyclonal			IB	611-132-122	IRDye® 800	ND	1/10000

2.8.2 Flow cytometry

Flow cytometry allows analysis of a large population of cells by hydrodynamically focusing the cells into a single stream and passing a beam of laser light across the path of the stream, scattering the light. Detection of the scattered light allows profiling of the size (forward scatter) and complexity, such as granularity (side scatter). Application fluorochromes and different light detectors allow deeper analysis of immunolabelled cells based on their fluorescent profile.

2.8.2.1 Preparation of whole blood for flow cytometry

Whole human blood (200μL) was added to a flow cytometry tube. To this, 1.8mL of 1x FACS lysing solution (BD Biosciences) in dH_2O was added and mixed by vortex. The blood and FACS lysing solution was incubated for 30 minutes at ambient temperature. Following incubation, the samples were further diluted by adding 1mL of PBS containing 1% (v/v) heat inactivated FBS and 0.1% (v/v) sodium azide (NaN_3); referred to a 'FACS wash buffer'. The samples were mixed by vortex and centrifuged at 306g for five minutes at 4°C. The supernatant was discarded and the cells resuspended in 1mL FACS wash buffer. The cell suspension was centrifuged at 306g for five minutes at 4°C. The supernatant was discarded and the cells resuspended in 500μL of 1% (v/v) formalin in PBS and the cells mixed by vortex. The cells were then incubated at 4°C overnight.

2.8.2.2 Preparation of PBMC for flow cytometry

Isolated PBMC (described in Section 2.5.1.2) were resuspended in an appropriate volume of ice cold PBS. An aliquot of single PBMC suspension was diluted 1:10 (v/v) with 0.4% (w/v) Trypan blue solution and the cells counted on a haemocytometer as previously described and the cell suspension adjusted to $1x10^6$ cells.mL^{-1} in ice cold PBS. A volume of cell suspension was aliquoted into a flow cytometry tube as an unstained and unlabelled control. All cells were maintained on ice until use.

2.8.2.3 Preparation of adherent macrophages for flow cytometry

Medium was aspirated from the Petri dish and the cells washed twice with ice cold PBS. Ten millilitres of 1% (w/v) EDTA was added to the dish and incubated at 37°C for 10 minutes or until the cells had began to round up. The 1% (w/v) EDTA solution was exchanged for 5mL of ice cold PBS and the cells gently scraped with a sterile 25cm cell scraper (Sarstedt). The cell suspension was harvested to a sterile round-bottom centrifuge tube on ice. A further 5mL of ice cold PBS was added to the dish and any remaining cells gently scraped into the PBS. The cell suspension was combined and centrifuged at 306g for

five minutes at 4°C. The supernatant was discarded and the cells were resuspended in an appropriate volume of ice cold PBS and the number of cells enumerated using a ruled haemocytometer. The cell suspension was adjusted to $1x10^5$ cells.mL^{-1} in ice cold PBS. A volume of cell suspension was aliquoted into a flow cytometry tube as an unstained and unlabelled control. All cells were maintained on ice until use.

2.8.2.4 Staining of dead cells for flow cytometry

The cell suspension was incubated with an ultra violet (UV) LIVE/DEAD® Fixable Dead Cell Stain (Molecular Probes) at a final dilution of 1:1000 (v/v) for 30 minutes at ambient temperature before evenly distributing the stained cell suspension into separated flow cytometry tubes. All cell suspensions were centrifuged at 306g for five minutes at 4°C. The supernatant was discarded and the tubes tapped dry on paper towel. The cell pellets were agitated by flicking the tubes and resuspended in 1mL PBS containing 1% (v/v) heat inactivated FBS and 0.1% NaN_3. The cell suspensions were centrifuged and agitated by flicking as described above.

2.8.2.5 Surface labelling of cells for flow cytometry

Dilute cells in suspension were stained with the LIVE/DEAD® fixable dead cell stain as described in Section 2.8.2.4 before incubating with primary antibody or isotype control (Table 2-7), at a pre-determined concentration in tris buffered saline (TBS; Appendix I-II) in a total volume of 11µL. The cells were mixed by vortexing and protected from light before incubating for 30 minutes on ice on a rocking platform. FACS wash buffer (2mL) was added to each cell suspension before being centrifuged and resuspended by flicking as described above. Five hundred microlitres of 1% (v/v) formalin in PBS was added to each cell suspension and the cells mixed by vortexing. The cells were then incubated at 4°C over night.

2.8.2.6 Intracellular labelling of cells for flow cytometry

Fluorescent immunolabelling of intracellular antigens was performed using the Dako IntraStain kit (Dako). Dilute cells in suspension were stained with the LIVE/DEAD® fixable dead cell stain as described in Section 2.8.2.4. Intracellular antigens were immunolabelled according to the manufacturer's instructions. Briefly, extracellular antigens were labelled by incubating the cell suspensions with primary antibody or isotype control (Table 2-7), at a pre-determined concentration in TBS in a total volume of 11µL. The cells were mixed by vortexing and protected from light before incubating for 30 minutes on ice on a rocking platform. FACS wash buffer (2mL) was added to each flow cytometry tube and the cell

suspensions centrifuged and agitated by flicking as described. IntraStain Reagent A (fixative; 100μL) was added to each tube containing dilute cell suspension. The tubes were gently vortexed and incubated for 15 minutes at ambient temperature. FACS wash buffer (2mL) was added to each fixed cell suspension and the cells mixed by vortexing. The cell suspensions were centrifuged and agitated by flicking as described above. IntraStain Reagent B (permeabilisation fluid; 100μL) was added to each tube containing dilute cell suspension. Primary antibody or isotype control at a pre-determined concentration (Table 2-7), was added to the appropriate tube containing dilute cells and IntraStain Reagent B. The tubes were gently vortexed and protected from light before being incubated for 15 minutes at ambient temperature. The cells suspension was washed with 2mL of FACS wash buffer centrifuged and agitated by flicking the tubes as described above. Five hundred microlitres of 1% (v/v) formalin was added to each cell suspension, the cells were then incubated at 4°C over night.

2.8.2.7 Flow cytometry data collection and analysis

FACS wash buffer (500μL) was added to each fixed cell suspension and the cells mixed by vortexing. Forward scatter, side scatter and fluorescent events were detected on a three-laser CyAn flow cytometer (Dako). Data analysis was performed using the Dako Summit software package version 4.3.

2.8.3 Immunoblotting

Immunoblotting allows investigation of specific proteins by loading proteins, denatured using SDS, into a polyacrylamide gel and separating by mass through application of an electric current through the gel. The separated proteins can then be transferred onto a thermoplastic membrane by application of an electric current across the gel and membrane. The membrane is then probed for a specific protein of interest by immunodetection using commercially available antibodies.

2.8.3.1 Cell lysis

Harvested suspension or adherent cells were washed twice with ice cold PBS. The cells were then incubated on ice at a 45° angle for 5 minutes to ensure residual PBS ran off the cells and was removed. Cells were lysed by adding 50μL of 2% (w/v) SDS lysis buffer (Appendix I-V) containing 13mM Dithiothreitol (DTT) (Melford Laboratories or Sigma-Aldrich) and protease inhibitor cocktail (PIC) at a final dilution of 1:500 (Sigma-Aldrich; appendix I-V). Lysed cell pellets were transferred directly to 1.5mL microfuge tubes on ice. Adherent cells were scraped using a sterile 25cm cell scraper and collected into a 1.5mL

microfuge tube on ice. Cell lysates were sonicated (25 Watts (W)) on iced water for two ten second bursts with a ten second rest in between. The sonicated cell lysates were incubated on ice for 30 minutes before being centrifuged at 14,000 revolutions per minute (rpm) for 30 minutes at 4°C. The supernatants were removed and aliquoted into a 1.5mL microfuge tubes on ice. Cell lysates were stored at -20°C.

2.8.3.2 Coomassie protein assay

BSA standards were prepared from a stock of 2mg.mL^{-1} BSA (Thermo Fisher). BSA was diluted in dH_2O to 1000, 750, 500, 250, 125 and 25 μg.mL^{-1}. Cell lysates were diluted 1:12.5 by adding 2μL of cell lysate sample to 23μL of dH_2O. Two hundred microlitres of Coomassie Plus reagent (Thermo Fisher) at ambient temperature was added to 10μL of BSA standards and 10μL of dilute sample in duplicate in a 96 well plate (Corning). The absorbance was read on a Multiskan Ascent microplate reader (Thermo Electron Corporation) at 630 and 480 nanometer wavelengths and the protein concentration of each sample was interpolated from the BSA standard curve.

2.8.3.3 Sample preparation

Twenty microgram of protein from each sample was combined with lithium dodecyl sulfate (LDS) sample buffer (Life Technologies) at 1x concentration and reducing agent (Life Technologies) at 1x concentration. The preparations were made up to equal volumes with dH_2O and boiled at 70°C for 10 minutes. Where required, microsome preparations generated from whole human liver were used as a positive control for immunolabelling (BD Bioscience; catalogue number 452161).

2.8.3.4 Gel electrophoresis

One-dimensional SDS polyacrylamide gel electrophoresis (PAGE) was performed using the Life Technologies Novex system. Proteins of molecular weight between 200 and 14 kiloDaltons (kDa) were separated on a 4-12% (w/v) Bis-Tris NuPAGE® precast gel (Life Technologies). Proteins of molecular weight between 500 and 40 kDa were separated on a 3-8 % (w/v) Tris-Acetate NuPAGE® precast gel (Life Technologies). Gels were loaded into a gel tank and immersed in running buffer. The 4-12% (w/v) Bis-Tris NuPAGE® gels or 3-8% (w/v) Tris-acetate gels were run in 1x MOPS running buffer in dH_2O or 1x Tris-acetate running buffer in dH_2O respectively. Five microlitres of Precision Plus All Blue protein standard ladder (Bio-Rad) was added to well one of each gel. Each well was loaded with all of the protein sample preparation. Empty wells were loaded with 4xLDS sample buffer at a volume equal to that of the prepared samples. Antioxidant (Life Technologies; 200μL) was

added to the inner chamber of the gel tank. Bis-Tris NuPAGE® gels and Tris-acetate NuPAGE® gels were electrophoresed using a power pack set to 200 volts (V) and 150V respectively for one hour ensuring the dye front had migrated to the bottom of the gel.

2.8.3.5 Gel transfer

The gel was removed from the gel cassette and transferred onto a precut piece of filter paper soaked in transfer buffer (appendix I-V). A precut piece of Polyvinylidene fluoride (PVDF) Immobilon transfer membrane (Millipore), immersed in 100% methanol prior to pre-soaking in transfer buffer, was then placed onto the exposed gel face and covered with another piece of transfer buffer-soaked filter paper. The gel membrane sandwich was then placed on two blotting pads presoaked in transfer buffer, within the cathode core of the Novex blot module. Air bubbles were removed by rolling a Universal tube over the gel membrane sandwich. Further transfer buffer soaked blotting pads were added on top of the exposed filter paper ensuring they protruded from the top of the blot module cathode core by at least 0.5 cm. The blot module was sealed using the anode lid and sandwiched into a gel tank. The central chamber of the blot module was filled with transfer buffer and the outer chamber of the gel tank was filled with dH_2O. The proteins were transferred to the PVDF membrane using a power pack set to 25/30V for two hours on ice. The blot module was then disassembled and the PVDF membrane immersed in 'Western blot TBS' (Appendix I-V) in a dish.

2.8.3.6 Ponceau red staining of the PVDF membrane

The membrane was stained with 5-10mL of 1x Ponceau red stain (appendix I-V) in dH_2O for a few seconds to ensure the proteins had transferred correctly and the absence of any defects caused by trapped air bubbles. The Ponceau red stain was washed from the membrane with dH_2O.

2.8.3.7 Immunolabelling of the PVDF membrane

All work was performed at ambient temperature on a shaking platform unless otherwise stated. The membrane was blocked with 10mL of 50% (v/v) Odyssey blocking buffer (Li-Cor Biosciences) in Western blot TBS for one hour. The blocking buffer was removed and 5mL of primary antibody, diluted to a pre-titrated concentration (Table 2-7) in 50% (v/v) Odyssey blocking buffer in 0.1% (v/v) Tween® 20 in TBS (appendix I-V) was added. The membrane was incubated on a rocking table at 4°C overnight.

Following overnight incubation the primary antibody was removed and stored at 4°C. The membrane was washed for 4x5 minutes in 0.1% (v/v) Tween® 20 in TBS. Infrared (IR) secondary antibody (8mL; Molecular Probes) diluted to a predetermined concentration (Table 2-7) in 50% (v/v) Odyssey blocking buffer in 0.1% (v/v) Tween® 20 in TBS was added to the PVDF membrane. The PVDF membrane was protected from light from this point onwards. The PVDF membrane was incubated for one hour. Following incubation the secondary antibody was removed and the membrane washed for 4x5 minutes in 0.1% (v/v) Tween® 20 in TBS followed by a single wash in 'Western blot TBS' for five minutes to remove residual Tween® 20.

2.8.3.8 Scanning of the PVDF membrane

The membrane was positioned onto the scan surface of an Odyssey Infrared Imager 9120 (Li-Cor Biosciences) and air bubbles removed using a roller. Infrared fluorochromes were excited with a solid-state diode laser at 680 nanometer (nm) and a solid-state diode laser at 780nm. Fluorochrome emissons were detected with a silicon avalanche photodiode detector and acquired images of the scanned membrane were orientated, cropped and exported as JPEGS.

2.8.3.9 Stripping of the PVDF membrane

Where required, the PVDF membrane was stripped using a Western blot recycling kit (Autogen Bioclear). The stripper solution was diluted 1:10 in dH_2O and 1x stripper solution (8mL) added to the PVDF membrane for 15-30 minutes on a shaking platform at ambient temperature. Following incubation the stripper solution was discarded and the PVDF membrane was washed in Western blot TBS for five minutes on a shaking platform. The membrane was rescanned on the Odyssey Infrared imager to confirm the antibodies had been removed. The PVDF membrane was re-probed as described in Section 2.8.3.7.

2.8.4 Immunolabelling of tissue sections

Immunolabelling of tissue sections allows localisation and compartmentalisation of antigens within a tissue to be determined by application of antibodies against the protein of interest and amplification and detection of the signal using chromogenic or fluorescent probes.

2.8.4.1 Antigen retrieval

Due to cross-linking by formalin based fixatives some antigens become masked and require retrieval treatment prior to incubation with the primary antibody. Antigens in tissue fixed in 10% (v/v) formalin in PBSc were retrieved using one of three methodologies:

a) Trypsinisation

Tissue sections were incubated in 100mL 0.1% (w/v) trypsin from porcine pancreas (Sigma-Aldrich) in 0.1% (w/v) calcium chloride ($CaCl_2$) solution at pH 7.8 at 37°C for 10 minutes.

b) Microwaving

Tissue sections were place into a Pyrex® dish and glass marbles placed on either end of the slide. The tissue sections were then immersed in 350mL of either 10mM citric acid buffer at pH 6.0 or 1mM EDTA buffer at pH 8.0. The Pyrex® dish was covered in cling film and a number of holes punched into the film. The Pyrex® dish was then microwaved at 900 W for 13 minutes. Following microwaving the dish was set on ice and allowed to cool.

c) Trypsinisation and microwaving

Tissue were trypsinised in 100mL 0.1% (w/v) trypsin in 0.1% (w/v) $CaCl_2$ solution at pH 7.8 at 37°C for one minute. Following incubation the slides were washed under running tap water for one minute and placed into a Pyrex® dish. The tissue sections were boiled in 10mM citric acid buffer at pH 6.0 as described above and cooled on ice.

Following all antigen retrieval steps the tissue sections were washed under running tap water for one minute.

2.8.4.2 Immunoperoxidase labelling of tissue sections

All work was performed at ambient temperature unless otherwise stated. Tissue sections were dewaxed to water as described in Section 2.6.4.1. Endogenous peroxidase activity was blocked by immersing the tissue sections in 3% (v/v) H_2O_2 in dH_2O for 10 minutes in a Schieferdecker jar followed by washing under running tap water for 10 minutes. Sections cut from tissue that was fixed in 10% (v/v) formalin in PBSc required antigen retrieval using one of the methods described in section 2.8.4.1. Sections cut from tissue which had been fixed in zinc salt fixative could not be blocked for endogenous peroxidase activity using 3% (v/v) H_2O_2. Zinc salt fixed tissue sections did not require antigen retrieval. Tissue sections on slides were immersed in TBS and placed onto a Shandon Sequenza (Thermo Scientific)

coverplate. The coverplate and slide was placed into a Shandon sequenza unit and TBS run over the slide to ensure an adequate seal was created. The slides were blocked with avidin (100µL per slide; Vector Laboratories) for 10 minutes followed by washing the slides twice with TBS. The slides were then blocked with biotin (100µL per slide; Vector Laboratories) for 10 minutes followed by washing twice with TBS. Each slide was then blocked with 10% (v/v) serum (Dako) obtained from the host species of the secondary anti-IgG antibody for five minutes. Primary antibody (100µL), diluted to a pre-titrated concentration (Table 2-7) in TBS was added to the relevant slide. The Shandon sequenza unit was incubated at 4°C overnight.

The primary antibody was removed by washing the slides thrice with TBS and 100µL/slide of pre-titred biotinylated anti-IgG secondary antibody (Table 2-7) added for 30 minutes. Secondary antibodies applied to sections of porcine tissue were made up in 10% (v/v) swine serum in TBS. Streptavidin-Horseradish peroxidase (HRP) (Vector Laboratories) was prepared according to the manufacturer's instructions in TBS 30 minutes before use. The biotinylated secondary antibody was removed by washing the slides thrice with TBS and 100µL/slide of pre-prepared Streptavidin-HRP was added to each slide for 30 minutes. SigmaFAST Diaminobenzidine (DAB) tablets (Sigma-Aldrich) were prepared according to the manufacturer's instructions in dH_2O. The slides were washed twice with TBS and once with dH_2O before adding 200µL/slide soluble DAB reagent for 12 minutes. The tissue sections were washed a further two times with dH_2O before counterstaining in Mayer's Haematoxylin. The tissue sections were then dehydrated from water through graded ethanol to xylene and mounted in DPX as described in Section 2.6.4.1.

2.8.4.3 Alkaline phosphatase immunohistochemistry

Endogenous peroxidase activity cannot be quenched with 3% (v/v) H_2O_2 in dH_2O in tissue sections cut from tissue which had been fixed with zinc salt fixative. In order to combat this, alkaline phosphatase was used as the enzyme which catalyses a substrate to form an insoluble precipitate for detection instead of Horseradish peroxidase. Tissue sections were dewaxed to water as described in Section 2.6.4.1. The immunoperoxidase labelling of tissue sections protocol was followed as outlined in Section 2.8.4.2. Following the addition of pre-titred biotinylated anti-IgG secondary antibody added for 30 minutes, the streptavidin-alkaline phosphatase (AP) (Vector Laboratories) was prepared according to the manufacturer's instructions in TBS. The biotinylated secondary antibody was removed by washing the slides thrice with TBS and 100µL/slide of pre-prepared Streptavidin-AP was

added to each slide for 30 minutes. The alkaline phosphatase substrate (Vector Laboratories) was prepared according to the manufacturer's instructions in alkaline phosphatase TBS (Appendix I-VI). The slides were washed twice with TBS and once with alkaline phosphatase TBS before adding 200µL/slide the pre-prepared alkaline phosphatase substrate for 20 minutes. The slides were washed a further two times with dH_2O before counterstaining in Mayer's Haematoxylin. The tissue sections were then dehydrated and mounted following the immunoperoxidase labelling of tissue sections protocol outlined in Section 2.8.4.2.

2.8.4.4 Immunoperoxidase labelling using the catalysed signal amplification (CSA) kit

All work was performed at ambient temperature unless otherwise stated. The tissue sections on slides were dewaxed, rehydrated to water, 3% (v/v) H_2O_2 blocked and antigen retrieved as described in Sections 2.8.4.1 and 2.4.8.2. Tissue sections on slides were immersed in 0.1% (w/v) Tween® in TBS (TBST; appendix I-VII) and placed onto a Shandon Sequenza (Thermo Scientific) coverplate. The coverplate and slide was placed into a Shandon sequenza unit and TBST run over the slide to ensure an adequate seal was created. The slides were blocked with avidin (100µL per slide) for 10 minutes followed by washing the slides twice with TBST and blocking with biotin (100µL per slide) for 10 minutes. The slides were washed twice with TBST before 100µL of serum free protein block (Dako) was applied to each slide for five minutes. Primary antibody (100µL), diluted to a pre-titrated concentration (Table 2-7) in antibody dilution buffer (Dako) was then applied to the relevant slides for 15 minutes. Streptavidin-biotin complex (Dako) was prepared according to the manufacturer's instructions 30 minutes before use. The slides were washed thrice with TBST before 100µL rabbit anti-mouse biotinylated link antibody (Dako) was added to each slide for 15 minutes. The slides were washed thrice with TBST and 100µL pre-prepared streptavidin-biotin complex was added to each slide for 15 minutes. The slides were washed three times with TBST and 100µL amplification reagent (Dako) was added to each slide for 15 minutes. The slides were washed as described previously and 100µL streptavidin-HRP (Dako) was added to each slide for 15 minutes. SigmaFAST DAB tablets were prepared according to the manufacturer's instructions in dH_2O. The slides were washed thrice with TBST before adding 100µL per slide soluble DAB reagent for 5 minutes. The tissue sections were washed twice with dH_2O before counterstaining in Mayer's Haematoxylin, dehydrating and mounting in DPX as described in Section 2.8.4.2.

2.8.4.5 Indirect immunofluorescent labelling of tissue sections

All work was performed at ambient temperature on a shaking platform unless otherwise stated. Tissue sections were dewaxed to water as described in Section 2.6.4.1 and where required, antigens retrieved as described in Section 2.8.4.2. The tissue sections were incubated with 0.25% (v/v) PBS Tween® 20 for 15 minutes and the slides tapped dry on paper towel. The tissue was drawn around with a grease pen (Dako) and 100µL of 10% (v/v) of serum obtained from the host species of the secondary anti-IgG antibody was applied for one hour. The slides were washed for 10 minutes with TBS and 100µL primary antibody, diluted to a pre-titred concentration (Table 2-7) in TBS was added to the relevant tissue section. The slides were incubated at 4°C overnight in a humidified environment. Following incubation the slides were washed for 4x10 minutes in TBS. Fluorescent-conjugated anti-IgG secondary antibody (Molecular Probes) (100µL) diluted to a pre-titred concentration (Table 2-7) in TBS containing 0.1% (w/v) BSA and 0.1% (v/v) NaN_3 was added to the relevant tissue section. The slides were protected from light and incubated for one hour. The tissue sections were washed for 3x10 minutes in TBS and 5mL of Hoechst 33258 at 0.1µg.mL^{-1} was added to each slide for 10 minutes. The tissue sections were then washed 3x10 minutes in TBS and mounted in IF anti-fade mountant. Coverslips (22x50mm number 1.5; Scientific Laboratory Supplies) were applied to the IF anti-fade mountant and the slides sealed with clear nail varnish. The slides were protected from light and kept at 4°C.

2.8.5 Immunolabelling of cells

All work was performed at ambient temperature on a shaking platform unless otherwise stated. Methanol:acetone fixed cells on multiwell slides were thawed and incubated with 0.25% (v/v) PBS Tween® 20 for 15 minutes. The slides were tapped dry on paper towel and the wells drawn around with a grease pen. Thirty microlitres of 10% (v/v) of serum obtained from the host species of the secondary anti-IgG antibody was applied to each well for one hour. The slides were washed for 10 minutes with TBS and 30µL primary antibody, diluted to a pre-titred concentration (Table 2-7) in TBS was added to the relevant well. The slides were incubated at 4°C overnight in a humidified environment. Following incubation the slides were washed quickly four times with TBS followed by washing 4x10 minutes in TBS. Fluorescent-conjugated anti-IgG secondary antibody (30µL) diluted to a pre-titred concentration (Table 2-7) in TBS containing 0.1% (w/v) BSA and 0.1% (v/v) NaN_3 was added to the relevant well. The remaining procedure followed was as described in Section 2.8.4.5. Coverslips (22x64mm number 1.5; Scientific Laboratory Supplies) were applied to the IF

anti-fade mountant and the slides sealed with clear nail varnish. The slides were protected from light and kept at 4°C.

2.9 Microscopy

2.9.1 Brightfield imaging

Stained or peroxidase immunolabelled tissue sections on glass slides were viewed on an Olympus BX60 microscope. Images were captured with an Olympus DP50 Camera using Image Pro Plus software (version 4.5.1.29).

2.9.2 Fluorescent imaging

Fluorescent imunolabelling of tissue sections and cells on glass slides was visualised by exciting the fluorescent probes using a single light source from a mercury lamp and burner (Olympus) connected to an Olympus BX60 microscope. A three-colour filter wheel was rotated to change the emission wavelength of the light source in order to excite the different fluorchromes. Images were captured using an Olympus DP50 Camera with Image Pro Plus software (version 4.5.1.29). Colour channels merged using the Image Pro Plus software or ImageJ software (National Institute for Health).

2.10 Statistical analysis

All statistical analysis was performed using InStat® version 3.05 statistical software (GraphPad). Mann-Whitney U tests were performed to test if there was a statistical significance between data sets with a small sample size or with an uneven number of replicates. Data sets in which any observed difference in values had a probability of less than five percent ($P<0.05$) that the difference was a result of chance were consider significant.

3.0 Method development and characterisation

3.1 Chapter rationale and aim

This chapter provides details and characterisation of the materials, antibodies and methods of analysis used throughout the study. The validation of reagents and analysis methods provides greater confidence in the specificity of any future observations made and consequently, conclusions drawn from the data.

The aim of this chapter was to develop and characterise the tools required to investigate the human tissue and cellular response to a porcine-derived decellularised biomaterial.

3.2 Chapter objectives

Specific objectives of this chapter were to:

a) Confirm the decellularised porcine bladder biological scaffolds were devoid of cellular components and nuclear material and that the matrices were non-cytotoxic to primary human stromal cells.
b) Validate a panel of antibodies and stains for use in histological and cytometric analysis.
c) Define flow cytometric gating strategies to characterise and interrogate human peripheral blood-derived cells.

3.3 Experimental approach

3.3.1 Analysis of the porcine bladder biological scaffold

Confirmation of successful decellularisation of the porcine bladder was achieved using histological staining for DNA using Hoechst 33258. Haematoxylin and eosin staining was used to confirm removal of cellular components and maintenance of the porcine bladder matrix architecture. Human urinary tract stromal cells were cultured in the presence of a biopsy of the porcine bladder biological scaffold to determine if the material showed signs of cytotoxicity by impeding the survival of the human cells when compared to a positive control of known cytotoxicity.

3.3.2 Development of a panel of antibodies against function markers

In order to determine the response of tissue and cells when challenged with porcine bladder biological scaffold a panel of functional markers was identified. Commercially available candidate antibodies raised against the functional markers were initially selected based on the datasheets describing their characterised applications and, where appropriate, cross-reactivity between different species. To determine the optimum primary antibody concentration for tissue labelling, primary antibodies were titrated against control tissues known to express the antigen of interest. Formalin-fixed, paraffin wax-embedded control tissue sections were either microwaved in citric acid buffer or enzymatically digested using trypsin in order to expose antigens masked by cross-linking as a result of formaldehyde fixation. Primary antibodies were then titrated over a range of concentrations on multiple sections of the control tissues. Zinc-fixed, paraffin wax embedded control tissue did not require antigen retrieval therefore the range of primary antibody concentrations were applied directly to the dewaxed tissue sections. The optimum concentration of the primary antibody for use by immunohistochemical or fluorescent immunolabelling of tissue sections was determined by brightfield and epi-fluorescent microscopy respectively. Isotype control antibodies, matched to the immunoglobulin of the primary antibody, were performed for all immunolabelling experiments as a negative control of tissue labelling. The optimum concentration of the primary antibody for tissue labelling was defined as the antibody concentration which produced a strong signal-to-noise ratio and which was restricted to areas of the control tissue where the antigen expression was reported. For weak labelling or labelling which required a high antibody concentration to obtain a signal by standard immunohistochemistry techniques, the CSA kit was used to amplify the signal.

To determine the optimum primary antibody concentration for labelling of cells, primary antibodies were titrated against cytospun preparations of PBMC and primary antibody labelling was detected by a fluorescent secondary antibody. The optimum concentration of the primary antibody for labelling of cells was defined as the antibody concentration that produced a strong signal-to-noise ratio and was restricted to populations of cells within a heterogeneous cell preparation. It is important to note that the optimum antibody concentration for tissue or cell labelling was not defined as the lowest primary antibody concentration at which a signal was detected, as an excess of primary antibody was still required in order to detect changes in antigen expression. Positive control cells and isotype controls, matched to the immunoglobulin of the primary antibody, were included as part of

every immunolabelling experiment. Fluorescent immunolabelling of mononuclear phagocyte (adherent) and T cell (non-adherent) associated markers was used to characterise selective adherence as the method for isolating peripheral blood monocytes.

3.3.3 Characterisation of a flow cytometric analysis

Flow cytometric analysis was used to analyse larger populations of human PBMC, compared to immunofluorescent microscopy, in order to determine initial expression of selected markers and interrogate any changes in the expression of these markers upon differentiation of human peripheral blood monocytes to macrophages. Gating strategies used to analyse peripheral blood-derived monocytes and macrophages were established using the forward scatter and side scatter profile of the cells. Cells with a compromised membrane, which may result in non-specific uptake of antibody leading to a false positive for immunolabelling, were removed from analysis using a LIVE/DEAD cell fluorescent stain. The peripheral blood monocyte population was then confirmed by direct fluorescent immunolabelling of the PBMC with the fluorochrome-conjugated antibodies; anti-CD11b conjugated with APC, anti-CD14 conjugated with PE or anti-CD68 conjugated with APC. The monocyte-derived macrophage population was confirmed using an anti-CD11b antibody conjugated with APC.

3.4 Results: Characterisation of the porcine bladder tissue decellularisation process

3.4.1 Confirmation of porcine bladder tissue decellularisation

Porcine bladder tissue was decellularised using the method described by Bolland et al (Bolland et al., 2007). To confirm that the decellularisation process removed the cellular and nuclear material from the tissue, histological sections were cut from representative samples taken from the bladder dome and walls of each batch of biomaterial produced. Brightfield microscopy of sections of porcine bladder biological scaffold, also referred to as the porcine bladder matrix, stained with H&E determined that cellular components of the porcine bladder tissue had been removed in three different anatomical areas of the porcine bladder and that only the extracellular matrix remained (Figure 3-1). Fluorescent microscopy of sections of porcine bladder matrix stained with Hoechst 33258 (H33258) confirmed that the nuclear material had been removed from the decellularised porcine bladder matrix when compared to the porcine bladder tissue stained with H33258 (Figure 3-1).

Results confirming the decellularisation of batches of porcine bladder biological scaffold used in this study are shown in appendices II-I to II-III.

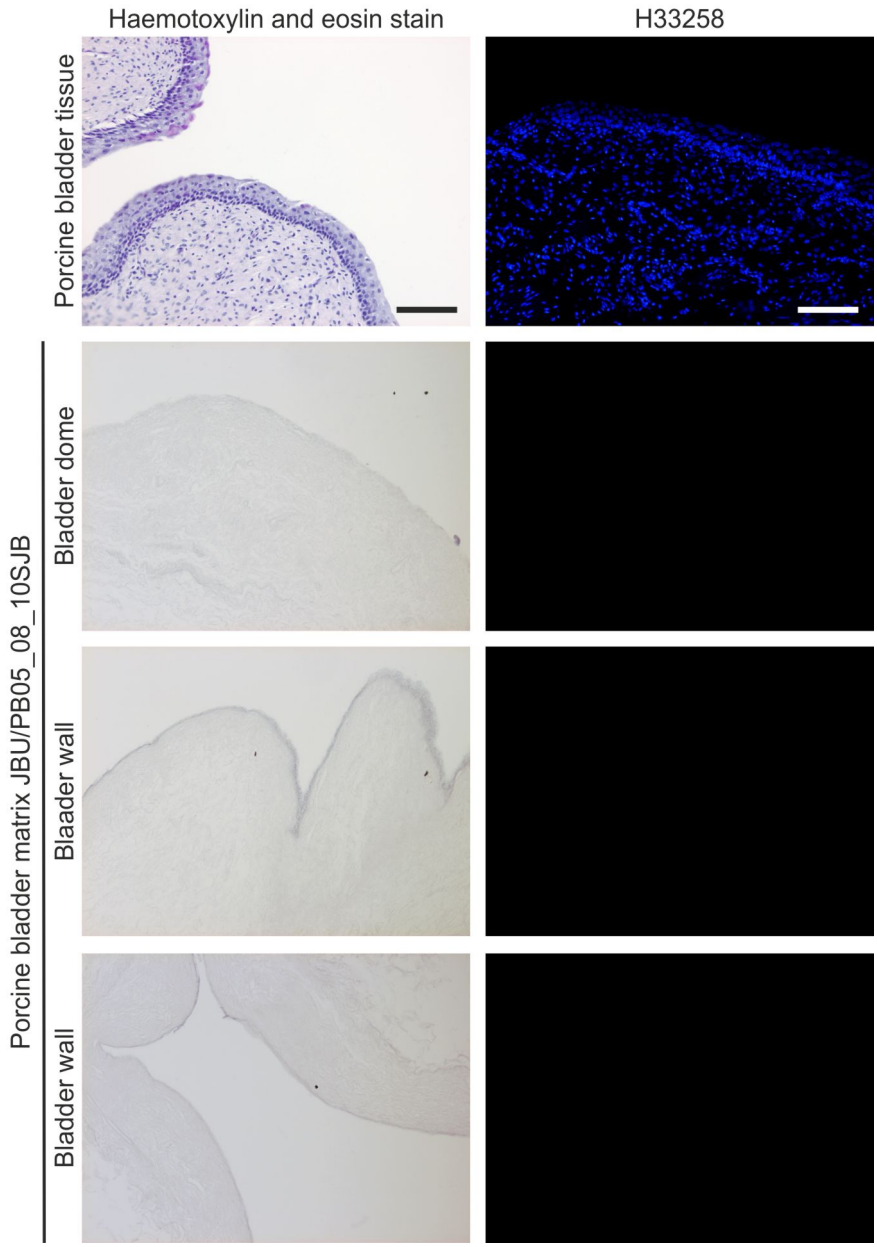

Figure 3-1. Confirmation of porcine bladder decellularisation of batch JBU/PB05_08_10SJB using H&E and H33258 staining. Following the decellularisation process, biopsies of the porcine bladder matrix from three anatomical areas of the bladder were processed into paraffin-wax and sections either stained with H&E or H33258 followed by visualisation with brightfield or fluorescent microscopy respectively. Camera exposures for fluorescent images were set using the porcine bladder tissue stained with H33258. Scale bars represent 100 microns.

3.4.2 Biocompatibility of porcine bladder biological scaffold

To determine if the decellularised porcine bladder tissue displayed any cytotoxic effects on cell cultures, human urinary tract stromal cells were cultured with biopsies of the porcine bladder matrix. Human urinary tract stromal cells were not observed growing up to and in contact with the porcine bladder matrix immersed in 10% (w/v) SDS in dH_2O overnight at ambient temperature, used as a positive control for cell cytotoxicity (Figure 3-2). Cells were observed growing up to and in contact with both the negative control (Steri-strip™ anchor only) and the decellularised porcine bladder matrix indicating that neither material was cytotoxic to human urinary tract stromal cells (Figure 3-2). Results of biocompatibility assays performed on other batches of porcine bladder matrix are shown in appendix II-IV.

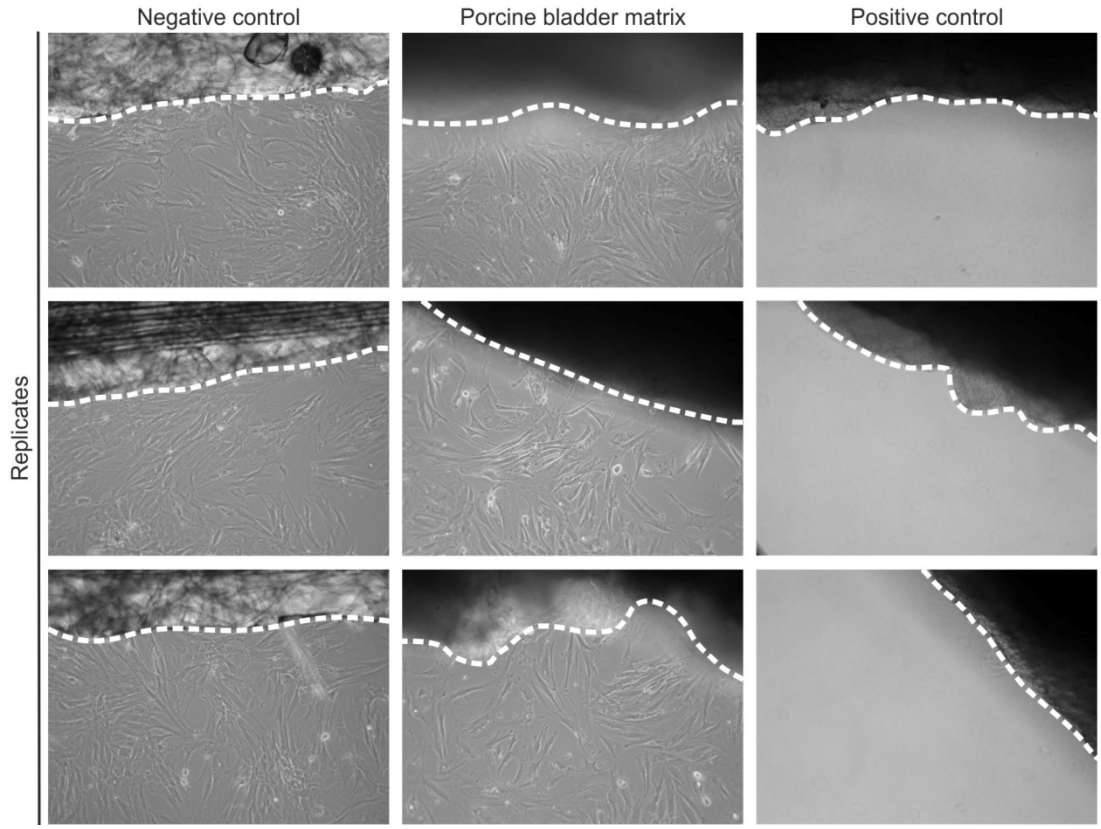

Figure 3-2. Phase contrast images of the contact cytotoxicity assay of porcine bladder matrix batch JBU/PB05_08_10SJB. Dotted line represents the interface between the Steri-strip™, native porcine bladder matrix or the SDS (10% w/v) pre-treated porcine bladder matrix. Human urinary tract stromal cells were cultured for 48 hours before phase contrast images were captured. Images from three intra-assay replicates are shown.

A complete list of porcine bladder biological scaffold generated and used throughout the study can be found in Table 3-1.

Table 3-1. Characterisation performed on batches of porcine bladder biological scaffold

Batches	Confirmation of decellularisation	
	H&E	Contact cytotoxicity
JBU/PB21_05_09SJB	✓	
JBU/PB14_10_09SJB	✓	
JBU/PB05_08_10SJB	✓	✓
JBU/PB02_10_10SJB	✓	✓

3.5 Results: Characterisation of a panel of tissue markers.

The panel of functional markers identified for use in the study and their reported cell association are summarised in Table 3-2.

All images shown represent the immunolabelling at the selected optimum antibody concentration; outlined in chapter 2, table 2-7. All antibodies characterised showed the correct localisation as reported on the antibody datasheets or within the literature. Representative images of isotype controls of tissue labelling using either immunofluorescence or immunohistochemical detection methods can be found in appendices II-V and II-VI respectively.

Table 3-2. Panel of functional markers and reported cell association

Antigen	Reported cell association
Arginase 1	Expressed by liver hepatocytes. Up-regulated by the anti-inflammatory cytokine, IL-4 in murine macrophages but not in human macrophages.
CD11b	Integrin-αM - Pan-macrophage and neutrophil marker.
CD14	Variable expression by different monocyte subsets.
CD3	T cell specific marker.
CD34	Haematopoietic progenitor cells and vascular endothelial cells.
CD36	Scavenger receptor of fatty acids and lipoproteins. Expressed on macrophages.
CD68	Member of the lysosome associated membrane protein (LAMP) family. Pan-macrophage marker.
CD80	Macrophage co-stimulatory molecule. Associated with inflammatory macrophages.
CD117	c-Kit – identifies stem cells and mast cells.
CD163	Haptoglobin:haemoglobin scavenger receptor. Associated with anti-inflammatory macrophages.
Glucocorticoid receptor	Nuclear receptor for anti-inflammatory glucocorticoids.
HLA-DR	MHC class II is expressed by antigen presenting cells and up-regulated by the pro-inflammatory cytokine IFNγ and the anti-inflammatory cytokine, IL-4.
Ki67	Identifies cells undergoing active cell cycle progression.
MAC387	Pan-macrophage marker.
PPARγ	Nuclear receptor for fatty acid metabolites.
Smooth muscle actin (αSMA)	Smooth muscle stromal cells and myofibroblasts.
CD107a	Member of the LAMP family. Pan-macrophage marker.

3.5.1 Porcine tissue

Spleen tissue was chosen to titrate the selected series of antibodies against macrophage-associated markers. The antibody specific to the porcine marker, CD107a was characterised on zinc-fixed, paraffin-embedded porcine splenic tissue using the alkaline phosphatase detection method.

The antibody raised against porcine CD107a reacted with the majority of cells in the porcine spleen (Figure 3-3). Some cells expressed CD107a more intensely than others (Figure 3-3 - arrows).

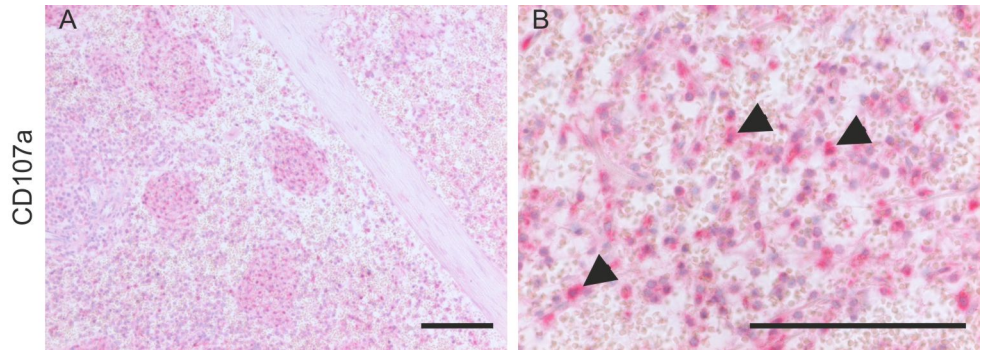

Figure 3-3. Alkaline phosphatase immunohistochemical detection of porcine CD107a+ cells in the porcine spleen. Image B is a higher magnification image of area in image A. Arrows indicate cells that label intensely positive for CD107a expression. Scale bars represent 100 microns.

3.5.2 Human tissue

Antibodies against human functional markers were characterised using a panel of formalin-fixed, paraffin wax-embedded control tissues known to express the antigen of interest. Antibodies were optimised for both concentration and antigen retrieval method using a combination of fluorescence and peroxidase detection methods.

3.5.2.1 Labelling of antigens using immunofluorescence on a panel of human tissues

Antigens were detected using indirect immunofluorescent labelling of tissues. Camera exposures were adjusted ensuring a representative image of the immunofluorescent labelling was captured. For comparisons between treatments exposures were set using

immunolabelling of controls. H33258 staining was used to detect cell nuclei while the Alexa fluorochrome shows indirect antibody labelling of the antigen. Images were merged to produce a colour composite image of nuclear staining (blue) and fluorescent labelling (green/red).

Splenic tissue

Indirect Immunofluorescence detection of antigens in human spleen localised CD36 (Figure 3-4), CD163 (Figure 3-5) and MAC387 (Figure 3-6) in the red pulp zone. Immunofluorescent labelling of CD68 (Figure 3-7) showed intense labelling of marginal zone macrophages in the spleen and weaker immunolabelling in the red pulp zone of the spleen. Immunofluorescent labelling of HLA-DR showed intense expression by marginal zone macrophages in the spleen (Figure 3-8).

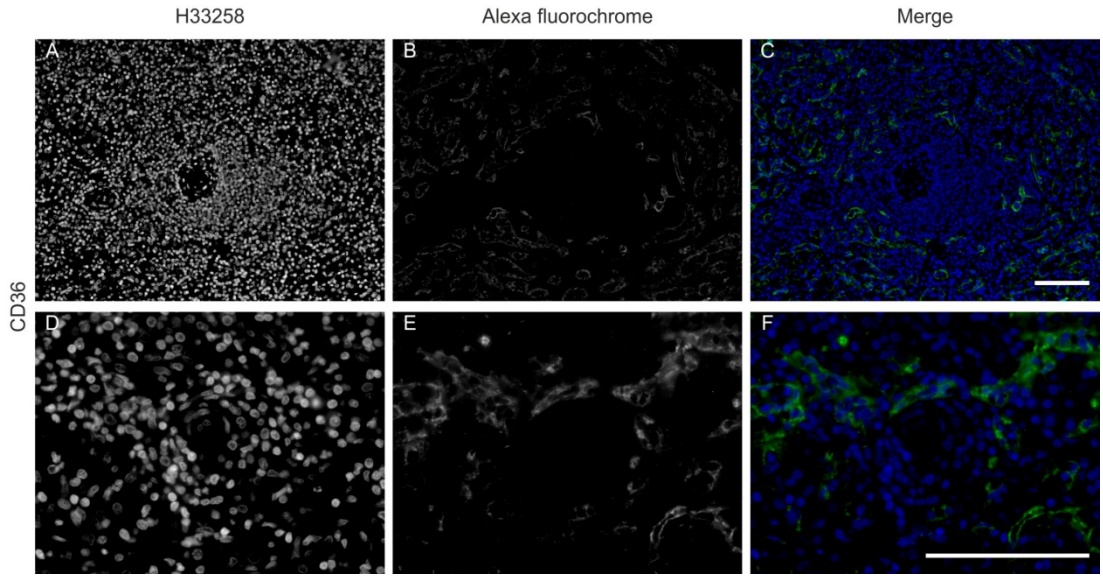

Figure 3-4. Fluorescent immunolabelling of human CD36+ cells in human splenic tissue. H33258 32-bit images (A and D) were combined with Alexa fluorochrome 32-bit images (B and E) to produce merged micrographs. Image F is a higher magnification image of area in image C. Scale bars represent 100 microns.

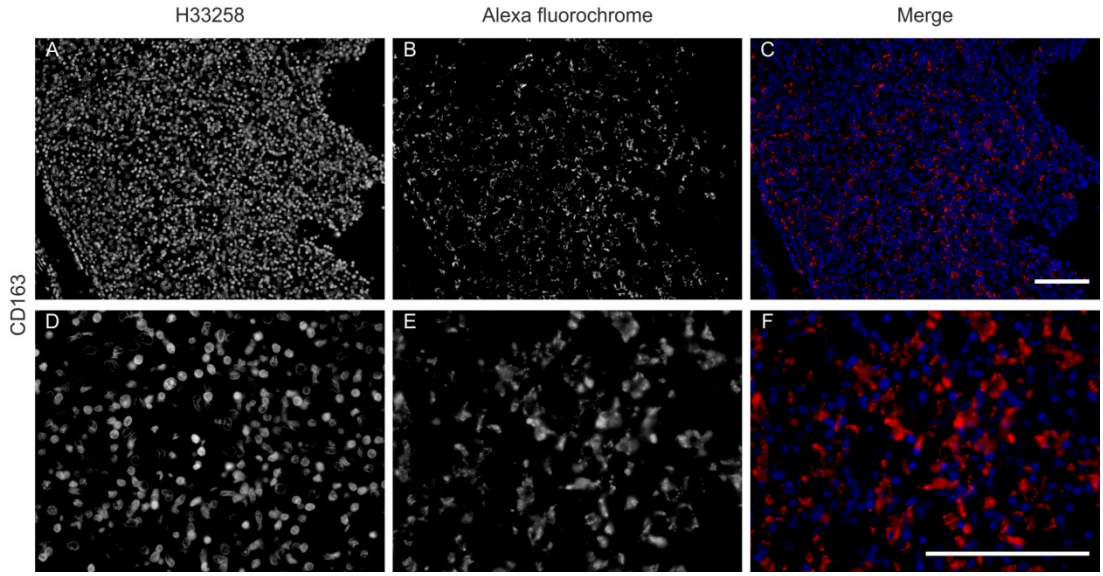

Figure 3-5. Fluorescent immunolabelling of human CD163+ cells in human splenic tissue. H33258 32-bit images (A and D) were combined with Alexa fluorochrome 32-bit images (B and E) to produce merged micrographs. Image F is a higher magnification image of area in image C. Scale bars represent 100 microns.

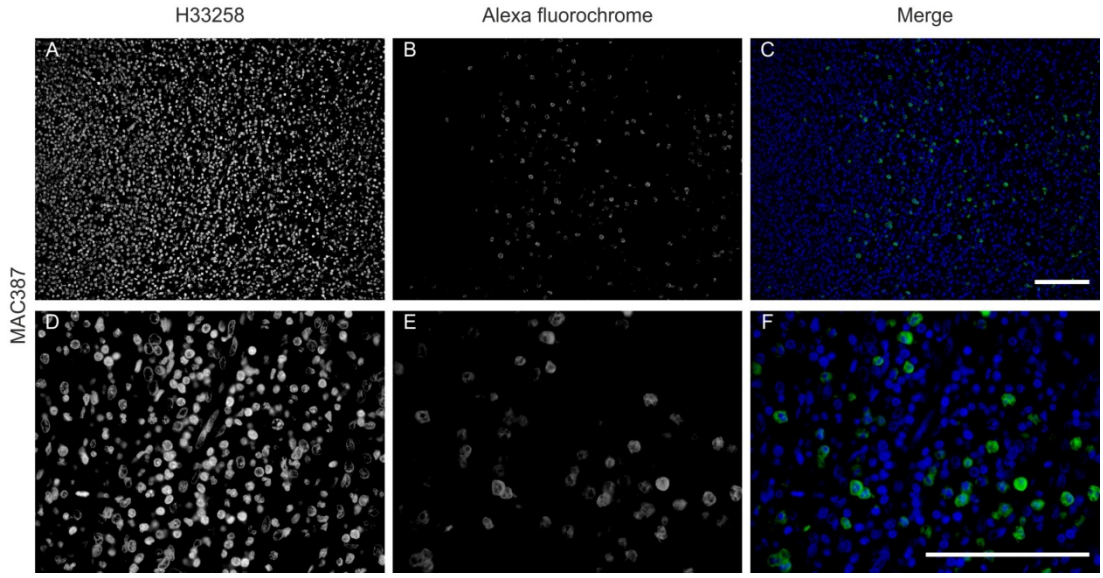

Figure 3-6. Fluorescent immunolabelling using the antibody, MAC387 on human splenic tissue. Alexa fluorochrome shows indirect antibody labelling of antigen. 32-bit images (A and B, D and E) were merged to produce a colour composite image of nuclear staining (blue) and fluorescent labelling (green). Scale bars represent 100 microns.

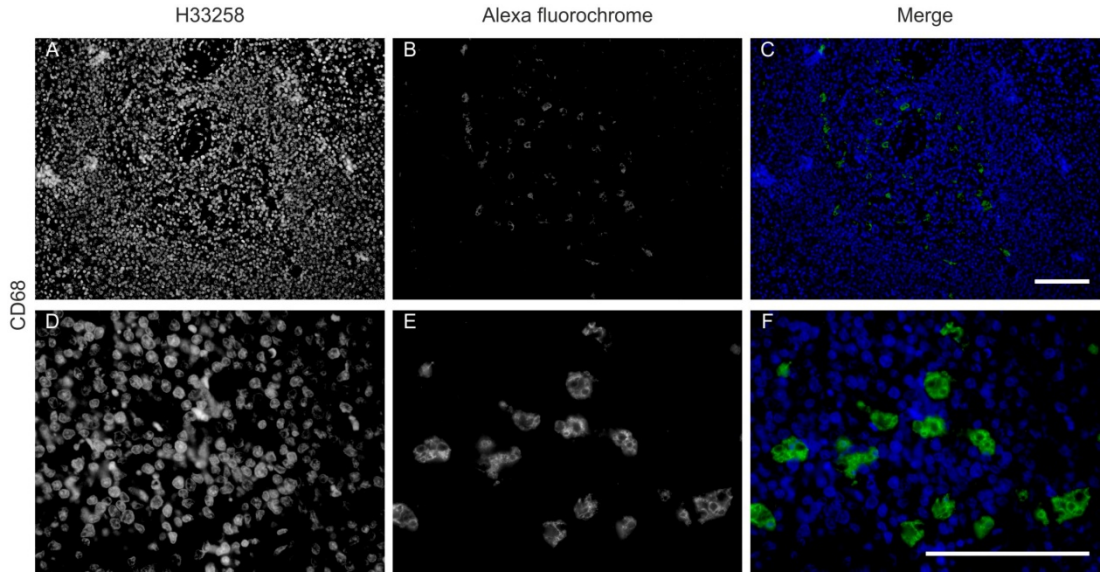

Figure 3-7. Fluorescent immunolabelling of human CD68+ cells in human splenic tissue. H33258 32-bit images (A and D) were combined with Alexa fluorochrome 32-bit images (B and E) to produce merged micrographs. Image F is a higher magnification image of area in image C. Scale bars represent 100 microns.

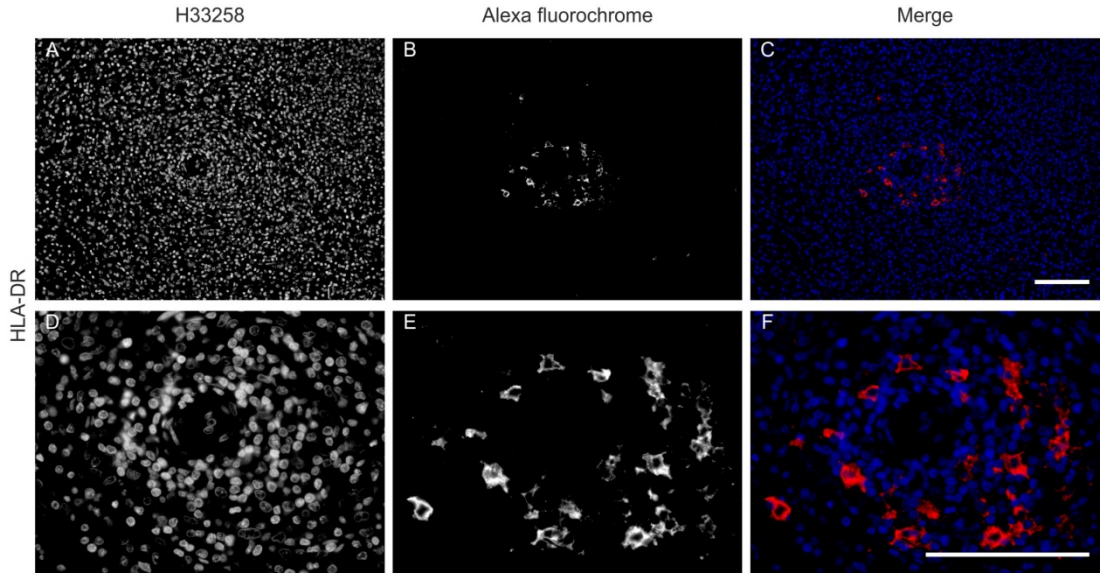

Figure 3-8. Fluorescent immunolabelling of HLA-DR+ cells in human splenic tissue. H33258 32-bit images (A and D) were combined with Alexa fluorochrome 32-bit images (B and E) to produce merged micrographs. Image F is a higher magnification image of area in image C. Scale bars represent 100 microns.

Other tissues

Human arginase 1 was detected in human liver hepatocytes (Figure 3-9). Immunolabelling of CD117 expression in freshly isolated normal human ureter showed a small population of CD117+ cells was present in the epithelial lining of human ureter (Figure 3-10).

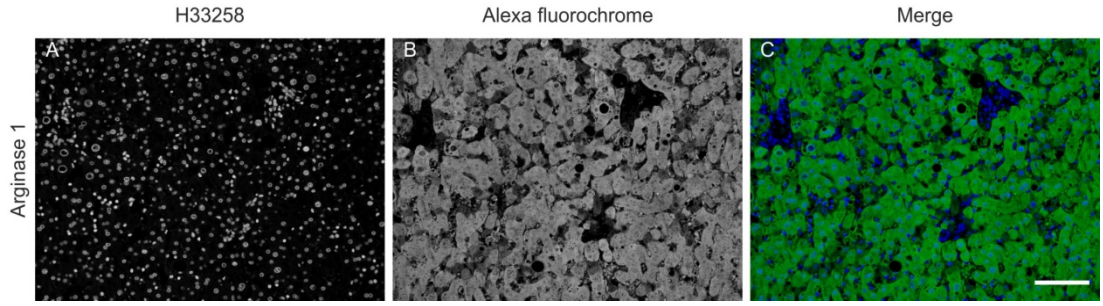

Figure 3-9. Fluorescent immunolabelling of human arginase 1+ cells in human liver tissue. H33258 32-bit image (A) was combined with Alexa fluorochrome 32-bit image (B) to produce merged micrograph (C). Scale bars represent 100 microns.

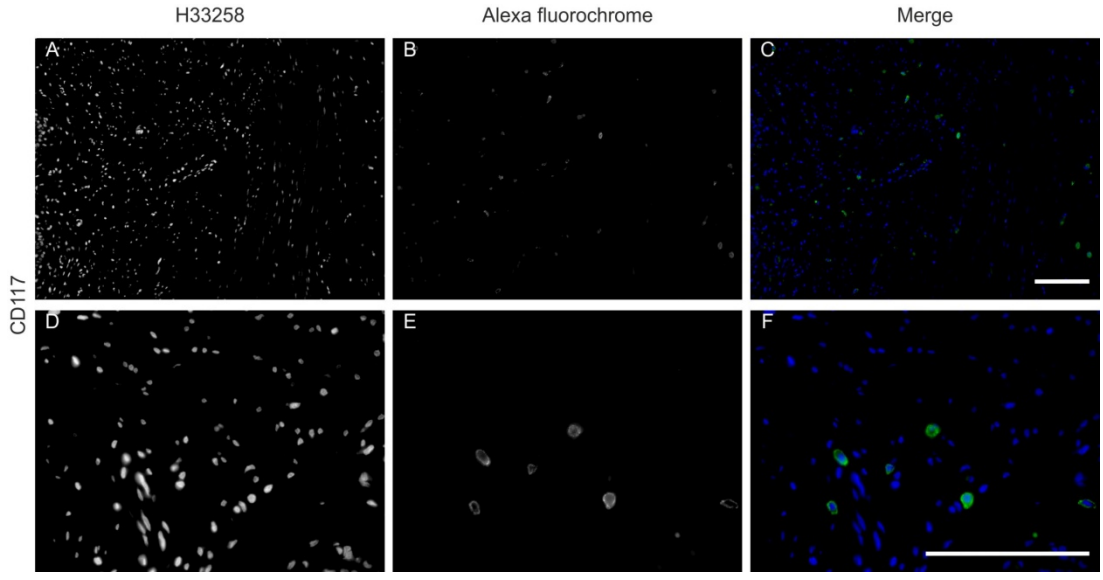

Figure 3-10. Fluorescent immunolabelling of human CD117+ cells in normal human ureter. H33258 32-bit images (A and D) were combined with Alexa fluorochrome 32-bit images (B and E) to produce merged micrographs. Image F is a higher magnification image of area in image C. Scale bars represent 100 microns.

3.5.2.2 Labelling of multiple antigens using immunofluorescence on a panel of human tissues

Multiple tissue antigens were detected using indirect immunofluorescent labelling of tissues. Dual labelling was achieved by combining primary antibodies against different antigens, which were raised in different species. These primary antibodies were then detected using fluorochrome-conjugated antibodies raised in a single species against the immunoglobulin type of the primary antibodies. Camera exposures were adjusted for each colour channel ensuring the optimal and most representative image of the immunofluorescent labelling was captured.

CD163+ cells were identified within the liver, however, CD163 expression and arginase 1 expression did not co-localise (Figure 3-11). CD163 expression in the human spleen also did not co-localise with CD36 expression indicating that two populations of cells were present in the red pulp of the spleen (Figure 3-12). CD163 expression did not co-localise with CD117 expression in the human ureter (Figure 3-13).

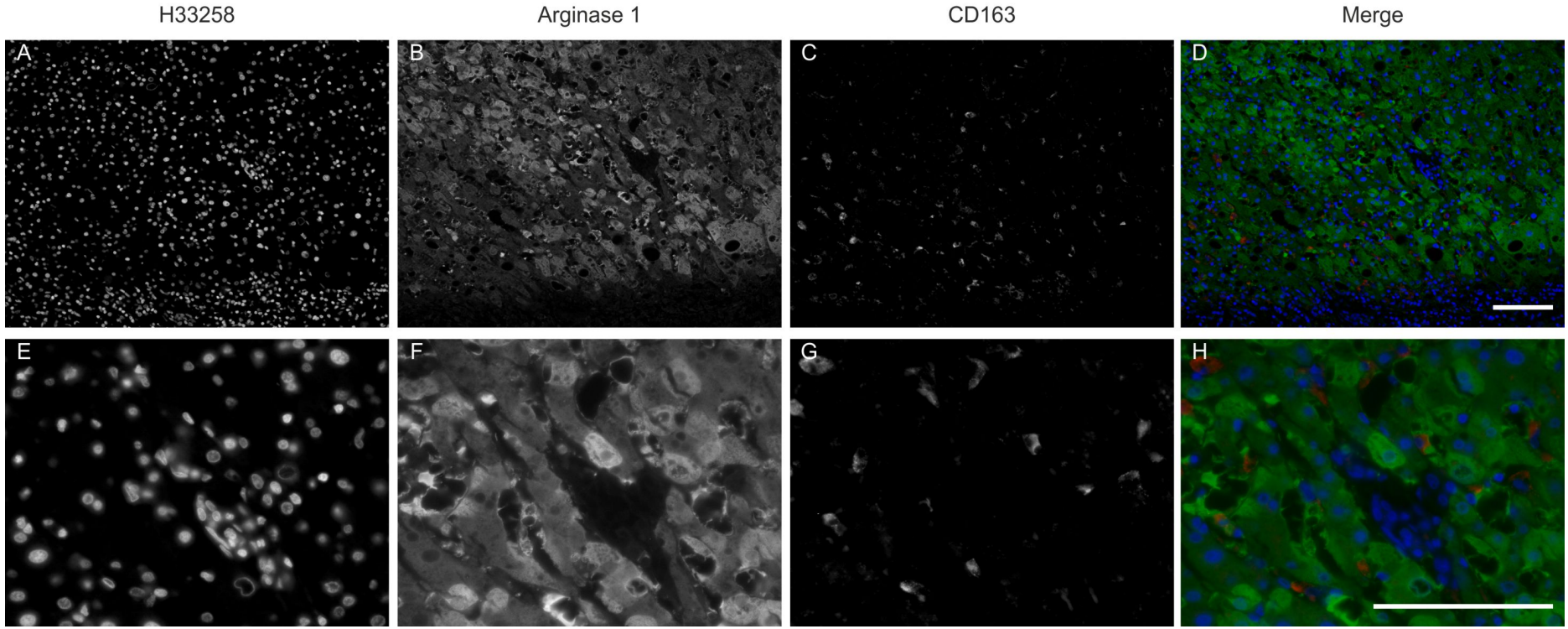

Figure 3-11. Fluorescent immunolabelling of human arginase 1 and CD163 positive cells in human liver. H33258 indicates nuclei. 32-bit images (A-C, E-G) were merged to produce a colour composite image (D and H) of nuclear staining (blue) and fluorescent labelling of arginase 1 (green) and CD163 (red). Scale bars represent 100 microns.

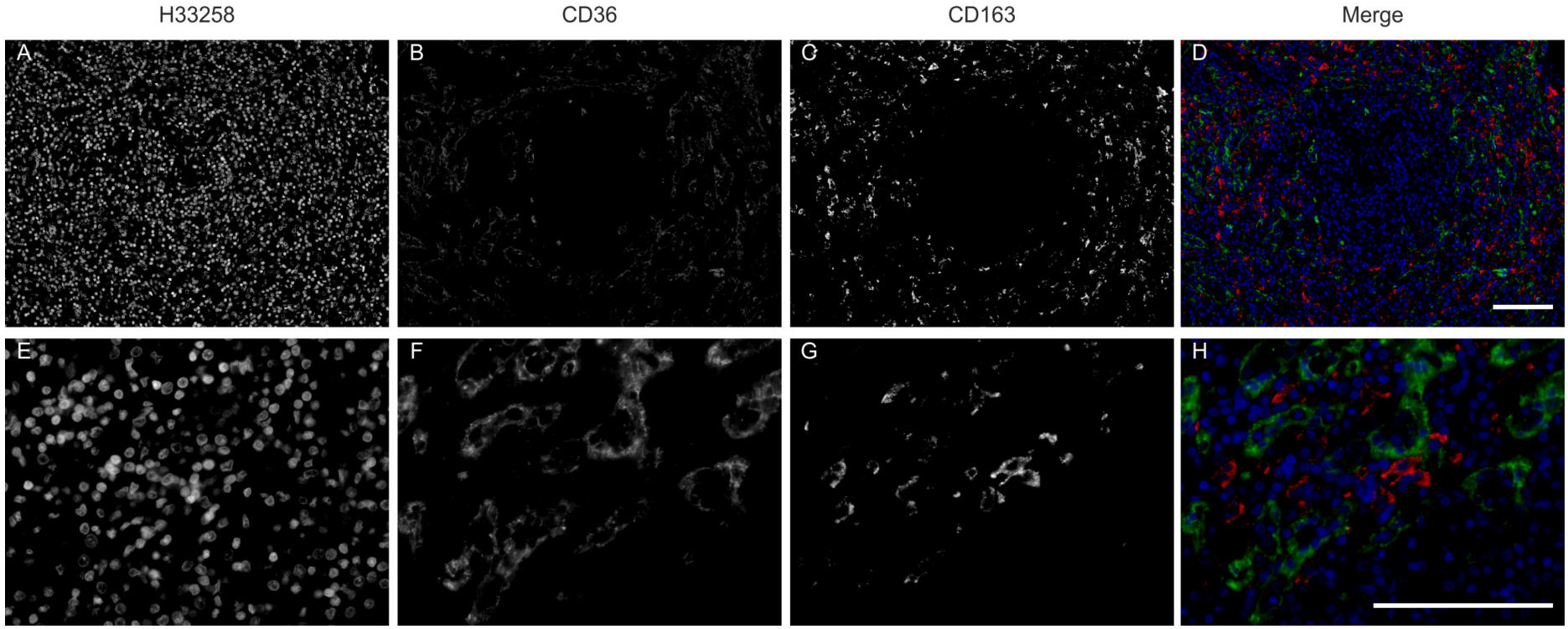

Figure 3-12. Fluorescent immunolabelling of human CD36 and CD163 in human splenic tissue. H33258 indicates nuclei. 32-bit images (A-C, E-G) were merged to produce a colour composite image (D and H) of nuclear staining (blue) and fluorescent labelling of CD36 (green) and CD163 (red). Scale bars represent 100 microns.

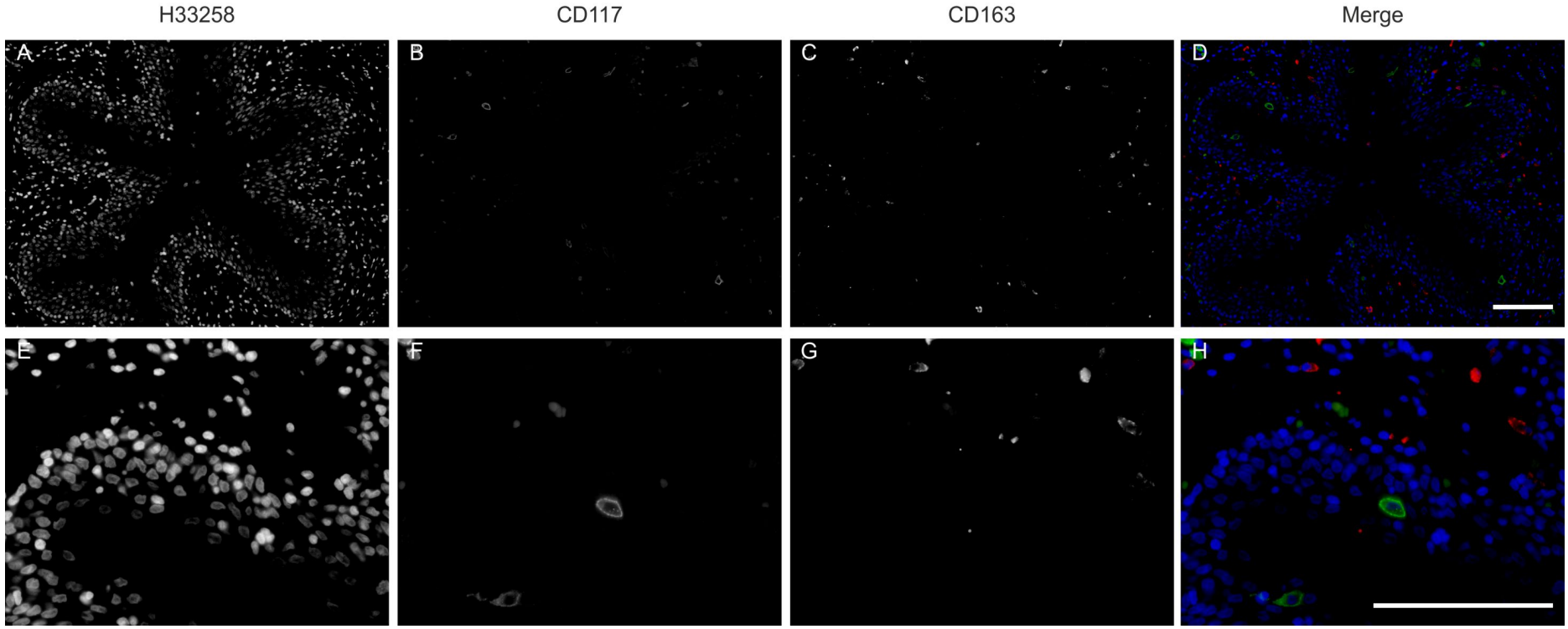

Figure 3-13. Fluorescent immunolabelling of human CD117 and CD163 positive cells in normal human ureter. H33258 indicates nuclei. 32-bit images (A-C, E-G) were merged to produce a colour composite image (D and H) of nuclear staining (blue) and fluorescent labelling of CD117 (green) and CD163 (red). Scale bars represent 100 microns.

3.5.2.3 Immunohistochemistry on a panel of human tissues

Antibodies against selected human markers were characterised using horseradish peroxidase immunohistochemistry (HRP-IHC). In addition to marker characterisation, HRP was used as a alternate detection method of primary antibody labelling, in order to confirm the cell specificity of the fluorescent immunolabelling. HRP-IHC allowed tissue architecture to be imaged by using a weak haematoxylin counterstain obviating multiple antibody labelling techniques to investigate tissue structure in addition to the functional marker labelling. The use of HRP-IHC also removed the potential issue of tissue auto-fluorescence, which can result from the fixation of tissue with 10% (v/v) formalin. All images shown represent the immunolabelling of the selected optimum antibody concentration outlined in chapter 2, table 2-7.

Lymph node

The T cell antigen CD3 and the macrophage antigens CD68 and CD163 were all identified within the cortex and paracortex region but not the germinal centres of the human lymph node (Figure 3-14). The antigen presenting cell marker, HLA-DR was observed within the cortex and paracortex of the lymph node and was weakly expressed in the B-cell follicles. A strong signal-to noise- ratio indicated that the antibody concentration selected identified the respective cells with intense labelling (Figure 3-14).

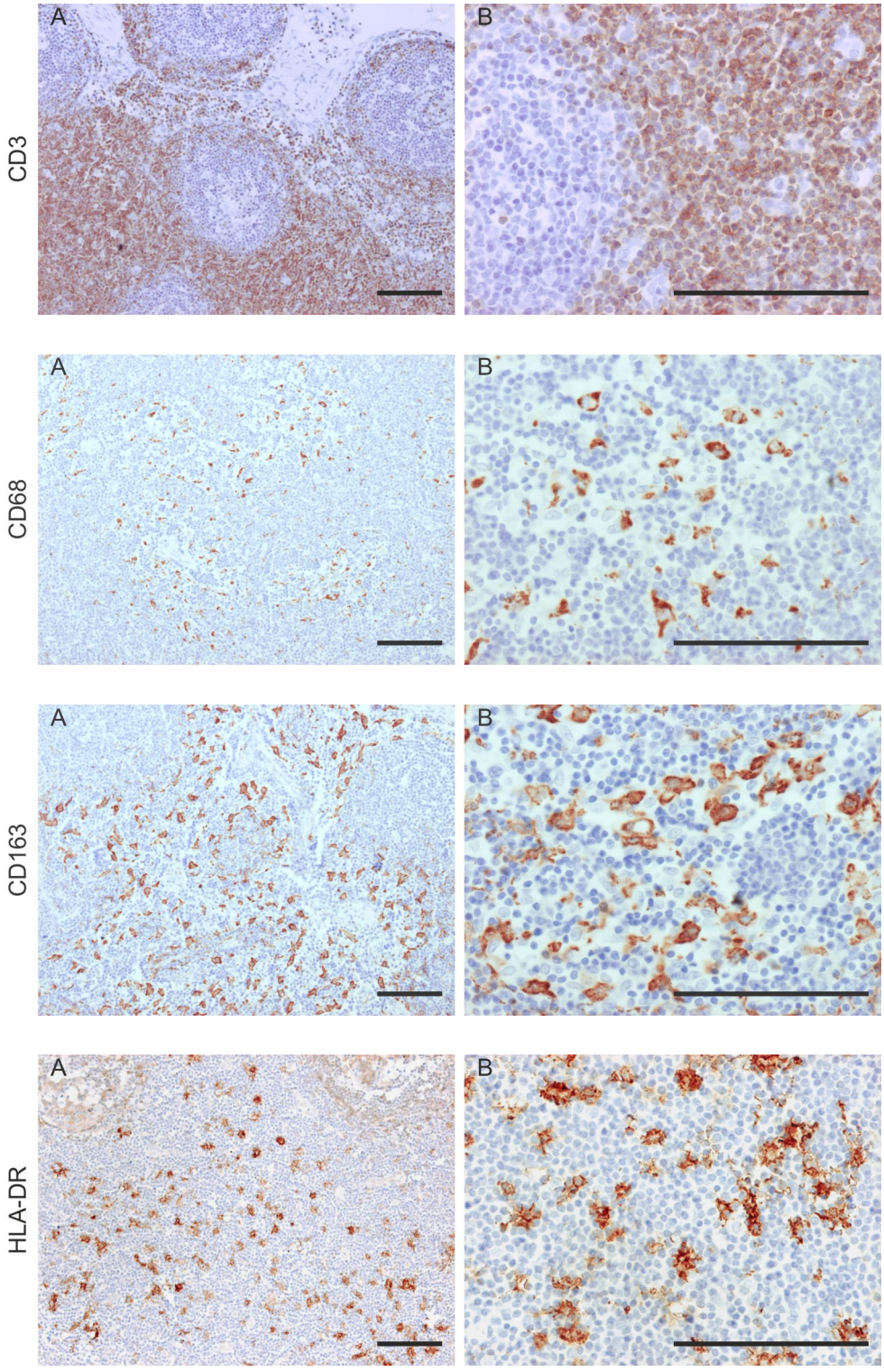

Figure 3-14. HRP immunohistochemical detection of human CD3, CD68, CD163 and HLA-DR positive cells in human lymph node. Image 'B' represents a higher magnification image of an area within image 'A' for all photomicrographs captured. Scale bars represent 100 microns.

Ureter

Human ureter was used to identify CD34+ endothelial cells and alpha smooth muscle actin positive cells. CD34 was intensely expressed by cells within the lamina propria of the human ureter (Figure 3-15, top image A) while CD34 immunolabelling showed diffuse expression within the muscularis regions of the tissue (Figure 3-15, top image B). αSMA was expressed within the smooth muscle bundles of the ureter tissue (Figure 3-15, bottom images).

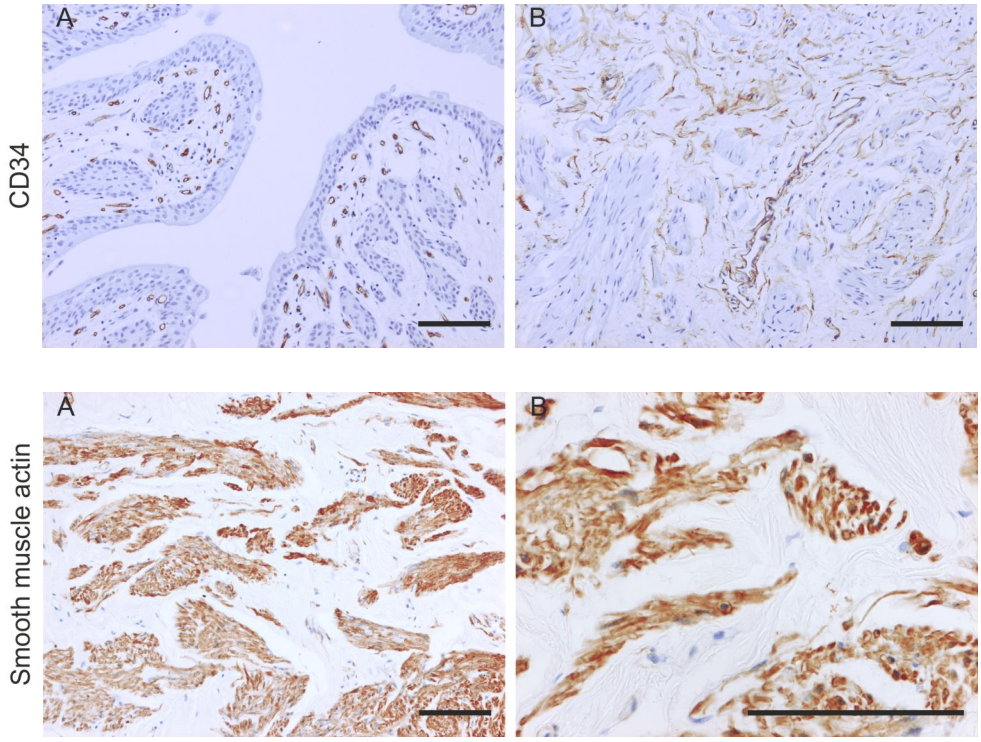

Figure 3-15. HRP immunohistochemical detection of αSMA and CD34 positive cells in sections of normal human ureter. Images of CD34 labelling in both the lamina propria (Top, A) and muscularis regions (Top, B) were captured. Images of smooth muscle actin labelling in the stromal regions of the normal human ureter were captured (Bottom panel A and B). Scale bars represent 100 microns.

Colon

Human colon was used as a positive control tissue for CD80 and Ki67 expression. CD80+ cells were observed in the lamina propria of the colon tissue (Figure 3-16, top images). Ki67+ cells were observed within the crypts of the villi indicating cells that were in cell cycle progression (Figure 3-16, bottom images).

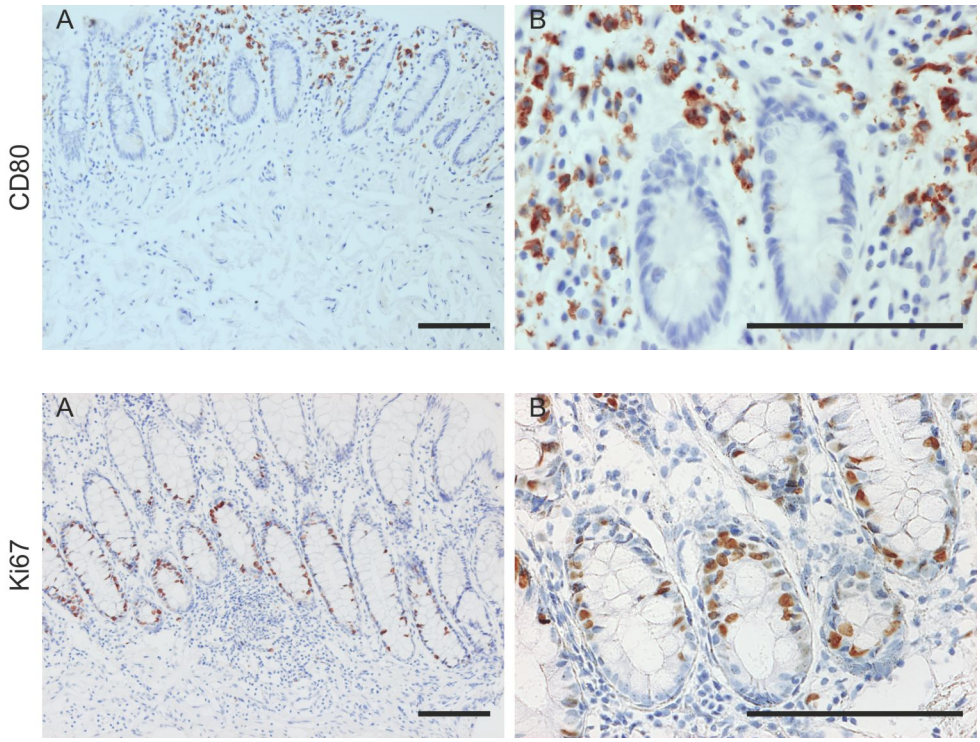

Figure 3-16. HRP immunohistochemical detection of CD80 and Ki67 positive cells in multiple tissue sections of human colon. Image 'B' represents a higher magnification image of an area within image 'A' for all photomicrographs captured. Scale bars represent 100 microns.

Liver

Confirmation of the expression of arginase 1 in human liver hepatocytes, observed by fluorescent immunolabelling, was performed using HRP-IHC (Figure 3-17).

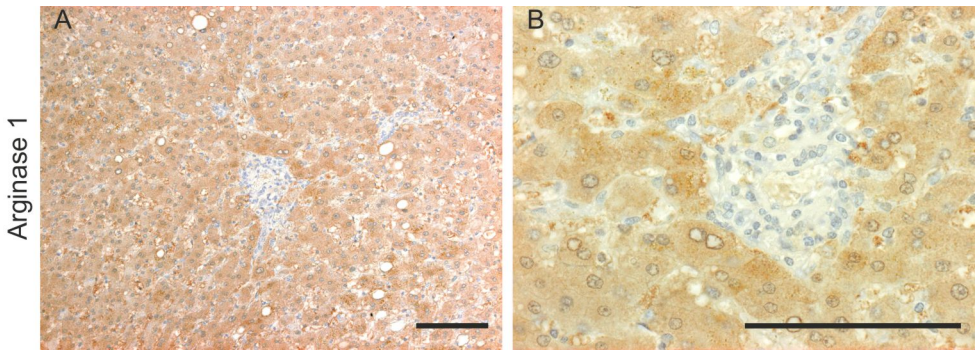

Figure 3-17. HRP immunohistochemical detection of arginase 1+ cells in a tissue section of human liver. Image B represents a higher magnification image of an area within image A. Scale bars represent 100 microns.

Nuclear receptors

Nuclear localisation of the glucocorticoid receptor was observed in human liver tissue (Figure 3-18, top images). Nuclear localisation of PPARγ was observed in the epithelial lining of the ureter (Figure 3-18, bottom images)

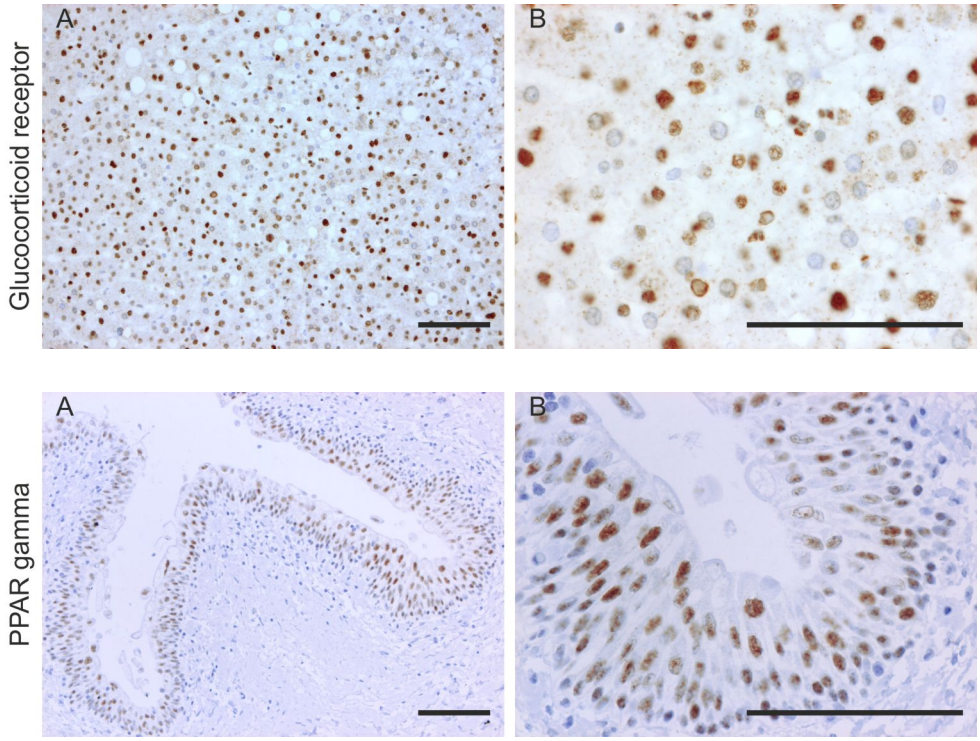

Figure 3-18. Immunohistochemical detection of the glucocorticoid receptor and PPARγ. Dako CSA kit HRP detection of PPARγ+ cells in normal human ureter and glucocorticoid receptor positive cells in human live**r.** Image B represents a higher magnification area of image A. Scale bars represent 100 microns.

3.6 Results: Characterisation of a panel of markers on PBMC.

Fluorescent microscopy allowed a large panel of functional markers to be characterised using a small number of isolated cells. Initial characterisation of all antibodies was performed by titration on cytospun preparations of PBMC. The optimum antibody concentration was then determined using indirect fluorescent microscopy techniques. An advantage of performing antibody titration using fluorescent microscopy on a heterogeneous cell population was that, for all antibodies characterised here, only sub-populations of cells were positive for the antigen of interest. This methodology produced an internal negative control per field of view, allowing greater confidence in the specificity and chosen concentration of the selected primary antibody. All images shown represent the immunolabelling using the selected optimum antibody concentration.

Human PBMC in suspension were centrifuged onto glass slides using a three-chamber microscope slide coverplate followed by fixation of the cells with methanol:acetone. Antibodies were titrated on the fixed cytospun cells on the slides and the optimum primary antibody concentration determined by fluorescent microscopy (Figure 3-19 and Figure 3-20). A representative isotype control image for cell labelling using the immunofluorescence detection method is shown in appendix II-VII.

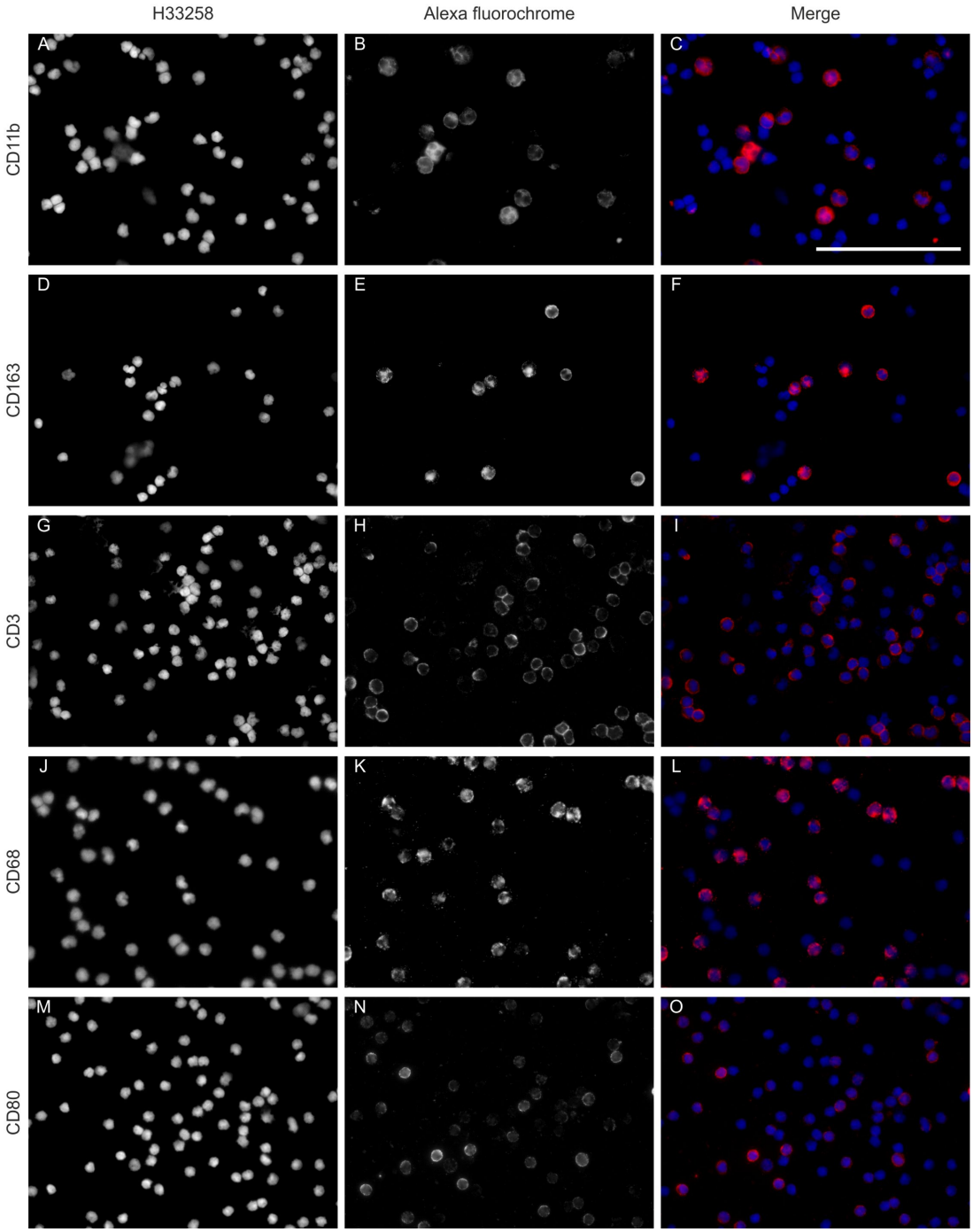

Figure 3-19. Characterisation of anti-CD11b, anti-CD163, anti-CD3, anti-CD68 and anti-CD80 primary antibodies on cytospun preparations of PBMC using immunofluorescence. 32-bit images were merged to produce a colour composite image (C, F, I, L and O) of nuclear staining (blue) and fluorescent labelling of the antigen (red). Scale bar represents 100 microns.

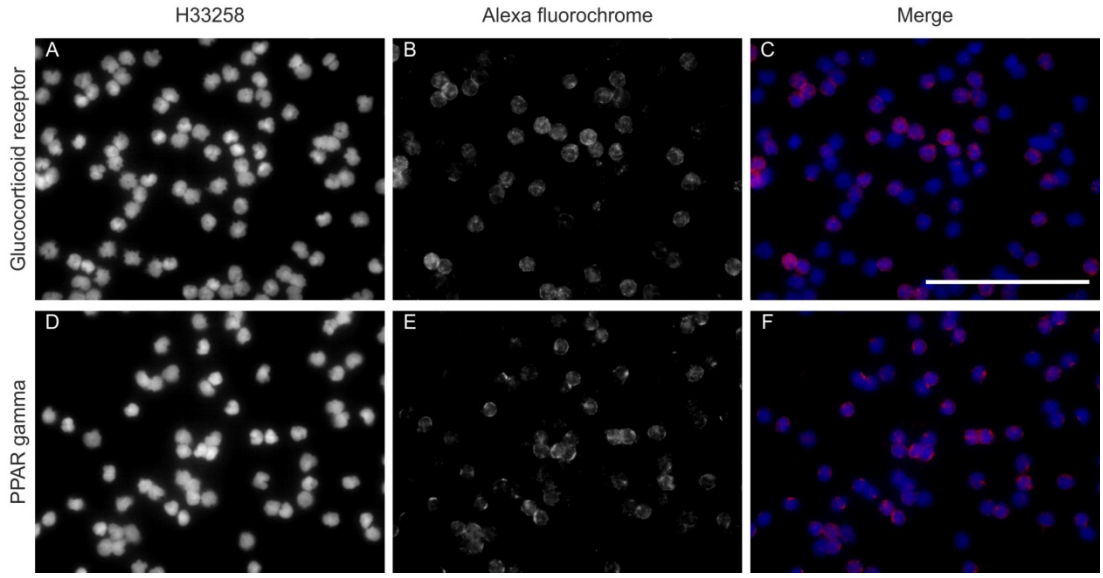

Figure 3-20. Characterisation of anti-glucocorticoid receptor and anti-PPAR gamma primary antibodies on cytospun preparations PBMC using immunofluorescence. 32-bit images were merged to produce a colour composite image (C and F) of nuclear staining (blue) and fluorescent labelling of the antigen (red). Scale bar represents 100 microns.

3.7 Results: Characterisation of selective adherence to isolate macrophages

Selective adherence is used to isolate monocytes for culture of monocyte-derived macrophages (For example (Ingham, 1990; Fox et al., 2011)). Selective adherence was used to isolate monocytes from peripheral blood mononuclear cell preparations. The methodology relies on the premise that within the heterogeneous PBMC population, only the monocytes will adhere to the surface that the cells have been seeded onto, allowing other non-adherent cells to be removed by washing.

In order to characterise the selective adherence methodology to select human peripheral blood monocytes, cells were selected using adherence and the adherent cells characterised using fluorescent immunolabelling. The T cell marker, CD3 was used to confirm that non-adherent PBMC were removed from the culture. H33258 staining of the DNA revealed that the cells that had adhered to the glass substrate had kidney-shaped nuclei, indicative of mononuclear phagocytes and were negative for CD3 (figure 3-21, A-C). Immunolabelling of the monocyte and macrophage-associated markers, CD11b and CD68 showed that selective adherence enriched for CD68 and CD11b positive cells after three hours, although not all adherent cells were CD11b and CD68 positive (figure 3-21, D-I).

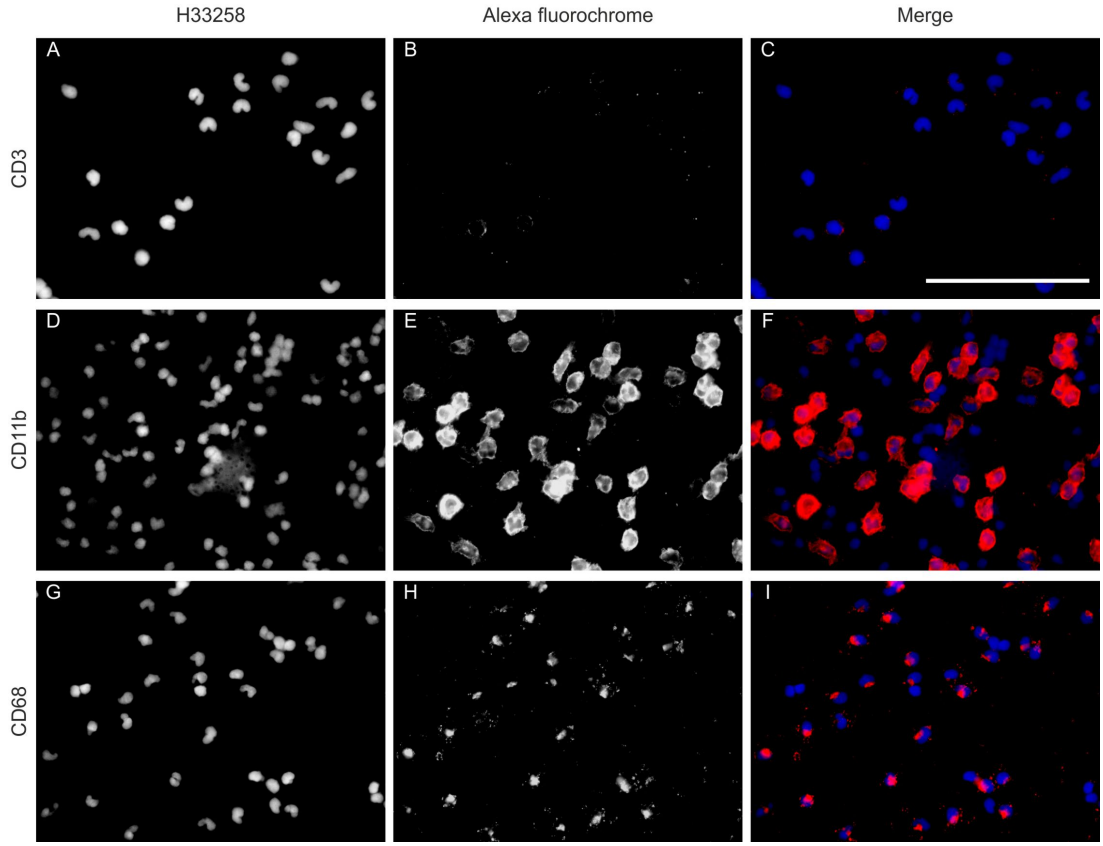

Figure 3-21. Characterisation of cells isolated by selective adherence. Cells were seeded onto glass multiwell slides and incubated for three hours in complete PBMC medium at 37°C in 5% (v/v) CO_2 in air to allow cells to adhere to the substrate. Following incubation, non-adherent cells were removed by washing. Cells that had adhered to the substrate were fixed with 1:1 (v/v) methanol:acetone and immunolabelled with antibodies against CD3, CD11b or CD68 and visualised using epi-fluorescent microscopy. Scale bar represents 100 microns.

3.8 Results: Characterisation of human monocytes and monocyte-derived macrophages using flow cytometric methods and analysis

Flow cytometry analysis was selected to analyse larger populations of cells compared to immunofluorescent imaging. Flow cytometric analysis of whole blood following the lysis of erythrocytes showed three distinct populations of cells based on forward scatter linear (FS Lin) and side scatter linear (SS Lin) profiles which are well defined. These three populations represented peripheral blood granulocytes, monocytes and lymphocytes (Figure 3-22). Lymphocytes are small in size, defined by FS Lin and have low granularity, defined by SS Lin, relative to the other cell populations. Monocytes are larger in size than lymphocytes, as defined by a shift in FS Lin profile compared to the lymphocytes and more granular as defined by a shift in SS Lin profile. Granulocytes are similar in size to monocytes based on their FS Lin profile, but are much more granular (Figure 3-22). Density centrifugation of diluted blood over Lymphoprep™ removed the granulocyte population allowing analysis of only the PBMC population (Figure 3-22, B versus C).

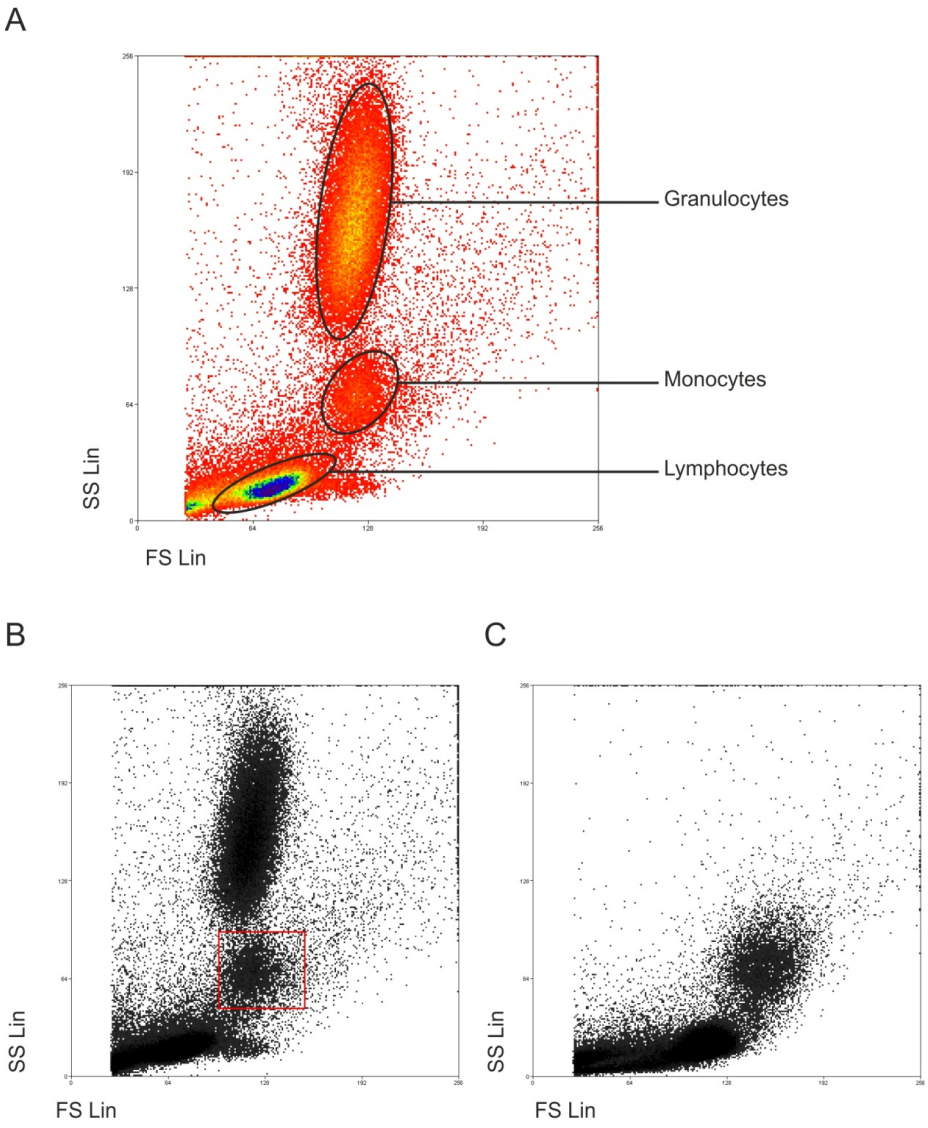

Figure 3-22. Flow cytometric analysis of human blood leukocyte populations pre- and post-density gradient centrifugation. Three distinct populations of leukocytes were identified by forward scatter (FS Lin) and side scatter (SS Lin) by flow cytometry. Granulocyte populations were removed from analysis by isolation of mononuclear cells over Lymphoprep™ (B versus C). Red box in image B highlight monocytes defined by FS Lin and SS Lin.

In order to characterise the isolated PBMC preparations and to confirm the monocyte cell population identified by FS Lin and SS Lin expressed monocyte-associated markers, initially a region of analysis was drawn around both the monocyte and lymphocyte populations (Figure 3-23). This region of analysis was used to characterise the dead cell population in section 3.8.1.1 and the monocyte population in section 3.8.3.

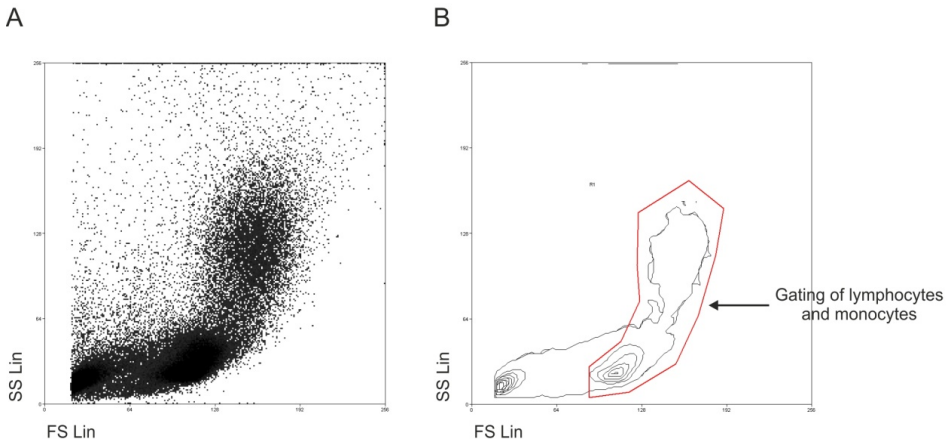

Figure 3-23. Gating of the lymphocyte and monocyte populations based on forward scatter and side scatter analysis of PBMC preparations. (A) Dot plot of flow cytometric analysis of the FS Lin and SS Lin profiles of unlabelled PBMC. (B) Contour analysis of the FS Lin and SS Lin dot plot (A) showing the region of analysis around the monocyte and lymphocyte populations in red.

3.8.1 Characterisation and exclusion of dead cells by flow cytometric analysis

3.8.1.1 Exclusion of 'dead' PBMC from flow cytometric analysis

A fixable LIVE/DEAD stain was used to exclude dead cells from flow cytometric analysis. The stain labelled the amine groups of all proteins resulting in labelling of the external proteins on all cells. Dead cells were defined as cells with a compromised membrane, which may take up antibody non-specifically. Cells with a compromised membrane exposed internal amine groups to the stain resulting in greater staining intensity compared to cells with a non-compromised membrane. In order to provide a positive control for the fixable violet LIVE/DEAD stain, isolated PBMC were permeablised using 70% (v/v) methanol in dH_2O for 30 minutes at ambient temperature. Flow cytometric analysis of PMBC permeablised with 70% (v/v) methanol using the region of analysis defined in figure 3-23 showed a shift in the

forward scatter properties of the cells indicating a decrease in cell size due to the dehydrating effect of the methanol (Figure 3-24, A). Therefore the region of analysis was moved to compensate for this shift in the size of the dead cell population (Figure 3-24, A; Red gate versus red gate with blue dots). Analysis of this population showed high intensity staining of the cells in the violet two detection channel of the flow cytometer, indicating the cells had taken up the dye (Figure 3-24, B).

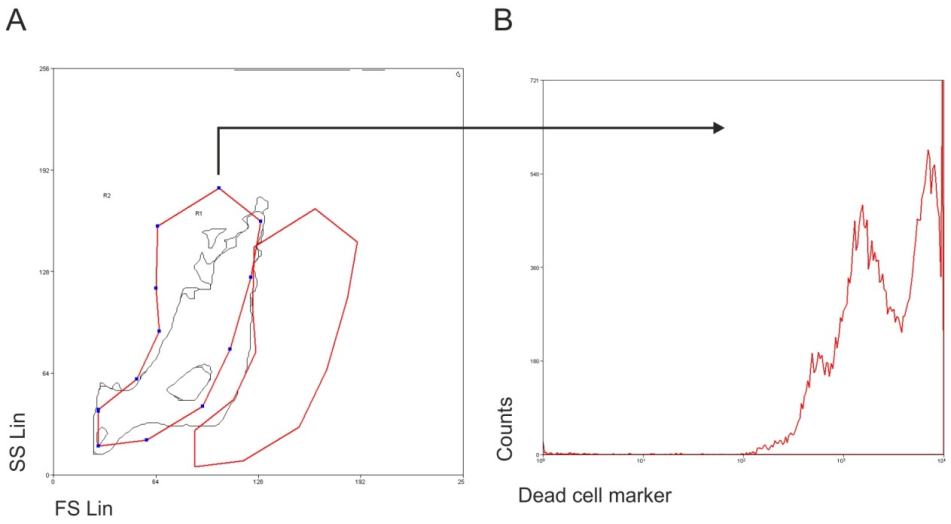

Figure 3-24. Flow cytometric analysis of the shift in forward scatter properties of 'dead' PBMC and the corresponding increase in fluorescent intensity of the fixable LIVE/DEAD cell marker. Use of methanol to permeablise the cells led to dehydration of the PBMC altering the FS Lin scatter properties of the cells compared to the untreated cells (figure 3-23). Therefore the region of analysis was shifted left (A). Gating of the cell population stained with a LIVE/DEAD cell marker showed intense fluorescence in the UV channel (B - red line).

To determine the staining intensity of non-permeablised ('live') cells stained with the LIVE/DEAD cell marker relative to 'dead' cells, which had been permeablised and stained with the LIVE/DEAD cell marker as described above, the 'live' and 'dead' cell populations were mixed 50:50 and analysis performed on both cell types for comparison to the unlabelled control cells. Overlay of the flow cytometric histograms of unlabelled cells and stained 'live' cells demonstrated the shift in emission intensity of the whole population when stained with the fixable violet LIVE/DEAD stain (Figure 3-25). Addition of

permeablised cells stained with the fixable LIVE/DEAD stain illustrated the shift in staining intensity between the 'live' and 'dead' populations (Figure 3-25).

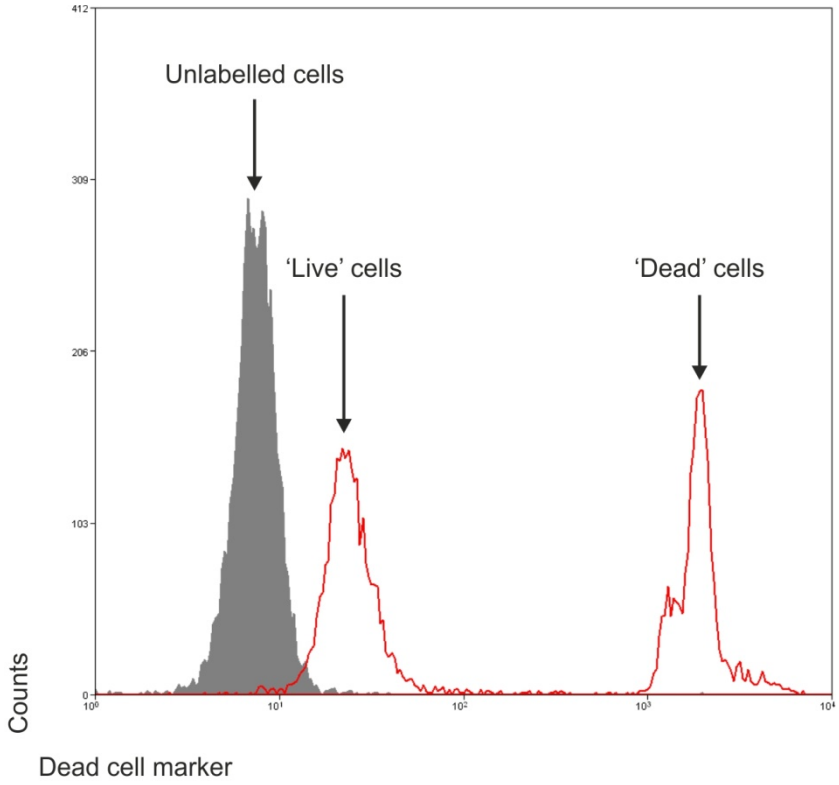

Figure 3-25. Summary of the fluorescence profile of the fixable LIVE/DEAD staining of human 'live' and 'dead' PBMC compared to unlabelled cells. Unlabelled PBMCs are represented by the gray histogram. The red line shows the shift in the fluorescent intensity of the 'live' PBMC stained with the LIVE/DEAD fixable stain compared to the unlabelled control and a greater shift in fluorescence intensity of the 'dead' PBMC following permeablisation.

'Live' cells were analysed by gating on the cells that displayed a low fluorescent intensity of the dead cell marker in the violet two detection channel of the flow cytometer.

3.8.1.2 Exclusion of 'dead' adherent macrophages from flow cytometric analysis

Gentle scraping was used to retrieve adherent macrophages from the glass substrate into suspension. This method of isolation produced a high percentage of cells with a

compromised membrane. These 'dead' cells could be distinguished from the population by increased intensity in fluorescent emission when stained with the fixable LIVE/DEAD stain. The population of cells that displayed lower intensity staining was selected as the 'live' cell population and all future analysis of antibody labelling was performed on this population (Figure 3-26).

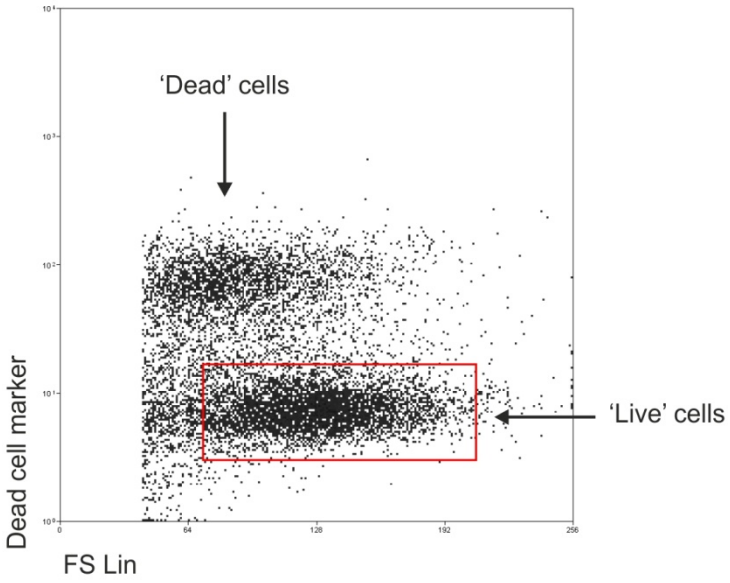

Figure 3-26. Gating strategy used to analyse the 'live' human monocyte-derived macrophages population following isolation by scraping. Isolated human monocyte-derived macrophages were stained with the fixable LIVE/DEAD stain and the 'live' cell population selected for analysis by gating on the cells which showed a lower fluorescent intensity with the fixable LIVE/DEAD stain (red box).

3.8.2 Characterisation of human peripheral blood monocytes using flow cytometry

To confirm that peripheral blood monocytes identified based on FS and SS profiles were monocytes (Figure 3-22), PBMC were labelled with fluorochrome-conjugated antibodies against monocyte-associated markers. PBMC were labelled with an APC conjugated anti-human CD11b antibody or a PE-conjugated anti-human CD14 antibody. Again, the monocytes and lymphocyte populations were gated based on FS Lin and SS Lin as illustrated in Figure 3-23 and dead cells excluded from all analysis as described in section 3.8.1.1.

Labelling of monocytes and lymphocytes with an anti-human CD11b-APC antibody produced a peak of cells displaying high expression of CD11b within the gated lymphocytes and monocytes (Figure 3-27, A). Using the fluorescent intensity of the labelling in the APC channel plotted against the FS Lin profile of the cells the $CD11b^{hi}$ population were gated (Figure 3-27, B – black circle). Colour back-gating of the $CD11b^{hi}$ cells (Figure 3-27, C and D) onto the FS Lin and SS Lin gated lymphocyte and monocyte populations showed that the $CD11b^{hi}$ population was restricted to the monocyte population (Figure 3-27, E).

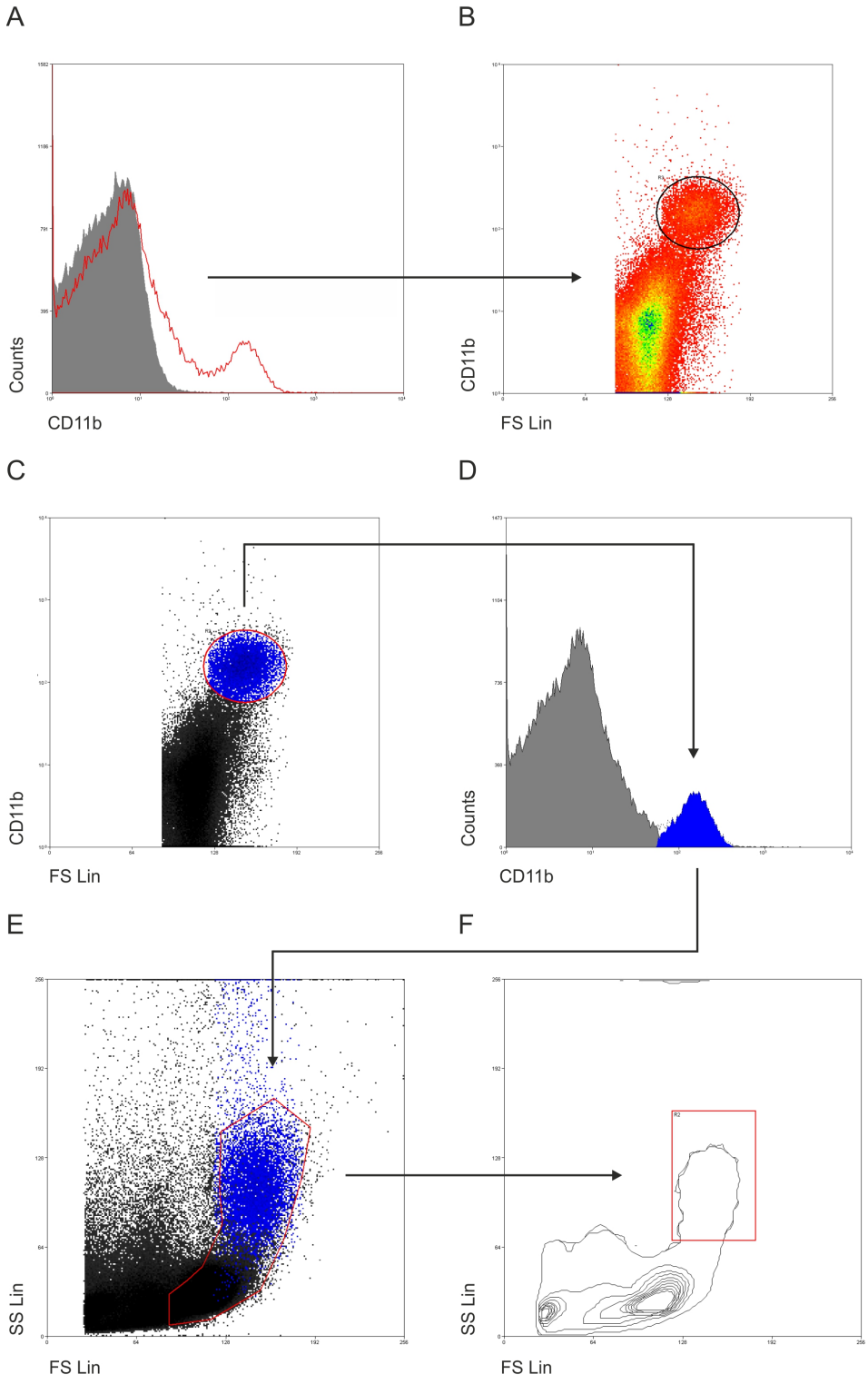

Figure 3-27. Identification of CD11b+ PBMC. Isolated PBMC were labelled with an anti-CD11b APC conjugated antibody and analysis was performed on the monocytes and lymphocytes based on FS Lin and SS Lin as described in figure 3-23. CD11b expression was plotted against the matched isotype control (A - red line vs grey histogram). Events were plotted on a plot of CD11b labelling versus FS and the $CD11b^{hi}$ population were selected for

analysis by gating (black circle - B). Colour gating of the selected CD11b high population (C) was restricted to the CD11b peak on the histogram of CD11b labelling versus counts (D). Application of the colour back-gating the SS Lin versus FS Lin dot plot of the gated monocytes and lymphocytes (red gate, E) revealed the $CD11b^{hi}$ population to be restricted to the monocyte population defined by FS and SS (E). Gating of human peripheral blood monocytes was restricted based on FS and SS (F – red square).

The gating strategy was refined so only human peripheral blood monocytes were selected based on the FS Lin and SS Lin profiles within the whole PBMC population. This allowed analysis of marker expression by the monocyte population only (Figure 3-28, A). Analysis of CD11b-APC immunolabelling of the monocyte population identified by FS Lin and SS Lin showed the majority of this population to be CD11b positive (Figure 3-28, B).

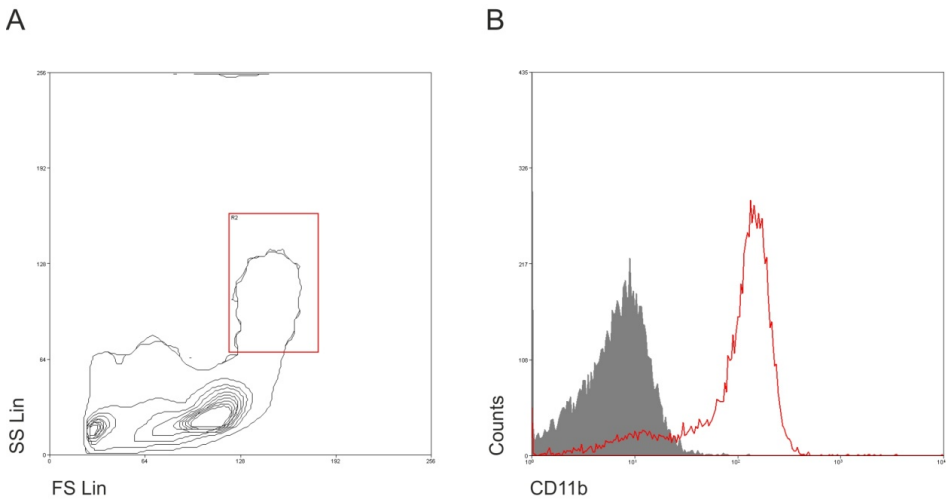

Figure 3-28. Reanalysis of extracellular CD11b labelling of the monocyte population based on FS Lin and SS Lin profile only. Human peripheral blood monocytes were selected for analysis based on FS Lin and SS Lin (A - red box). Analysis of CD11b labelling by the human monocyte population showed a shift in fluorescent intensity by the majority of the population (B - red line) when compared to the fluorescent IgG isotype control (B - grey histogram).

To confirm the CD11b high population expressed other monocyte-associated markers, PBMC were labelled with anti-human CD14 antibody conjugated with the fluorochrome PE.

Again, the lymphocyte and monocyte populations were gated based on FS Lin and SS Lin as previously illustrated (Figure 3-23) and dead cells excluded from the analysis as described in section 3.8.1.1. Flow cytometry analysis was performed using the same procedure outline in the analysis of CD11b expression (Figure 3-27). Labelling of monocytes and lymphocytes with an anti-human CD14 PE antibody produced a peak of cells with high expression of CD14 within the gated lymphocytes and monocyte populations (Figure 3-29, A). Using the fluorescent intensity of the labelling in the PE channel plotted against the FS Lin profile of the lymphocytes and monocytes the $CD14^{hi}$ population were gated (Figure 3-29, B). Colour back-gating of the $CD14^{hi}$ cells (Figure 3-29, C and D) onto the FS Lin and SS Lin gated lymphocyte and monocyte populations showed that the $CD14^{hi}$ population was restricted to the monocyte population defined by FS Lin and SS Lin (Figure 3-29, E).

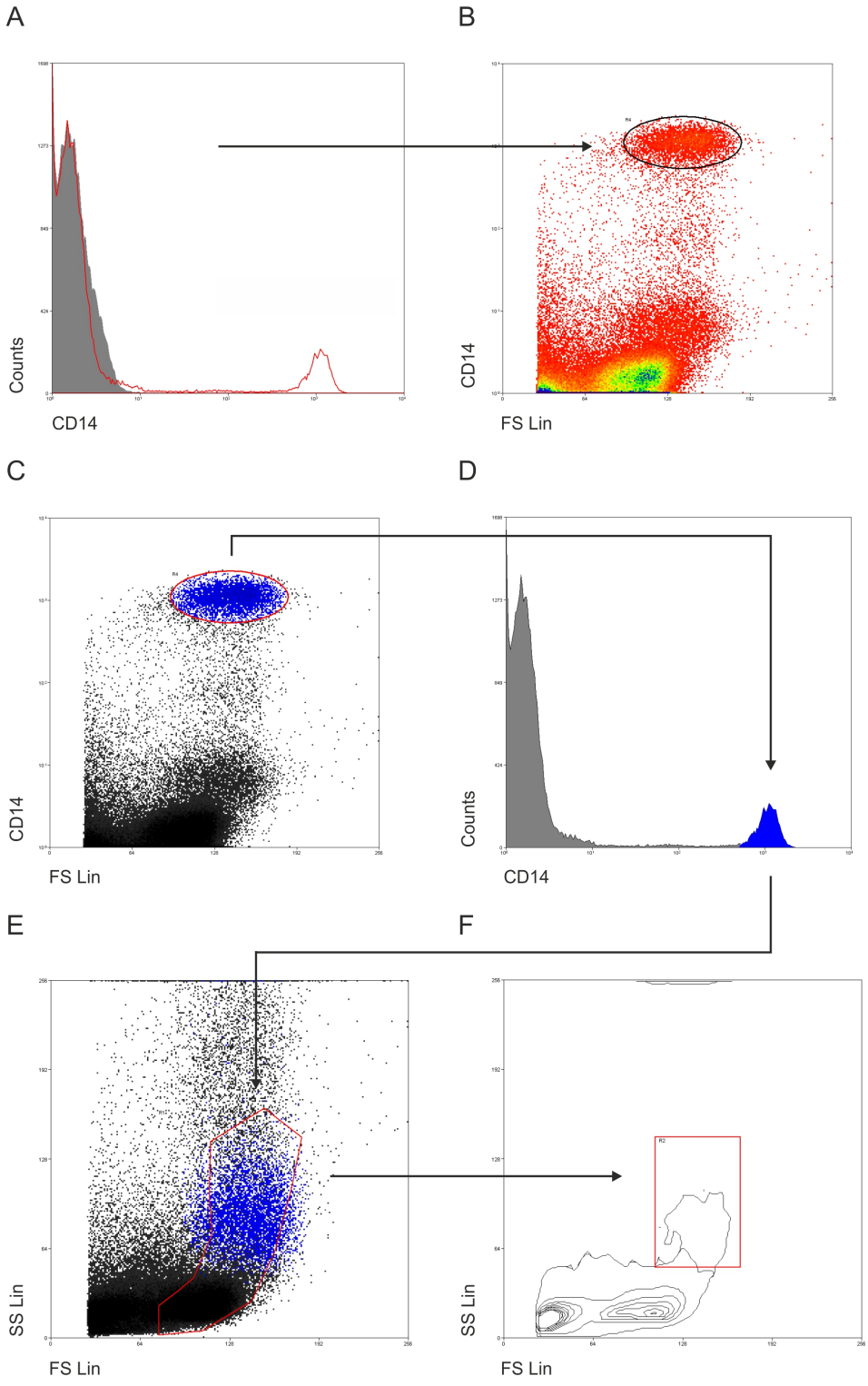

Figure 3-29. Identification of CD14+ PBMC. Isolated PBMC were labelled with an anti-CD14 PE conjugated antibody and analysis was performed on the monocytes and lymphocytes based on FS and SS as described in figure 3-23. CD14 expression was plotted against the matched isotype control (A - red line vs grey histogram). Events were plotted on a plot of CD14 labelling versus FS and the $CD14^{hi}$ population were selected for analysis by gating

(black oval - B). Colour gating of the selected CD14 high population (C) was restricted to the CD14 peak on the histogram of CD14 labelling versus counts (D). Application of the colour back-gating the SS Lin versus FS Lin dot plot of the gated monocytes and lymphocytes revealed the $CD14^{hi}$ population to be restricted to the monocyte population defined by FS Lin and SS Lin (E). Gating of human peripheral blood monocytes was restricted based on FS Lin and SS Lin (F – red square).

Analysis of the CD14-PE immunolabelling on the monocyte population identified by FS Lin and SS Lin showed the majority of the monocyte population were CD14 positive (Figure 3-30 – red line versus grey histogram).

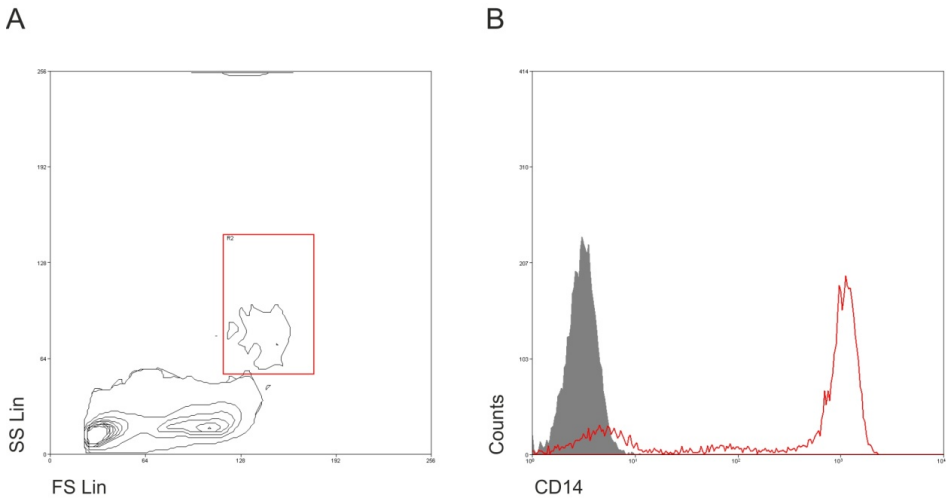

Figure 3-30. Reanalysis of extracellular CD14 expression by human peripheral blood monocytes identified by FS Lin and SS Lin. Isolated PBMC were labelled with an anti-CD14 PE conjugated antibody and flow cytometric analysis was performed on the human peripheral blood monocytes selected based on FS Lin and SS Lin (A). Analysis of CD14 labelling on the human monocyte population showed a shift in fluorescent intensity by the majority of the population (B - red line) when compared to the fluorochrome conjugated isotype control (B - grey histogram).

Permeablisation and immunolabelling of the human peripheral blood monocyte intracellular antigen CD68 was also performed. Gating of the monocyte population based on FS Lin and SS Lin (Figure 3-31, A) showed a subtle shift in CD68 expression compared to the isotype control histogram (Figure 3-31, B – red line versus gray histogram). As the shift in fluorescent intensity of the CD68 labelling compared to the isotype control histogram (Figure 3-31, B) was not as convincing as the shift in fluorescent intensity observed with the extracellular antigen CD11b and CD14; CD68 was not used to identify human peripheral blood monocytes by flow cytometry in further investigations.

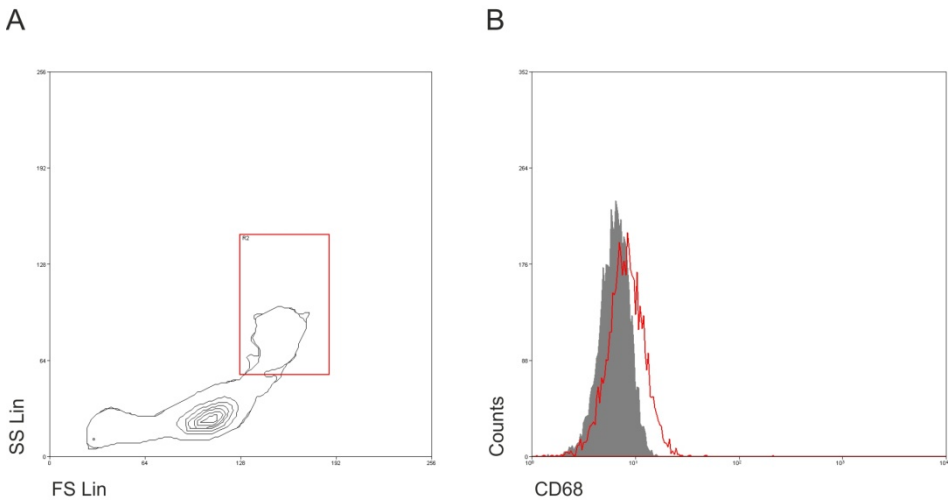

Figure 3-31. Flow cytometric analysis of intracellular CD68 expression by human peripheral blood monocytes identified by FS Lin and SS Lin. Isolated PBMC were permeablised using the Dako IntraStain kit and immunolabelled with an anti-CD68 APC conjugated antibody and flow cytometric analysis was performed on the human peripheral blood monocytes selected based on FS Lin and SS Lin (A). Analysis of CD68 labelling on the human monocyte population showed a subtle shift in fluorescent intensity by the majority of the population (red line) when compared to the fluorochrome conjugated isotype control (B - gray histogram).

All future gating strategies of PBMC using flow cytometric analysis was restricted to the human monocyte population based on FS Lin and SS Lin and use of the extracellular monocyte marker, CD11b.

3.8.3 Characterisation of human peripheral blood monocyte-derived macrophages using flow cytometry

Macrophages that had been matured from peripheral blood monocytes for 11 days on a glass substrate showed a mixture of a 'fried egg'-like morphologies and elongated morphologies (Figure 3-32), associated with human peripheral blood monocyte-derived macrophages *in vitro* (Verreck et al., 2006).

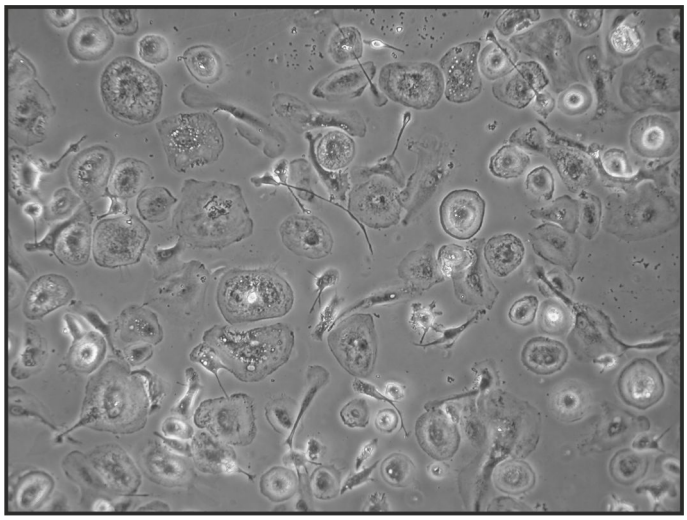

Figure 3-32. Phase contrast image of human monocyte-derived macrophages cultured on a glass substrate for 11 days.

Adherent macrophages were isolated by gentle scraping and labelled with an anti-human CD11b antibody conjugated with the fluorochrome, APC. 'Dead' cells were excluded from the analysis as described in section 3.8.1.2. The adherent macrophages were positive for the expression of CD11b (Figure 3-33).

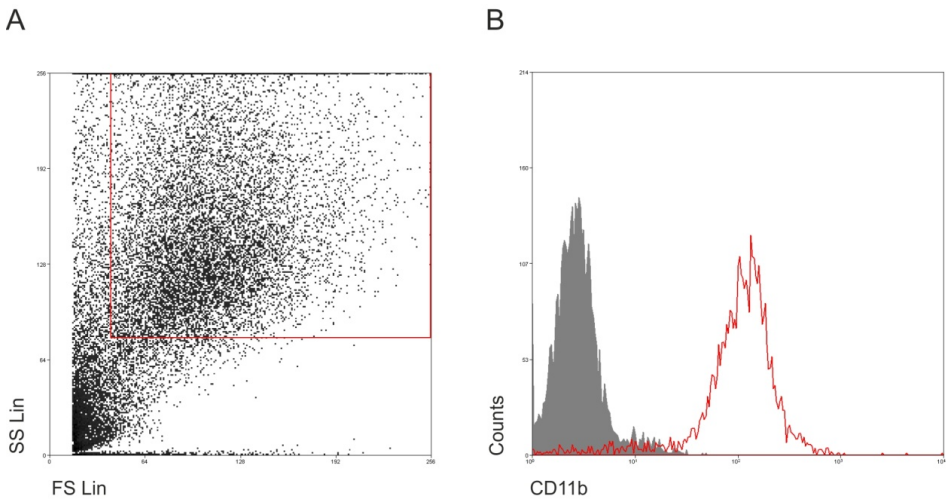

Figure 3-33. Flow cytometric analysis of CD11b expression by human monocyte-derived macrophages. Human monocyte-derived macrophages cultured on a glass substrate for 11 days were isolated and labelled with anti-CD11b antibody conjugated with APC. Monocyte-derived macrophages were gated using FS Lin and SS Lin (A). Analysis of CD11b labelling on monocyte-derived macrophages showed a high fluorescent intensity of the majority of cells (B – red line) compared to the APC conjugated isotype control (B – grey histogram).

Future analysis of monocyte-derived macrophages by flow cytometry was restricted to cells gated based on FS Lin and SS Lin and CD11b expression.

3.9 Summary

- Batches of porcine bladder tissue were successfully decellularised to produce a porcine bladder matrix which retained its extracellular matrix architecture; was devoid of porcine cells and did not show signs of toxicity towards human ureteric stromal cells
- An antibody against the porcine macrophage-associated marker, CD107a, was characterised on zinc-fixed, paraffin-embedded porcine splenic tissue sections using and alkaline phosphatase detection method and showed expected tissue localisation.
- A panel of antibodies selected against a series of markers were characterised for use on formalin-fixed, paraffin wax-embedded human tissue known to express the antigen of interest using both immunofluorescent and peroxidase detection methods.
- Application of a panel of antibodies against functional markers, to fixed human peripheral blood-derived cells showed antigen expression could be detected by immunofluorescence.
- Immunofluorescent labelling of fixed human cells isolated by selective adherence on a glass substrate demonstrated successful isolation of human monocytes from PBMC preparations.
- Flow cytometry gating strategies of human peripheral blood monocytes and human monocyte-derived macrophages and the elimination of dead cells from the analysis were established.

4.0 Development of a biomaterial-organ culture system to interrogate events at a urinary tract-biomaterial interface

4.1 Introduction

4.1.1 Structure and function of the urinary tract

The urinary bladder is a vessel that gradually fills with urine, which it stores until micturition (voiding). A key feature of bladder function is its ability to distend and maintain a low pressure, protecting the upper urinary tract against damage from the build up of backpressure. The bladder wall is made of three different layers of smooth muscle collectively known as the detrusor muscle. The bladder is lined by a transitional epithelium known as the urothelium, which provides a barrier between the urine and underlying tissues. The urinary bladder has three orifices that make up the trigone at the base of the bladder. Urine enters the bladder through two of these orifices from the ureters; two thin tubes that connect the kidneys to the bladder and allow a constant flow of urine in to the bladder by peristalsis. The third orifice allows passing of urine down the urethra at the neck of the bladder. An internal urethral sphincter located at the neck of the bladder is contracted and closed allowing retention of urine. The external urethral sphincter is a muscle further down the urethra and is under control of the voluntary nervous system. Both sphincters must open to allow passage of urine from the bladder (further reviews of the function of the urinary bladder can be found in (Bro-Rasmussen et al., 1965; HICKS, 1975; de Groat, 1993)).

4.1.2 Urinary bladder reconstruction – current practice

Urinary tract reconstruction is required clinically when the function or capacity of the bladder as a low-pressure storage vessel is compromised. This can be as a result of diseases such as multiple sclerosis and cancer and as a result spinal cord damage, as in spina bifida or spinal cord injury. When the spinal cord is damaged, the urinary bladder becomes hyperreflexic and coordination of the urinary bladder sphincter is impaired. This results in urinary incontinence or delayed micturition leading to urinary retention and bladder overdistension. This in turn leads to diverticular formation in the bladder wall and upper urinary tract infection or upper urinary tract damage (Urakami et al., 2007). The primary aims of urinary bladder reconstruction are to increase the capacity and compliance of the bladder and prevent renal deterioration. Currently, the surgical procedure of enterocystoplasty, in which a vascularised segment of autologous bowel is used to augment the urinary bladder, represents the 'gold standard' for increasing bladder capacity (Dawson and Whitfield, 1996). This procedure has serious clinical ramifications which stem from using bowel including; mucus production, stone formation, infections and electrolyte abnormalities ((Merguerian et al., 2000) reviewed in (Wezel et al., 2011)).

4.1.3 Urinary bladder reconstruction - prospective practice

Research into alternative methods of urinary bladder reconstruction to combat the effects of using autologous bowel have focused on; a) cell-based approaches to replace intestinal epithelial tissue with urinary tract epithelial cells; b) tissue engineering of the bladder or c) the use of biomaterials as an 'off-the-shelf' approach to bladder reconstruction. Turner et al described a method for bladder reconstruction in pigs. Autologous porcine urothelial cell sheets, which had been propagated and differentiated in culture, were transported on a Vicryl mesh and transplanted onto de-epithelialised, vascularised intestinal tract tissue. The composite was then used to augment the porcine bladder (Turner et al., 2011). Histological analysis of the porcine bladder reconstruction three months post implantation showed that the augmented sections were lined with continuous urothelium that bridged the native tissue and the implant. In addition the procedure was reported to show none of the complications associated with the use of bowel (Turner et al., 2011). Approaches in which new bladders are 'engineered' have involved taking biopsies from the bladders of patients with spina bifida, expanding the epithelial and stromal cells in culture and seeding them onto collagen-polyglycolic acid composite matrices or a decellularised bladder submucosa (of undescribed origin) (Atala et al., 2006). These 'engineered human bladders' were then implanted into patients and covered in the omentum, used as a vascular bed to promote

neo-vascularisation of the implant. An increase in bladder capacity was reported 49-61 months post-procedure in four of seven patients receiving the implants however, limited total patient numbers (n=7) and the loss of patients from follow-up urodynamic studies, coupled with the variation in protocol used i.e. decellularised bladder submucosa either covered or not covered in omentum or collagen composite matrices covered by omentum, which were not optimised in pre-clinical studies, made it difficult to assess the long term clinical benefits of the procedure. Moreover, seven weeks were required for cell expansion after obtaining the initial biopsy prior to implantation and therefore the treatment required two invasive procedures (Atala et al., 2006). Studies have also questioned the ability of urothelial cells from diseased or abnormal pediatric bladders to be expanded in culture for use in bladder tissue engineering strategies (Subramaniam et al., 2011).

4.1.3.1 Bladder augmentation using biological scaffolds

There is a growing interest in urinary tract reconstruction using biological scaffolds or synthetic biomaterials (reviewed in (Wood and Southgate, 2008; Wezel et al., 2011)). Decellularised biological scaffolds are excellent candidates for use in bladder reconstruction and porcine SIS has been used in the experimental bladder augmentation of canine (Kropp et al., 1996) rabbit (Ayyildiz et al., 2008) and porcine bladder partial cystectomy models (CALVANO et al., 2000; Reddy et al., 2000). *In vivo* experimental models have employed a 'like-for-like' approach when using biological scaffolds in bladder augmentation. Therefore, many bladder-derived biological scaffolds have been described with the aim of using these materials in bladder augmentation (reviewed in (Aitken and Bägli, 2009)). Incorporation of rat bladder extracellular matrix was shown to increase bladder capacity and compliance following partial cystectomy (>50%) in Sprague-Dawley rats (Piechota et al., 1999). Functional regeneration of the bladder detrusor smooth muscle was demonstrated using electrical field stimulation experiments (Piechota et al., 1998). Bladder augmentation using rat bladder extracellular matrix was also shown to improve bladder capacity of low capacity neuropathic bladders of Sprague-Dawley rats, which were experimentally-induced by transection of the spinal cord (Urakami et al., 2007). In a more size-relevant model, implantation of canine urinary bladder submucosa-derived biological scaffold in a canine partial cystectomy model, in which approximately 50% of the bladder volume was reduced, increased the capacity of the urinary bladder by 30%. The authors also reported that the bladder capacity could be further increased by 99% when the scaffold was seeded with autologous urinary bladder smooth muscle cells and urothelial cells (Yoo et al., 1998). The canine urinary bladder biological scaffold was prepared by

microdissection and isolation of the submucosa from the serosal and muscular layers of a canine urinary bladder before irradiating the material with UV light for 24 hours (Yoo et al., 1998). This method of preparation of a urinary bladder biological scaffold has also been applied to the porcine urinary bladder (Chen et al., 1999) and the porcine bladder biological scaffold has been used to repair ventral urethral defects in male New Zealand white rabbits. Histological analysis of the implanted scaffold was reported to show infiltration of host cells accompanied by angiogenesis and no signs of fibrosis six months post surgery (Chen et al., 1999). Porcine bladder matrix has also been prepared using detergent extraction of porcine cells and RNAse and DNAse treatment (Farhat et al., 2008). This biological scaffold was used to augment the bladder in a porcine partial cystectomy model. The implant was shown to be infiltrated by stromal cells and showed migration and stratification of the epithelial lining of the bladder over the luminal surface at four weeks post surgery, as assessed by histological staining (Merguerian et al., 2000). A follow-up study in which the porcine bladder matrix was used to repair larger defects in a porcine bladder partial cystectomy model showed vascularisation and smooth cell infiltration at 22 weeks at the periphery of the implanted scaffold, but limited luminal recellularisation by the epithelium within the central regions of the porcine bladder implant (Brown et al., 2002). Porcine urinary bladder matrix, produced by mechanical delamination and mechanical removal of the serosa, muscularis and submucosal regions has also been used to augment a partial cystectomy (35% of the anterior dome) in a canine model (Boruch et al., 2010). Augmented bladders were subject to short term cyclic distension via catheterisation and were shown to be constructively remodelled at 12 weeks post-surgery, characterised by formation of a stratified epithelial lining and the presence of smooth muscle bundles within the porcine bladder matrix implant (Boruch et al., 2010).

4.1.4 Towards better models of urinary tract-biomaterial biocompatibility

Studies using large animal models of urinary tract reconstruction have not included analysis the inflammatory cell infiltration into the biological scaffold as described in rodent abdominal wall defect models (Section 1.6.3). In particular, little is known about the functional markers of macrophage phenotypes in larger animal models compared to rodents. Despite the attraction of large animal models, which can be used for more clinically relevant defect size models to infer functional properties of biological scaffolds, little has been inferred regarding the cellular response to different biological scaffolds at different implantation sites. Therefore these large animal models can only be used to speculate the human urinary tract tissue response to the biological scaffolds, but in a more

size relevant model. Emphasis should be made on the need for better models of human tissue-biomaterial interactions in order to determine the biocompatibility of biomaterials for use in the clinic. Development of *in vitro/ex vivo* models using relevant human tissues will give a greater insight into the tissue-specific human cell interaction with biomaterials that have potential clinical applications and reduce the number of animal implantation studies used for medical device safety testing or biocompatibility testing.

4.2. Chapter aim

The aim of this chapter was to investigate the human tissue response to the porcine bladder biological scaffold through development of an *ex vivo* biomaterial-tissue interface model. These studies were based on the supposition that it was possible to produce an organ culture/biological scaffold model to examine the early cellularisation events *ex vivo*.

4.3 Objectives

Specific objectives of this chapter were to:

a) Establish a biomaterial-organ culture model by maintaining fresh porcine urinary tract tissue and biomaterial juxtaposed in culture.
b) Adapt the biomaterial-organ culture system to incorporate surgically-excised human urinary tract tissue.
c) Determine the cellular events entrained at the biomaterial-tissue interface during a short-term period (11 days) by investigating changes in cell localisation and expression of functional cell markers over time, with focus on mononuclear phagocyte-associated markers.
d) Examine the model to determine potential signalling mechanisms that were active at the *ex vivo* biomaterial-tissue interface.

4.4 Biomaterial-organ culture nomenclature

The development of a biomaterial-organ culture model allowed the formation of a biomaterial-tissue interface, where the biomaterial refers to the porcine bladder biological scaffold. The porcine bladder biological scaffold:porcine split-thickness bladder tissue organ culture is referred to as a porcine:porcine biomaterial-organ culture system. The porcine bladder biological scaffold:human ureteric tissue organ culture is referred to as a porcine:human biomaterial-organ culture system.

4.5 Experimental approach

In order to create an *ex vivo* biomaterial-tissue interface studies used fresh porcine and human urinary tract tissue, which was maintained in close apposition with porcine bladder biological scaffold for up to 11 days. In order to achieve this, a method for culturing tissue at an air-liquid interface was adapted to incorporate the porcine bladder matrix. Initial investigations optimised the approach with split-thickness porcine bladder tissue. The biomaterial-organ culture system was then adapted to incorporate 0.5cm^2 surgical resection specimens of normal human ureter tissue. A construct was created for each time point analysed i.e. three time points meant three constructs from each donor. The porcine:human biomaterial-organotypic culture model was reproduced using three donor tissues, Y1050 using decellularised porcine bladder biological scaffold batch JBU/PB21_05_09SJB and Y1129 and Y1132 using decellularised porcine bladder biological scaffold batch JBU/PB02_10_10SJB (characterised in section 3.4 of chapter three).

The porcine tissue constructs were fixed in zinc salt fixative and embedded into paraffin wax blocks. Human tissue constructs were fixed using 10% (v/v) formalin in PBSc and processed into paraffin wax in the same manner as human control tissues. The tissues were examined by histology, using standard staining and immunoperoxidase or immunofluorescence techniques using the panel of markers characterised in chapter three, to determine the functions and characteristics of the cells within the system. Immunolabelling and isotype controls were performed on control tissues for each histological procedure that used antibodies. Analysis focused on comparing the central regions of the tissue with the biomaterial-tissue interface over an 11-day time course. Where possible, observations were confirmed by immunolabelling constructs comprising of ureteric tissue from all three human donors (Table 4-1).

Changes in expression of the mononuclear phagocyte-associated markers, CD68 and CD163 were assessed semi-quantitatively using ImageJ software. Multiple sections ≥100 microns apart were cut from the biomaterial-organ culture Y1050 to obtain a total of four sections for each time point harvested. Primary antibody labelling was detected using secondary antibodies conjugated with a fluorescent probe and images captured at a set exposure for each marker. Using ImageJ, regions of analysis (ROA) were overlaid on binary images of the fluorescent micrographs to allow a defined region for quantification. The central point of the central regions of the tissue was defined based on the X-Y coordinates of the images. The biological-scaffold-tissue interface was defined using H33258 staining to demarcate the

edge of the tissue and ensure objective analysis of the marker expression. These regions were then applied to the separate immunolabelled images and the expression of the marker within the ROA determined by automated counting the number of positive areas of expression using ImageJ, referred to a 'particles'. Significant differences in temporal or spatial number of positive areas of CD68 and CD163 expression was determined using the Mann-Whitney U test.

To determine if selected medium supplements contributed to the cell phenotypes observed in the porcine:human biomaterial-organ culture constructs, the constituents of the organ culture medium were altered. Biomaterial-organ culture constructs assembled using ureteric tissue from donor Y1083 and decellularised porcine bladder biological scaffold batch JBU/PB02_10_10SJB were cultured on Waymouth's medium minus ferrous sulphate. Biomaterial-organ culture constructs assembled using ureteric tissue from donor Y1093 and decellularised porcine bladder biological scaffold batch JBU/PB02_10_10SJB were cultured over Waymouth's medium plus or minus hydrocortisone hemisuccinate. The tissue constructs were cultured for 11 days before fixing and processing for histological analysis and immunolabelling was performed using selected markers (Table 4-2). Due to constraints on tissue size, Y1093 porcine:human biomaterial-organ culture constructs could only be assembled for harvesting at two time points.

4.6 Results: Porcine:porcine biomaterial-organ culture system

The biological scaffold-organ culture system was initially established and optimised by inserting a segment of split-thickness porcine urinary bladder tissue into a segment of the porcine bladder biological scaffold. The constructs, one for each time point analysed, were cultured at an air-liquid interface over complete Waymouth's medium on the porous membrane of a six well plate well insert (Figure 4-1).

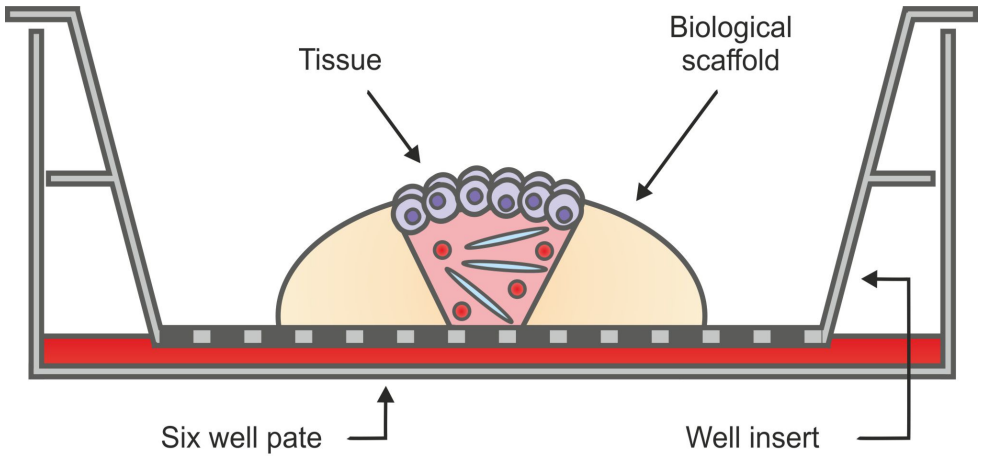

Figure 4-1. Schematic diagram of the biomaterial-organ culture system. Urinary tract tissue was inserted within the porcine bladder biological scaffold and cultured for up to 11 days.

The apical aspect of the constructs showed the yellow colour of the tissue surrounded by the white porcine bladder biological scaffold giving the constructs a 'fried egg' appearance (Figure 4-2).

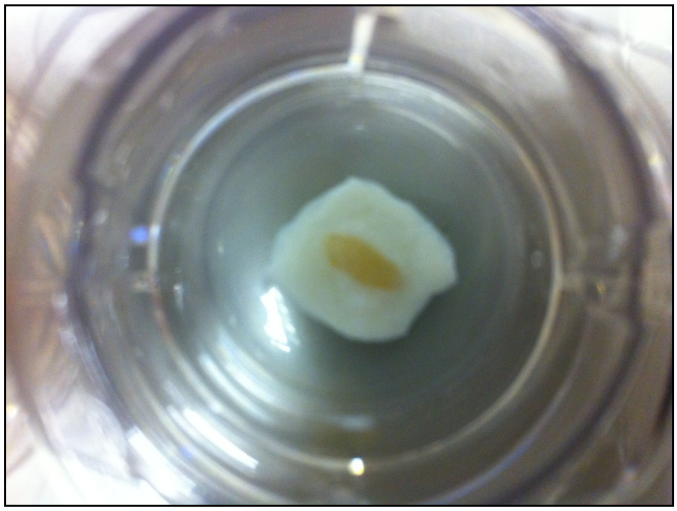

Figure 4-2. Photograph of the apical aspect of the porcine:porcine biomaterial-organ culture construct within the culture well insert. Porcine split-thickness tissue appears yellow in colour and is surrounded by the white biological scaffold. For scale, the base of the well insert has an effective growth are of 4.2cm^2. Constructs were cultured at an air-liquid interface over complete Waymouth's medium at 37°C in a humidified atmosphere of 5% (v/v) CO_2 in air before fixing and processing for histological analysis.

A whole section slide scan of a histological section of the porcine:porcine biomaterial-organ culture construct harvested at day 11 illustrated the organisation of the constructs following processing. The 'live' component of the organ culture system was observed centrally and was flanked either side by porcine bladder biological scaffold producing two, *ex vivo* biomaterial-tissue interfaces (Figure 4-3). The epithelial cells of the porcine bladder tissue could be observed covering the surface of the porcine bladder biological scaffold indicating that the cells had migrated from the porcine bladder tissue onto the scaffold during the culture period (Figure 4-3 - arrows).

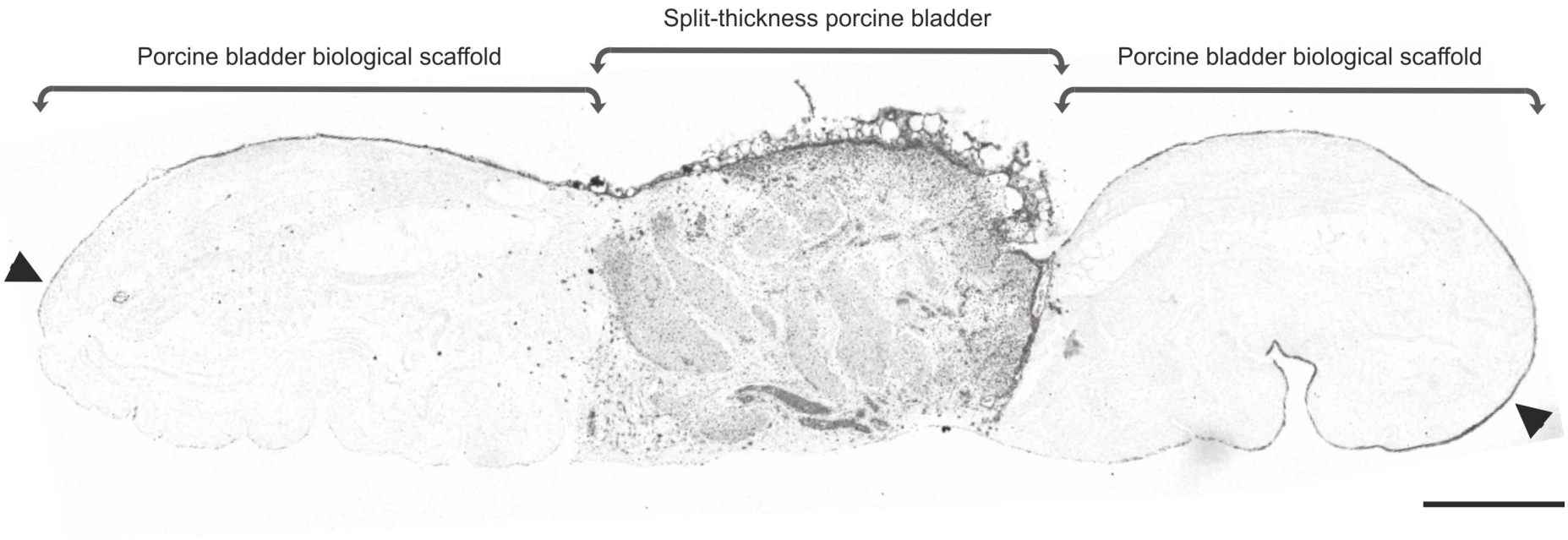

Figure 4-3. Greyscale image of a whole section slide scan of a biological scaffold-porcine bladder tissue section. Porcine split-thickness bladder tissue was cultured within the porcine bladder biological scaffold and harvested at the day 11-time point and fixed in zinc fixative followed by histological processing. The section was immunolabelled with anti-porcine CD107a and the whole section captured on a MetaSystems slide scanner. The tissue can be seen within the central region of the section and is flanked either side by porcine bladder biological scaffold. Arrows indicate bladder epithelial cells covering the surface of the porcine bladder biological scaffold. Scale bar represents 700 microns.

4.6.1 Haematoxylin and eosin staining

Histological analysis of H&E stained sections from the porcine:porcine biomaterial-organ culture constructs harvested at days 2, 6 and 11 showed that the biomaterial-tissue interface was maintained in culture (Figure 4-4). Over this culture period, the interface became harder to distinguish. At the day 11 time point, the biomaterial-tissue interface was harder to define and cells were observed within the biological scaffold indicating that cells from the split-thickness porcine bladder 'live' component had infiltrated laterally into the porcine bladder biological scaffold. These cells had the morphology of mononuclear phagocytes, defined by kidney-shaped nuclei and a large volume of cytoplasm (Figure 4-4, D - arrows). In addition, other smaller unidentified cells were also observed within the biological scaffold at this time point (Figure 4-4, D).

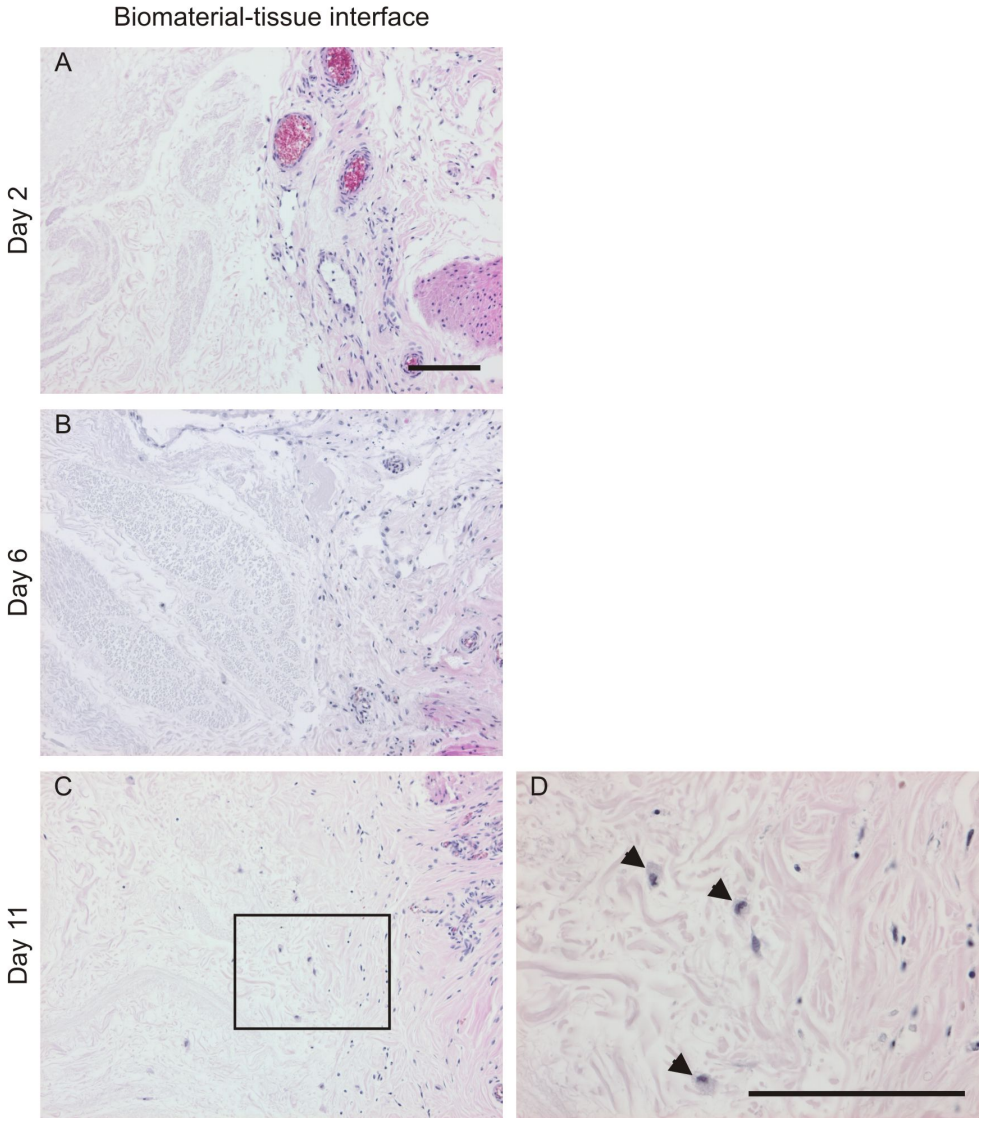

Figure 4-4. Haematoxylin and eosin staining of sections from the porcine:porcine-biomaterial organ culture model. Histological staining of sections of the porcine:porcine biological scaffold-organ culture constructs at days 2 (A), 6 (B) and 11 (C) showed a gradual increase of cells within the biological scaffold. Box on image C highlights location of higher magnification image D at day 11. Cells present in the biological scaffold showed a mononuclear phagocyte-like morphology (D; arrows). Scale bars represent 100 microns.

4.6.2 Immunohistochemical analysis of porcine:porcine biomaterial-organ cultures

Immunohistochemistry was used to investigate if the cells with a mononuclear phagocyte-like morphology also displayed makers associated with porcine macrophages. The porcine:porcine biomaterial-organ culture system was immunolabelled with the pan porcine macrophage marker, CD107a. Immunolabelling revealed a time-dependent increase in cells expressing CD107a at the biomaterial-tissue interface and an increase of CD107a+ cells within the porcine bladder biological scaffold with increased culture time (Figure 4-5, A, C and E). By contrast, little expression of CD107a by cells with the same morphology was observed within the central regions of the split thickness porcine bladder tissue (Figure 4-5, B, D and F). Smaller CD107a+ cells were observed within the central region of the tissue at the day two time point however, the expression of CD107a in the central regions of the tissue decreased over the culture period (Figure 4-5, B, D and F).

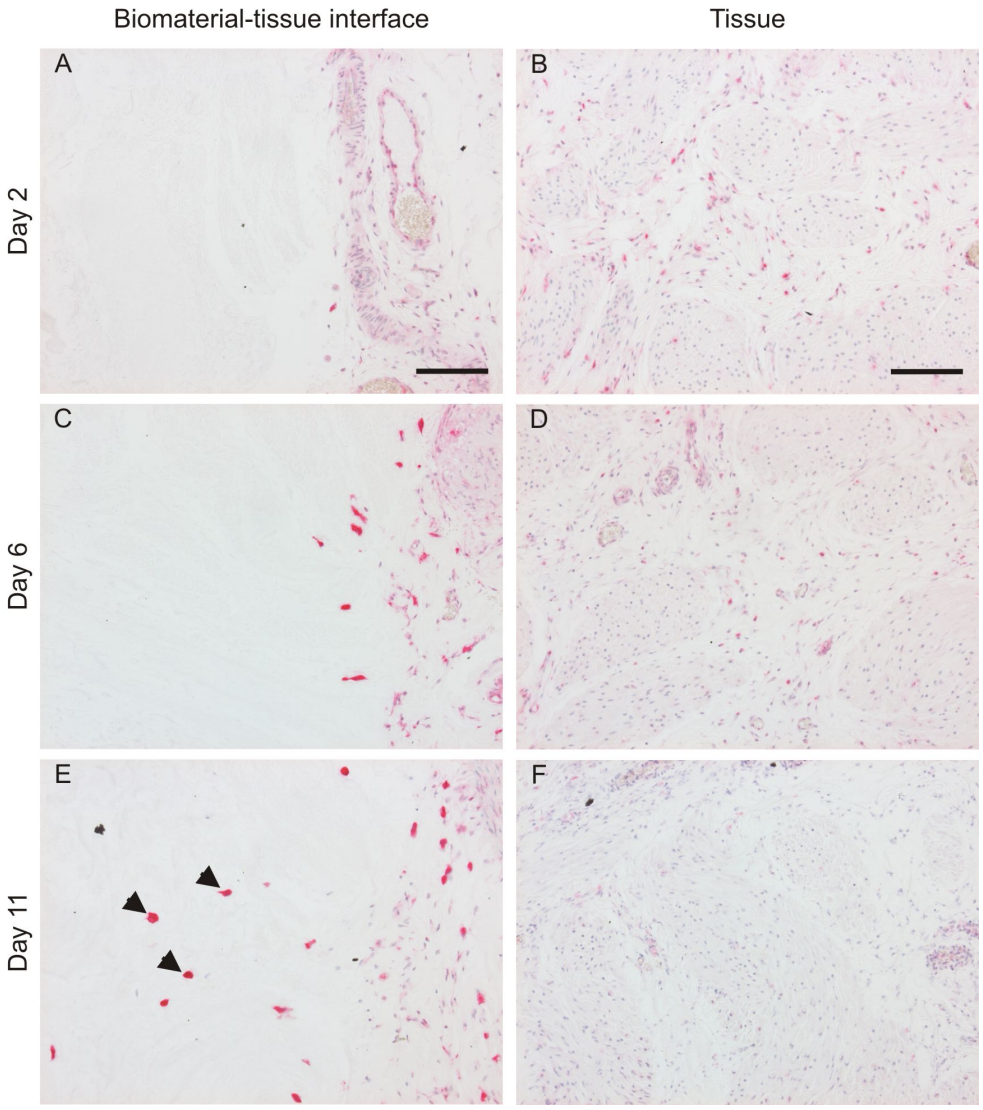

Figure 4-5. Alkaline phosphatase immunolabelling of porcine CD107a expression in tissue sections from the porcine:porcine biomaterial-organ culture system. Images were captured at the biological scaffold-tissue interface (A, C, E) and within the central regions of the tissue (B, D, F). Cells that were present in the biological scaffold labelled intensely for porcine CD107a expression (arrows). Scale bars represent 100 microns.

4.7 Results: Identification of resident or captured populations of mononuclear phagocytes in human ureter

The studies with the porcine:porcine biomaterial-organ culture system clearly demonstrate the utility of the approach. Hence studies progressed to incorporate human ureteric tissue into the model. It was however necessary to first demonstrate whether human ureteric tissue had a population of resident or captured mononuclear phagocytes.

To determine the presence of captured or resident mononuclear phagocytes within the surgically excised human ureteric tissue, freshly excised tissue from three separate donors was immunolabelled with the MAC387 antibody. Multiple images taken of each donor sample highlighted the presence of cells that labelled positive using the MAC387 antibody within the vasculature and stromal regions of the urinary tract tissues (Figure 4-6).

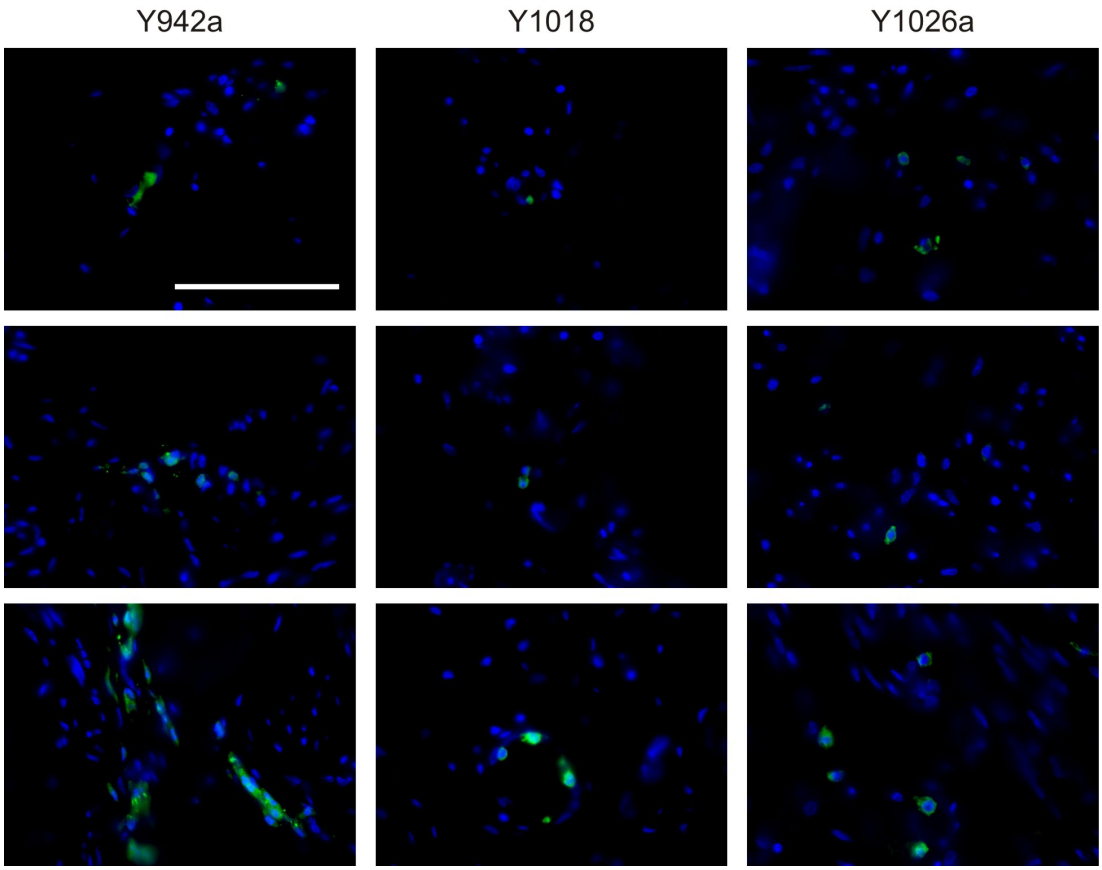

Figure 4-6. Immunolabelling of tissue sections from three separate excised human ureter samples Y492a, Y1018 and Y1026a using the MAC387 antibody. Three images were captured from each donor. MAC387 labelling is indicated by green. H33258 staining is indicated by blue. Scale bar represents 100 microns.

4.8 Results: Porcine:human biomaterial-organ culture model

The 'live' component of the biological scaffold-organ culture system was exchanged to incorporate human urinary tract tissue instead of split-thickness porcine bladder tissue. The constructs were cultured at an air-liquid interface as shown in Figure 4-1 and harvested at days 2, 6 and 11 for histological analysis. The experimental procedure was repeated in three independent experiments using tissue from three donors. Three constructs were created from each donor tissue for harvest at three time points. Where possible, IHC was performed on constructs from more than one donor. Immunolabelling of tissue sections from the porcine:human organ culture systems is summarised in Table 4-1.

Table 4-1. Marker expression investigated in donor ureter tissues

Antigen	Biomaterial-organ culture donor tissue code		
	Y1050	Y1129	Y1132
MAC387	✓	✓	
CD68	✓	✓	✓
HLA-DR		✓	✓
CD3		✓	
CD80		✓	✓
CD163	✓	✓	✓
αSMA		✓	
CD34		✓	
CD117			✓
Arginase I	✓		
CD36		✓	✓
Glucocorticoid receptor		✓	
PPARγ		✓	✓
Ki67		✓	

To determine the potential effects of selected components of the complete Waymouth's medium, constituents of the medium were omitted. Porcine:human biomaterial-organ culture constructs using tissue from donor Y1083 were cultured over Waymouth's medium in the absence of ferrous sulphate. Porcine:human biomaterial-organ culture constructs using tissue from donor Y1193 were cultured over Waymouth's medium in the presence or absence of hydrocortisone hemisuccinate. Investigation into the effects of selected medium supplements on the expression of selected markers using ureteric tissue from donors Y1083 and Y1193 is summarised in Table 4-2.

Table 4-2. Marker expression investigated in donor ureter tissues cultured on modified Waymouth's medium

Antigen	Biomaterial-organ culture donor tissue code	
	Y1083	Y1193
CD68		✓
CD163	✓	✓
PPARγ		✓
Glucocorticoid receptor		✓

4.8.1 Haematoxylin and eosin staining

Analysis of H&E stained tissue sections from the porcine:human biomaterial-organ culture constructs Y1050, showed cells infiltrating the biological scaffold from the human tissue at the day 11 time point. The cells bridging the biomaterial-tissue interface had an elongated morphology. Small cells with a round morphology were also observed within the biological scaffold at the day 11 time point (Figure 4-7)

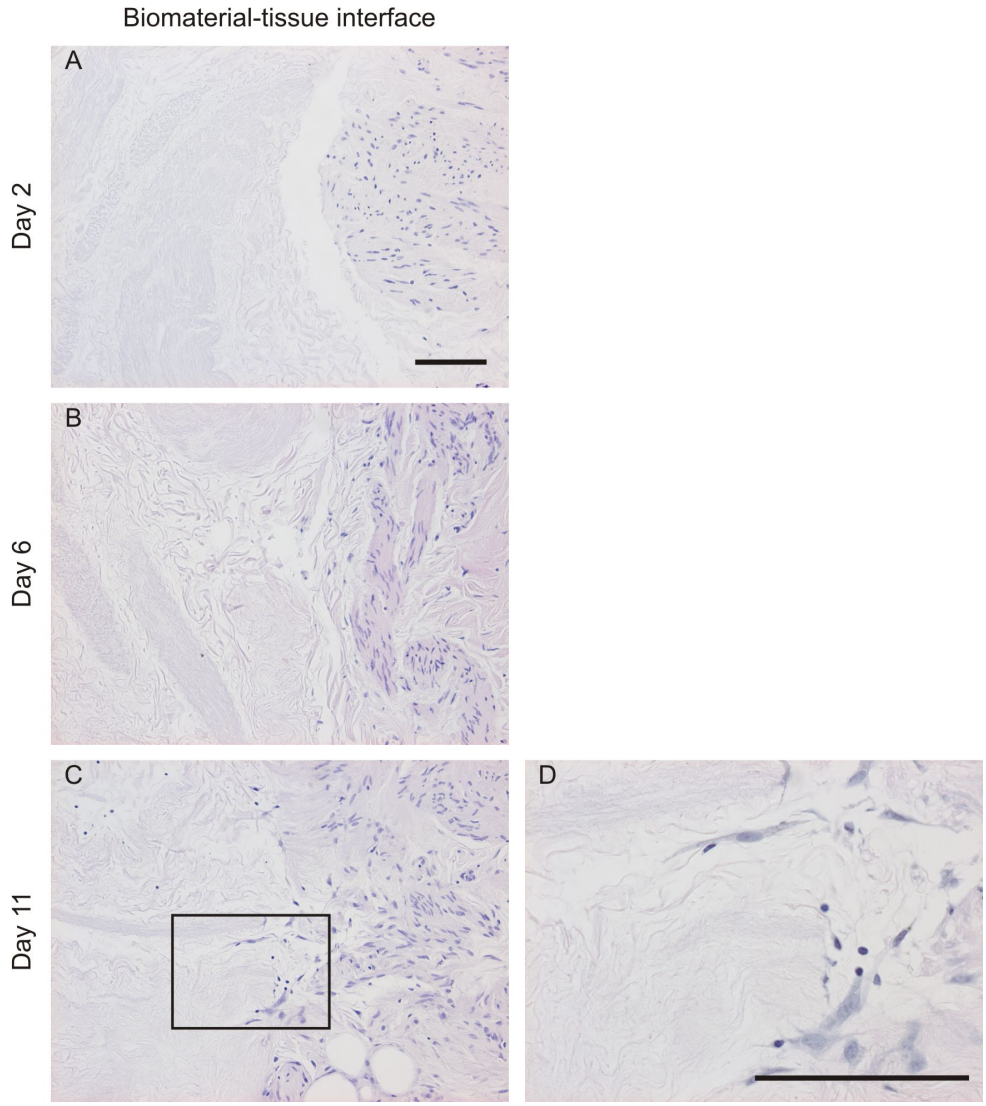

Figure 4-7. Haematoxylin and eosin stained histological sections from biological scaffold-human organ culture system using human ureter Y1050. Micrographs show the biomaterial-tissue interfaces on day 2 (A), day 6 (B) and day 11 (C). Box on image C highlights location of higher magnification image D. Scale bars represent 100 microns.

4.8.2 Immunolabelling of mononuclear phagocyte-associated markers

In order to determine the localisation of mononuclear phagocytes within the porcine:human biomaterial-organ culture system, immunolabelling with the MAC387 antibody was performed and the biomaterial-tissue interface and the central regions of the tissue investigated (Figure 4-8).

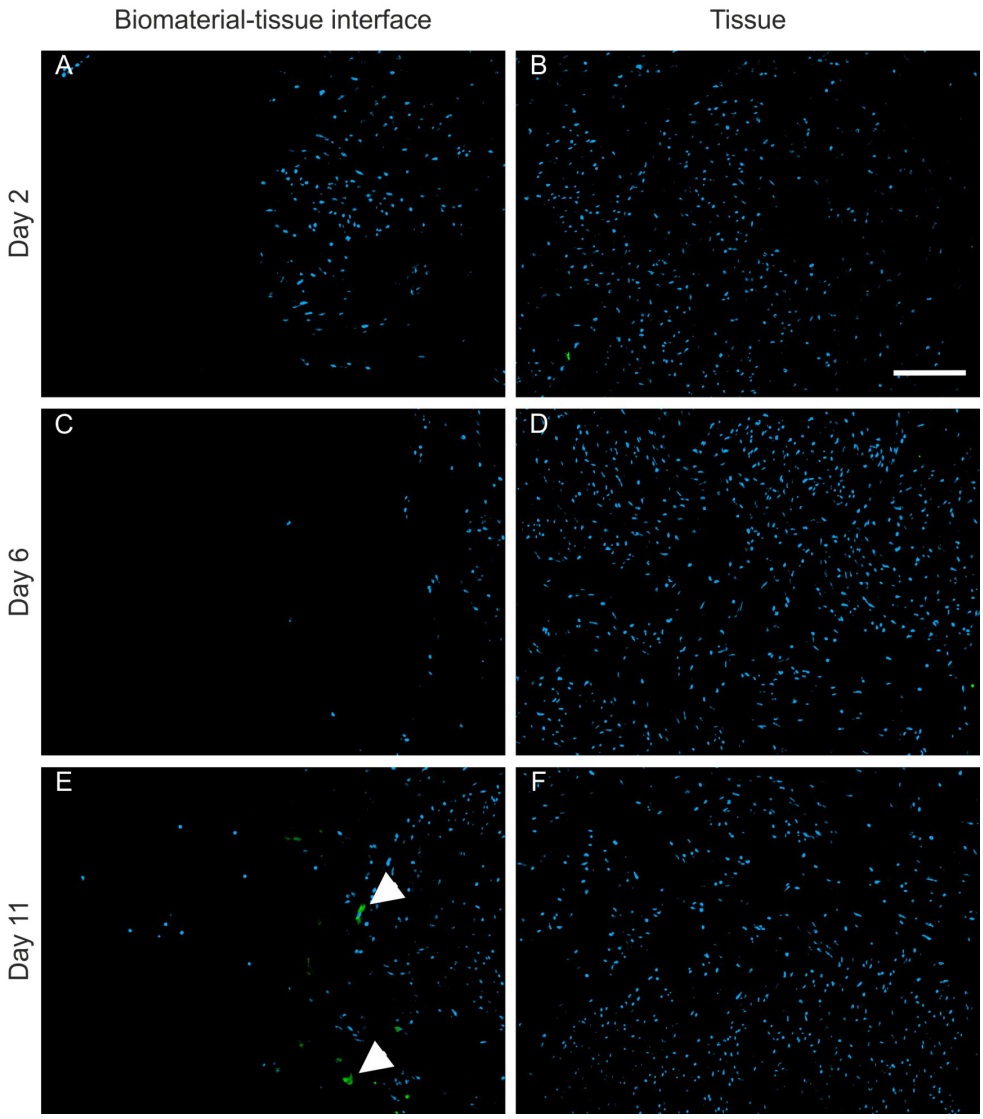

Figure 4-8. Fluorescent immunolabelling of tissue sections from the porcine:human biomaterial-organ culture system using human ureter Y1050 with the MAC387antibody. The biological scaffold-tissue interface is shown in micrographs A, C and E and the central regions of the tissue are shown in micrographs B, D and F. Labelling with MAC387 (green and arrows) was observed at the biological scaffold-tissue interface at day 11. H33258 staining is shown in blue. Scale bars represent 100 microns.

Immunolabelling of sections of the constructs with MAC387 did not show intensively labelled cells at days two or six at the biological scaffold-tissue interface (figure 4-8). A single, weakly positive cell was observed within the central region of the tissue at the day two time point (Figure 4-8, B) however, no MAC387 labelled cells were observed within the central region of the tissue at the day six time point (Figure 4-8, D). Immunolabelling using MAC387 showed labelled cells at the interface between the porcine bladder biological scaffold and the human ureteric tissue at the day 11 time point (Figure 4-8, E). These cells were not observed within the central region of the tissue at the same time point (Figure 4-8, F). This observation was confirmed in the porcine:human-biomaterial organ culture constructs using tissue from donor Y1129 (Appendix III-I). Immunolabelling of tissue sections of the day 11 biological scaffold-organ culture constructs from donor Y1129 with MAC387 showed labelled cells at the biological scaffold-tissue interface and within the biological scaffold (Appendix III-I). High magnification images of the biological scaffold-tissue interface of tissue obtained from donor Y1129 showed cells labelled with MAC387 had an elongated mononuclear phagocyte-like morphology (Figure 4-9).

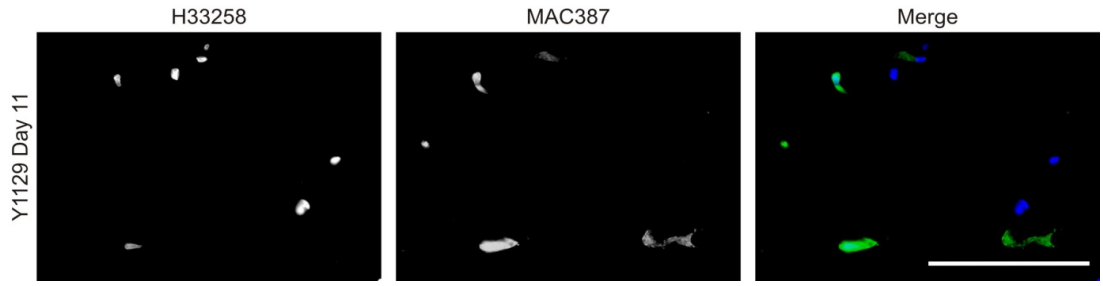

Figure 4-9. High magnification images of MAC387 labelling on porcine:human biomaterial-organ culture construct Y1129 at day 11. The tissue is located to the right of the photomicrographs. Positive cells were observed within the biological scaffold. Grey scale images of H33258 staining and MAC387 labelling were combined to produce merged image. Scale bar represents 100 microns.

The pan-macrophage marker CD68 was also evaluated. Fluorescent immunolabelling for CD68 expression on tissue sections from porcine:human biomaterial-organ culture constructs Y1050 showed an increase in CD68 positive cells at the biological scaffold-tissue

interface and within the biological scaffold. By contrast, no CD68 immunolabelling was observed within the central regions of the tissue at any time point (Figure 4-10). These observations were confirmed with the porcine:human-biomaterial organ culture constructs in an independent experiment using tissue from donor Y1129 (Appendix III-II).

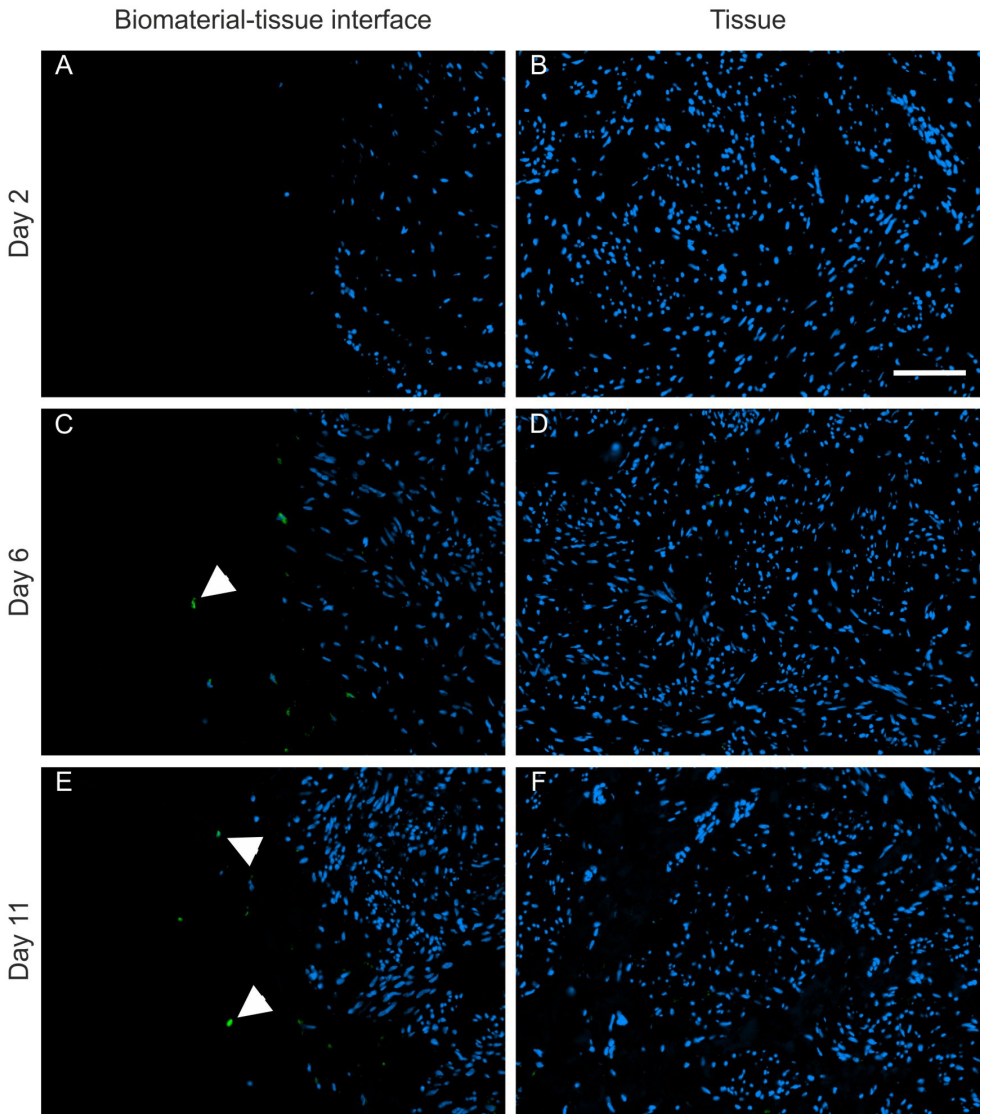

Figure 4-10. Fluorescent immunolabelling of CD68 expression in the porcine:human biomaterial-organ culture system using donor human ureter Y1050. The biological scaffold-tissue interface is shown is micrographs A, C and E and the central regions of the tissue are shown in micrographs B, D and F. CD68+ cells were observed at the biological scaffold-tissue interface at days 6 and 11 only (green and arrows). H33258 staining is shown in blue. Scale bars represent 100 microns.

The presence of CD68+ cells at the biological scaffold-tissue interface and within the biological scaffold at day 11 was confirmed using donor tissue Y1132 in an independent experiment using immunoperoxidase as the detection method (Figure 4-11).

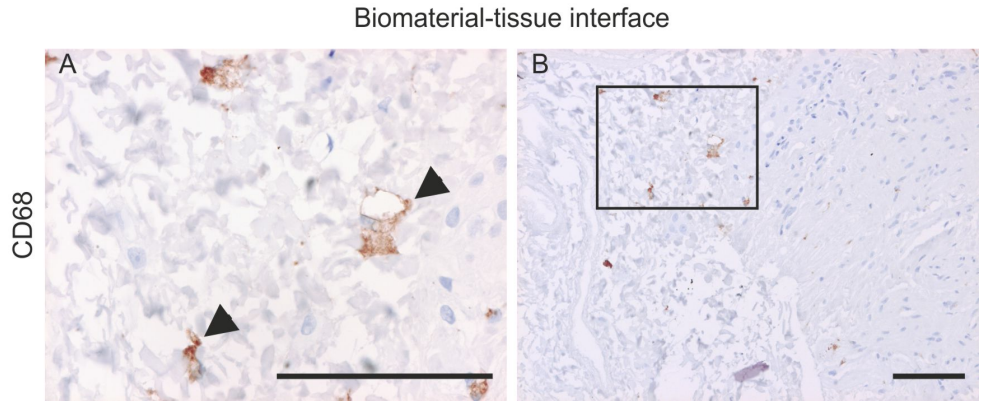

Figure 4-11. Detection of CD68+ cells present within the biological scaffold and at the interface between the biomaterial and the tissue at the day 11 time point in the porcine:human biomaterial-organ culture using tissue from donor Y1132. Black box on image B highlights location of higher magnification in image A. Arrows on image A highlights CD68+ cells within the biological scaffold. Scale bars represent 100 microns.

4.8.2.1 Quantification of mononuclear phagocyte-associated marker expression in the porcine:human biomaterial-organ culture system

The expression of CD68 at the biomaterial-tissue interface was quantified to determine if the temporal or spatial expression of CD68 was significantly different and if the pattern of CD68 expression was consistent throughout the whole construct. The methodology of quantification of binary version of fluorescent images is shown in Figure 4-12. Regions of analysis (ROA), a quarter of the width of the whole image diameter and the complete height of the image were defined at the biological scaffold-tissue interface based on H33258 nuclei staining. The central region of interest was defined using the X-Y coordinates of the image. Histological analysis resulted in only partial capture of some cells. Captured positive cells were analysed as 'particles' using the image J software, which allowed quantification of expression using parameters set by the software, removing bias from the analysis. These regions of interest were then applied to the separated images of immunolabelled antigen and the number of positive 'particles' quantified automatically

(Figure 4-12). This process was repeated for four separate images taken from four sections >100μm apart within a biological scaffold-tissue construct, Y1050.

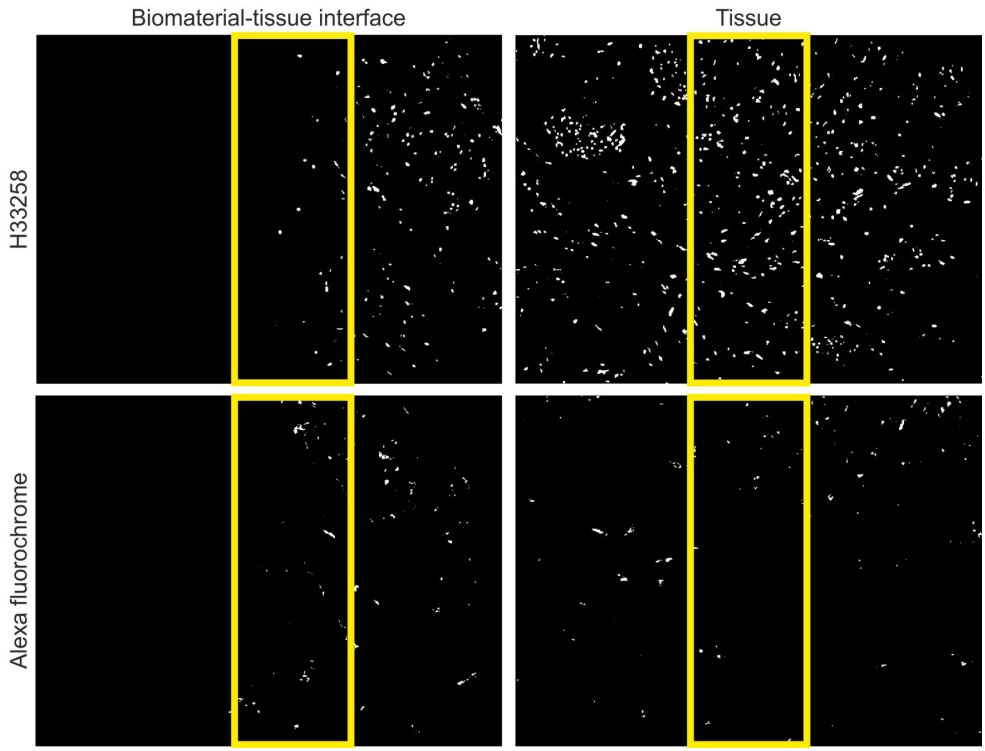

Figure 4-12. Example fluorescent image analysis of Alexa fluorochrome labelling in the porcine:human biomaterial-organ culture system using Image J software. Rectangular ROA are highlighted in yellow. ROA were applied to binary H33258 images of both the biomaterial-tissue interface and central tissue regions. The defined regions were then applied to the binary images of the macrophage marker expression detected using Alexa fluorochrome labelling at the biomaterial-tissue interface and in the central regions of the human ureter Y1050**.**

Application of this methodology of analysis was applied to CD68 expression in multiple tissue sections from the porcine:human biomaterial-organ culture construct, Y1050 (Figure 4-13). A temporal increase in mean CD68 particle counts was observed over four tissue sections at the biomaterial-tissue interface from day two to day six. The mean particle count of CD68 labelling decreased at the day 11 time point from the day six time point. The counts of CD68 immunolabelling were highly variable throughout the tissue and differences CD68 particle counts were not found to be significant.

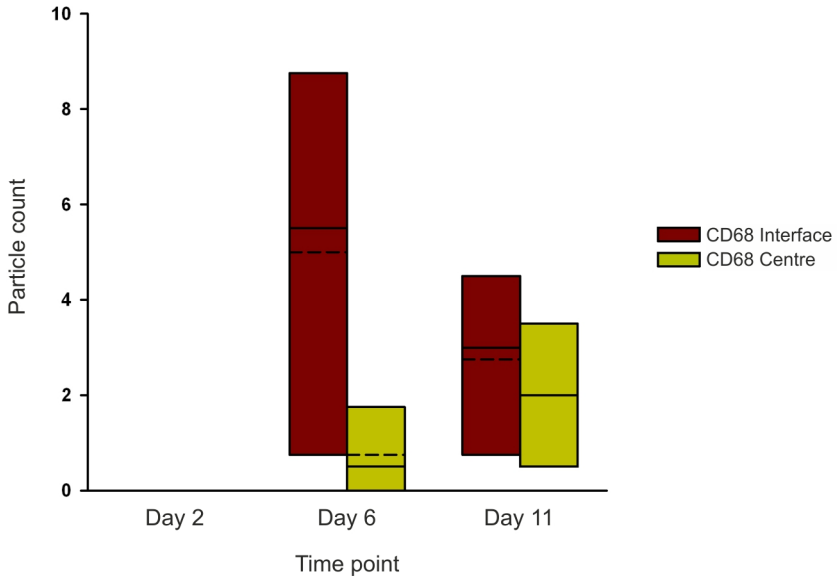

Figure 4-13. Quantification of CD68 expression at the biomaterial-tissue interface versus the central region of the tissue in the porcine:human biomaterial-organ culture system Y1050 over the 11-day time course. Data derived from n=4 sections. The top and bottom of the box plots represent the range of the data set. The solid line in the centre of each box represent the median value of each data set and the dashed line represents the mean value of each data set. No significant differences were found using the Mann-Whitney U-test.

4.8.3 Evaluation of mononuclear phagocyte-associated phenotypic markers

Mononuclear phagocytes are professional antigen presenting cells that can present antigen to lymphocytes using MHC class II. As discussed in chapter one, the modulation of MHC class II expression has also been associated with defined macrophage phenotypes therefore, sections from biological scaffold-organ culture constructs were immunolabelled for HLA-DR expression.

HLA-DR expression was observed within the central regions of the tissue and at the biological scaffold-tissue interface in the biomaterial-organ culture constructs Y1129 at days 2, 6 and 11. Maintenance of a set camera exposure for all images captured revealed a temporal, qualitative decrease in the intensity of expression of HLA-DR at the biological scaffold-tissue interface and within the central regions of tissue (Figure 4-14, A versus E).

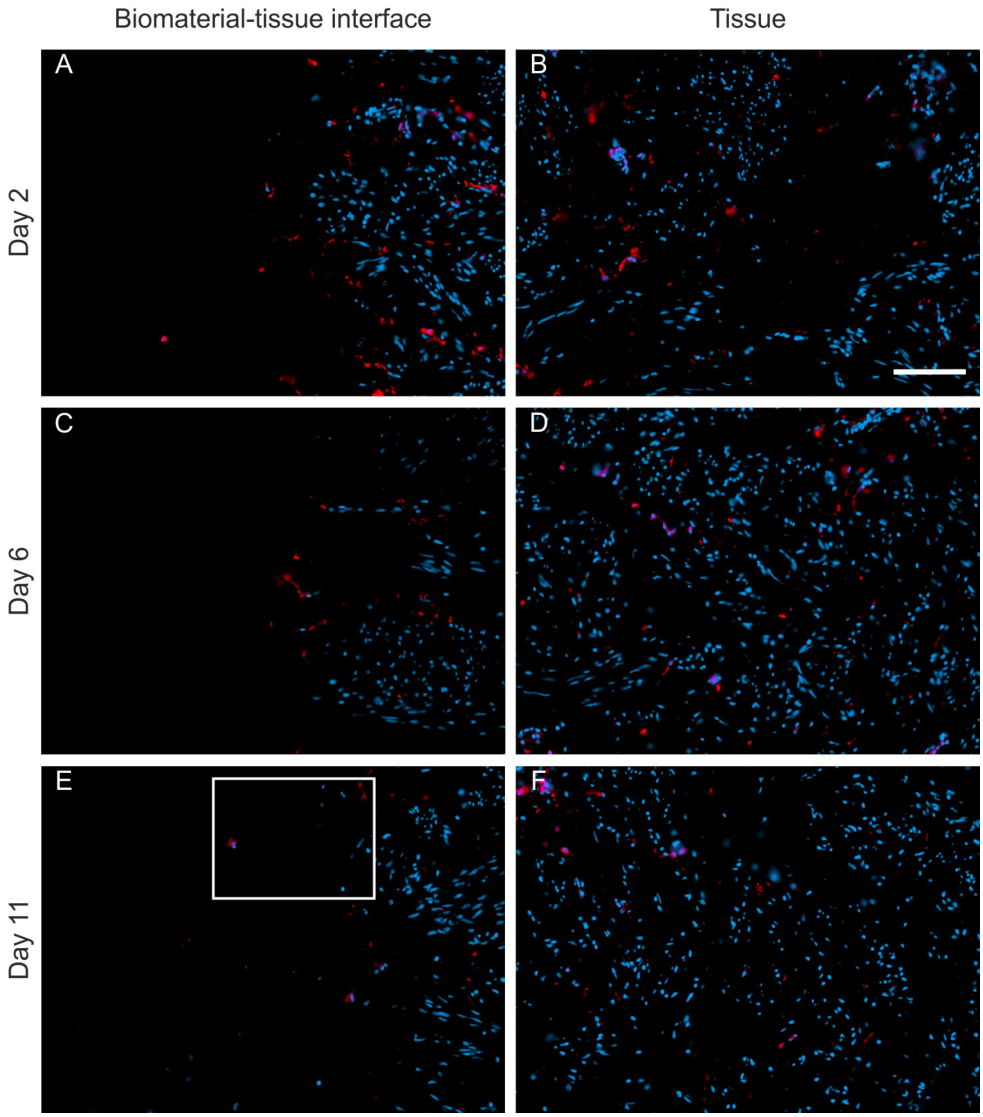

Figure 4-14. Fluorescent immunolabelling of HLA-DR expression in the porcine:human biomaterial-human organ culture system using donor human ureter Y1129. The biomaterial-tissue interface is shown is micrographs A, C and E and the central regions of the tissue are shown in micrographs B, D and F. Labelling of HLA-DR expression (red) is observed at the biomaterial-tissue interface and within the centre of the tissue at days 2, 6 and 11. H33258 staining is shown in blue. Scale bars represent 100 microns.

Higher magnification images the biological scaffold-tissue interface showed that HLA-DR+ cells were present within the biological scaffold and displayed kidney-shaped nuclei, indicative of mononuclear phagocytes (Figure 4-15).

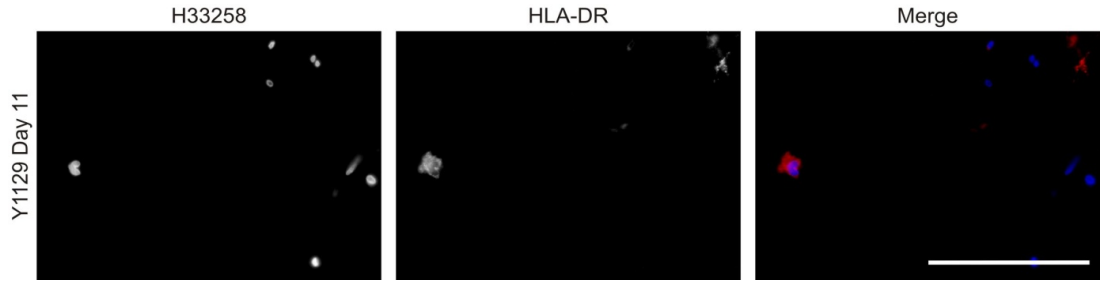

Figure 4-15. High magnification images of fluorescent immunolabelling of HLA-DR+ cells in the porcine:human biomaterial-organ culture construct Y1129 at day eleven. Image is a higher magnification image of area depicted by the white box in figure 4-14, E. The tissue is located to the right of the photomicrographs. Positive cells were observed within the biological scaffold. Grey scale images of H33258 staining and HLA-DR labelling were combined to produce merged image. Scale bar represents 100 microns.

Immunoperoxidase labelling for HLA-DR expression in tissue sections from an independent experiment using donor tissue, Y1132, showed weak HLA-DR expression by cells present at the biological scaffold-tissue interface and within the biological scaffold (Figure 4-16) supporting the observations made using donor tissue, Y1129.

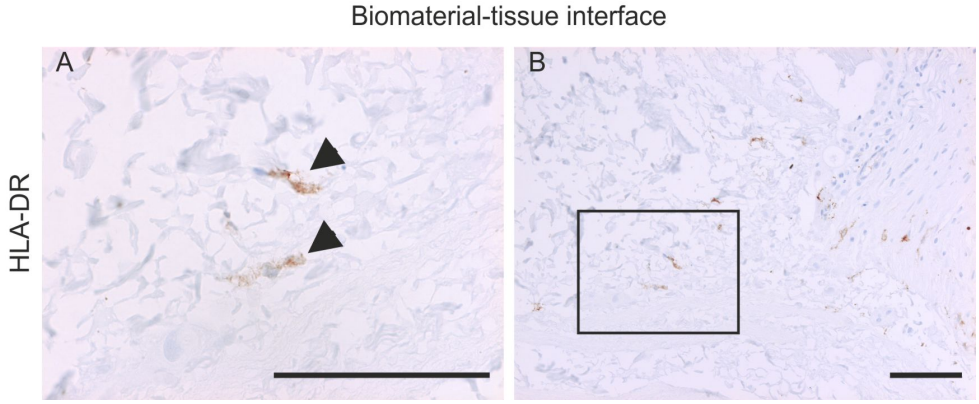

Figure 4-16. Detection of HLA-DR+ cells present within the biological scaffold and at the interface between the biomaterial and the tissue at the day 11 time point in the porcine:human biomaterial-organ culture construct Y1132. Black box on image B highlights location of higher magnification image A. Arrows on image A highlights HLA-DR+ cells within the biological scaffold. Scale bars represent 100 microns.

Immunolabelling of the antigen presenting cell co-stimulatory molecule CD80 in the porcine:human biomaterial-organ culture constructs showed no expression of CD80 throughout the culture period either at the biomaterial-tissue interface or within the central regions of the tissue using donor tissue Y1129 (Figure 4-17). The absence of CD80 expression in the culture model was confirmed in another biomaterial-organ culture system using donor tissue Y1132 (Appendix III-III).

Figure 4-17. Immunoperoxidase labelling for CD80 expression on histological sections of the biomaterial-organ culture construct Y1129. The biomaterial-tissue interface is shown is micrographs A, B, E, F, I and J the central regions of the tissue are shown in micrographs C, D, G, H, K and L. Black box on image (F and J) highlights location of the respective higher magnification image (E and I). Cells present in the biological scaffold are negative for CD80 expression (arrows). Positive control labelling was confirmed using human colon tissue as shown on chapter 3. Scale bars represent 100 microns.

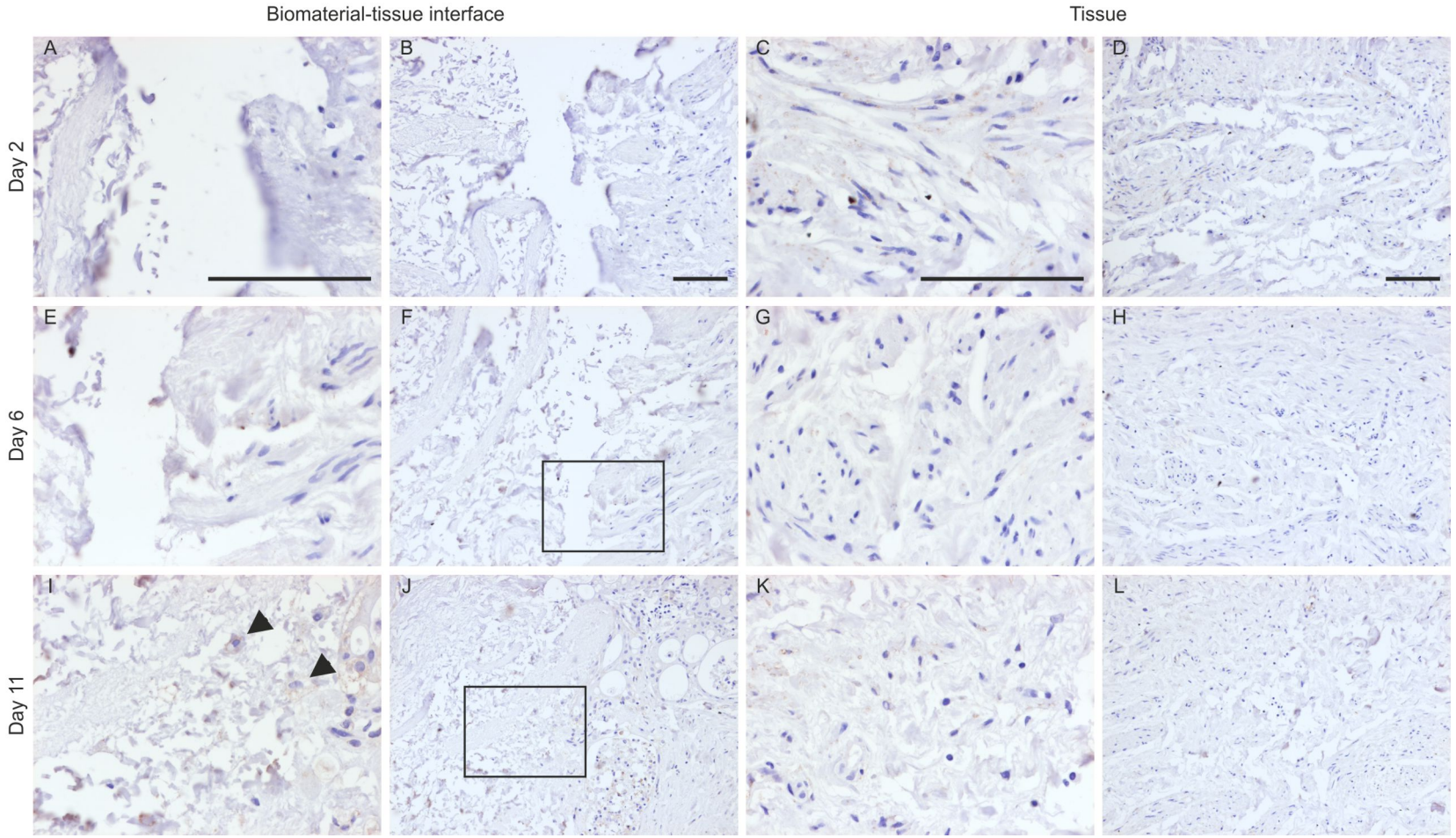
Biomaterial-tissue interface
Tissue
Day 2
Day 6
Day 11
A
B
C
D
E
F
G
H
I
J
K
L

Immunolabelling for the anti-inflammatory macrophage marker, CD163 on the porcine:human biomaterial-organ culture using donor tissue Y1050 showed CD163+ cells in the porcine bladder biological scaffold over the 11 day time course (Figure 4-18). This observation was also confirmed in constructs using tissue from donors Y1129 and Y1132 (Appendices III-IV and III-V, respectively).

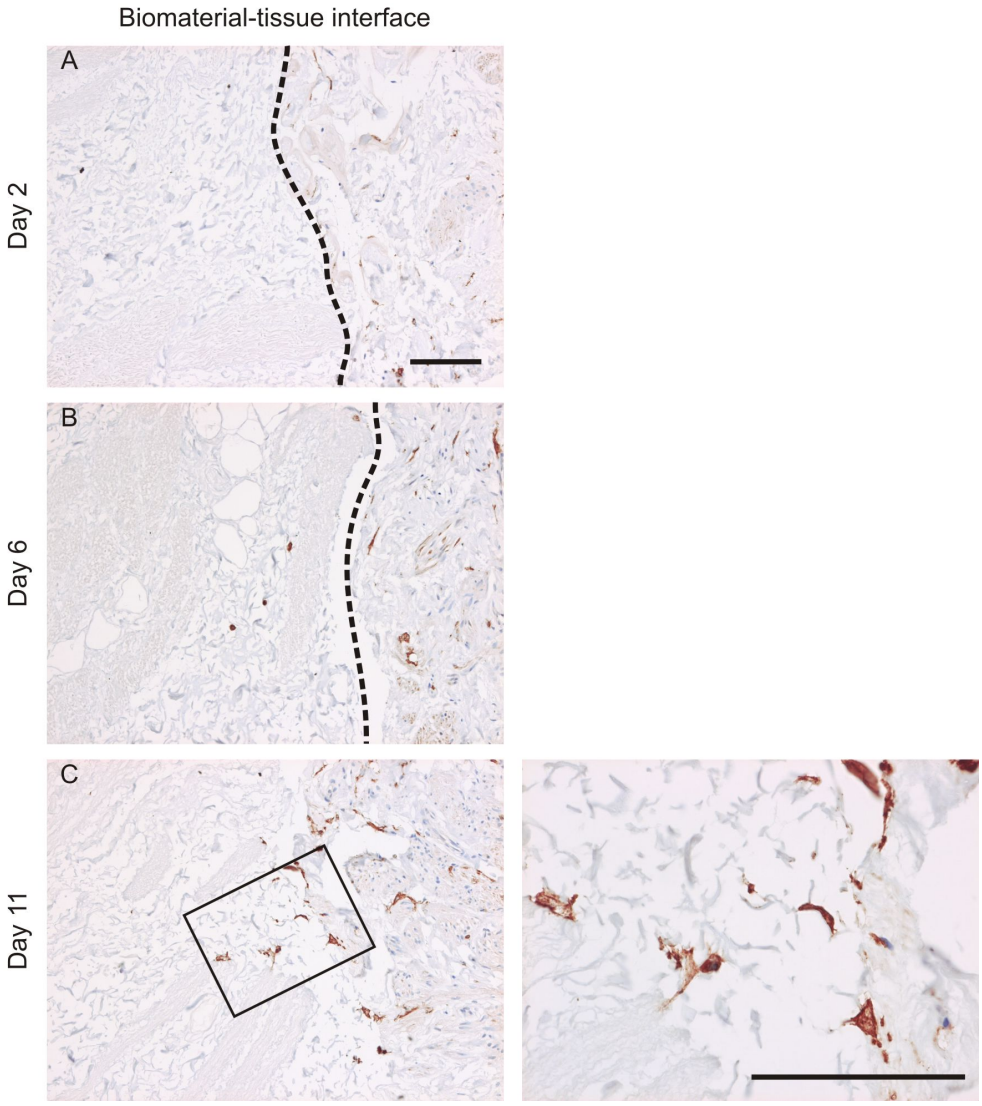

Figure 4-18. Immunoperoxidase labelling of CD163+ cells in the porcine:human biomaterial-organ culture system Y1050. Photomicrographs show biomaterial-tissue interface over the 11-day time course (A-C). Dotted line on photomicrographs A and B highlight biological scaffold-tissue interface. Black box on day 11 photomicrograph (C) indicates orientation and location of higher magnification image. Scale bars represent 100 microns.

Comparisons between the central regions of the tissue and the biomaterial-tissue interface using fluorescent immunolabelling revealed a striking upregulation in CD163 expression at the biomaterial-tissue interface versus the central region of the tissue (Figure 4-19).

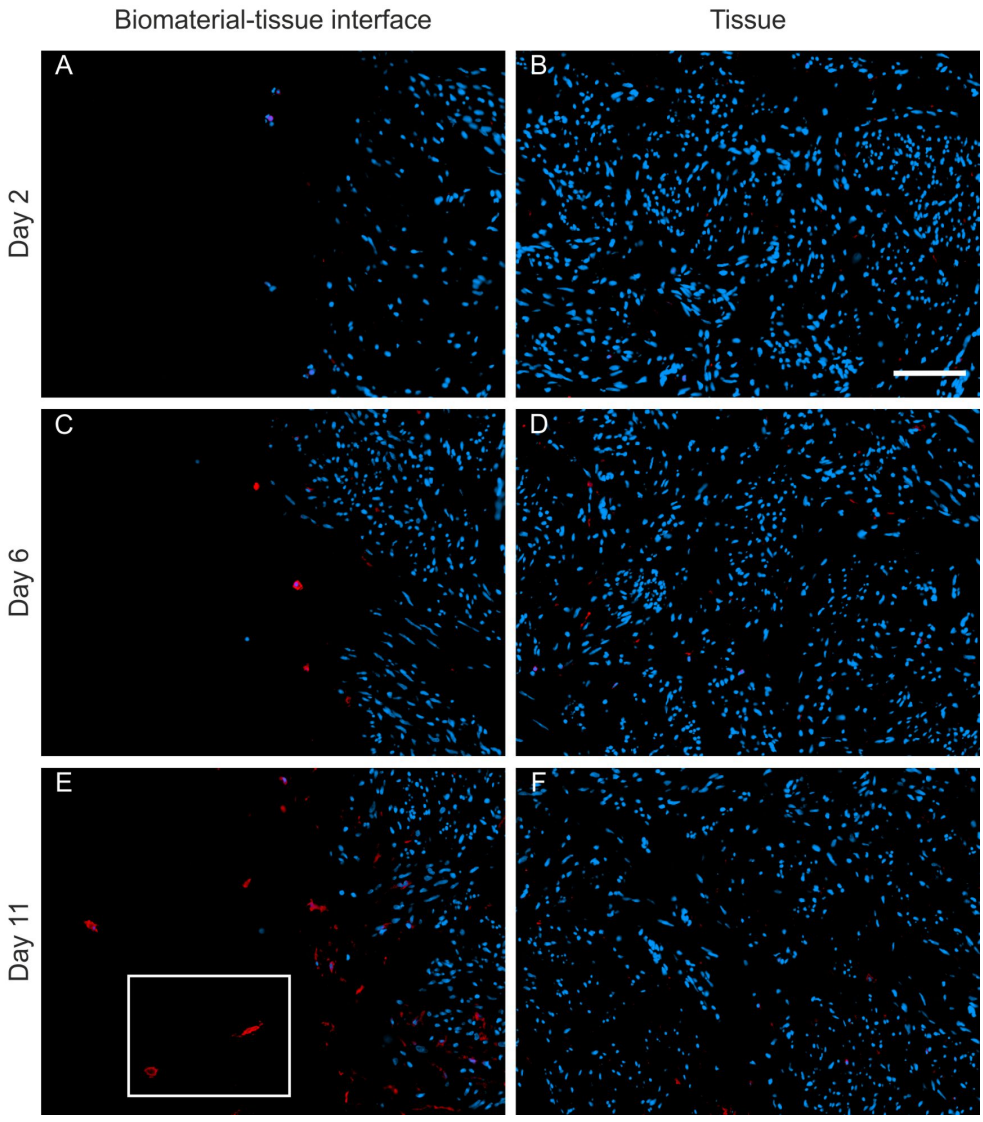

Figure 4-19. Fluorescent immunolabelling of CD163 expression in the porcine:human biomaterial-organ culture system using donor human ureter Y1050. The biological scaffold-tissue interface is shown is micrographs A, C and E and the central regions of the tissue are shown in micrographs B, D and F. CD163 labelling (red) was observed at the biomaterial-tissue interface at days 6 and 11. H33258 staining is indicated in blue. White box on image (E) highlights the presence of CD163+ cells in the biological scaffold. Scale bars represent 100 microns.

High magnification images of CD163+ cells within the biological scaffold showed that the cells had both an elongated and rounded morphology (Figure 4-20).

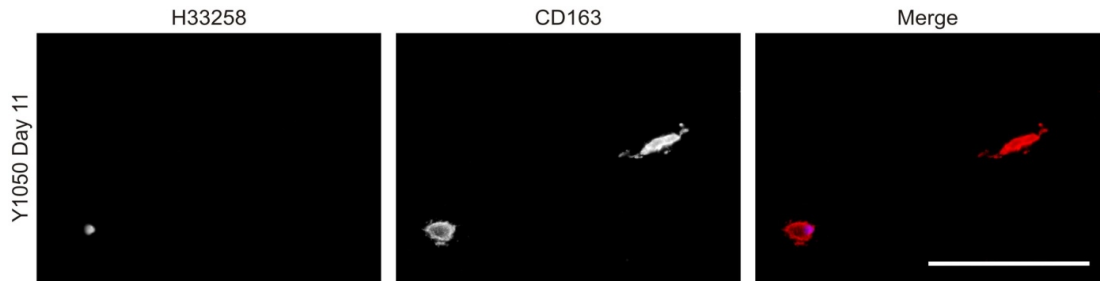

Figure 4-20. High magnification images of fluorescent immunolabelling of CD163+ cells within the biological scaffold of the porcine:human biomaterial-organ culture, using donor Y1050 highlighted in white box in Figure 4-19, E. The tissue located to the right of the photomicrographs. Positive cells were observed within the biological scaffold. Grey scale images of H33258 staining and CD163 labelling were combined to produce merged image. Scale bar represents 100 microns.

Quantification of CD163 expression at the biomaterial-tissue interface and in the central regions of tissue using ImageJ showed a significant increase ($P<0.05$) in CD163 expression at the interface between the porcine bladder biological scaffold and tissue between day two and day eleven (Figure 4-21). A significant difference ($P<0.05$) was found between the CD163 expression at the interface and CD163 expression within the central region of the tissue at the day six and day eleven time points using the non-parametric Mann Whitney U-test. There was no significant difference in CD163 expression between the central regions of the tissues at all time points sampled (Figure 4-21).

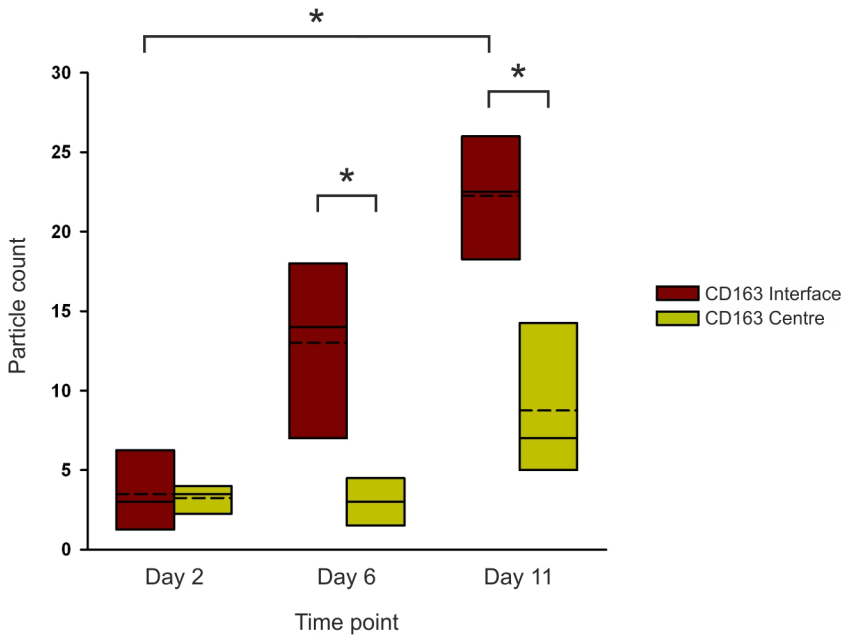

Figure 4-21. Quantification of CD163 expression at the biomaterial-tissue interface versus the central region of the tissue in the biomaterial-organ culture system Y1050 over the 11-day time course. Data derived from n=4 sections. The top and bottom of the box plots represent the range of the data set. The solid line in the centre of each box represent the median value of each data set and the dashed line represents the mean value of each data set. * represents a significant difference in the median values of $P<0.05$ by the non-parametric Mann-Whitney U test.

Serial sections of the porcine:human biomaterial-organ culture construct, Y1132 harvested at day 11 were immunolabelled for CD68 and CD163 and the biomaterial-tissue interface investigated. Investigation of the same region of the biomaterial-tissue interface showed that CD68 and CD163 were both expressed within the same regions examined (Figure 4-22). There was qualitative difference in CD68 and CD163 expression levels by immunoperoxidase analysis (Figure 4-22). CD68 expression was qualitatively weaker compared to expression on control tissue (chapter 3) and compared to CD163 expression.

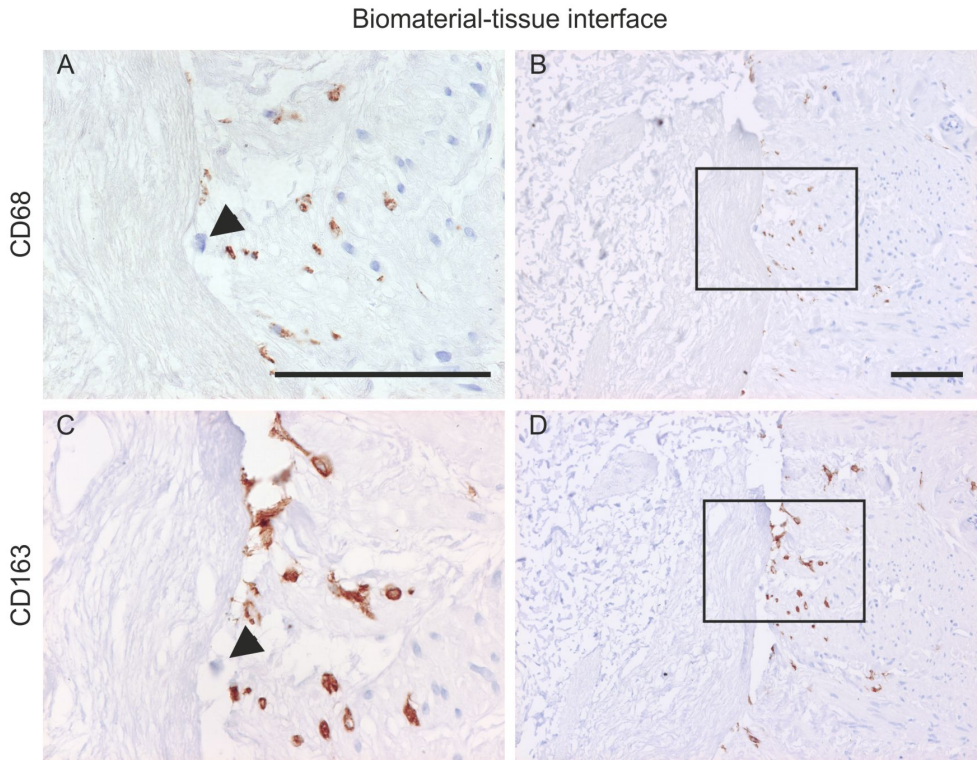

Figure 4-22. Immunoperoxidase labelling of CD68 and CD163 expression at the biomaterial-tissue interface on serial sections of the biomaterial-organ culture Y1132 at day 11. Box boxes on images (B and D) represent the respective higher magnification images (A and C). Arrow indicates the same cell on a different tissue section (A and C). Scale bars represent 100 microns.

4.8.4 Dual labelling of functional markers associated with CD163+ cells

Further investigation into the phenotype of the CD163+ cells observed in the biomaterial-organ culture constructs was performed using dual immunofluorescent labelling.

4.8.4.1 CD163 and arginase 1

Due to its association with anti-inflammatory macrophages and role in wound-healing the porcine:human biomaterial-organ culture system was labelled with arginase 1 and CD163 to determine if CD163+ cells expressed arginase 1. Arginase 1 expression was not observed throughout the biomaterial-organ culture constructs at all time points sampled (Figure 4-23) but was positive on control tissue (chapter three).

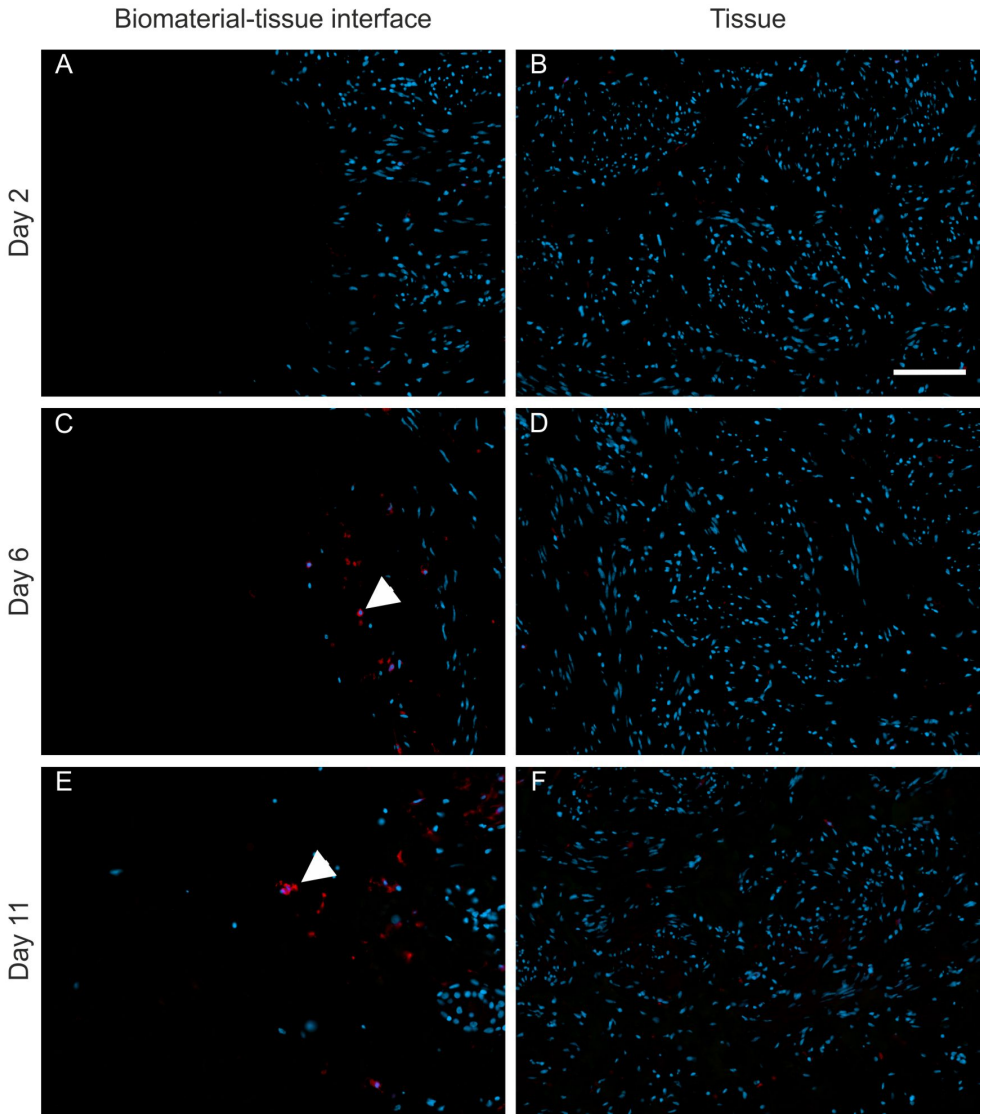

Figure 4-23. Dual fluorescent immunolabelling for CD163 and arginase 1 expression in porcine:human biomaterial-organ culture Y1050. The biological scaffold-tissue interface is shown is micrographs A, C and E and the central regions of the tissue are shown in micrographs B, D and F. Labelling for CD163 expression (red) is observed at the biomaterial-tissue interface at days 6 and 11. Arginase 1 (green) expression is not observed. H33258 staining is shown in blue. Scale bars represent 100 microns.

4.8.4.2 CD163 and CD36

Dual labelling of the scavenger receptor, CD36 with CD163 was performed to determine if CD163+ cells expressed other macrophage-associated scavenger receptors. As observed in the human spleen control tissues, immunofluorescence indicated the presence of separate populations of CD36+ and CD163+ cells. CD36+ cells were predominantly within the central regions of the tissue at day 11 (Figure 4-24, I) while a few cells at the biological scaffold-tissue interface were positive for CD36 expression at the same time point (Figure 4-24, G). CD163+ cells were dominant at the biomaterial-tissue interface at day 6 (Figure 4-24, E).

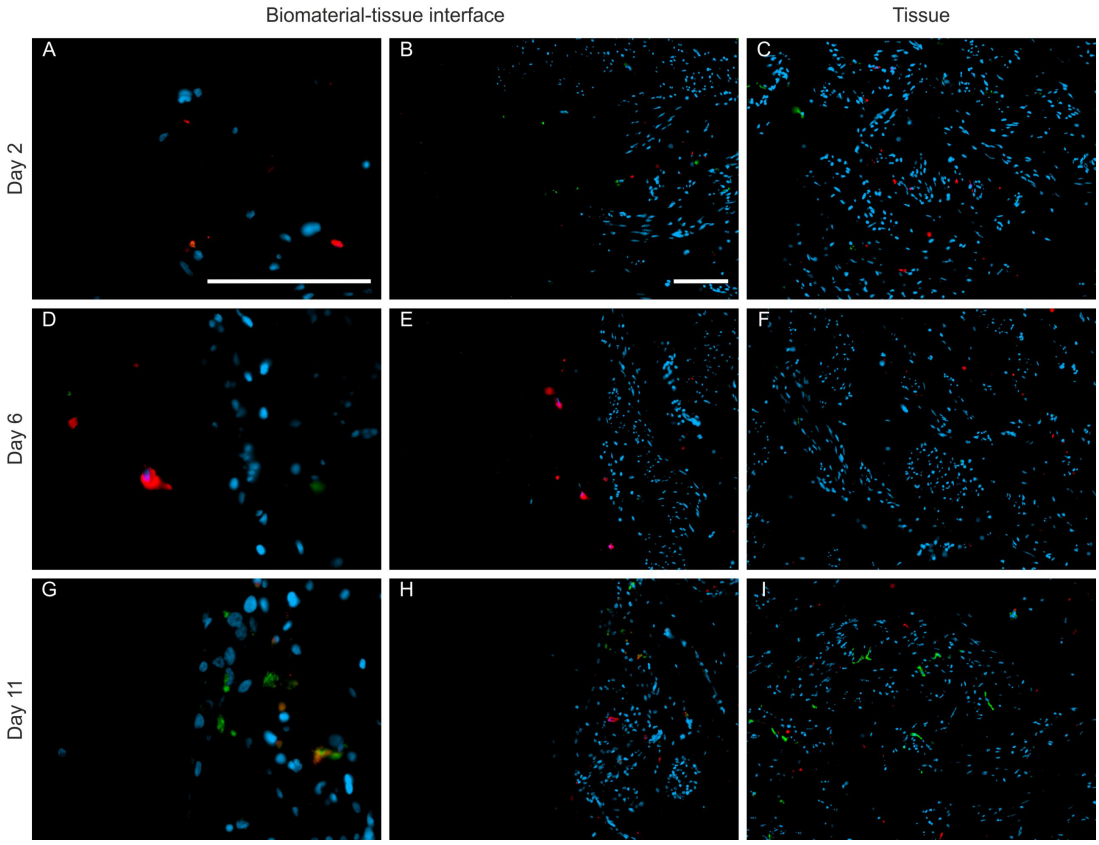

Figure 4-24. Dual fluorescent immunolabelling of CD163 and CD36 expression in biomaterial-organ culture constructs Y1129. The biomaterial-tissue interface is shown is micrographs A, B, D, E, G and H and the central regions of the tissue are shown in micrographs C, F and I. Labelling for CD163 (red) and CD36 (green) expression is observed. H33258 staining is shown in blue. Scale bars represent 100 microns.

4.8.5 Assessment of infiltration into the biological scaffold by other cells

4.8.5.1. Stromal cells

Investigation into other cell types, which potentially had the ability to infiltrate the porcine bladder biological scaffold, was performed. αSMA was investigated as a marker of stromal cells such as smooth muscle cells and myofibroblasts. Serial sections of the biomaterial-organ were immunolabelled for CD163 and αSMA to investigate the potential contribution of stromal cells in the cell infiltration of the porcine bladder biological scaffold. CD163+ cells were observed migrating into the biological scaffold (Figure 4-25). Regions of CD163 expression did not show αSMA expression by serial section (Figure 4-25). In addition, no αSMA+ cells were observed within the porcine bladder biological scaffold (Figure 4-26).

Figure 4-25. Photomicrographs of immunoperoxidase labelling of CD163 and αSMA on serial sections of the porcine:human biomaterial-organ culture Y1129. Serial section compared the αSMA and CD163 immunolabelling within the same regions of tissue. The biomaterial-tissue interface is shown is micrographs A, B, E, F, I and J the central regions of the tissue are shown in micrographs C, D, G, H, K and L. Black box highlights region of CD163 expression on image I which is negative for αSMA labelling (Image J). Scale bar represents 100 microns.

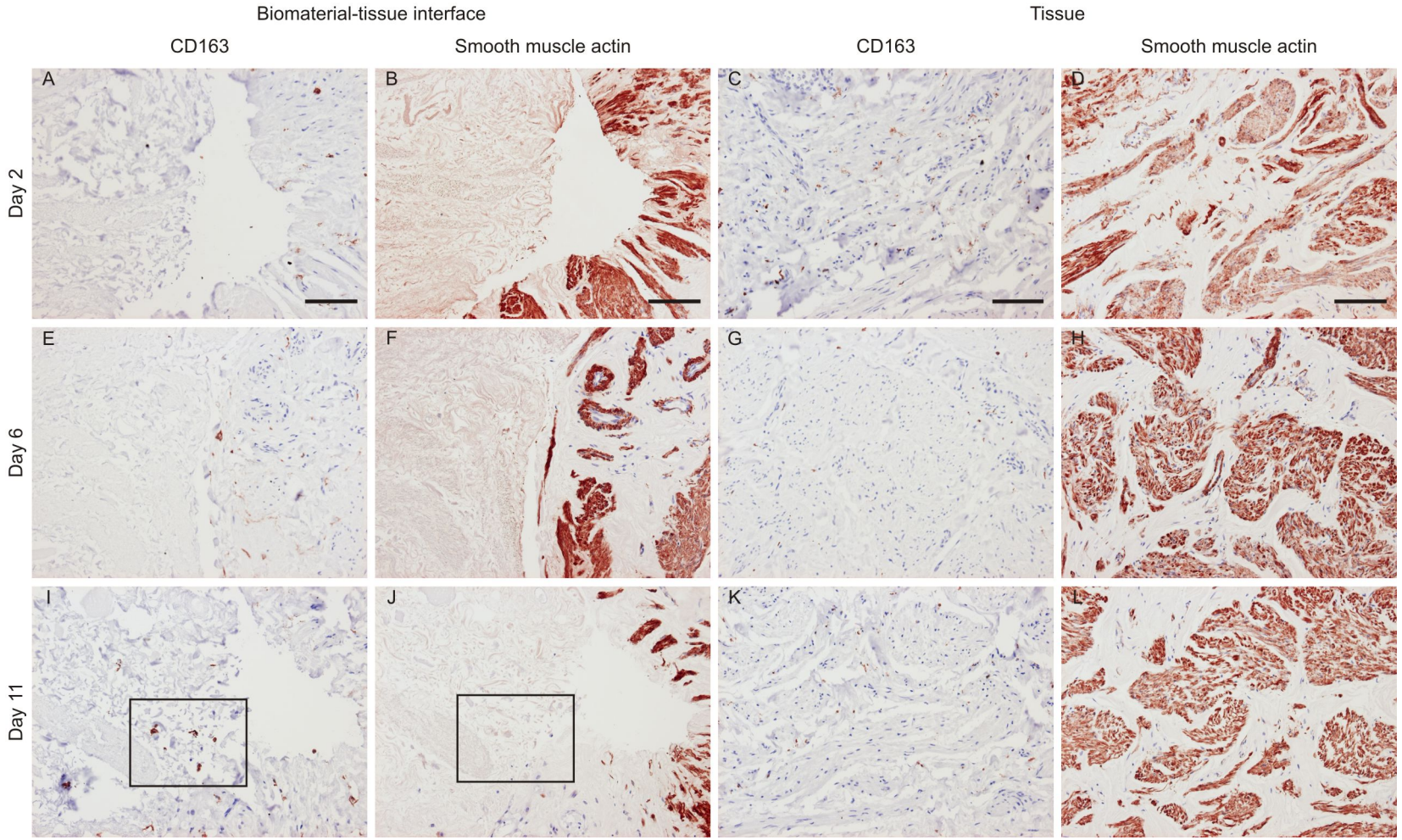
Biomaterial-tissue interface
Tissue
CD163
Smooth muscle actin
CD163
Smooth muscle actin
Day 2
Day 6
Day 11
A
B
C
D
E
F
G
H
I
J
K
L

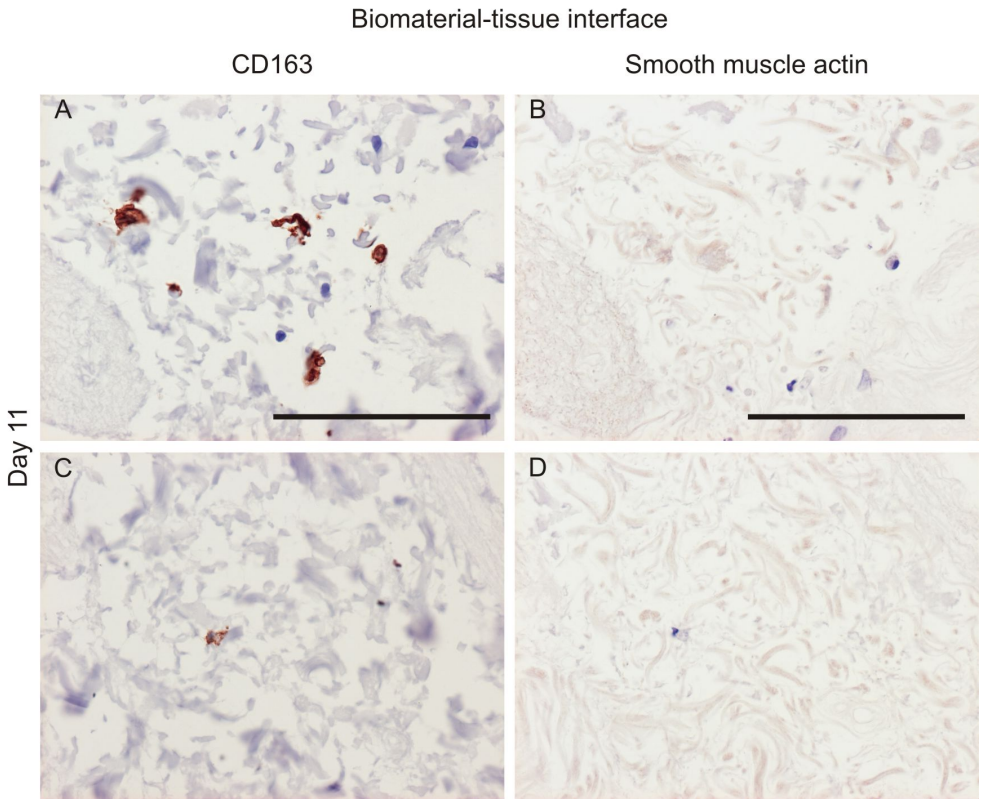

Figure 4-26. Photomicrographs of immunoperoxidase labelling of CD163 and αSMA on serial sections of the porcine:human biomaterial-organ culture system Y1129. Images A and B are high magnification images of areas outlined with black boxes in Figure 4-25, image I and J respectively. Images A and C show a CD163 positive, αSMA negative cells within the biological scaffold. Scale bars represent 100 microns.

4.8.5.2. CD3+ T-cells

To investigate if the presence of the mononuclear phagocyte-associated markers, CD68, MAC387, HLA-DR and CD163 was accompanied by the presence of lymphocytes at the biological scaffold-tissue interface, the T cell specific marker, CD3 was investigated by immunoperoxidase labelling. Immunolabelling of the biomaterial-organ culture constructs using donor tissue Y1129 showed no CD3+ T cells at the biological scaffold-tissue interface (Figure 4-27). Furthermore, CD3+ cells were only observed at the day two time point within the central regions of the tissue (Figure 4-27, C) and were not observed within constructs at later time points.

Figure 4-27. Immunoperoxidase labelling of CD3 expression on histological sections of the porcine:human biomaterial-organ culture construct Y1129. The biomaterial-tissue interface is shown is micrographs A, B, E, F, I and J the central regions of the tissue are shown in micrographs C, D, G, H, K and L. Black box on image (F and J) highlights location of the respective higher magnification image (E and I). Cells migrating from the tissue into the biological scaffold were negative for CD3 expression (arrows). Scale bars represent 100 microns.

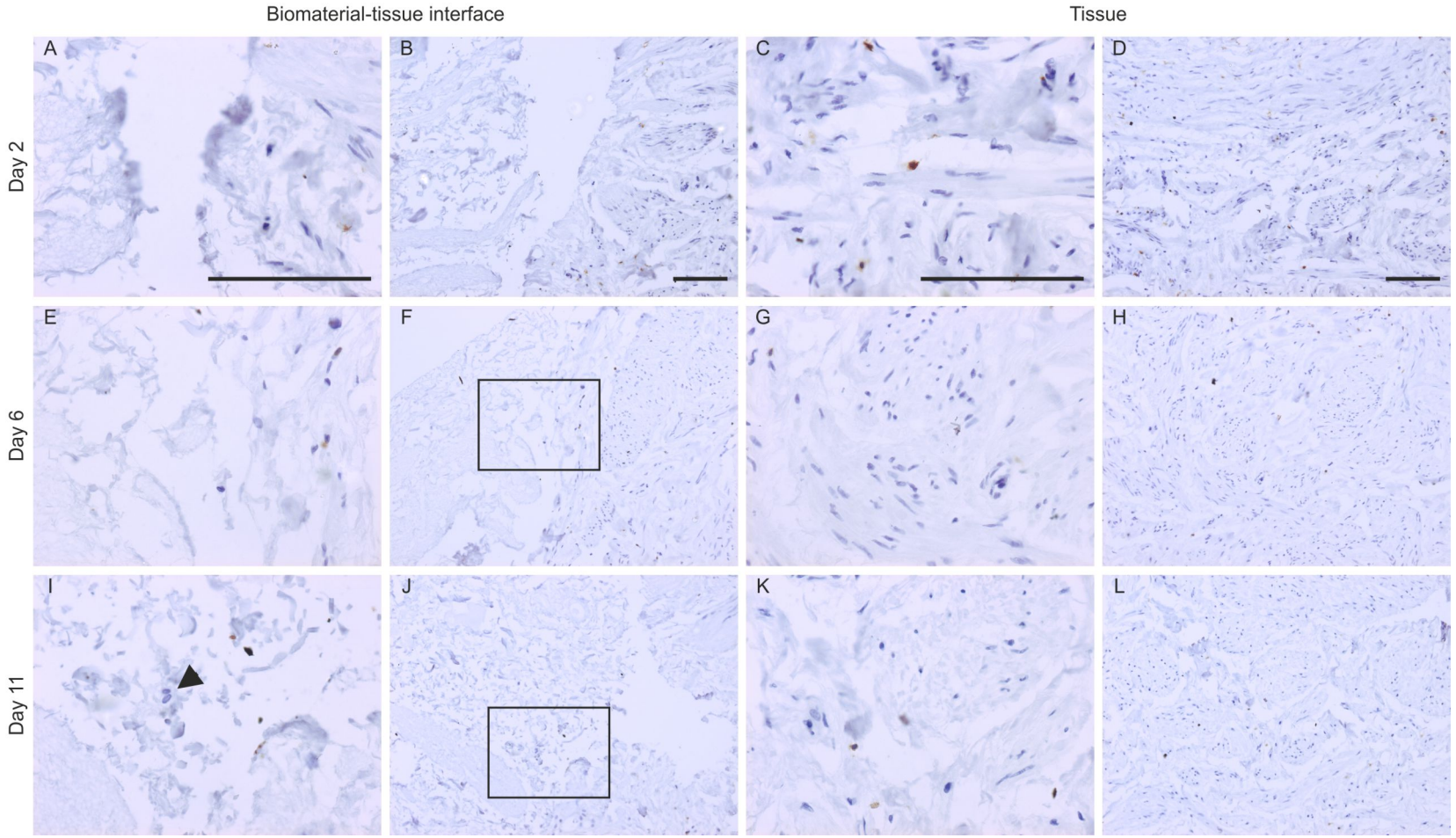
Biomaterial-tissue interface
Tissue
Day 2
Day 6
Day 11
A
B
C
D
E
F
G
H
I
J
K
L

4.8.5.3. Vascular endothelial cells

In order to determine if cells of vascular endothelial origin infiltrated the biological scaffold, the porcine:human biomaterial-organ culture Y1129 was immunolabelled for CD34 expression. The cells within the biological scaffold at days six and 11 were negative for CD34 (Figure 4-28, E and I, arrows). The central regions of the human ureteric tissue showed weak expression of CD34 by some cells within the ureter stroma (Figure 4-28, D. H and L).

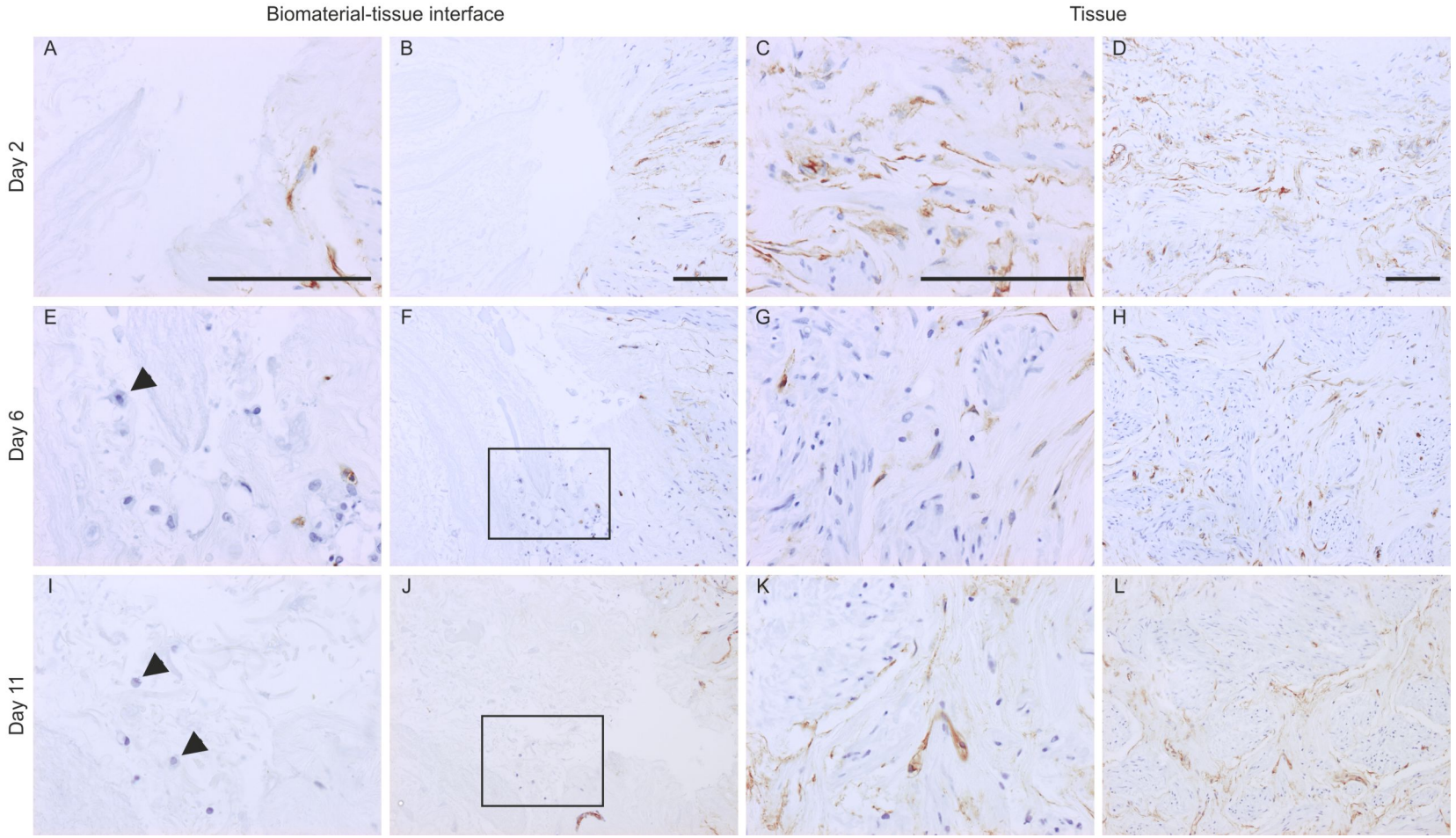

Figure 4-28. Immunoperoxidase labelling of CD34 in the porcine:human biomaterial-organ culture Y1129. Black boxes and arrows highlight areas were cells are observed migrating into the biological scaffold. Arrows show cells within the biological scaffold. All scale bars represent 100 microns.

4.8.5.4. Mast cells

Investigation into the expression of c-kit (CD117) was performed in the biological-scaffold organ culture system Y1132 using dual fluorescent immunolabelling with CD163 (Figure 4-29). CD163+ cells were identified at the biomaterial-tissue interface at days six and 11 as previously shown however, CD117 expression was not observed at the biomaterial-tissue interface at either time point (Figure 4-29). A few CD117+ cells were observed within the central regions of the tissue. These CD117+ cells potential represent mast cells resident within the tissue (Figure 4-29, B and D).

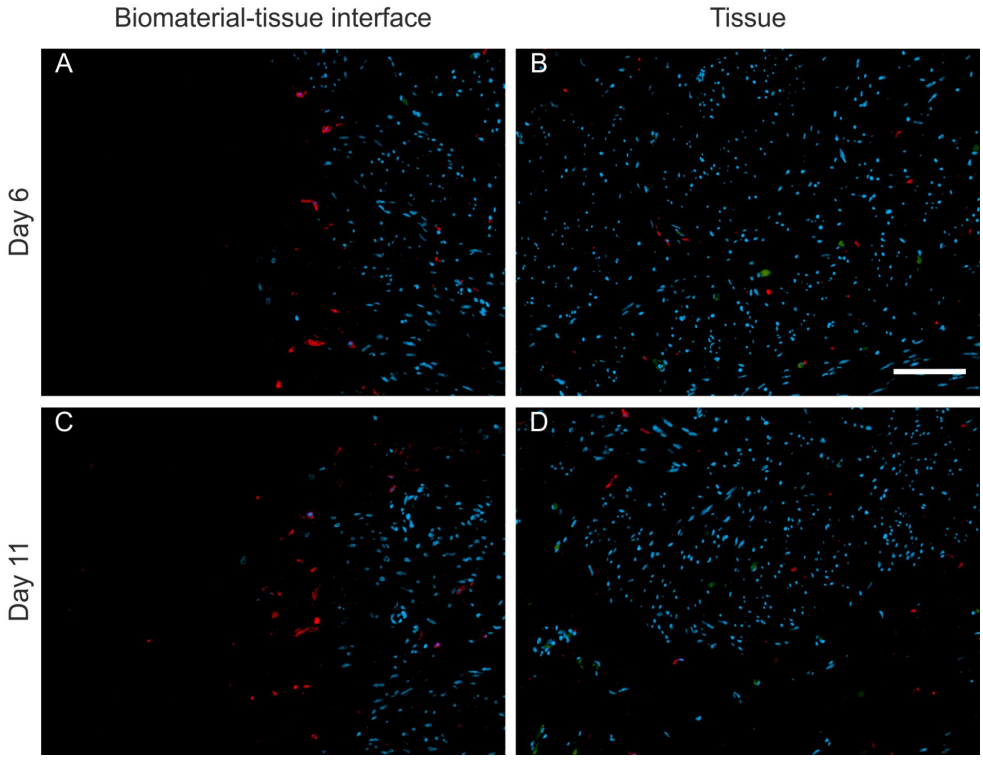

Figure 4-29. Dual immunofluorescence imaging of CD163 and CD117 labelling on the porcine:human biomaterial-organ culture construct Y1132 harvested at days six and eleven. The biomaterial-tissue interface is shown is micrographs A and C and the central regions of the tissue are shown in micrographs B and D. Labelling for CD163 (red) expression is observed at the biomaterial-tissue interface (A and C). CD117 (green) expression is observed in the central regions of the constructs (B and D). H33258 staining is shown in blue. Scale bar represents 100 microns.

4.8.5.5. Proliferative cells

In order to determine if proliferation contributed to the colonisation of the biological scaffold by tissue-derived cells expression of the cell cycle marker, Ki67 was determined using immunoperoxidase labelling (Figure 4-30). Ki67 labelling was not observed within the central regions of the tissue or at the biomaterial-tissue interface at days 2, 6 and 11, indicating that the colonisation of the porcine bladder biological scaffold was unlikely to involve proliferation (Figure 4-30).

Figure 4-30. Immunoperoxidase labelling for Ki67 expression in the porcine:human biomaterial-organ culture system Y1129. The biomaterial-tissue interface is shown in micrographs A, B, E, F, I and J the central regions of the tissue are shown in micrographs C, D, G, H, K and L. Box on image F highlights area of higher magnification on image E. Arrow (image I) indicates Ki67 negative cells within the biological scaffold. Scale bar represents 100 microns.

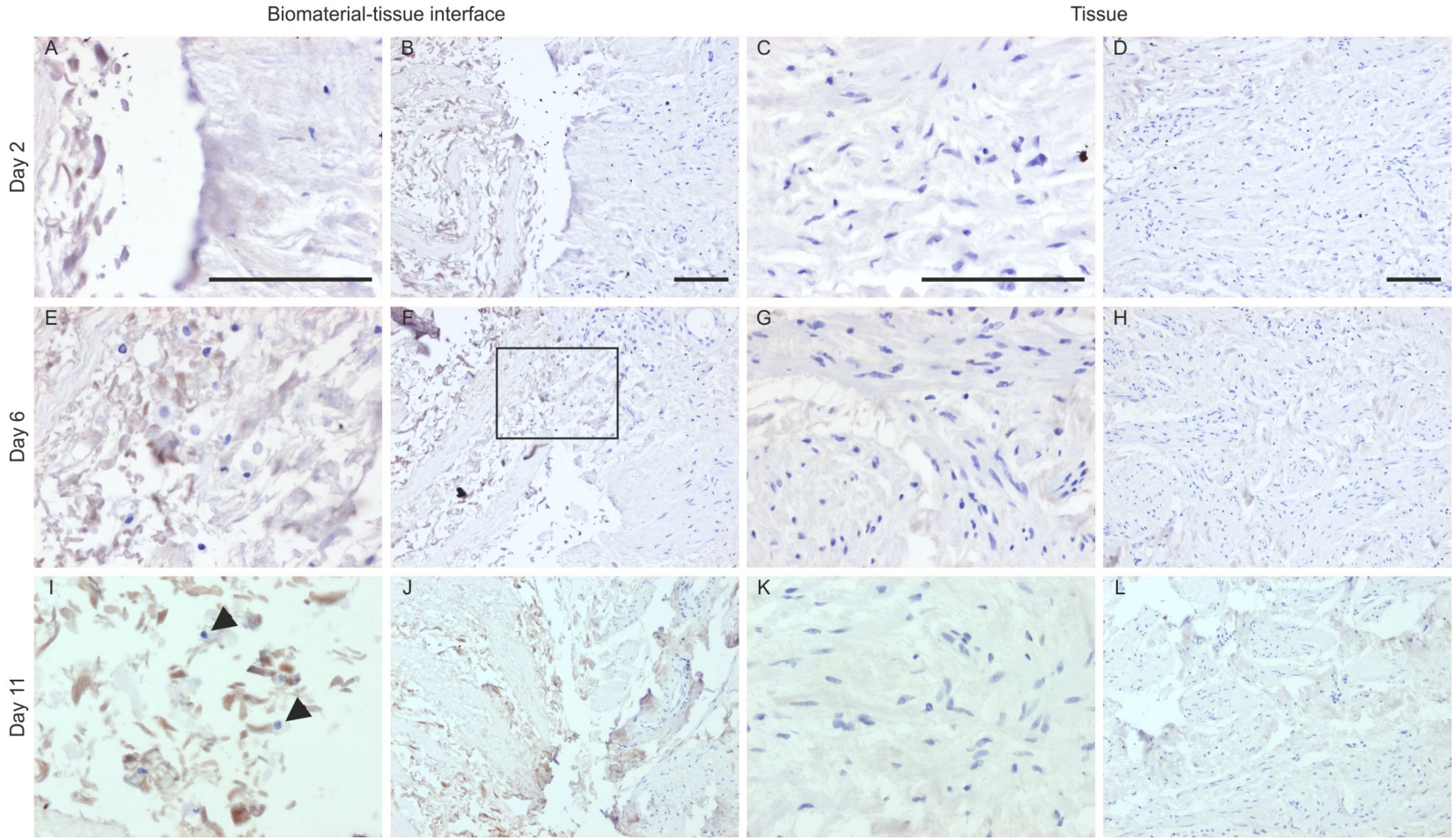
Biomaterial-tissue interface
Tissue
Day 2
Day 6
Day 11
A
B
C
D
E
F
G
H
I
J
K
L

4.8.6 Identification of nuclear receptor expression

To identify potential signalling mechanisms involved in governing the expression of functional markers by cells at the porcine:human biomaterial-tissue interface, nuclear receptor expression was investigated. The glucocorticoid receptor, a known regulator of CD163 expression, was initially investigated as a potential driver of CD163 expression at the biomaterial-tissue interface. Immunoperoxidase labelling for the glucocorticoid receptor showed predominantly cytoplasmic localisation by cells within the central regions of the tissue and nuclear localisation by cells at the biomaterial-tissue interface at days 2, 6 and 11 (Figure 4-31).

Further investigation into the expression pattern of another nuclear receptor, PPARγ, showed nuclear PPARγ expression by cells at the biomaterial-tissue interface at days 2, 6 and 11 while nuclear PPARγ expression was not observed within the central regions of the tissue (figure 4-32). Furthermore, nuclear PPARγ+ cells were observed within the porcine bladder biological scaffold at the day 11 time point. These cells displayed a kidney-shaped nucleus, a defining feature of mononuclear phagocytes (Figure 4-32, I).

Figure 4-31. Immunoperoxidase labelling of human glucocorticoid receptor on porcine:human biomaterial-organ culture using donor tissue Y1129, harvested at days 2, 6 and 11. The biomaterial-tissue interface is shown is micrographs A, B, E, F, I and J the central regions of the tissue are shown in micrographs C, D, G, H, K and L. Inset images show digital zoom micrographs of cell nuclei at the biomaterial-tissue interface (B, F and J) and within the central regions of the tissue (D, H and L). Scale bars represent 100 microns.

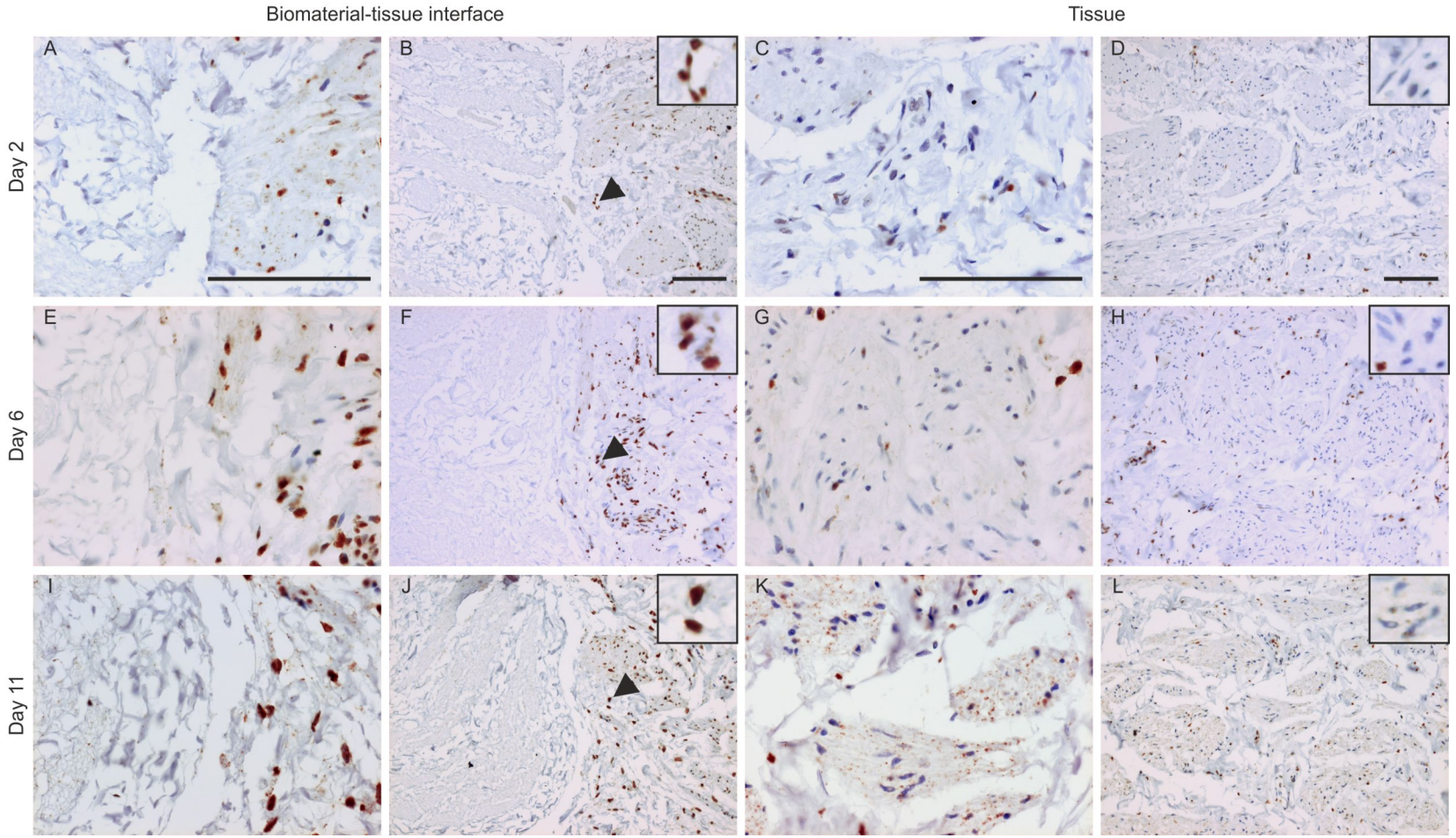
Biomaterial-tissue interface
Tissue
Day 2
Day 6
Day 11
A
B
C
D
E
F
G
H
I
J
K
L

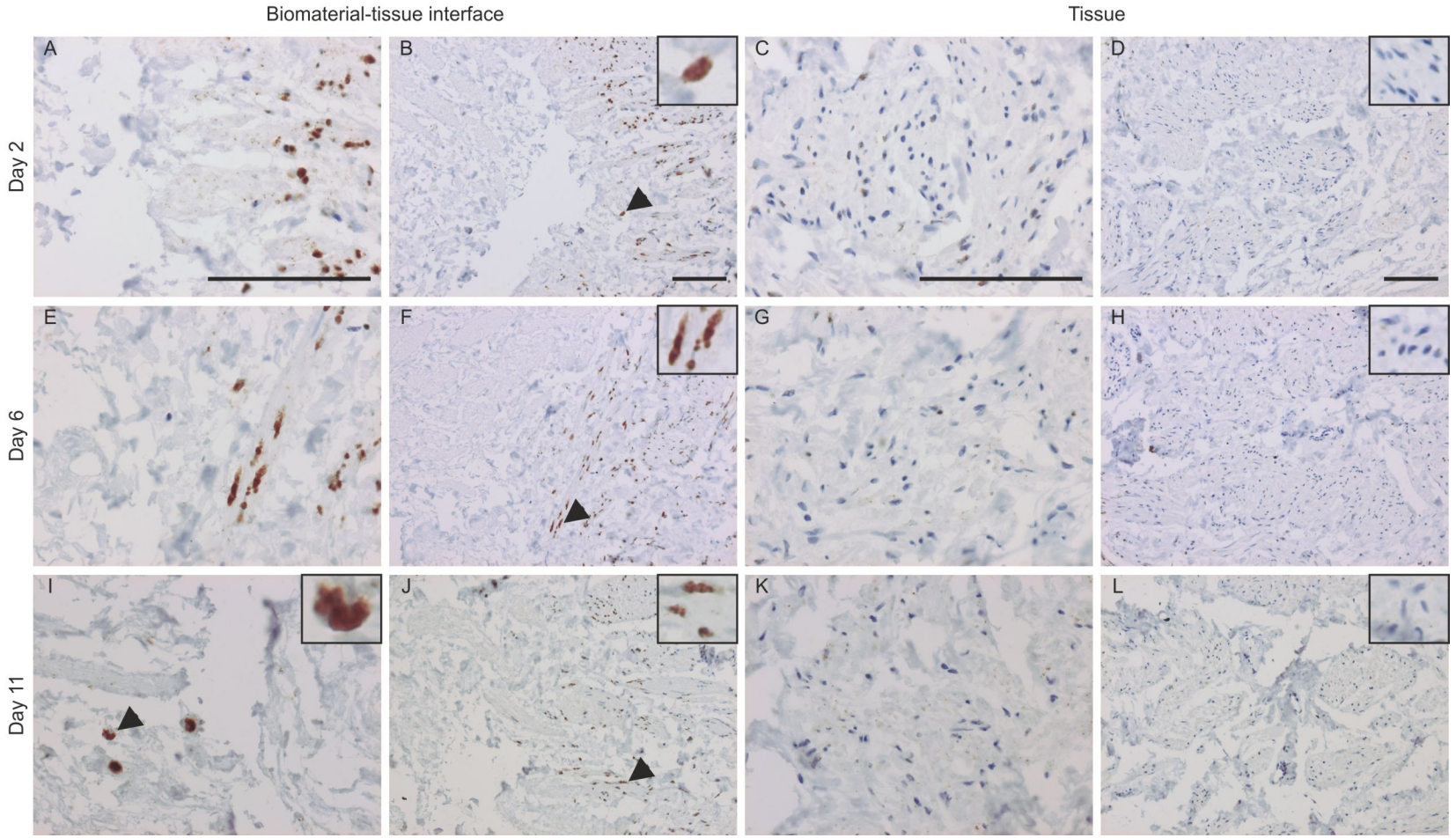

Figure 4-32. Immunoperoxidase labelling of the nuclear receptor PPARγ on biomaterial-organ culture Y1129. Scale bars represent 100 microns.

4.8.7 Modification of Waymouth's medium components

To investigate if components of the Waymouth's medium affected the expression of functional markers observed in the porcine:human biomaterial-organ culture system, selected supplements were omitted.

4.8.7.1. Ferrous sulphate

Culture of the porcine:human biomaterial-organ culture constructs using donor tissue Y1083 over Waymouth's medium from which the ferrous sulphate had been omitted showed the presence of CD163+ at the biomaterial-tissue interface at day 11 of the culture period (Figure 4-33).

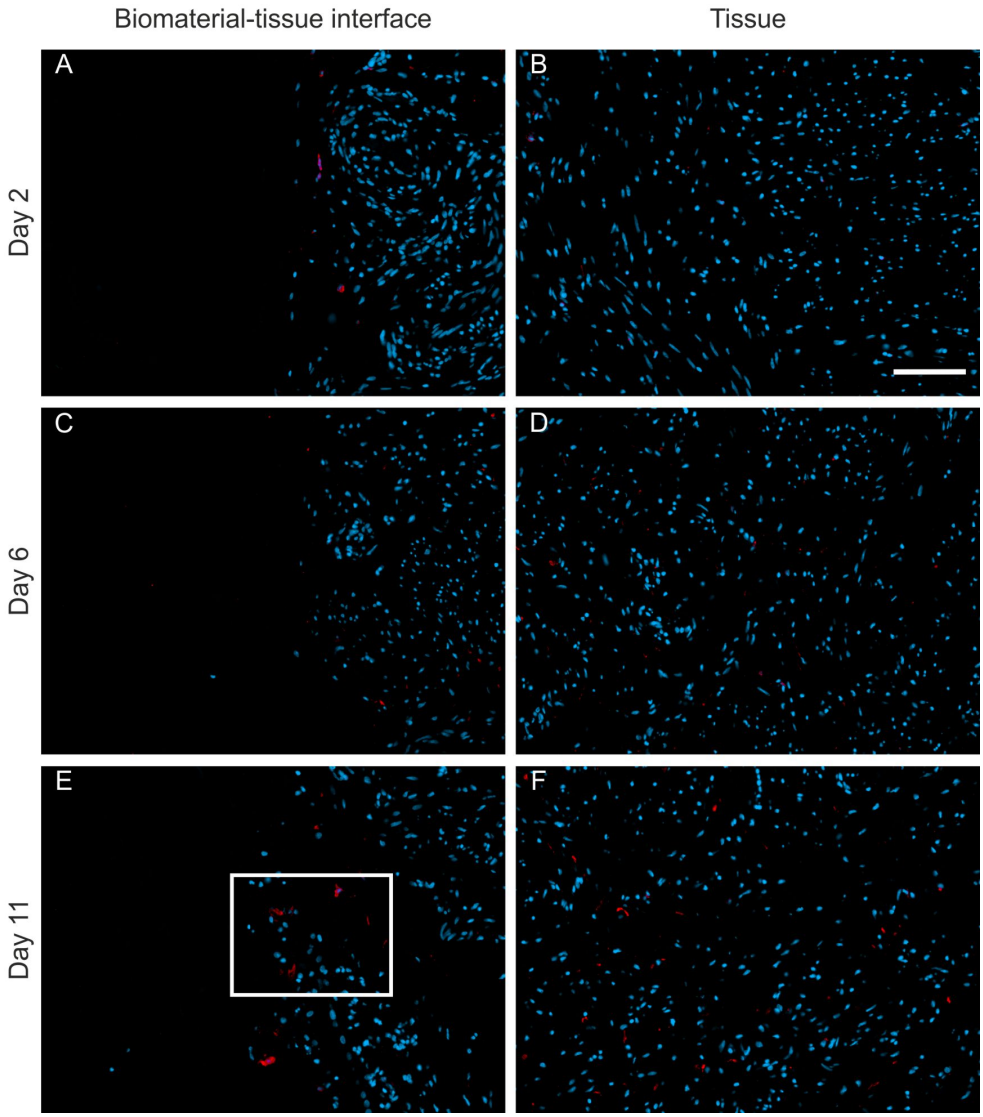

Figure 4-33. Fluorescent immunolabelling of CD163 expression in the porcine:human biomaterial-organ culture system in the absence of ferrous sulphate using donor human ureter Y1083. The biomaterial-tissue interface is shown is micrographs A, C and E and the central regions of the tissue are shown in micrographs B, D and F. Labelling of CD163 expression (red) is observed at the biomaterial-tissue interface at days 6 and 11. H33258 staining is indicated in blue. White box on image (E) highlights the infiltration of CD163+ cells into the biological. Scale bars represent 100 microns.

High magnification images of the day 11 biomaterial-tissue interface showed that the observed CD163+ cells had a mononuclear phagocyte-like morphology (Figure 4-34).

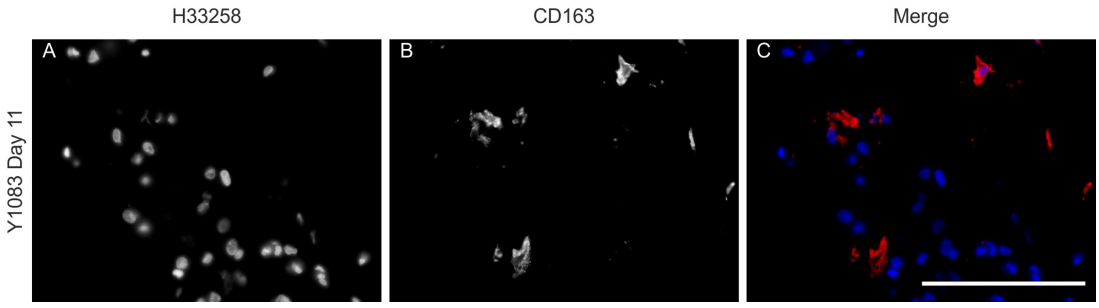

Figure 4-34. Fluorescent immunolabelling of CD163+ cells within the biological scaffold, highlighted in white box in figure 18, E, of the biomaterial-organ culture construct Y1083, cultured in the absence of ferrous sulphate. The tissue located to the right of the photomicrographs. Positive cells were observed at the biomaterial-tissue interface. Grey scale images of H33258 staining and CD163 labelling were combined to produce merged image. Scale bar represents 100 microns.

4.8.7.2. Hydrocortisone hemisuccinate

Culture of porcine:human biomaterial-organ constructs using donor tissue Y1193 over Waymouth's medium from which the hydrocortisone hemisuccinate was omitted and immunolabelling of the histological sections of the constructs showed the presence of CD68+ cells at the biomaterial-tissue interface and within the porcine bladder biological scaffold at days 6 and 11 (Figure 4-35). Immunoperoxidase labelling of CD163 in the biomaterial-organ culture system Y1193, showed cells that were positive for CD163 expression at the biomaterial-tissue interface at days 6 and 11 (Figure 4-36). CD163+ cells were observed within the biological scaffold at day 11 (Figure 4-36, E). Immunolabelling of CD68 and CD163 on tissue sections from biomaterial-organ culture construct, Y1193 cultured in the presence of hydrocortisone hemisuccinate is shown in appendices III-VI and III-VII, respectively. Immunoperoxidase labelling of the glucocorticoid receptor and PPARγ expression in donor tissue Y1193 showed nuclear localisation of both receptors in cells within the biological scaffold at day 11 in the absence of hydrocortisone hemisuccinate. Equivalent cells were not observed within the central regions of the tissue constructs at the same time points (Figure 4-37).

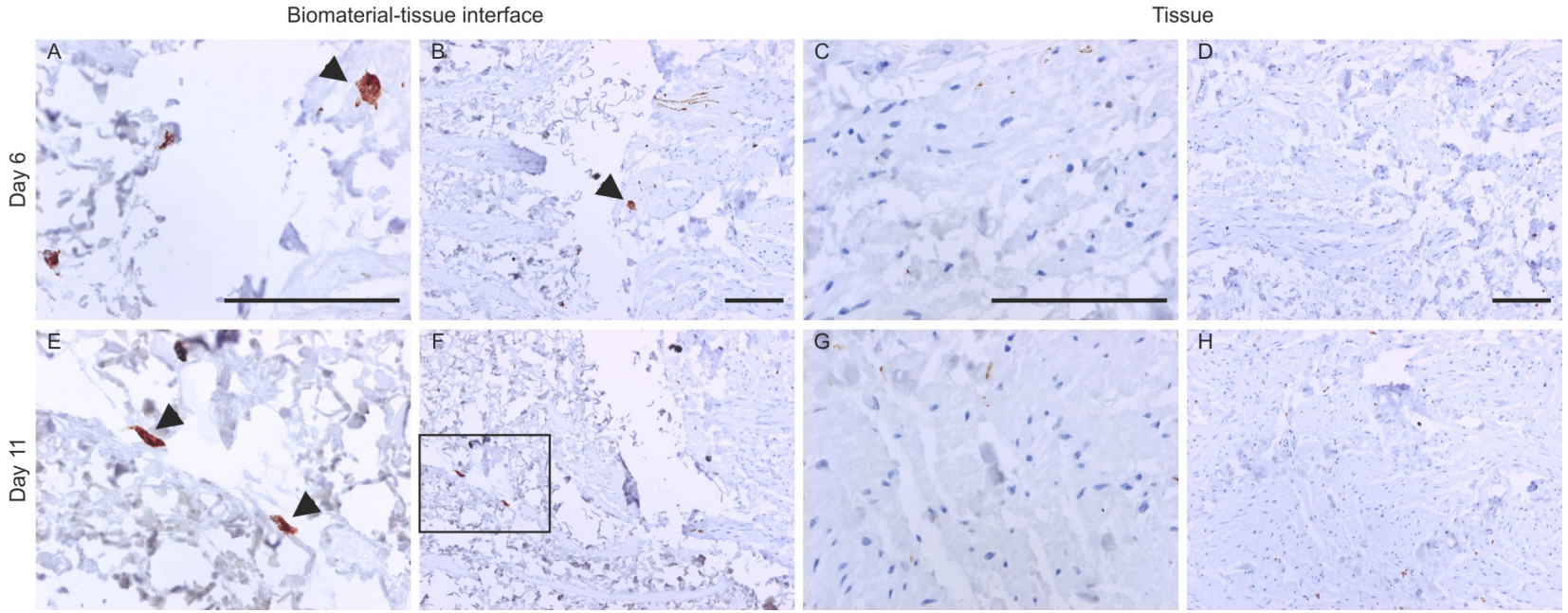

Figure 4-35. Immunoperoxidase labelling of CD68 on histological sections of porcine:human biomaterial-organ culture using donor tissue Y1193 in the absence of hydrocortisone hemisuccinate. Constructs were harvested at days 6 and 11. The biomaterial-tissue interface is shown is micrographs A, B, E and F the central regions of the tissue are shown in micrographs C, D, G and H. Arrow on image B shows indicated cell in image A. Black box on image F represent area of high magnification image E. Scale bars represent 100 microns.

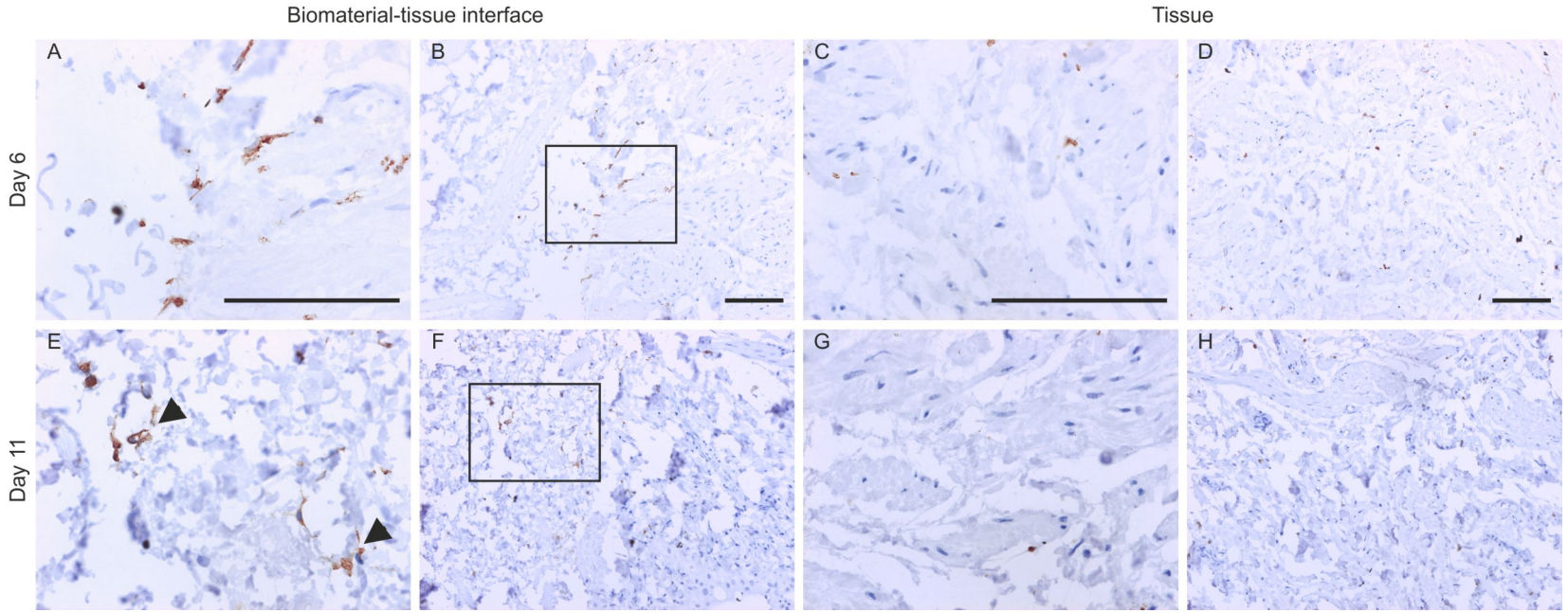

Figure 4-36. Immunoperoxidase labelling of CD163 on histological sections porcine:human biomaterial-organ culture using donor tissue Y1193 in the absence of hydrocortisone hemisuccinate. Constructs were harvested at days 6 and 11. The biomaterial-tissue interface is shown is micrographs A, B, E and F the central regions of the tissue are shown in micrographs C, D, G and H. Black box on image B represent area of high magnification image A. Black box on image F represent area of high magnification image E. Scale bars represent 100 microns.

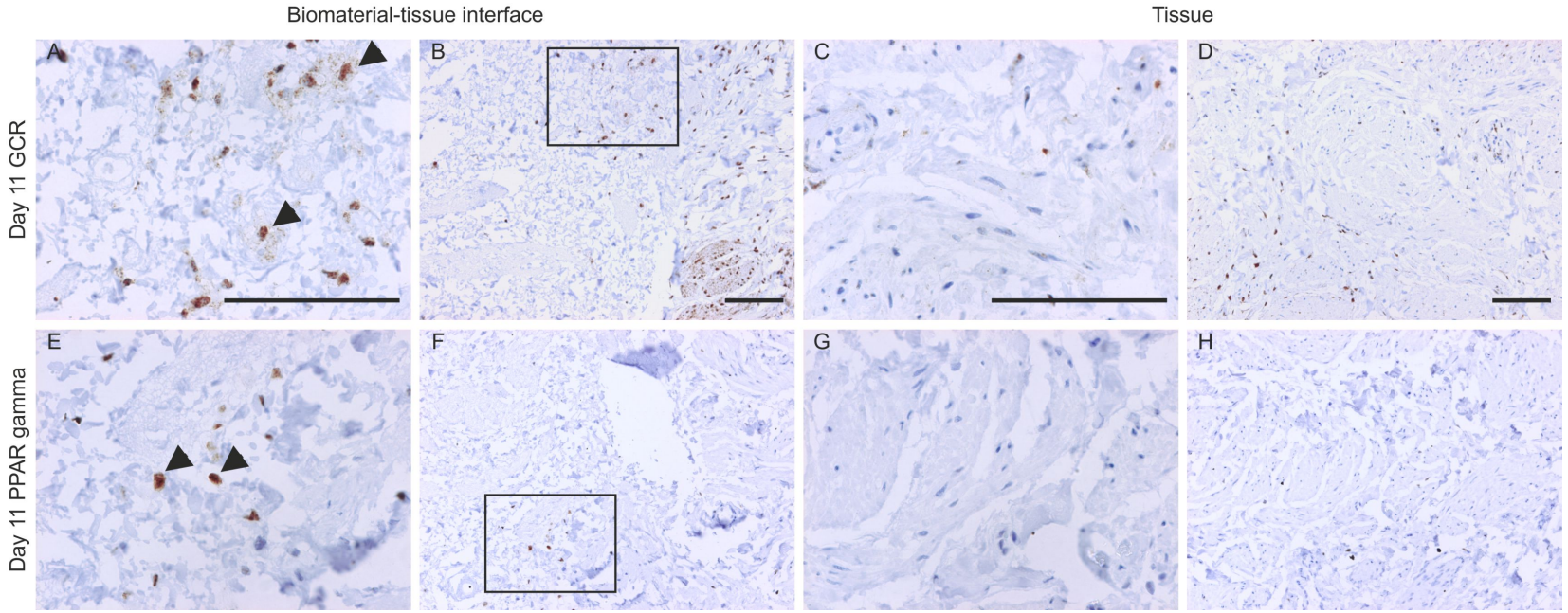

Figure 4-37. Immunoperoxidase labelling of the GCR and PPARγ on histological sections porcine:human biomaterial-organ culture using donor tissue Y1193 in the absence of hydrocortisone hemisuccinate. Constructs were harvested at day 11. The biomaterial-tissue interface is shown is micrographs A, B, E and F the central regions of the tissue are shown in micrographs C, D, G and H. Black box on image B represent area of high magnification image A. Black box on image F represent area of high magnification image E. Scale bars represent 100 microns.

4.9 Discussion

4.9.1 Maintenance of human tissue in culture

Many different tissues have been maintained in organ culture including human skin (Le Poole et al., 1994; Vukelic et al., 2010; Bedoni et al., 2007), human and bovine cornea (Foreman et al., 1996) and human urinary tract tissue (Scriven et al., 1997; Wang et al., 2012) (reviewed in (Varley and Southgate, 2011)). These organ cultures have been extensively used to investigate cell migration, differentiation and wound healing in the context of three-dimensional tissue in culture and have been adapted to incorporate biomaterials.

4.9.2 Biomaterial-organ culture systems

Biomaterial-organ culture models offer an attractive alternative to *in vivo* implantation and a number of studies have exploited organ culture systems to investigate the regeneration and cellular infiltration of biomaterials *ex vivo*. Many of these studies used the culture models to determine the 'wound-healing' capabilities of human tissues in the presence of synthetic biomaterials; a few examples are described here. Histological evaluation of 4mm discs of polyurethane-based scaffolds inserted into a pocket created in the stroma of human corneas and maintained suspended in medium for 7 weeks showed limited interactions between the stroma and polymers (Sandeman et al., 2003). In a similar study perfluoropolyether (PFPE) and polycarbonate membranes were implanted into a pocket created in bovine corneas. The excised corneas when then cultured at an air-liquid interface for eights days before processing for histology (Evans et al., 2002). The authors reported a similar wound-healing process to that reported *in vivo* however, the synthetic materials showed reduced stratification of the epithelium compared to the epithelium which had migrated over the stroma in the 'sham' control procedure (Evans et al., 2002).

Human skin samples have also been used as the tissue component of a biomaterial-organ culture system. Human breast skin explants, obtained by biopsy punch, threaded with a surgical fixature pin provided a biomaterial-tissue interface (Peramo et al., 2009). The constructs were cultured at an air-liquid interface for five days before being harvested, fixed and processed for histology. Limited analysis of haematoxylin and eosin stained sections examined the morphology of the tissue following culture with or without the fixature pin in place (Peramo et al., 2009).

Other skin biomaterial-organ culture models used human newborn foreskin, punctured with 4mm biopsy punch, followed by threading of poly(2-hydroxyethyl methacrylate) (poly(HEMA)) into the punched hole using an 18G needle. The constructs were maintained at an air-liquid interface by rafting on a metal mesh for up to seven days (Fukano et al., 2006; Beckstead et al., 2009). Histological examination of the constructs revealed that the keratinocytes failed to attach to the polyHEMA scaffold but instead showed epithelial migration between the tissue edge and the polyHEMA biomaterial, a process which is also observed *in vivo,* termed marsupialisation (Recum, 1984). Despite the histological analysis of *in vitro* biomaterial-tissue interactions, analysis of these biomaterial-organ cultures failed to comment on the presence of inflammatory cells within the tissue and biomaterials.

4.9.3 The development of a biomaterial-urinary tract organ culture model

In this study development of a porcine:porcine and a porcine:human biomaterial-organotypic culture model in which urinary tract tissue was maintained in close apposition with a porcine bladder-derived biological scaffold was achieved. This model revealed that mononuclear phagocytes, identified morphologically and by antigen expression, infiltrated the biological scaffold over an 11-day time culture period. This study is the first to describe culture of human urinary tract tissue with a decellularised porcine bladder biological scaffold to date. Furthermore, this is also the first study to make observations of mononuclear phagocytes at the biomaterial-human urinary tract tissue interface and provides a tool to investigate the temporal and spatial expression of antigens at a biomaterial-human tissue interface.

4.9.4 Cells at the *ex vivo* biomaterial-tissue interface

4.9.4.1 Porcine:porcine biomaterial-organ culture system

Culture of porcine urinary tract tissue in close apposition to a porcine bladder biological scaffold showed that cells with a kidney-shaped nuclei and large volume of cytoplasm increased in number within the biological scaffold over time. Porcine models have been proposed to be a superior model for studies of immunological mechanisms compared to murine models (Kapetanovic et al., 2012) however, there are a limited number of recognised macrophage-associated markers and reagents to porcine cells. In addition, porcine immunology is not as well understood, compared to rodent and human immunology. The antibody clone 4E9/11 used in this study identifies an antigen associated with a member of the LAMP-1 family. CD107a identifies porcine monocytes and tissue

macrophages ((Bullido et al., 1997), reviewed in (Ezquerra et al., 2009)). In addition to identifying mononuclear phagocytes on formalin-fixed, paraffin embedded porcine tissues (Domenech et al., 2003), 4E9/11 also identifies, to a lesser extent, granulocytes (Bullido et al., 1997). H&E staining of the biomaterial-organ culture constructs and investigation of cell and nuclear morphology did not indicate that polymorphonuclear granulocytes were present in the biological scaffold at any time points sampled.

4.9.4.2 Porcine:human biomaterial-organ culture system

Adaptation of the biomaterial-organ culture system to incorporate human urinary tract tissue showed that the biomaterial-human tissue interface was maintained in culture. Cells observed at the biological scaffold-tissue interface and within the biological scaffold were positive for mononuclear phagocyte-associated markers MAC387, CD68 and CD163. The cells weakly expressed HLA-DR at the day 11 time point and were negative for the pro-inflammatory marker, CD80. This data supports *in vivo* observations that macrophages, which were defined as CD80- CD163+, interact and infiltrate biological scaffolds implanted into rats (Badylak et al., 2008).

HLA-DR expression is indicative of human antigen presenting cells and is expressed by macrophages and dendritic cells. The distinction between macrophages and dendritic cells has been contested due to functional similarities (Hume, 2008) however, HLA-DR expression within the 'M1/M2' macrophage activation paradigm has been associated with pro-inflammatory 'M1' macrophages. MHC II^{hi} macrophages are highly efficient at presenting antigen while 'M2' macrophages have a decreased ability to present antigen to T cells (reviewed in (Biswas and Mantovani, 2010)). In this biomaterial-organ culture model, HLA-DR expression qualitatively decreased over the 11-day culture period suggesting an absence of signals, which could maintain MHC II expression, however further work is required to confirm this supposition. CD80 expression was not observed in the human urinary tract-biological scaffold culture model at all time point samples. CD80 was shown to be expressed on classical activated 'M1' monocyte-derived macrophages induced by GM-CSF *in vitro* and expression of CD80 by M1 macrophages was further enhanced in the presence of LPS (Verreck et al., 2006). CD80 has also been shown to be expressed in inflammatory lesions in multiple sclerosis using histology (Windhagen et al., 1995). This indicates that the mononuclear phagocytes present at the biomaterial-tissue interface did not have an 'inflammatory' phenotype. The presence of mononuclear phagocytes in the biological scaffold was not accompanied by the presence of αSMA+ stromal cells or CD3+

human lymphocytes, in agreement with *in vivo* implantation studies (Baker et al., 2011). The temporal increase in CD163+ cells at the biomaterial-tissue interface and within the biological scaffold indicated that these cells had an 'anti-inflammatory' phenotype.

4.9.4.3 Origin of human urinary tract interface mononuclear phagocytes

The origin of the mononuclear phagocytes observed at the biomaterial-tissue interface was not clear. The biomaterial-organ culture model is a 'closed' system in which the only cells that can be observed are those isolated in the tissue specimen as such, the system does not model cells recruited from the periphery to the same extent as *in vivo* systems. This limits the interpretation in the observations made in the systems compared to animal implantation studies. Histological evaluation of surgically resective specimens of human ureter from three donors showed MAC387 immunolabelled cells resident within the tissue stroma and 'captured' within the tissue vasculature. There has been little exploration into the resident leukocyte populations within the urinary tract tissue. The regenerative mechanisms of the epithelial lining of the urinary tract has been extensively investigated both *in vitro* (Kreft et al., 2005; Shabir and Southgate, 2008) and computationally (Walker et al., 2004). Leukocyte biology is context dependent; as an epithelial barrier it is possible to speculate that the urinary tract may represent a specialised tissue environment like other epithelial-lined tissues, such as gastrointestinal tract or the epidermis. During an immune response, there are potential contributions from both resident macrophage populations and macrophages derived from monocytes captured in the vasculature. Use of histological methods of analysis over three time points resulted in difficulty in determining if these biomaterial-tissue interface mononuclear phagocytes were a) originally blood monocytes which extravasated from the vasculature to the interface; b) originally mature macrophages within the stroma which migrated towards the wound-edge; or c) if the cells originated from a combination of these potential sources. No loss of macrophage-associated antigens within the central regions of the tissue indicated that these cells may have been derived from an immature population either localised within the vasculature or diffuse within the stroma however further analysis is required.

4.9.4.4 Prevalence of CD163+ macrophages at the biomaterial-tissue interface

The most striking observation was the significant up-regulation of CD163 expression at the biomaterial-tissue interface over time and compared to the central regions of the tissue. CD163 is described as being expressed exclusively on monocytes and macrophages (Van Gorp et al., 2010), furthermore, the expression of the scavenger receptor was described as

being restricted to 'M2' monocyte-derived macrophages, induced using M-CSF (Verreck et al., 2006). These 'M2' macrophages produced greater levels of IL-10 in response to LPS compared to GM-CSF induced 'M1' macrophages, which predominately secreted IL-12p40 (Verreck et al., 2006). CD163 expression was observed and quantified at the day two time point however, CD68 expression was not observed at the same time point. Disparity in the expression of CD68 and CD163 has been observed following implantation of a particulate-leached, cross-linked poly(ε-caprolactone) scaffold into a ventral subcutaneous pocket in Piebald-Viral-Glaxo rats (Baker et al., 2011). The authors suggested that the expression of CD163 by these CD68 negative cells may represent expression by stromal cells (Baker et al., 2011). Candidate stromal cells in human ureteric tissues are smooth muscle cells and myofibroblasts both of which express αSMA ((Baker and Southgate, 2008; Darby et al., 1990), reviewed in (Tomasek et al., 2002)). Serial sections of the biomaterial-organ culture constructs showed that the CD163+ cells present within the biological scaffold were αSMA negative. CD163 has also been reported to be expressed on a small subpopulation of CD34+ haematopoietic progenitors derived from human bone marrow and umbilical cord blood (Matthews et al., 2006). Immunolabelling for CD34 expression showed that the CD34+ cells did not infiltrate the biological scaffold. This observation also indicated that vascular endothelial cells did not infiltrate into the biological scaffold over the culture period. Immunoperoxidase labelling of CD163 and CD68 on serial sections of a biomaterial-tissue interface showed weaker expression of CD68 compared to CD163 expression in the same region, indicating a potential preference in the expression of CD163 by mononuclear phagocytes, over the expression of the LAMP-1 family member, CD68. These CD163+ mononuclear phagocytes did not show expression of the 'M2'-associated antigen, arginase 1 and CD163 expression did not co-localise with another macrophage scavenger receptor, CD36.

4.9.5 Nuclear receptor localisation at the biological scaffold-tissue interface

A goal of this chapter was to identify potential factors or signalling mechanisms that can drive the expression of mononuclear phagocyte-associated markers at a biomaterial-tissue interface. The mechanisms driving the presence of the mononuclear phagocytes within biological scaffold-tissue interface is most likely in response to the wound-event, however other factors, such as the biological scaffold, which may influence the cell phenotype at the biomaterial-tissue interface should be considered. To understand potential mechanisms involved in governing the phenotype of the human mononuclear phagocytes at the biomaterial-tissue interface, nuclear receptor expression and localisation was investigated.

PPARγ has been identified as having an orchestrating role in wound healing processes following tissue injury ((Kapoor et al., 2007), reviewed in (Michalik and Wahli, 2006)). In this study PPARγ was found to localise to the nucleus in cells present at the biomaterial-tissue interface and within the biological scaffold but not within the central regions of the tissue. In addition the PPARγ target gene, CD36 showed expression by cells at the biomaterial-tissue interface and within the central regions of the tissue.

The activation of the glucocorticoid receptor has been shown to inhibit epithelialisation and wound healing in a human skin wound healing model (Vukelic et al., 2010). Over-expression of keratinocyte specific murine glucocorticoid receptor was shown to delay wound healing relative to wild type mice and was reported to reduce recruitment of Ly6G+ granulocytes and F4/80+ macrophages in the wound skin (Sanchis et al., 2012). In this study, the glucocorticoid receptor showed a similar expression pattern to that of PPARγ in the biomaterial-organ culture system indicating that the receptor was active at the interface. Investigation into factors which may drive the significant up-regulation of CD163 expression by cells at the biomaterial-tissue interface and within the porcine bladder biological scaffold showed that CD163 was expressed in the absence of the medium supplements, ferrous sulphate and hydrocortisone hemisuccinate indicating that these supplements in the medium were not driving the expression of CD163 and that other factors may be regulating CD163 expression. In addition, both the glucocorticoid receptor and PPARγ showed nuclear localisation by cells present within the biological scaffold in the absence of the medium supplement, hydrocortisone hemisuccinate; a glucocorticoid. The glucocorticoid receptor is known to drive the expression of CD163 (Högger et al., 1998) however, little is known about the role of PPARγ in the expression of CD163. Mechanisms and regulation of expression of CD163 will be explored in chapter five.

4.10 Summary

- Establishment of a porcine:porcine biomaterial-organ culture system showed the infiltration of CD107a+ cells with mononuclear phagocyte-like morphology into the biological scaffold over time.
- Maintenance of a porcine bladder biological scaffold juxtaposed with human urinary tract tissue in culture showed the presence of CD68+ and MAC387+ human mononuclear phagocytes at the biomaterial-tissue interface and within the porcine bladder biological scaffold.
- Cells at the biomaterial-tissue interface showed weak expression of HLA-DR and there was absence of the inflammatory marker, CD80 throughout the biomaterial-organ culture constructs, implying that the mononuclear phagocytes at the biomaterial-tissue interface were 'non-inflammatory'.
- CD163 expression was significantly up-regulated at the biomaterial-human tissue interface over an 11-day culture period however, the origin of these CD163+ cells is not currently known.
- T cells, vascular endothelial cells, mast cells and αSMA+ stromal cells did not accompany the human mononuclear phagocytes within the porcine bladder biological scaffold.
- The glucocorticoid receptor and PPARγ showed nuclear localisation in cells at the biomaterial-human tissue interface indicating that the receptor signalling pathways were active at the interface.

5.0 Nuclear receptor modulation of CD163 expression

5.1 Introduction

5.1.1 CD163

CD163 is a member of the scavenger receptor cysteine-rich (SRCR) domain family type B (Madsen et al., 2004) and was characterised as the macrophage haptoglobin:haemoglobin scavenger receptor by Kristiansen and colleagues in 2001 (Kristiansen et al., 2001). CD163 functions to remove toxic haem from the tissue environment and is described as being expressed by monocytes and up-regulated upon differentiation to mature macrophages (for a complete review see Van Gorp et al (Van Gorp et al., 2010)). CD163 is known to be up-regulated by anti-inflammatory mediators, in particular, agonists of the nuclear glucocorticoid receptor (Högger et al., 1998). The striking up-regulation of CD163 in response to glucocorticoids, as well as the regulatory cytokine IL-10 (Sulahian et al., 2000), coupled with a down-regulation of CD163 mRNA expression by human peripheral blood monocytes and macrophages in response to the inflammatory stimuli, IFNγ and TNFα (Buechler et al., 2000), resulted in CD163 becoming an indicative marker of an anti-inflammatory macrophage phenotype (Biswas and Mantovani, 2010).

5.1.2 Nuclear receptor signalling in leukocytes

5.1.2.1 Glucocorticoid receptor signalling

Glucocorticoids are potent anti-inflammatory agents and are widely prescribed as anti-inflammatory drugs (for a complete review see (Smoak and Cidlowski, 2004)). The glucocorticoid receptor, a member of the nuclear receptor superfamily, resides in the cytoplasm, where it is sequestered and inactivated by a multimeric complex of proteins. Upon ligand binding the glucocorticoid receptor dissociates from the complex and translocates to the nucleus where it binds a glucocorticoid response element (GRE) upstream of a transcription start site and initiates transcription of anti-inflammatory genes (Figure 5-1; (Smoak and Cidlowski, 2004)) such as the decoy receptor, IL-1RII and IL-10 as shown in human peripheral blood monocytes (Ehrchen et al., 2007) and inhibitor of NF-κB (IκB) as shown in murine cells (Auphan et al., 1995). In addition, inhibition of the glucocorticoid receptor with the antagonist RU486 has shown reduced expression of IL-10 by primary human whole blood cultures (Visser et al., 1998).

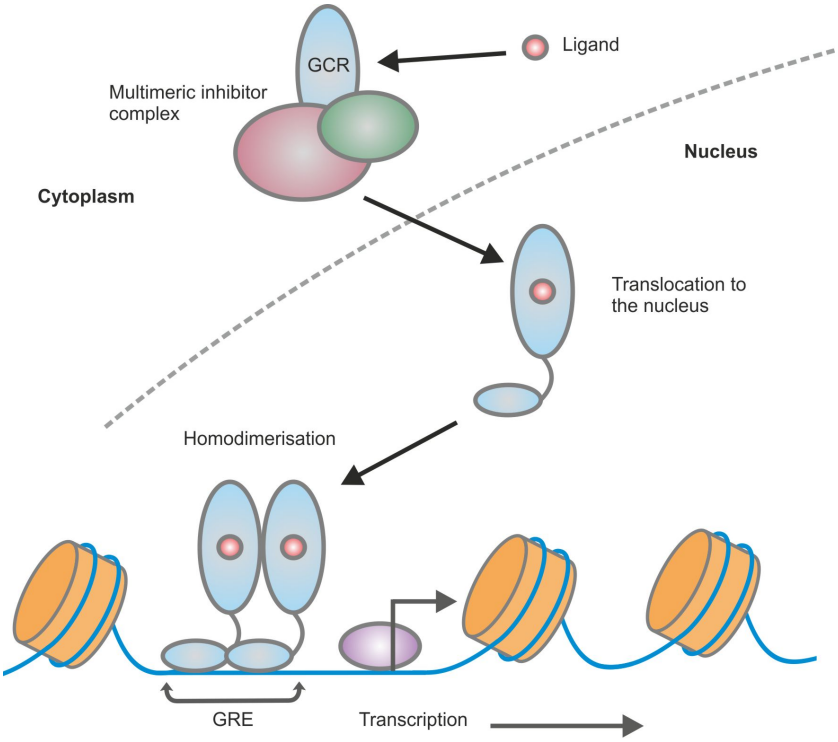

Figure 5-1. Schematic diagram of the basic glucocorticoid receptor signalling mechanism. Upon ligand binding the glucocorticoid receptor (GCR) dissociates from its inhibitory complex and translocates to the nucleus where it homodimerises and binds to a consensus sequence (GRE) upstream of the target gene transcription start site to initiate transcription.

5.1.2.2 PPARγ signalling

Another member of the nuclear receptor superfamily is PPARγ. PPARγ activates transcription of an array of genes in response to a variety of fatty acid metabolites culminating in a diverse range of cellular functions. Upon ligand binding to the ligand binding domain (LBD) of PPARγ the receptor translocates to the nucleus where it heterodimerises with its binding partner, retinoid X receptor α (RXRα). PPARγ:RXRα complexes activate transcription through binding to a PPAR response element (PPRE) upstream of the gene transcription start site (figure 5-2; for a more complete review of PPARγ signalling see (Feige et al., 2006)).

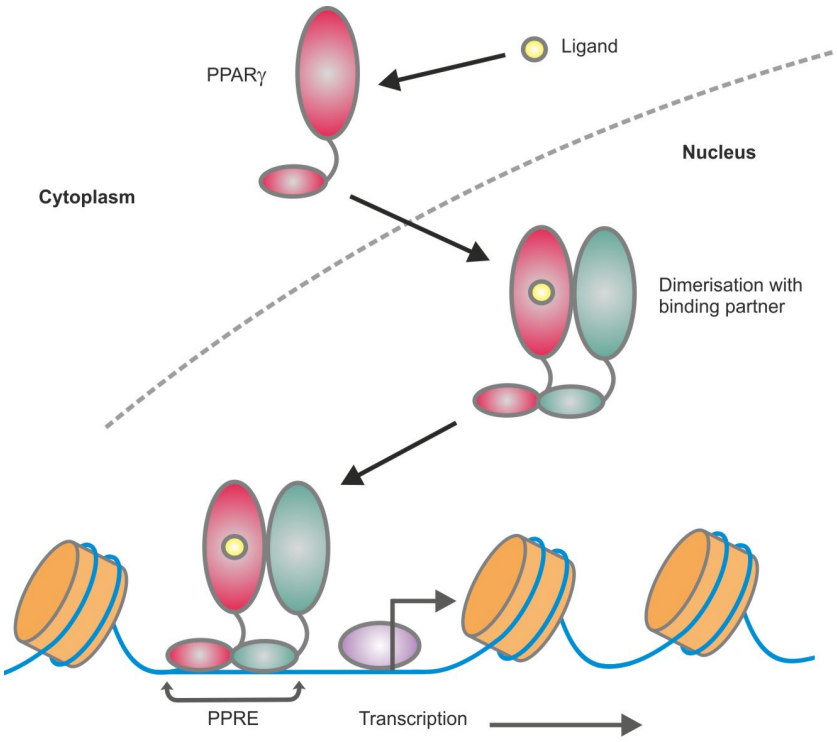

Figure 5-2. Schematic diagram of the basic PPARγ signalling mechanism. Upon ligand binding PPARγ translocates to the nucleus where it binds to its nuclear receptor-binding partner. The receptor dimer then binds to a consensus sequence, known as a PPRE, upstream of the target gene transcription start site and initiates transcription.

The function of PPARγ in a variety of cells of the immune system has been extensively investigated (reviewed by (Széles et al., 2007; Szanto and Nagy, 2008). A few roles of PPARγ in cellular immunity are discussed here.

5.1.3 Suppression of inflammation by PPARγ

PPARγ activation has been implicated in modulating many inflammatory responses by inhibiting pro-inflammatory processes in antigen presenting cells. PPARγ activation with the synthetic PPARγ agonist troglitazone has been shown to reduce secretion of the pro-inflammatory cytokines IL-12, TNFα and IL-6 by human monocyte-derived dendritic cells (Nencioni et al., 2002) and reduce the phorbol 12-myristate 13-acetate (PMA)-induced TNFα, IL-1β and IL-6 production by human monocyte-derived macrophages (Jiang et al., 1998). PPARγ activation with the natural arachidonic acid-derived ligand, 15-deoxy-$\Delta^{12,14}$-PGJ_2 (15d-PGJ_2) showed inhibition of combined LPS and IFNγ-induced promoter activity of the iNOS gene (*Nos2)* in the murine macrophage cell line, RAW 264.7 transfected with a

PPARγ expression plasmid (Ricote et al., 1998). In concordance, mice with a macrophage-specific depletion of PPARγ showed elevated gene expression of *Nos2* and IL-6 by white adipose-derived macrophages (Odegaard et al., 2007). PPARγ activation in human monocyte-derived dendritic cells by the synthetic PPARγ agonist, rosiglitazone for 24 hours was shown to significantly reduce the LPS induced expression of the co-stimulatory molecule, CD80 (Gosset et al., 2001). The PPARγ-dependent reduction in LPS-induced CD80 expression by human-monocyte-derived dendritic cells was also observed by Nencioni et al following treatment of the cells for six days using troglitazone before challenging with LPS for 24 hours (Nencioni et al., 2002). In addition to repression of inflammatory genes, PPARγ activation with either rosiglitazone or pioglitazone has also been shown to enhance protein expression of the immunoregulatory cytokine, IL-10 in lung tissue in a mouse model of asthma (Kim et al., 2005). Together, these observations indicate a key role for PPARγ in suppressing the propagation of inflammatory responses.

5.1.3.1 Mechanism of suppression

Activation of PPARγ with oxidized low-density lipoprotein revealed that LPS-stimulated production of IL-12 by murine macrophages was inhibited by PPARγ through a potential interaction between PPARγ and p50 and p65 subunits of the transcription factor, NF-κB (Chung et al., 2000). In a more targeted approach using *Nos2* gene expression as a readout, Pascual et al demonstrated that SUMOlayted PPARγ stabilised the nuclear receptor co-repressor (NCoR) at the *Nos2* promoter, preventing the LPS-induced degradation of the repressor complex and *Nos2* gene expression (Pascual et al., 2005) (reviewed in (Li and Yang, 2011)). This mechanism of NCoR degradation leading to de-repression of gene transcription had earlier been described for activator protein -1 (AP-1) target genes in macrophages (Ogawa et al., 2004) and illustrations of NCoR stabilisation by SUMOylated PPARγ have indicated this mode of activity to be through AP-1 (Figure 5-3; illustrated in (Glass and Saijo, 2010; Ogawa et al., 2004)).

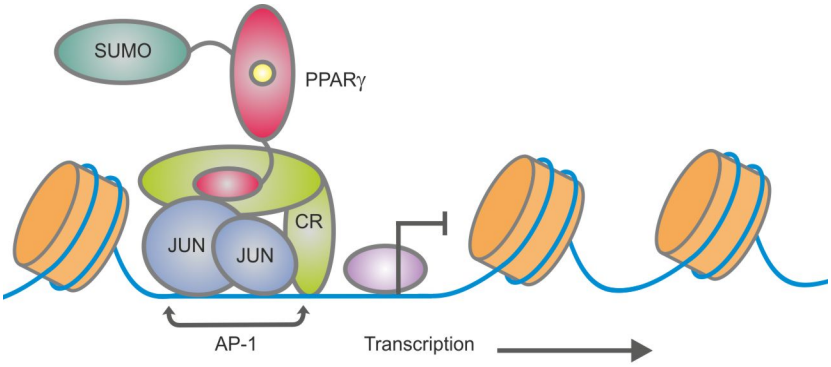

Figure 5-3. Transrepression of AP-1 target genes by stabilisation of co-repressors by SUMOylated PPARγ. SUMOylated PPARγ targets the nuclear receptor corepressor (NCoR - CR) and prevents ubiquitin dependent degradation of the repressor complex. As a result, NCoR complexes are not removed from the promoter region and transcription is not initiated. (Adapted from (Glass and Saijo, 2010)).

5.1.4 PPARγ and macrophage scavenger receptors

Macrophage scavenger receptors, such as CD163, are described as having key roles in regulating immune responses by binding and removing inflammatory stimuli (reviewed by (Peiser and Gordon, 2001; Peiser et al., 2002)). In line with this associated function, activation of PPARγ has been shown to up-regulate CD36, the oxidized LDL, class B scavenger receptor (Chawla et al., 2001) through direct binding of PPARγ to the promoter of the CD36 gene (Tontonoz et al., 1998). Conversely, investigation into PPARγ-dependent down-regulation of macrophage specific genes found that the promoter activity of the macrophage scavenger receptor A gene (*SR-A*) was down-regulated in U937 cells in response to the PPARγ ligand, 15d-PGJ_2 (Ricote et al., 1998), suggesting a dual association of PPARγ activation and scavenger receptor expression.

5.2 Chapter rationale and aim

The striking expression of CD163 by cells at the biomaterial-tissue interface and the observed nuclear localisation of PPARγ in cells within the biological scaffold, coupled with the known 'anti-inflammatory' roles of PPARγ, led to the supposition that PPARγ activation has a role in modulating CD163 expression by macrophages.

The aim of this chapter was to understand the factors that modulate CD163 expression with particular focus on the role of PPARγ and how the nuclear receptor can influence human monocyte-derived macrophage phenotype.

5.3 Hypothesis

PPARγ activation modulates CD163 expression in human monocyte-derived macrophages.

5.4 Objectives

Specific objectives of this chapter were to:

a) Confirm the expression of key functional markers and receptors by human peripheral blood monocytes and monocyte-derived macrophages.
b) Determine the expression pattern of CD163 from monocytes to monocyte-derived macrophages.
c) Investigate the consequence of manipulating PPARγ function on the expression of CD163.
d) Examine if the expression of functional markers, associated with defined macrophage phenotypes, is influenced by culture substrate (biological scaffold versus glass).

5.5 Experimental approach

5.5.1 Macrophage expression of CD163

To determine the expression profile of functional markers and receptors, whole cell lysates were prepared from human PBMC and monocyte-derived macrophages cultured on a glass substrate for 11 days from matched donors and the expression of proteins of interest determined by Western blot. To determine the expression of functional markers and receptor by adherent monocytes, peripheral blood monocytes were enriched by adherence onto glass for three hours and proteins extracted and investigated by Western blot analysis. CD163 protein expression by monocytes and monocyte-derived macrophages was assessed by flow cytometric analysis of CD11b+ monocytes from peripheral blood mononuclear cell preparations of six healthy donors and CD11b+ monocyte-derived macrophages from three donors. Further confirmation of the pattern of CD163 expression was achieved using immunofluorescent imaging of monocyte-derived macrophages cultured on a glass substrate.

The expression of CD163 in response to IL-10 was examined by stimulating monocyte-derived macrophages with IL-10 at 1, 10 or 100ng.mL^{-1} for 48 hours and quantifying the expression by fluorescent intensity of cells labelled with the EDhu monoclonal antibody using image analysis software. The up-regulation of CD163 protein expression on macrophages by activation of the glucocorticoid receptor using synthetic corticosteroid, dexamethasone was confirmed using the human monocytic cell line, THP-1. THP-1 cells were selected for use, as a large number of cells could be generated in culture for assessment by Western blot. Proteins were extracted from THP-1 cells in suspension, PMA (100nM)-stimulated adherent THP-1 cells and PMA-stimulated adherent THP-1 cells treated with dexamethasone (250nM). CD163 protein expression by THP-1 cells was determined by Western blot analysis.

Potential GCR and PPARγ DNA binding sites proximal to the transcription start site of selected genes were predicted using online resources. Nucleotides 2000 base pairs upstream of the transcription start site of the gene of interest were identified using the Ensembl online genome resource (ensembl.org) and input into an online transcription-factor binding profile database (JASPAR.genereg.net). Consensus sequences with putative binding sites for the glucocorticoid receptor (NR3C1) and PPARγ:RXRα heterodimers within the 2000 DNA base pair sequence and with a score threshold above 85% were identified.

5.5.2 Manipulation of nuclear receptor activity

PPARγ function was manipulated using the PPARγ agonist troglitazone and the PPARγ antagonist, T0070907. PPARγ activation was stimulated by treating adherent monocytes for 48 hours with troglitazone (1μM) before exchanging the agonist for control medium for the remainder of the culture period. PPARγ function was inhibited by maintaining the cells in T0070907 (5μM) throughout the cell culture period. Glucocorticoid receptor activation was stimulated in monocyte-derived macrophages by maintaining the cells in dexamethasone (250nM) throughout the culture period. Agonist and antagonists were used in combination at the concentrations described above and the appropriate vehicle controls at equal concentration to the agonist and antagonists were included in all experiments. Changes in expression or localisation of selected markers and receptors following dexamethasone, T0070907, troglitazone and control treatment were determined using immunofluorescent imaging and confirmed using flow cytometric analysis.

5.5.3 Culture of monocyte-derived macrophages on the porcine bladder biological scaffold

To determine if the porcine bladder biological scaffold influenced the expression of functional markers by monocyte-derived macrophages, human PBMCs were seeded onto the decellularised porcine bladder matrix for 11 days and the expression and localisation of CD80, CD163 and PPARγ determined using immunohistochemistry. Expression and localisation of the markers was then compared to immunofluorescent imaging from multiple donors of selected marker expression by monocyte-derived macrophages cultured on glass.

5.6 Results: Expression of markers by monocytes and monocyte-derived macrophages

CD68 protein expression by peripheral blood mononuclear cells and monocyte-derived macrophages cultured on glass was determined by Western blot. CD68 was strongly expressed by monocyte-derived macrophages from two independent donors following 11 days of culture on a glass substrate (Figure 5-4). Despite detection of CD68 in cytospun preparations of PBMC (chapter 3), expression of CD68 was not detected by Western blot in PBMC preparations from either donor, suggesting CD68 expression was below the limit of detection by Western blot (Figure 5-4).

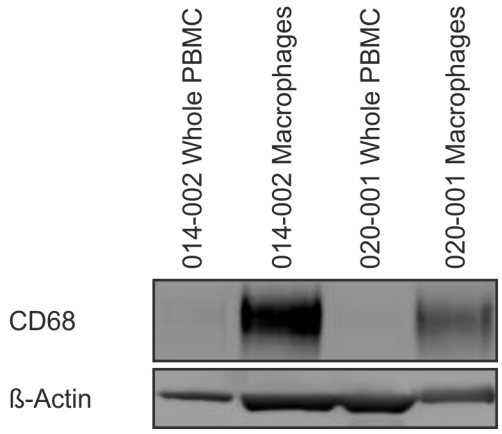

Figure 5-4. CD68 expression by PBMC and monocyte-derived macrophages. Protein lysates from matched whole PBMC, taken directly following isolation from peripheral blood and adherent mononuclear cells seeded onto a glass substrate for 11 days from two independent donors were separated on a 4-12% (w/v) Bis-Tris gel and CD68 expression detected. Labelling of β-Actin was used as a loading control. Whole gel image can be found in appendix IV-I.

Western blot analysis showed that the components to investigate of the role of PPARγ and GCR in the expression of CD163 by monocytes-derived macrophages were present (Figure 5-5). CD163 expression was not detected by Western blot in the whole PBMC preparation of either donor. The anti-CD163 antibody detected two bands at approximately 150kDa in lysates from monocyte-derived macrophages from both donors (Figure 5-5; CD163 lanes 2 and 4 – arrows). Western blot analysis showed that peripheral-blood mononuclear cells

expressed the glucocorticoid receptor and PPARγ and that monocyte-derived macrophages from both donors retained expression of these receptors (Figure 5-5). Detection of PPARγ expression by monocyte-derived macrophages showed the presence of two bands (Figure 5-5; PPARγ lanes 2 and 4 – arrows), suggesting monocyte-derived macrophages express alternative isoforms of the PPARγ protein not expressed by PBMC (Figure 5-5).

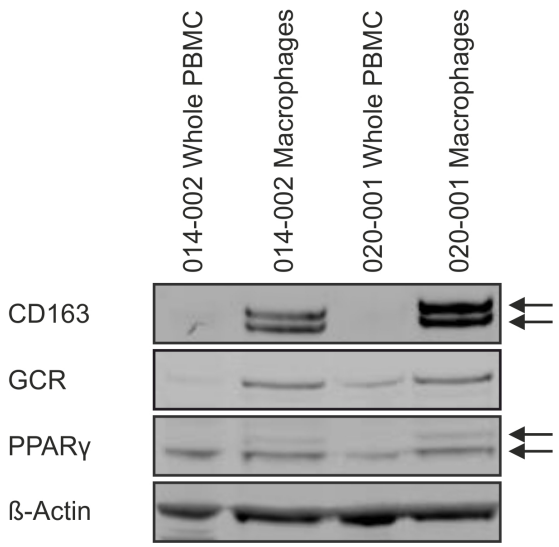

Figure 5-5. CD163, GCR and PPARγ expression by PBMC and monocyte-derived macrophages. Protein lysates from donor matched whole PBMC, taken directly following isolation from peripheral blood and adherent mononuclear cells seeded onto a glass substrate for 11 days were separated on a 4-12% (w/v) Bis-Tris gel. CD163, GCR and PPARγ expression was detected. Labelling of β-Actin was used as a loading control. Whole gel image can be found in appendix IV-II.

Analysis of cytospun preparations of PBMC showed that CD163 expression could be detected by indirect immunofluorescence imaging (Section 3.6, chapter 3). It was postulated that within the heterogeneous PBMC preparations, the reported monocyte-restricted expression of CD68 and CD163 may have been low in proportion to other proteins in the preparations; and therefore below the limits of detection by immunoblotting. To overcome this potential problem, monocytes were enriched by selective adherence on a glass substrate for 3 hours and the proteins extracted for Western blot analysis. Detection of CD68 expression in the enriched peripheral blood monocyte preparations showed a weak band of CD68 protein expression in the lysates of cells from two independent donors (Figure 5-6). A weak band of CD68 expression was also observed in the human liver microsome positive control lane. Adherent monocytes also showed multiple bands of β-Actin expression (Figure 5-6).

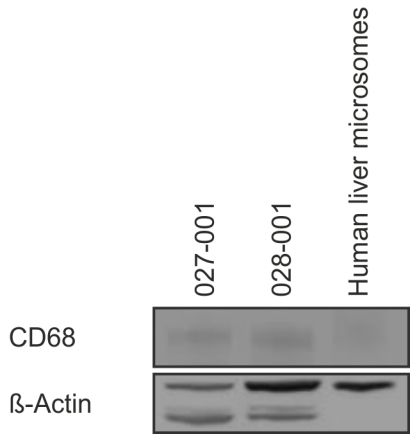

Figure 5-6. Detection of CD68 protein expression by adherent PBMC. Protein lysates from adherent peripheral blood mononuclear cells from two independent donors and protein lysates from microsomes generated from whole human liver were separated on a 4-12% (w/v) Bis-Tris gel and CD68 expression was detected by Western blot. Labelling of β-Actin was used as a loading control. Whole gel image can be found in appendix IV-III.

Western blot analysis of CD163 expression by adherent PBMC showed that CD163 was not detected in the enriched peripheral blood monocyte preparations (Figure 5-7).

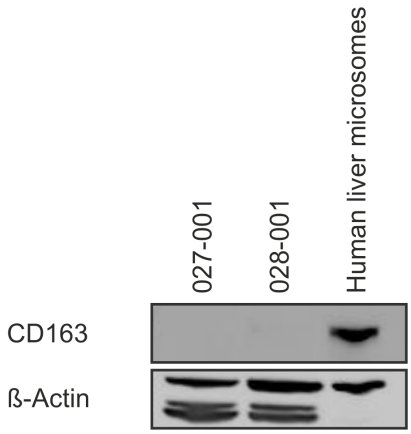

Figure 5-7. Determining expression of CD163 protein by adherent PBMC. Protein lysates from adherent PBMC from two independent donors and protein extracts from human liver microsomes were separated on a 4-12% (w/v) Bis-Tris gel and CD163 protein expression was detected by Western blot. Labelling of β-Actin was used as a loading control. Whole gel image can be found in appendix IV-IV.

Immunofluorescent labelling of CD163 in adherent PBMC revealed an absence of CD163 expression by the adherent cells suggesting either loss in expression of CD163 by the adherent peripheral blood monocytes or that the CD163+ cells observed in cytospun preparation of PBMCs did not adhere to the glass substrate (Figure 5-8).

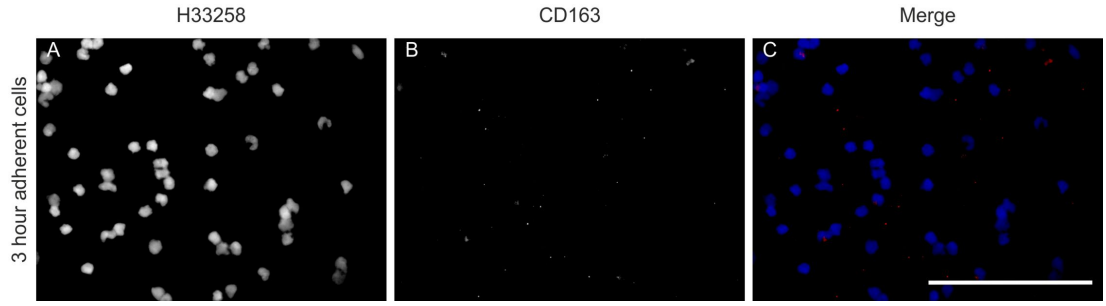

Figure 5-8. Immunofluorescent labelling for CD163 expression by adherent PBMC three hours post seeding. PBMC from donor 016-003. Following three hours of culture on a glass substrate, non-adherent cells were removed and the remaining adherent cells were fixed and labelled for CD163 expression. Scale bar represents 100 microns.

5.7 Results: Determining changes in CD163 expression from monocytes to macrophages

Western blot analysis showed that day 11 monocyte-derived macrophages expressed CD163 at the protein level but adherent PBMC were shown not to express CD163 three hours post seeding. In order to determine if peripheral blood monocytes expressed CD163, CD11b+ peripheral blood monocytes were investigated for expression of CD163 by flow cytometric analysis.

Flow cytometry of PBMC from six independent donors revealed that the majority of CD11b+ human peripheral blood monocytes were positive for CD163 expression (Figure 5-9 and appendix IV-VI). This observation indicated that the adherent peripheral blood monocytes should be positive for CD163 and that CD163 expression by these cells was lost following initial adherence to the glass substrate.

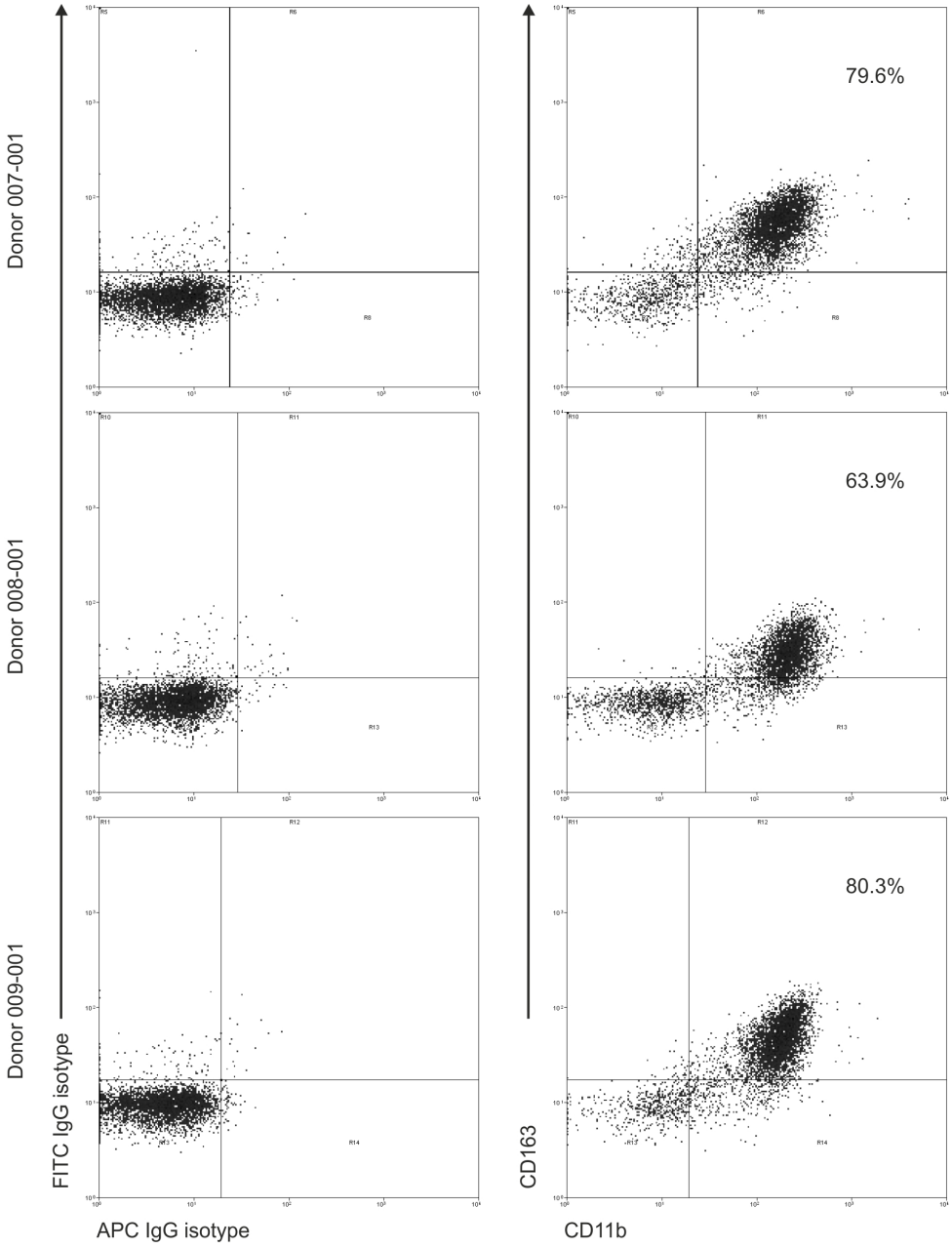

Figure 5-9. Analysis of CD163 expression by CD11b+ peripheral blood monocytes from donors 007-01, 008-001 and 009-001 using flow cytometry. Isolated peripheral blood mononuclear cells were labelled with APC conjugated anti-CD11b and FITC-conjugated anti-CD163 antibodies. Human peripheral blood monocytes were gated based on FS Lin and SS Lin and dead cells excluded from the analysis (Appendix IV-V). Analysis regions for CD11b, CD163 labelling were set using the fluorescent profiles of the APC-IgG and FITC-IgG isotype controls for each donor. Percentage of double positive cells shown. Figure shows three representative flow cytometry plots from a total of six donors.

In order to confirm the earlier observation in which CD163 expression was observed by monocyte-derived macrophages by Western blot (Figure 5-5), adherent peripheral blood monocytes were cultured on a glass substrate for 11 days to allow for differentiation to macrophages. Immunofluorescent imaging of monocyte-derived macrophages from two independent donors labelled with an anti-CD11b antibody showed the size and morphology associated with monocyte differentiation to macrophages (Figure 5-10).

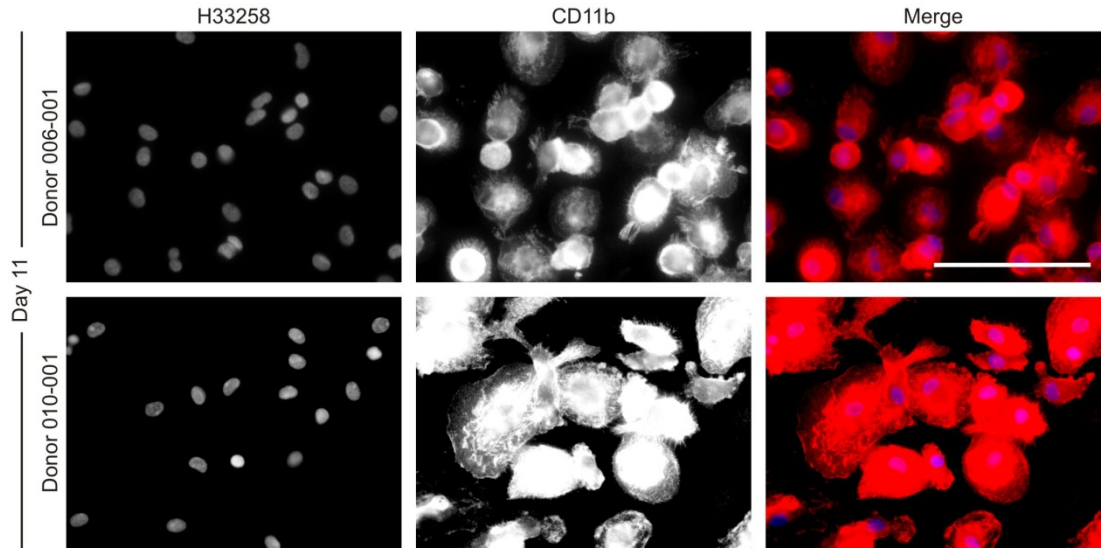

Figure 5-10. Immunofluorescence images of CD11b expression by human monocyte-derived macrophages. Day 11 monocyte-derived macrophages from two donors (006-001 and 010-001) cultured in complete PMBC medium only were immunolabelled for CD11b expression. 32-bit greyscale images of H33258 nuclear staining and CD11b expression were merged to produce colour images. Scale bar represents 100 microns.

Investigation into CD163 expression by the monocyte-derived macrophages at day 11 showed that expression of CD163 was restricted to a subpopulation of monocyte-derived macrophages (Figure 5-11).

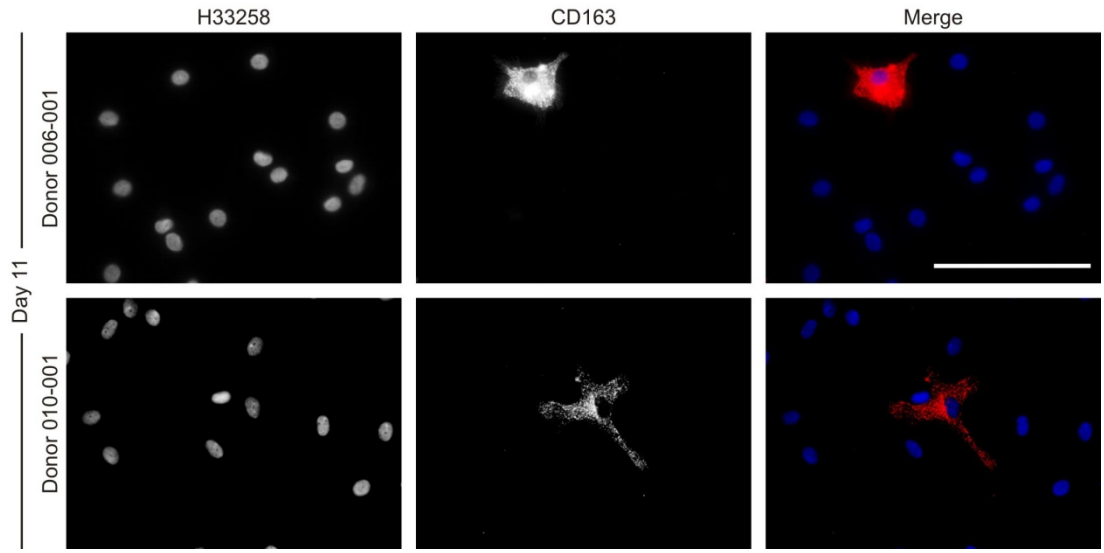

Figure 5-11. The expression of CD163 by monocyte-derived macrophages on a glass substrate. Day 11 monocyte-derived macrophages from two donors (006-001 and 010-001) cultured in complete PMBC medium only were immunolabelled for CD163 expression. 32-bit greyscale images of H33258 nuclear staining and CD163 expression were merged to produce colour images. Scale bar represents 100 microns.

To confirm the observation that a subpopulation of monocyte-derived macrophages expressed CD163 in culture, flow cytometry was used. Analysis of day 11 CD11b+ monocyte-derived macrophages from three independent donors by flow cytometry revealed a gradient of CD163 expression and showed that some cells were $CD163^{hi}$ while other cells were negative for CD163 expression (Figure 5-12). Cells showed high expression of CD11b indicating that these cells were macrophages (Figure 5-12).

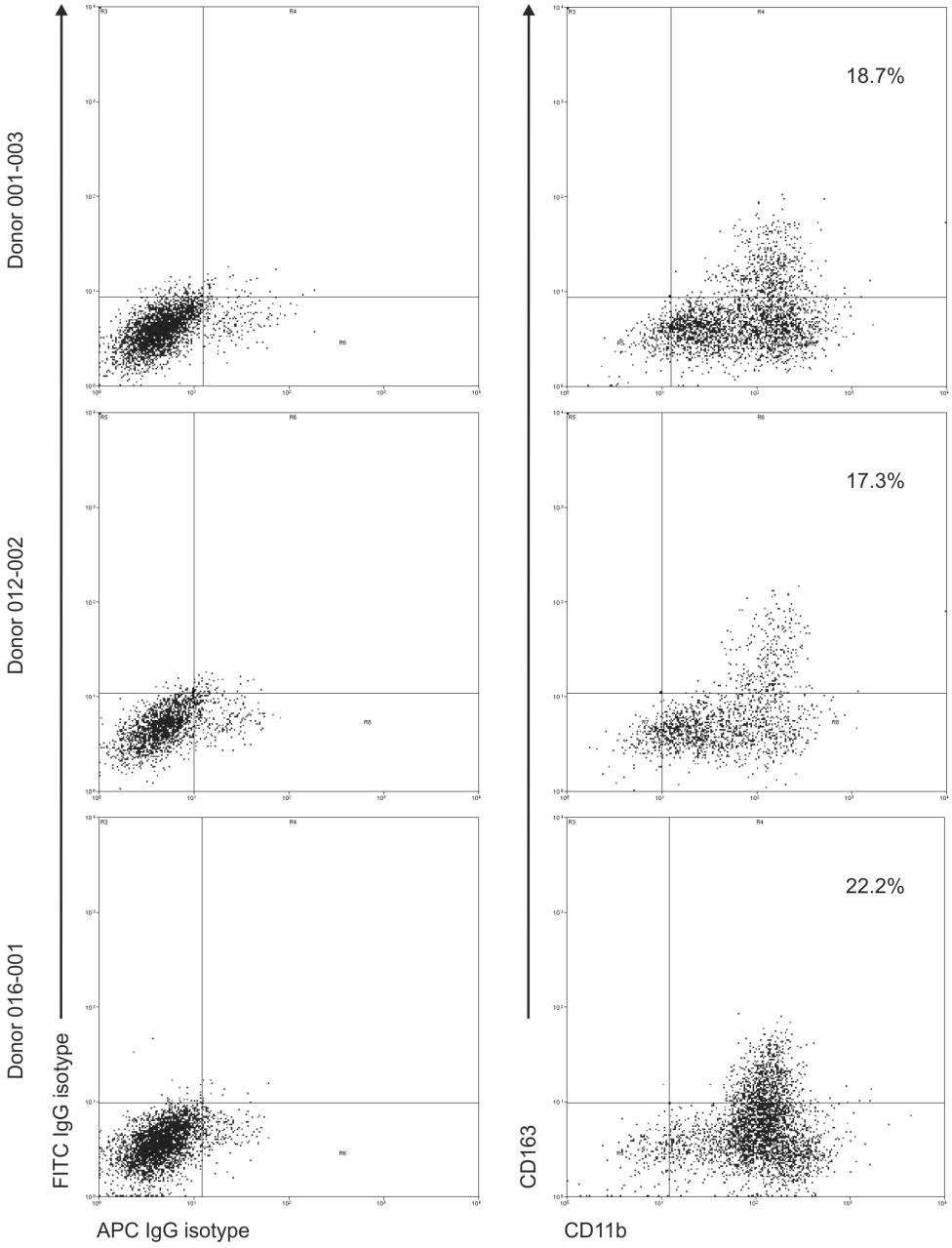

Figure 5-12. Analysis of CD163 expression by CD11b+ monocyte-derived macrophages from donors 001-003, 012-002 and 016-001 using flow cytometry. Monocyte-derived macrophages harvested at day 11 were labelled with APC-conjugated anti-CD11b and FITC-conjugated anti-CD163 antibodies. FS Lin and SS Lin plots and gating of 'live' cells can be found in Appendix IV-VIII. Analysis regions for CD11b, CD163 labelling were set using the fluorescent profiles of the APC-IgG and FITC-IgG isotype controls for each donor (left dot plots). Percentage of double positive cells shown.

Analysis of the percentage of CD11b+CD163+ peripheral blood monocytes and the percentage of CD11b+CD163+ monocyte-derived macrophages showed a significant change (P<0.05) in CD163 expression from peripheral blood monocytes to monocyte-derived macrophages in *in vitro* culture (Figure 5-13). Approximately 80% of human peripheral blood CD11b+ monocytes were positive for CD163 expression (n=6 donors) and approximately 17% of CD11b+ monocyte-derived macrophages were $CD163^{hi}$ (n=3 donors) (Figure 5-13).

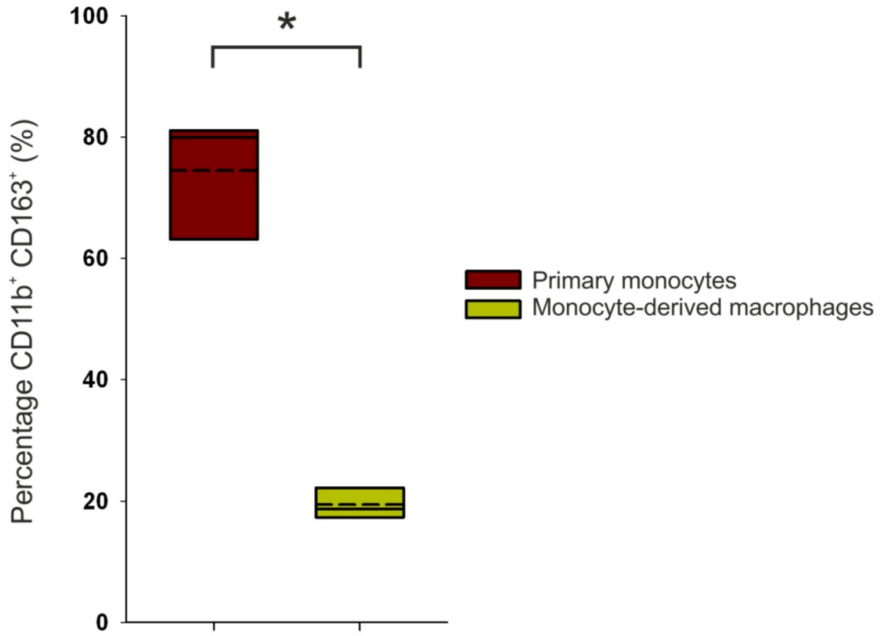

Figure 5-13. Box plots showing the change in CD163 expression from peripheral blood monocytes to monocyte-derived macrophages. The percentage of CD11b+CD163+ monocytes (n=6) and day 11 monocyte-derived macrophages (n=3) determined by flow cytometry were plotted using a box plot. Solid line within each box represents the median value of each dataset and the broken line represents the mean value within each dataset. The top and bottom of the boxes represent the range of each dataset. The statistical significance in the difference in the median values between the two cell types was determined using the Mann-Whitney U test. * Represents significance of P<0.05.

5.8 Results: Known modulators of CD163 expression

In order to further investigate the pattern of CD163 expression by monocyte-derived macrophages and to confirm that the antibody clone EDhu detected changes in expression of CD163, the reported modulation of CD163 by IL-10 and the corticosteroid, dexamethasone, was assessed by immunofluorescent labelling and Western blot analysis respectively.

5.8.1 Modulation of CD163 by IL-10

Fluorescent intensity of CD163 immunolabelling was used to quantify the changes in CD163 expression by monocyte-derived macrophages cultured in the presence of IL-10 for 48 hours compared to monocyte-derived macrophages cultured in complete PBMC medium only. Fluorescent intensity was quantified on 32-bit greyscale images of the fluorescent labelling by setting a threshold of pixel intensity to establish a defined area of analysis and to eliminate background fluorescence from the image analysis (Figure 5-14). The median fluorescent intensity of all cells, which had a fluorescent intensity above that of the threshold, was then plotted for each treatment.

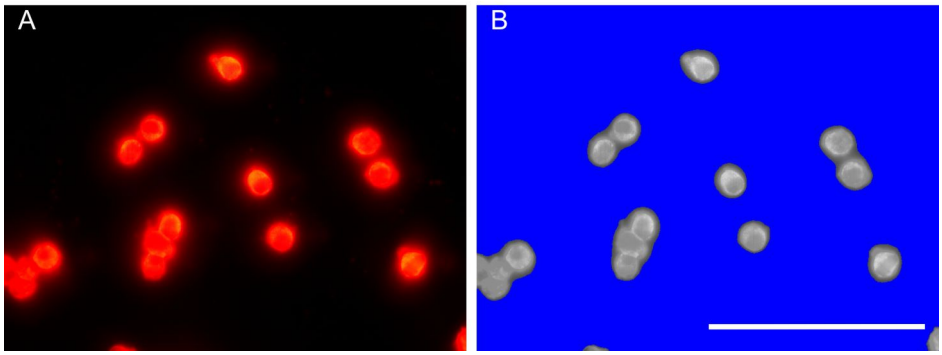

Figure 5-14. Setting an intensity threshold on an immunofluorescence image. Images were captured at a set exposure for the antigen based on the control treatment (A). Images were then converted to 32-bit greyscale and a threshold automatically set using ImageJ (B). The median fluorescence intensity of all the pixels within the image that were above the threshold were measured using the ImageJ software. Scale bar represents 100 microns.

The fluorescent imaging of the IgG isotype control showed low background fluorescent for cells treated with all concentrations of IL-10 and the medium only treated monocyte-

derived macrophages (Figure 5-15). Immunolabelling with the anti-CD163 primary antibody and quantification of the fluorescence showed an increase in CD163 expression by monocyte-derived macrophages following 48 hour treatment with IL-10 at either 1, 10 or 100ng.mL^{-1} compared to the immunolabelled medium only treated cells (Figure 5-15).

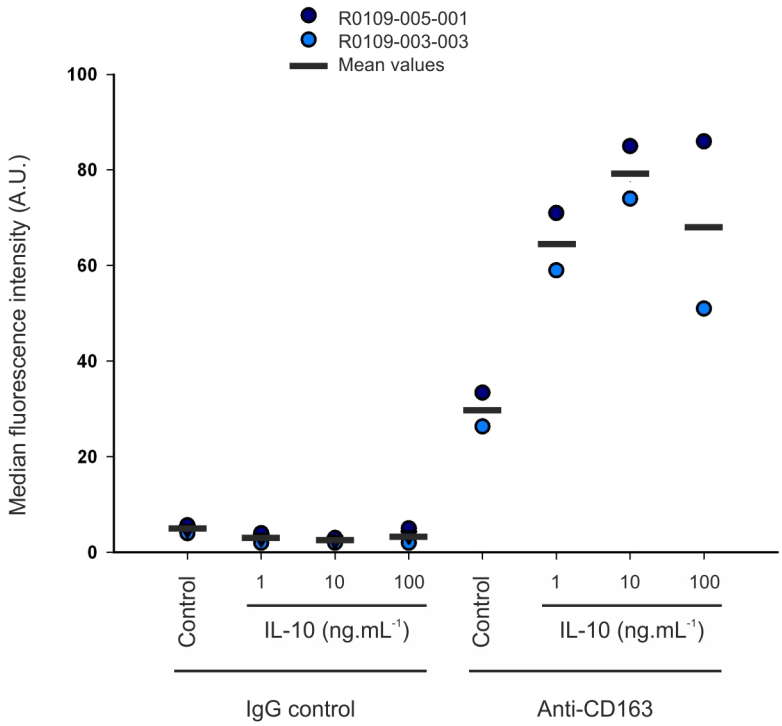

Figure 5-15. Change in fluorescent intensity of CD163 immunolabelling of monocyte-derived macrophages cultured in the presence of IL-10 for 48 hours. Fluorescent intensity of monocyte-derived macrophages from two donors, represented by different coloured dots, either cultured in control conditions (complete PBMC medium) or IL-10 at 1, 10 or 100ng.mL^{-1} in complete PBMC medium for 48 hours. The fixed cells were either incubated with an IgG isotype control or an anti-CD163 monoclonal primary antibody. The mean values of the fluorescent intensity of each donor for each treatment is represent by the bar. A.U is arbitrary units.

Fluorescent intensity analysis of CD163 expression by monocyte-derived macrophages indicated expression of CD163 at the day two time point (Figure 5-15). This observation was confirmed using immunofluorescent labelling of monocyte-derived macrophages from two donors, which showed expression of CD163 by subpopulation of cells at day 11 (Figure

5-16, also see Figure 5-11). These observations indicated that CD163 expression re-emerged 48 hours post-seeding. All cells responded to IL-10 stimulation and showed enhanced expression of CD163. The fluorescent intensity analysis also confirmed that the EDhu clone antibody detected the up-regulation of CD163 expression by monocyte-derived macrophages in the presence of the anti-inflammatory stimulus compared to the control treatment (Figure 5-15).

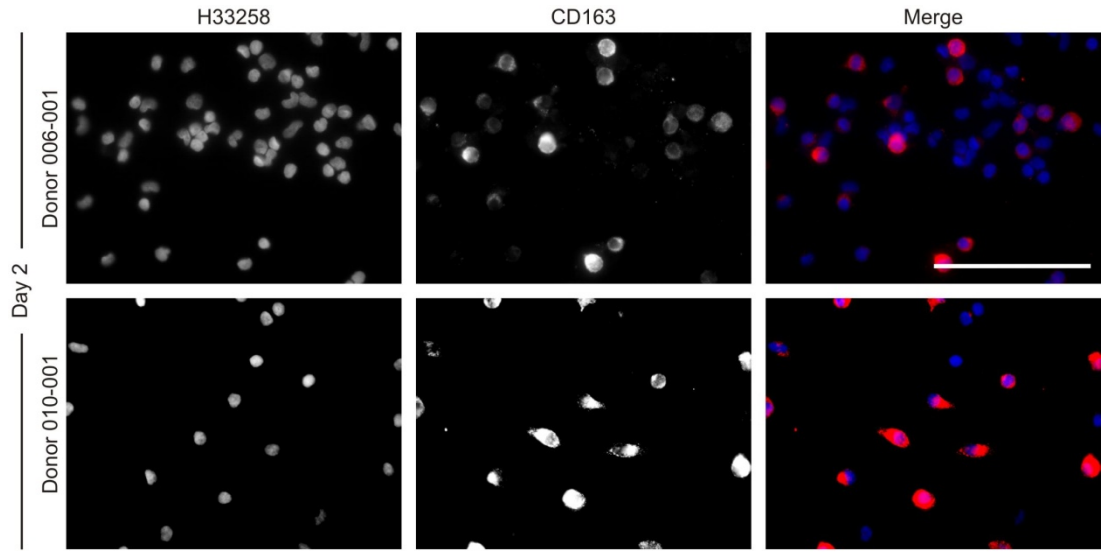

Figure 5-16. CD163 expression by monocyte-derived macrophages following 48 hours of culture on a glass substrate. Monocyte-derived macrophages from two donors (006-001 and 010-001) were cultured on a glass substrate in complete PBMC medium only for 48 hours were immunolabelled for CD163 expression. 32-bit greyscale images of H33258 nuclear staining and CD163 expression were merged to produce colour images. Scale bar represents 100 microns.

5.8.2 Modulation of CD163 by dexamethasone

The monocytic cell line, THP-1 was used to confirm the glucocorticoid receptor-mediated up-regulation of CD163 in response to a synthetic corticoid using Western blot analysis. Monocytic THP-1 cells did not show expression of CD163 by Western blot analysis as observed with human PBMC analysed by Western blot (Figure 5-17). Differentiation of suspension THP-1 cells to an adherent cell type using PMA showed up-regulation of CD163 expression. Expression of CD163 was further increased using dexamethasone (Figure 5-17).

The glucocorticoid receptor was not detected in monocytic THP-1 cells. Differentiation of the THP-1 cells to an adherent macrophage-like phenotype showed expression of the glucocorticoid receptor. Treatment of the macrophage-like THP-1 cells with dexamethasone showed a loss of the glucocorticoid receptor expression by the adherent THP-1 cells (Figure 5-17). All changes in CD163 expression were independent of the vehicle.

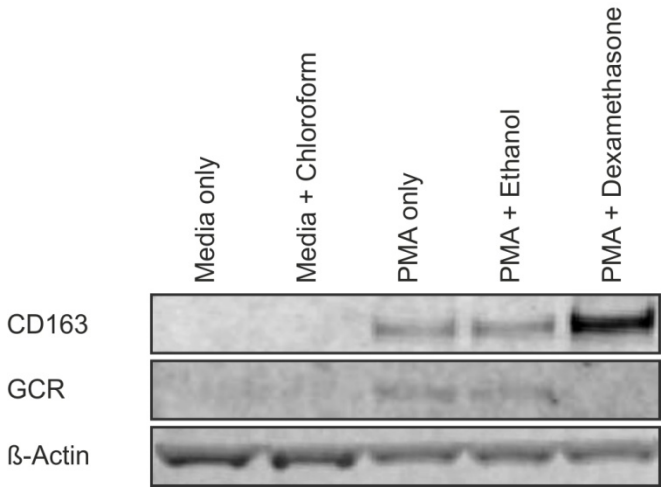

Figure 5-17. Western blot analysis of CD163 and glucocorticoid receptor expression by THP-1 cells. THP-1 cell protein lysates were separated on a 3-8% (w/v) Tris-Acetate gel and CD163 and GCR expression determined by Western blot. Medium plus chloroform was the vehicle control for the PMA. PMA plus ethanol was the vehicle control for the dexamethasone. Labelling of β-Actin was used as a loading control. Whole gel image can be found in appendix IV-IX.

5.9 Results: Identification of putative nuclear receptor DNA binding sites

Investigation into the potential role of PPARγ in the regulation of CD163 expression initially employed bioinformatics analysis of the promoter region of the CD163 gene. Putative glucocorticoid receptor and PPARγ DNA binding site consensus sequences were determined using the online transcription-factor binding profile database (JASPARgenereg.net) (Figure 5-18). The PPARγ binding sequence was also confirmed (Juge-Aubry et al., 1997; Heinäniemi et al., 2007).

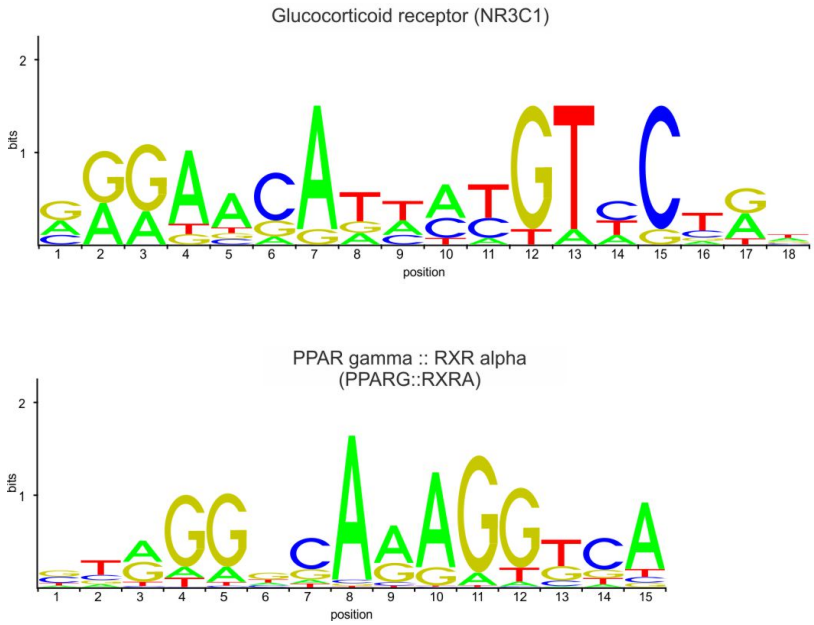

Figure 5-18. Sequence logos of the putative DNA binding sequences of the glucocorticoid receptor (NR3C1) and PPARγ heterodimerised with its binding partner, RXRα. Each nucleotide is scaled based on its relative occurrence at that position (reviewed in (Wasserman and Sandelin, 2004)).

Sequence searches for PPARγ:RXRα (PPARG::RXRA) or glucocorticoid receptor (NR3C1) putative binding sites upstream of the transcription start of selected genes confirmed that the CD36 gene had a putative PPARγ:RXRα DNA binding site (Table 5-1). CD163 was also confirmed to have a consensus sequence for glucocorticoid receptor binding upstream of the transcription start site. Sequence analysis of the upstream region of the NR3C1 gene indicated that there were no putative binding sites for either the glucocorticoid receptor or PPARγ:RXRα when the relative score threshold was set to ≥85% (Table 5-1). Interestingly,

PPARγ was found to have both putative PPARγ:RXRα and glucocorticoid receptor DNA binding motifs upstream of the PPARγ transcription start site suggesting that both nuclear receptors might regulate the expression of PPARγ. CD11b was used as a control gene for transcript which is not thought to be driven by either PPARγ or glucocorticoid receptor (Table 5-1). Emphasis should be made that use of promoter analysis to search for transcription factor binding sites only offers limited indication as to whether the transcription factor can bind within the defined upstream region.

Table 5-1. Output from JASPAR transcription-factor binding profile database

Gene transcribed	Transcription factor	Relative score	Start base	End base	DNA binding sequence
CD36	PPARG::RXRA	0.88	54	68	CCAGGCCAGAGTGCA
CD163	NR3C1	0.86	1168	1185	AGGGAAATCCTGTCCTTT
Glucocorticoid receptor	NI	NI	NI	NI	NI
PPAR gamma	PPARG::RXRA	0.87	640	654	GGGAGGCAGAGGTTA
	NR3C1	0.88	1678	1695	TGGAGCATACTGTTCTGG
	NR3C1	0.85	1679	1696	CAGAACAGTATGCTCCAG
CD11b	NI	NI	NI	NI	NI

NI – Not identified

5.10 Results: Modulation of CD163 expression by PPARγ

To determine if PPARγ activation affected the expression of CD163 by human monocyte-derived macrophages, the PPARγ agonist troglitazone and the PPARγ antagonist, T0070907 were employed. As described in the introduction to this chapter, PPARγ can modulate the expression of the co-stimulatory molecule, CD80. Therefore, CD80 expression was used as an indicator of PPARγ stimulation and inhibition. Monocyte-derived macrophages at day 11 in culture on a glass substrate showed a basal level of CD80 expression (Figure 5-19). Inhibition of monocyte-derived macrophage PPARγ activation using T0070907 for 11 days showed a marked increase in CD80 expression (Figure 5-19). Stimulation of PPARγ with troglitazone for 48 hours followed by culture in control medium showed a qualitative decrease in CD80 immunolabelling at day 11. No qualitative difference in CD80 immunolabelling was observed following stimulation of the glucocorticoid receptor with dexamethasone however, culture in the presence of dexamethasone for 11 days reduced the number of cells that adhered to the glass substrate (Figure 5-19). This immunofluorescent dataset provided qualitative readout of the activation or inhibition of PPARγ using the pharmacological agonist or inhibitor.

Preliminary data of the effects of PPARγ modulation on CD163 and CD80 expression can be found in appendices IV-X to IV-XVI.

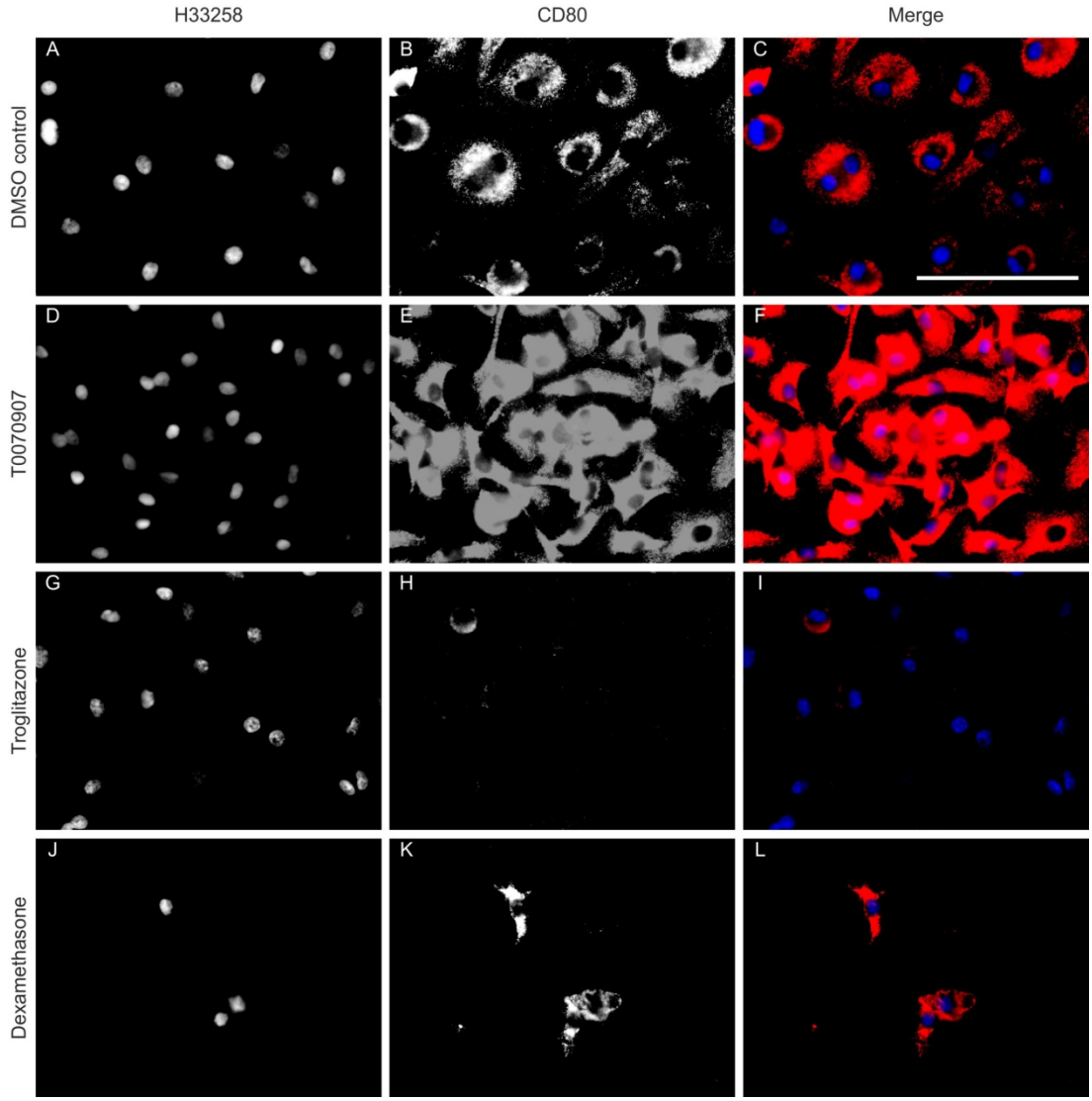

Figure 5-19. The effect of PPARγ activation and inhibition and glucocorticoid receptor activation on the expression of CD80 by monocyte-derived macrophages. Day 11 monocyte-derived macrophages from donor 012-003 were cultured in complete PBMC medium containing either DMSO control for 11 days (A-C), T0070907 for 11 days (D-F), troglitazone for 48 hours followed by nine days in DMSO control medium (G-I) or dexamethasone for 11 days (J-L). Fixed cells were immunolabelled for CD80 expression and all images captured at the same exposure, set using the control cells. 32-bit greyscale images of nuclei (H33258) and CD80 expression were merged to produce a colour image. Scale bar represents 100 microns.

5.10.1 Modulation of CD163 expression by activation of PPARγ

Investigation of CD163 expression in PPARγ-activated monocyte-derived macrophages did not show a qualitative increase in the level of immunofluorescent intensity, corresponding to an up-regulation of CD163 expression compared to the control cells. However, there was a noticeable increase in the number of CD163 positive cells per field of view following PPARγ activation (Figure 5-20). The total number of CD163+ cells per field of view was quantified manually and the percentage of CD163+ cells determined using H33258 staining as an indicator of total cell number (Table 5-2). This method of analysis showed a subtle increase in the percentage of CD163+ cells in troglitazone treatment cultures versus medium only cell cultures by two independent donors (Table 5-2). Images from donor 015-002 can be found in appendix IV-XVII.

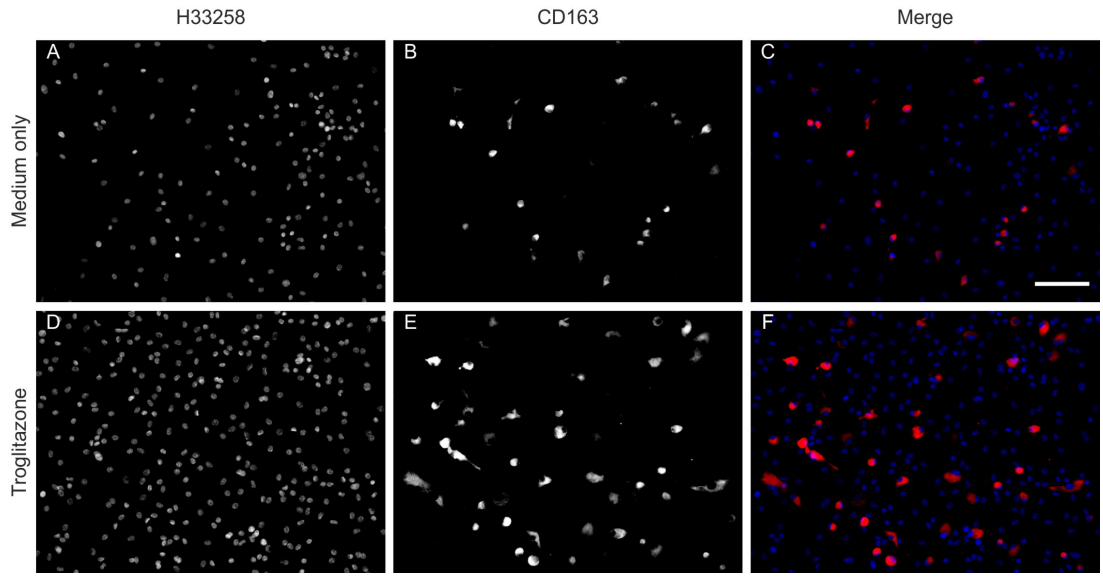

Figure 5-20. The effect of PPARγ activation on the expression of CD163 by monocyte-derived macrophages. Day 11 monocyte-derived macrophages from donor 005-003 were either cultured in complete PBMC medium only (A-C) or complete PBMC medium containing troglitazone for 48 hours followed by nine days in complete PBMC medium (D-F). Fixed cells were immunolabelled for CD163 expression. 32-bit greyscale images of H33258 staining and CD163 expression were merged to produce a colour image. Scale bar represent 100 microns.

Table 5-2. Quantification of CD163+ monocyte-derived macrophages cultured in the presence or absence of troglitazone

Donor	Treatment	Number $CD163^+$ cells	Total cell number	Percentage $CD163^+$ cells (%)
005-003	Medium only	34	375	9
	Troglitazone	94	659	14
015-002	Medium only	11	144	8
	Troglitazone	11	96	11

The increase in CD163+ cell number following stimulation with the PPARγ agonist, troglitazone was further quantified using flow cytometric analysis. Previously, approximately 17% of CD11b+ monocyte-derived macrophages were shown to be $CD163^{hi}$ when cultured in medium only and analysed by flow cytometry (Figure 5-12). Following stimulation of PPARγ with troglitazone for 48 hours and culture of a further nine days in control medium, 36.1% of CD11b+ monocyte-derived macrophages were positive for CD163 (Figure 5-21). These cells could also be more clearly defined as CD163+. A population of CD11b+ cells that did not express CD163 following treatment with the PPARγ agonist was observed both by immunofluorescence (figure 5-20) and flow cytometry (Figure 5-21).

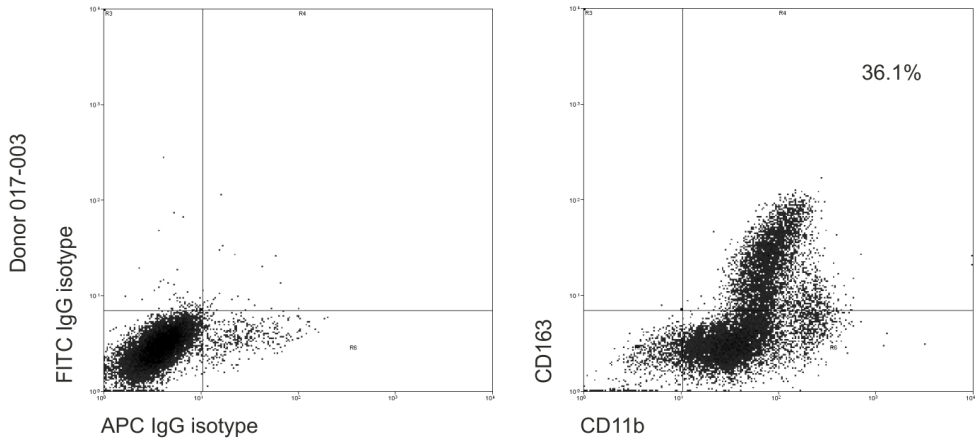

Figure 5-21. **Flow cytometric analysis of CD11b+ monocyte-derived macrophages following activation of PPARγ**. Day 11 monocyte-derived macrophages from donor 017-003 were harvested for flow cytometric analysis following activation of PPARγ for 48 hours with complete PBMC medium containing troglitazone followed by culture for a further nine days in DMSO control medium. The cells were labelled with APC conjugated anti-CD11b and FITC-conjugated anti-CD163 antibodies. FS Lin and SS Lin plots and gating of live cells can be found in appendix IV-XVIII. Analysis regions for CD11b, CD163 labelling were set using the fluorescent profiles of the APC-IgG and FITC-IgG isotype controls (left dot plot).

5.10.2 Modulation of CD163 expression by inhibition of PPARγ function

To further investigate the potential role for PPARγ in regulating CD163 expression, the nuclear receptor was pharmacologically inhibited using T0070907. Inhibition of PPARγ function had a profound effect on the morphology of the monocyte-derived macrophages. Culture in the presence of the PPARγ antagonist resulting in the macrophages becoming elongated in morphology compared to a more rounded 'fried egg' morphology observed when cultured in complete PBMC medium only (Figure 5-22).

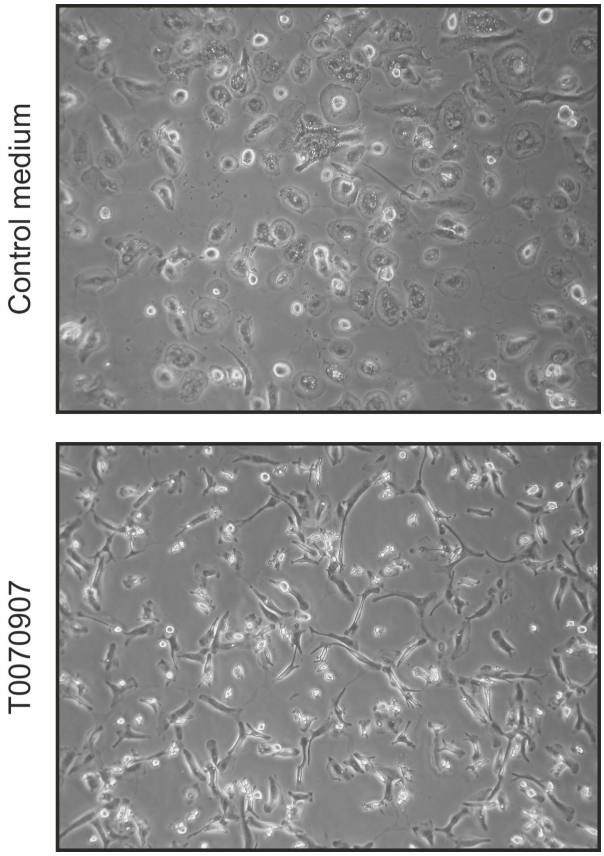

Figure 5-22. Phase contrast images of day 11 monocytes-derived macrophages cultured either in control medium or in the presence of T0070907. Monocyte-derived macrophages from donor 013-002 were cultured on a glass substrate in complete PBMC medium in the absence (control medium) or in complete PBMC medium in the presence of T0070907.

In concordance with the observation that T0070907 treatment up-regulated the 'pro-inflammatory' marker CD80 by monocyte-derived macrophages, PPARγ inhibition showed a loss of expression of CD163 by the subpopulation by monocyte-derived macrophages (Figure 5-23). Furthermore, in the presence of T0070907, the glucocorticoid receptor agonist, dexamethasone failed to up-regulate CD163 expression, indicating that the glucocorticoid receptor-mediated up-regulation of CD163 was dependent on PPARγ activation (Figure 5-23). Again a greater number of CD163+ cells were observed following PPARγ activation with troglitazone (Figure 5-23, I).

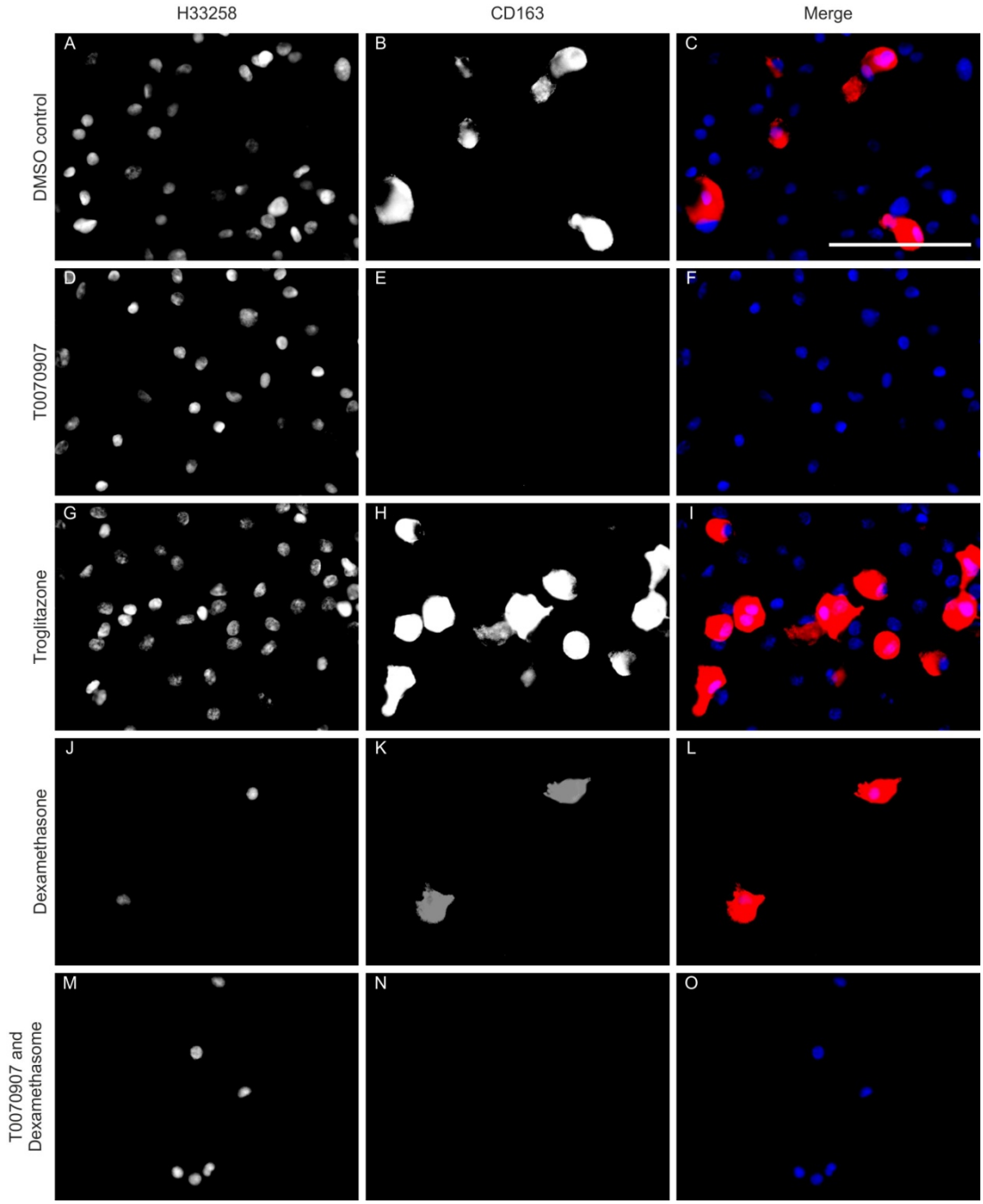

Figure 5-23. The effect of PPARγ activation and inhibition and glucocorticoid receptor activation on the expression of CD163 by day 11 monocyte-derived macrophages. Day 11 monocyte-derived macrophages from donor 012-003 were cultured in complete PBMC medium containing either DMSO control for 11 days (A-C), T0070907 for 11 days (D-F), troglitazone for 48 hours followed by nine days in DMSO control medium (G-I), dexamethasone for 11 days (J-L) or dexamethasone in the presence of T0070907 for 11 days (M-O). Fixed cells were immunolabelled for CD163 expression and all images captured at the same exposure, set using the control cells. 32-bit greyscale images were merged as previously described. Scale bar represents 100 microns.

To determine the pattern of the PPARγ-dependent changes in CD80 and CD163 expression, an earlier time point was investigated. Inhibition of PPARγ with T0070907 for six days and immunofluorescence labelling of CD80 showed a marked increase in immunofluorescence which corresponded to an increase in CD80 expression as observed at day 11 (Figure 5-24). Monocyte-derived macrophages stimulated for 48 hours with troglitazone followed by culture for a further four days in control medium did not show a loss in CD80 immunolabelling as observed at day 11 (Figure 5-24). This observation was consistent for two donors (Appendix IV-XIX).

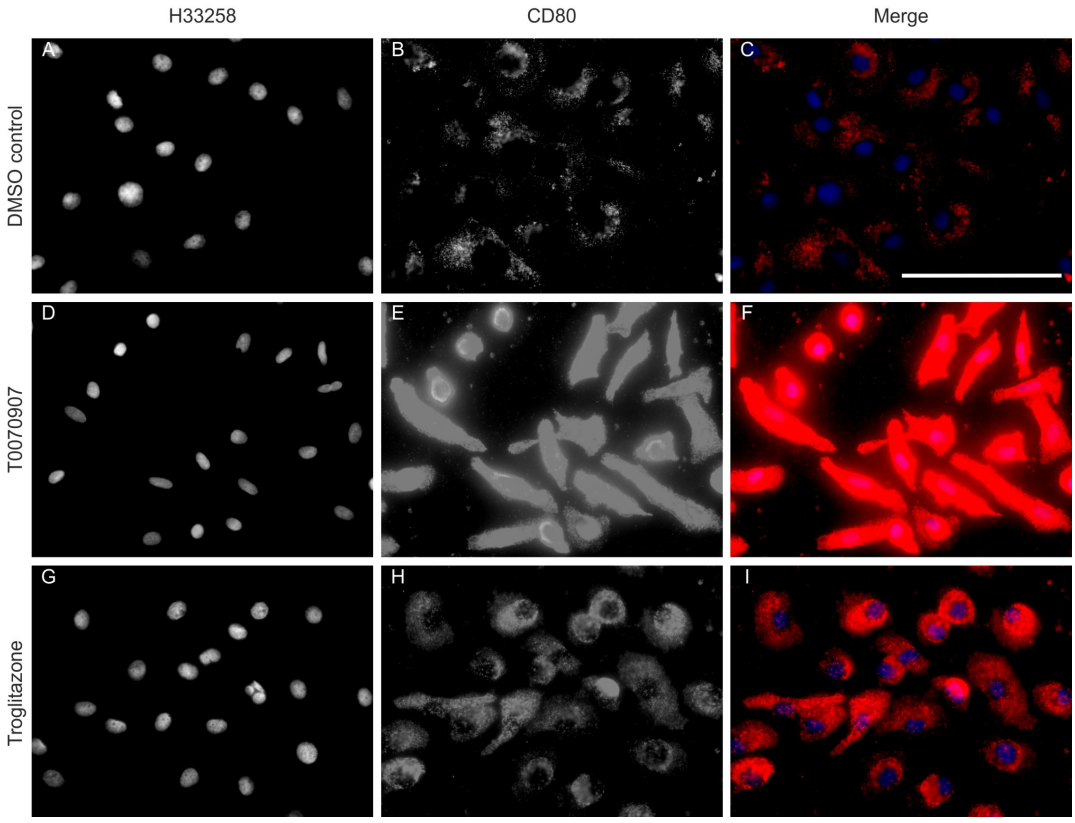

Figure 5-24. The effect of PPARγ activation and inhibition on CD80 expression by monocyte-derived macrophages. Day 6 monocyte-derived macrophages from donor 017-002 were cultured in complete PBMC medium containing either DMSO control for 6 days (A-C), T0070907 for 6 days (D-F), troglitazone for 48 hours followed by four days in DMSO control medium (G-I). Fixed cells were immunolabelled for CD80 expression and all images captured at the same exposure, set using the control cells. 32-bit greyscale images were merged as previously described. Scale bar represents 100 microns.

Immunofluorescence labelling of monocyte-derived macrophages cultured in control medium for six days showed a subpopulation of CD163+ cells as observed at the day 11 time point (Figure 5-25). CD163 expression was absent at day six in the presence of T0070907 (Figure 5-25). In line with the distinct difference in CD80 expression at day six compared to day eleven following PPARγ activation, no qualitative difference in CD163 expression by monocyte-derived macrophages was observed at day six following 48 hours of troglitazone treatment. Dexamethasone also maintained the ability to up-regulate CD163 expression in the presence of T0070907 (Figure 5-25). This observation was consistent for two donors (Appendix IV-XX).

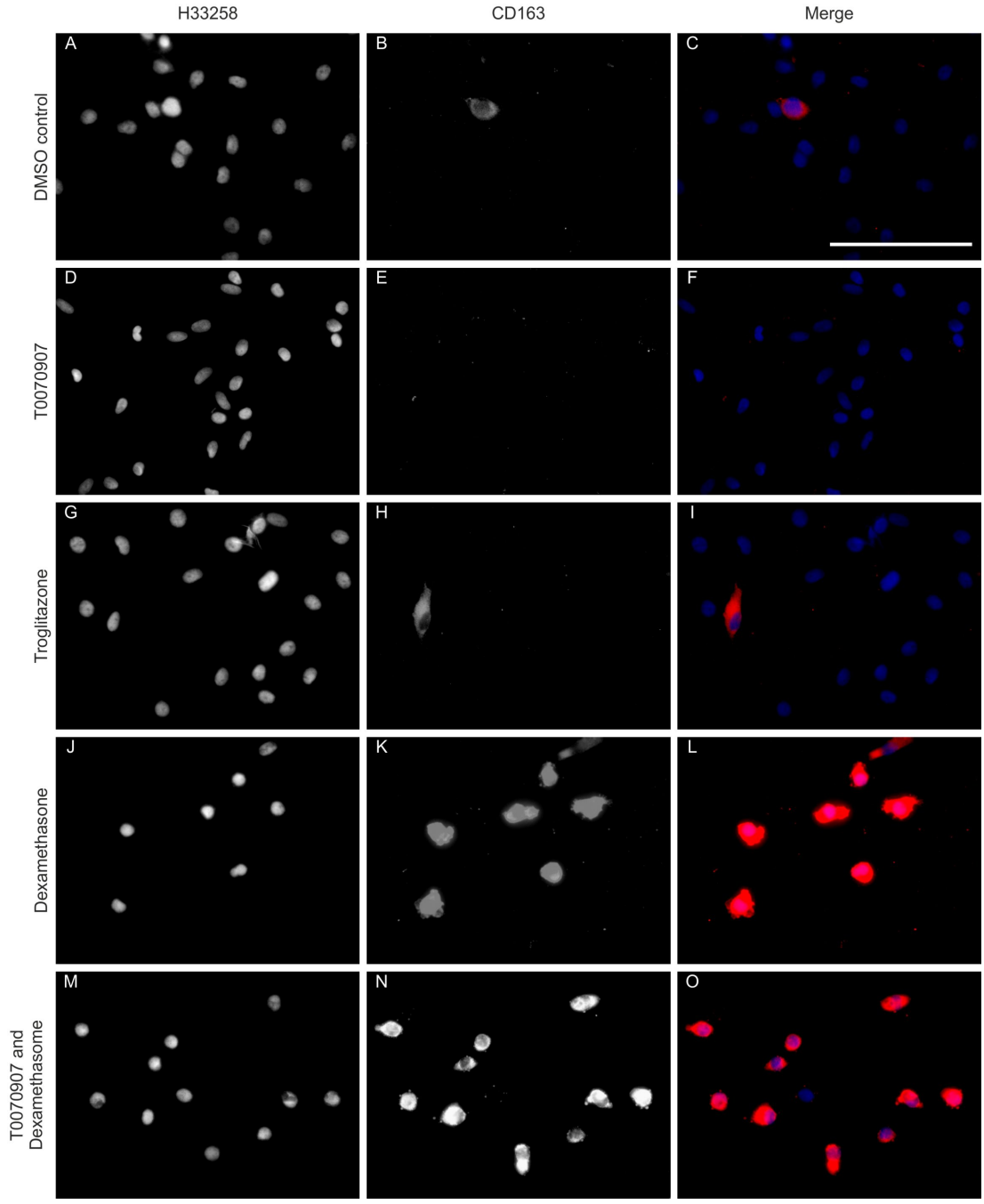

Figure 5-25. The effect of PPARγ activation and inhibition and glucocorticoid receptor activation on the expression of CD163 by day six monocyte-derived macrophages. Day 6 monocyte-derived macrophages from donor 017-002 were cultured in complete PBMC medium containing either DMSO control for 11 days (A-C), T0070907 for 11 days (D-F), troglitazone for 48 hours followed by nine days in DMSO control medium (G-I), dexamethasone for 11 days (J-L) or dexamethasone in the presence of T0070907 for 11 days (M-O). Fixed cells were immunolabelled for CD163 expression and all images captured at the same exposure, set using the control cells. 32-bit greyscale images were merged to produce colour images. Scale bar represents 100 microns.

Flow cytometric analysis was used to determine if the whole population of monocyte-derived macrophages treated with T0070907 was negative for CD163 expression at day six in culture. Monocyte-derived macrophages at day six were gated based on FS Lin and SS Lin as previously described and CD163 expression determined by the comparison between the cells labelled with the primary antibody and cells incubated with the matched fluorochrome-conjugated isotype control (Figure 5-26).

Flow cytometric analysis of CD163 labelled monocyte-derived macrophages revealed a gradient of CD163 expression as previously observed at day eleven and agreed with the immunofluorescent data indicating a subpopulation of monocyte-derived macrophages were $CD163^{hi}$ (Figure 5-26). Culture of the monocyte-derived macrophages in the presence of T0070907 showed a complete absence of CD163 labelling at the day six time point indicating that PPARγ function was required for the maintenance of the CD163+ population. This observation was reproducible in two donors in two independent experiments (Figure 5-27).

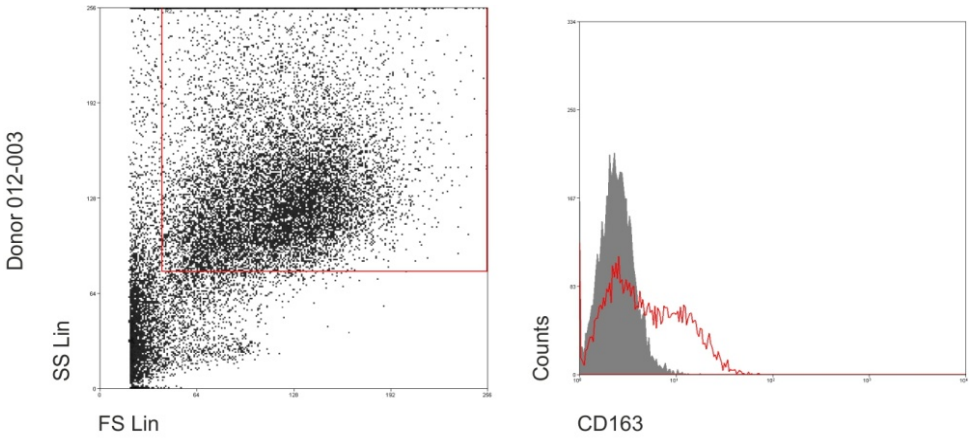

Figure 5-26. **Flow cytometric analysis of day six monocyte-derived macrophages cultured in DMSO control medium**. Human peripheral blood monocyte-derived macrophages from donor 012-003 were cultured for six days in DMSO control medium. Monocyte-derived macrophages were gated by FS Lin and SS Lin (left dot plots) and 'live' cells selected (Appendix IV-XXI). CD163 labelling is shown in histogram format (right histogram). The red line represents CD163 labelling and the grey histogram represents isotype control labelling.

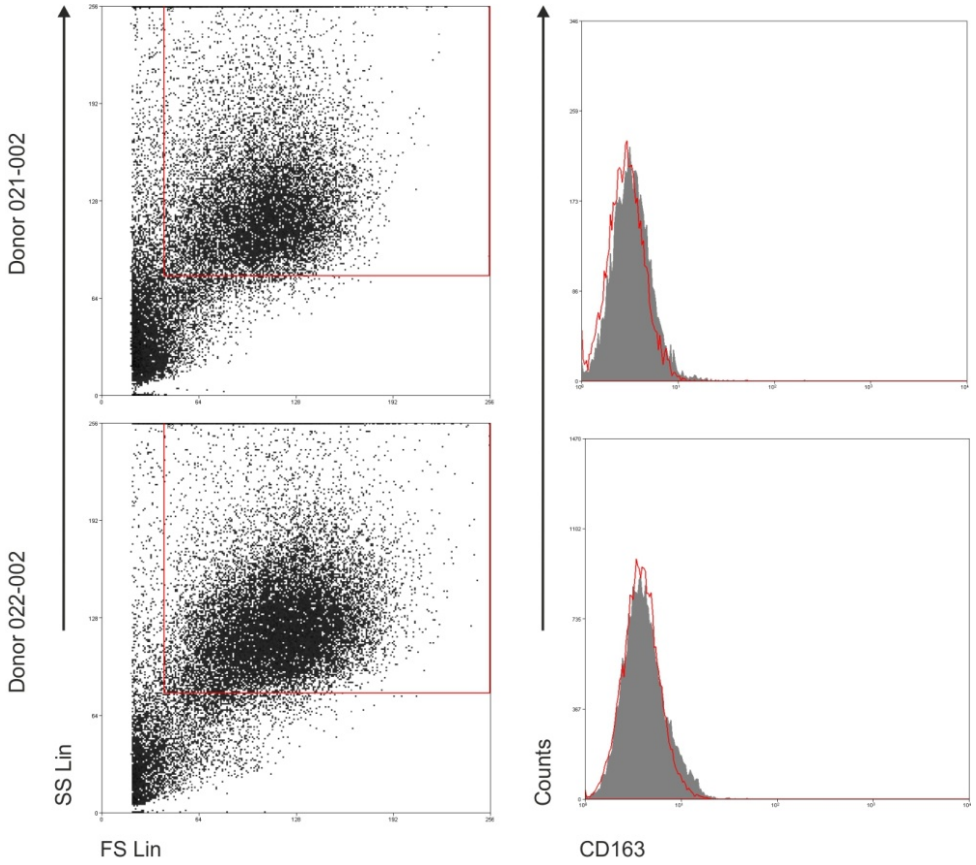

Figure 5-27. **Flow cytometric analysis of CD163 expression by day six monocyte-derived macrophages following inhibition of PPARγ**. Human peripheral blood monocyte-derived macrophages from two independent donors, 021-002 and 022-002, were cultured for six days in the presence of T0070907. Monocyte-derived macrophages were gated by FS Lin and SS Lin (left dot plots) and 'live' cells selected (Appendix IV-XXII). CD163 labelling is shown in histogram format (right histograms). The red lines represent CD163 labelling and the grey histogram represents isotype control labelling.

5.11 Results: Modulation of nuclear receptor expression

5.11.1 PPARγ

To determine the effects of the PPARγ and glucocorticoid receptor agonists and inhibitors on PPARγ and the glucocorticoid receptor expression and localisation, the nuclear receptors were immunolabelled and imaged. Fluorescent immunolabelling of PPARγ indicated a mixture of cytoplasmic and nuclear PPARγ in monocyte-derived macrophages cultured in control medium for 11 days however, culture in the presence of T0070907 showed intense cytoplasmic PPARγ immunolabelling. Treatment of monocyte-derived macrophages with troglitazone for 48 hours followed by culture in control medium for a further nine days also showed predominantly cytoplasmic PPARγ and very little presence of PPARγ within the nuclei of the cells (Figure 5-28). Dexamethasone treated monocyte-derived macrophages showed intense cytoplasmic PPARγ at day 11 with little qualitative difference between dexamethasone treatment in the presence or absence of T0070907 (Figure 5-28).

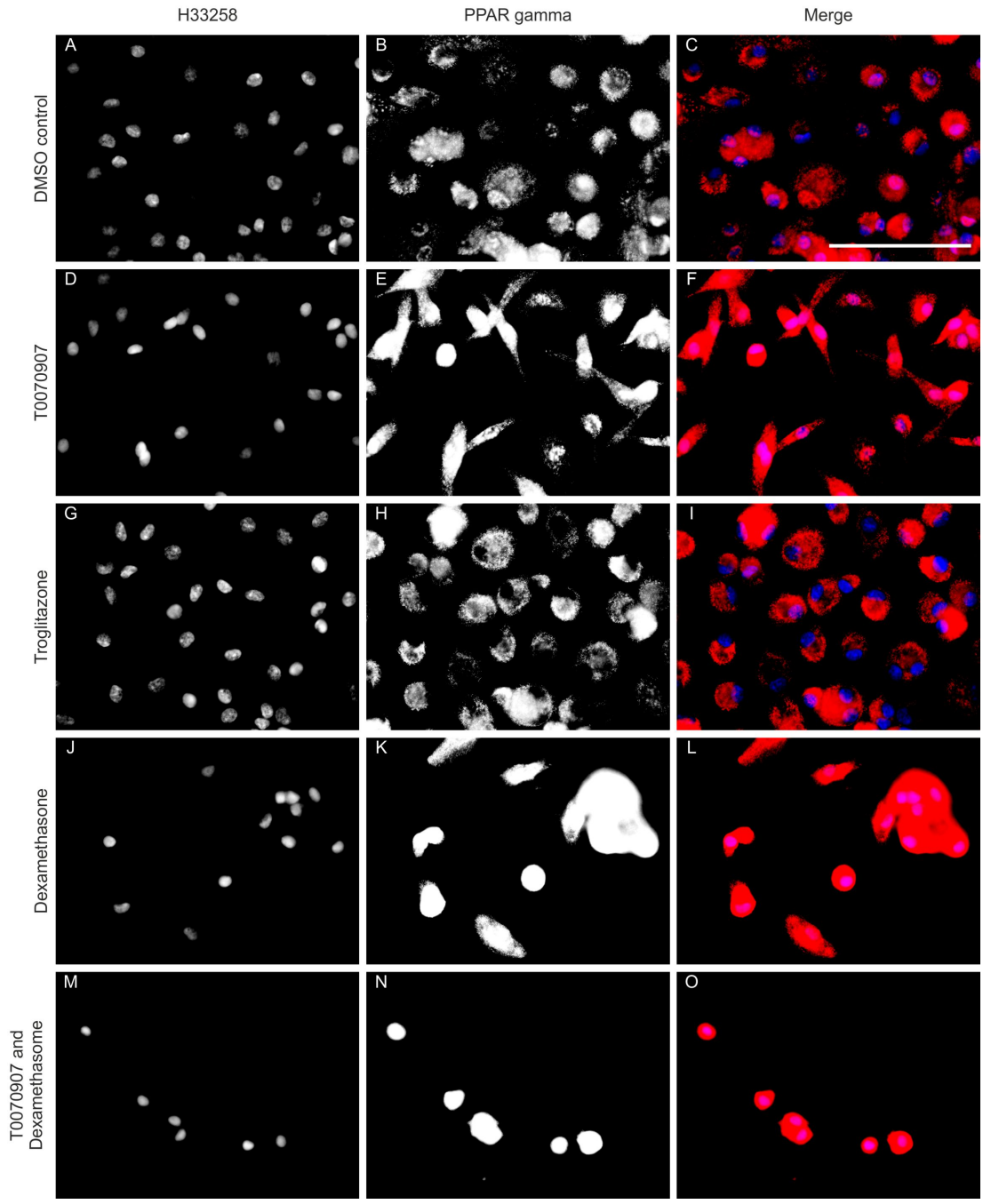

Figure 5-28. The effect of PPARγ activation and inhibition and glucocorticoid receptor activation on the expression of PPARγ by day 11 monocyte-derived macrophages. Day 11 monocyte-derived macrophages from donor 012-003 were cultured in complete PBMC medium containing either DMSO control for 11 days (A-C), T0070907 for 11 days (D-F), troglitazone for 48 hours followed by nine days in DMSO control medium (G-I), dexamethasone for 11 days (J-L) or dexamethasone in the presence of T0070907 for 11 days (M-O). Fixed cells were immunolabelled for PPARγ and images captured at a set exposure and merged as previously described. Scale bar represents 100 microns.

5.11.2 Glucocorticoid receptor

Fluorescent imaging of glucocorticoid receptor immunolabelling revealed a mixture of cytoplasmic and nuclear localised receptor in the DMSO control treated monocyte-derived macrophages at day 11 (Figure 5-29). The culture of monocyte-derived macrophages in the presence of T0070907 showed a loss in glucocorticoid receptor immunolabelling by the majority of cells (Figure 5-29). Conversely, PPARγ stimulation with troglitazone showed no qualitative difference in glucocorticoid receptor expression. Stimulation of the glucocorticoid receptor with dexamethasone showed a loss of glucocorticoid receptor expression in agreement with the observations made in the THP-1 cell line following treatment with dexamethasone (Figure 5-17). The dexamethasone-stimulated loss of glucocorticoid receptor expression was independent of the presence of T0070907. Again, culture of monocyte-derived macrophages in the presence of dexamethasone appeared to show a loss of cells compared to the other treatments (Figure 5-29).

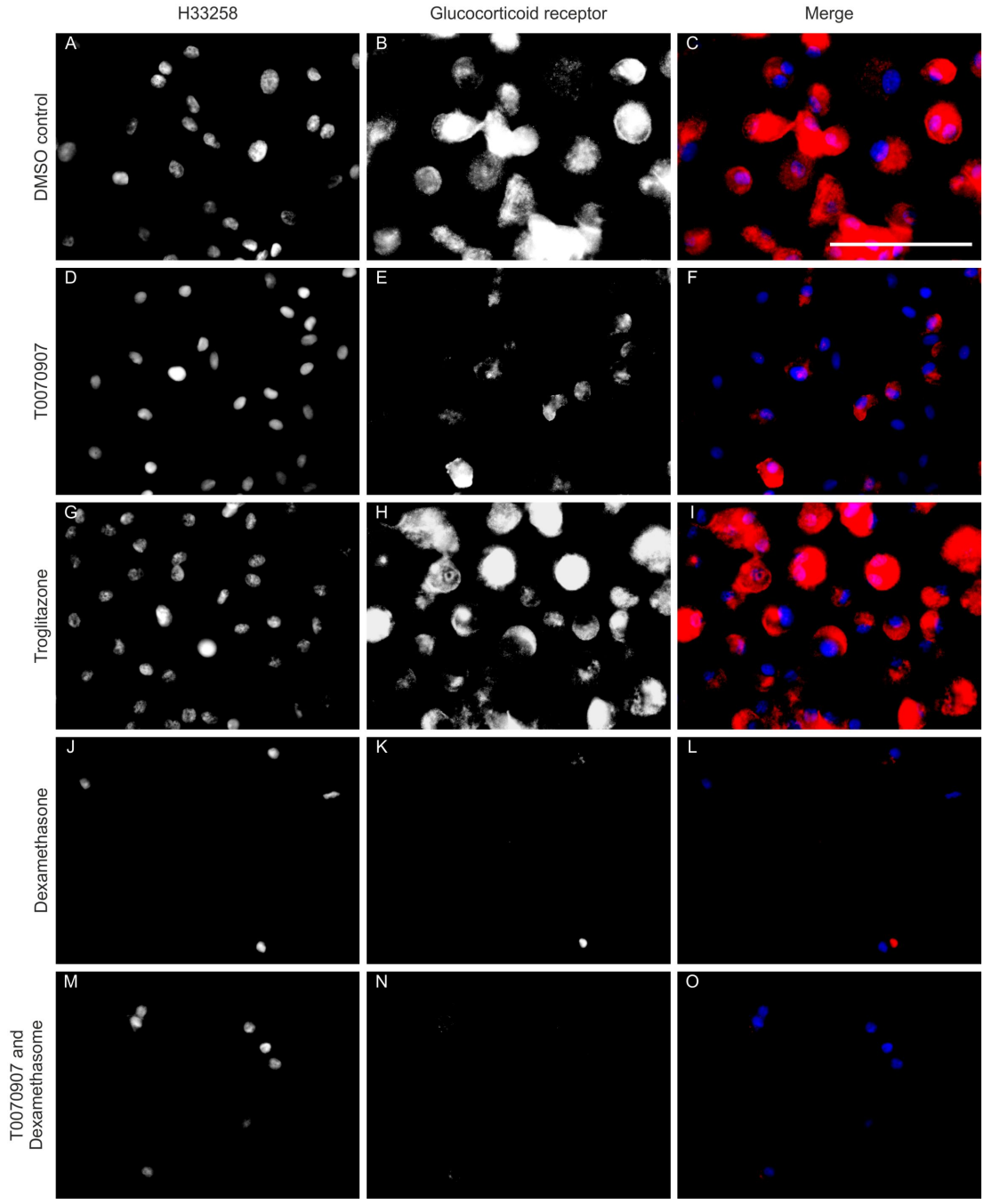

Figure 5-29. The effect of PPARγ activation and inhibition and glucocorticoid receptor activation on the expression of the glucocorticoid receptor by day 11 monocyte-derived macrophages. Day 11 monocyte-derived macrophages from donor 012-003 were cultured in complete PBMC medium containing either DMSO control for 11 days (A-C), T0070907 for 11 days (D-F), troglitazone for 48 hours followed by nine days in DMSO control medium (G-I), dexamethasone for 11 days (J-L) or dexamethasone in the presence of T0070907 for 11 days (M-O). Fixed cells were immunolabelled for GCR and images captured at a set exposure and merged as previously described. Scale bar represents 100 microns.

5.12 Results: CD80 expression by monocyte-derived macrophage cultured on different substrates

It was postulated that monocyte-derived macrophages seeded onto the decellularised porcine bladder biological scaffold would show differential expression of functional markers compared to monocyte-derived macrophages seeded onto a glass substrate and that the biomaterial may govern the monocyte-derived macrophage phenotype. Immunofluorescent analysis of CD80 immunolabelling of day 11 monocyte-derived macrophages from multiple donors indicated that all cells showed a basal level of CD80 expression when cultured on a glass substrate in complete PBMC medium only (Figure 5-30).

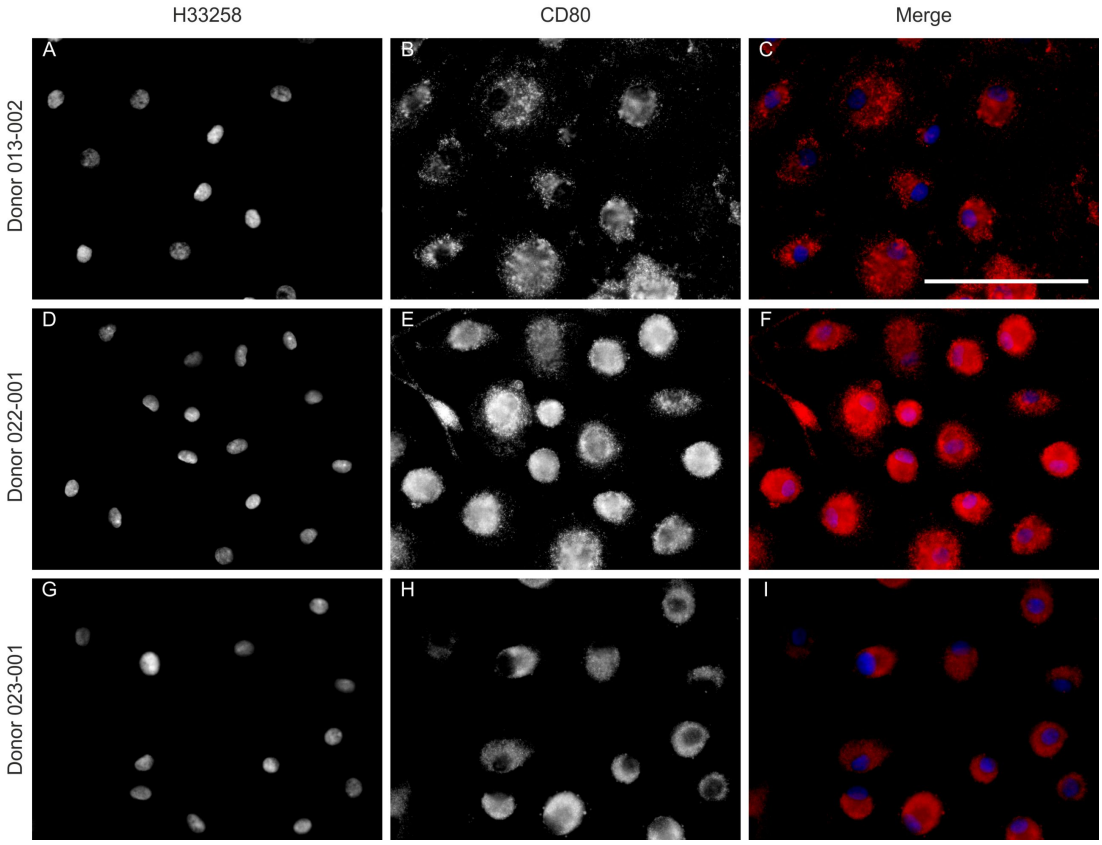

Figure 5-30. Immunofluorescent imaging of CD80 expression by day 11 monocyte-derived macrophages from multiple donors cultured on a glass substrate. Monocyte-derived macrophages from three independent donors 013-002 (A-C), 022-001 (D-F) and 023-001 (G-I) were cultured on a glass substrate for 11 days in complete PBMC medium. Fixed cells were immunolabelled for CD80 and captured images merged as previously described. Scale bar represents 100 microns.

Monocyte-derived macrophages cultured on the porcine bladder biological scaffold showed intense nuclear localisation of PPARγ and an absence of CD80 expression. A heterogeneous population of CD163 positive and negative cells was still observed by the macrophages seeded onto the porcine bladder matrix as observed of monocyte-derived macrophages cultured on a glass substrate for multiple donors (Figure 5-31).

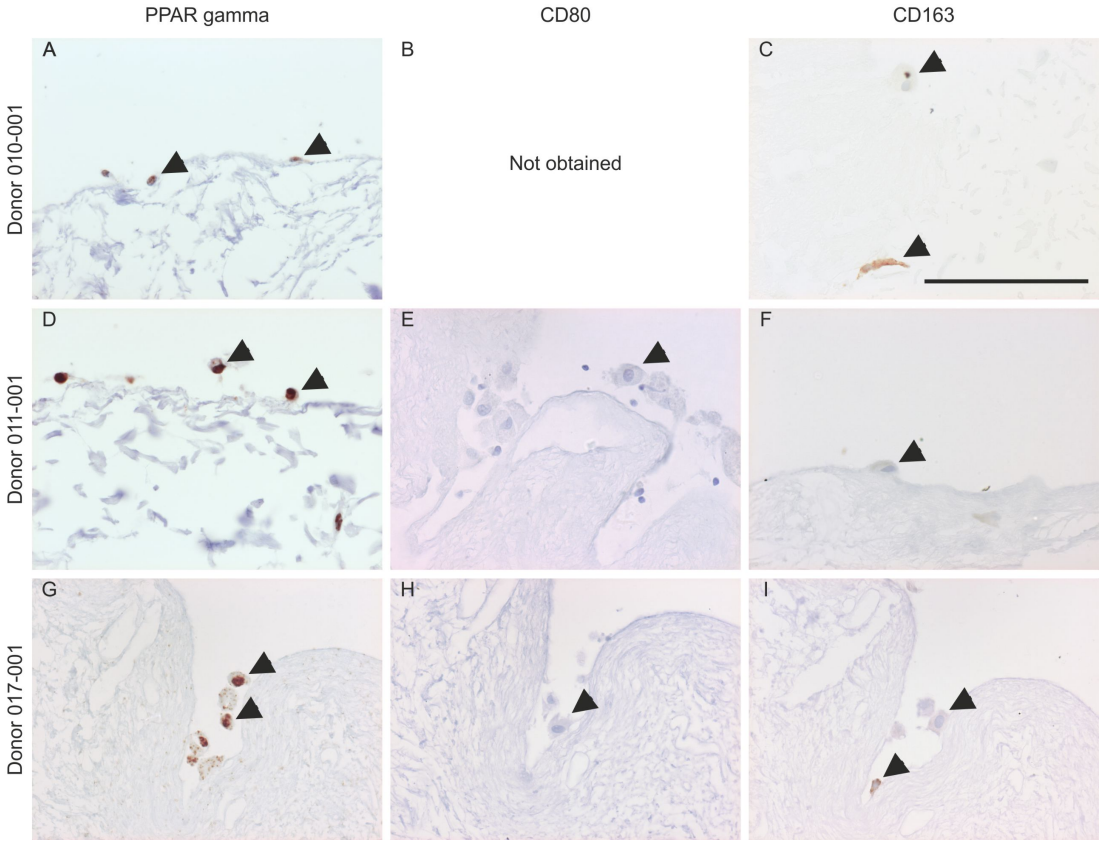

Figure 5-31. Immunoperoxidase labelling of PPARγ, CD80 and CD163 expression by monocyte-derived macrophages from three donors cultured on the porcine bladder biological scaffold for 11 days. Monocyte-derived macrophages from three independent donors were cultured on the porcine bladder biological scaffold for 11 days in complete PBMC medium. Fixed cell-biological scaffold constructs were processed for histology and immunolabelled for PPARγ (A, D and G), CD80 (E and H) and CD163 (C, F and I) expression. Scale bar represents 100 microns.

5.13 Discussion

5.13.1 Cellular expression of CD163

CD163 has been described as being exclusively expressed on monocytes and mature tissue macrophages (Pulford et al., 1992; Backé et al., 1991). Immunofluorescent imaging and flow cytometric analysis showed that the majority of CD11b+ peripheral blood monocytes expressed CD163. Reports of CD163 expression by human monocytes has varied from absent by human monocytes (Van den Heuvel et al., 1999) or <5% by human CD14+ monocytes (Philippidis et al., 2004) to >99% of human monocytes reported as being CD163 positive (Sulahian et al., 2000). It has been proposed that monocyte CD163 expression was dependent on the anti-coagulant in which the human blood was collected (Moniuszko et al., 2006). Work by Maniecki and colleagues addressed these varied reports of CD163 expression by human monocytes and determined that the reported expression of CD163 by monocytes was dependent on which region of the scavenger receptor the antibody clone recognised (Maniecki et al., 2011). Use of anti-CD163 antibodies that bind to the N-terminal of the scavenger receptor, such as the EDhu antibody (Madsen et al., 2004), showed that approximately 80% of CD14+ peripheral blood monocytes were CD163 positive (Maniecki et al., 2011), which agrees with observations of CD11b+ peripheral blood monocytes made in this study. Conversely, the RM3/1 antibody, which recognises the C-terminal domain of CD163 (Madsen et al., 2004), failed to identify any CD163 expression by CD14+ peripheral blood monocytes (Maniecki et al., 2011). Recent evidence has suggested that CD163 expression may vary on different monocyte subsets. Classical monocytes, defined as $CD14^{hi}$CD16-, were reported to express high levels of CD163 mRNA and protein, while $CD14^{hi}$CD16+ monocytes had a lower level of CD163 protein expression and significantly lower CD163 mRNA expression. Non-classical $CD14^{lo}$CD16+ monocytes were reported to be negative for both CD163 mRNA and protein (Tippett et al., 2011). This differential expression of CD163 between different monocyte subsets may explain why only 80% of CD11b+ peripheral blood monocytes isolated were observed to express CD163. Following culture of monocytes to macrophages for eight days in the presence of M-CSF all monocytes subsets were reported to be able to express CD163 however, the authors failed to comment on the observation that not all monocyte-derived macrophages derived from the different subsets expressed the scavenger receptor (Tippett et al., 2011). In this study, immunofluorescence imaging and flow cytometric analysis of monocyte-derived macrophages cultured for day 11 on glass indicated that some cells had a higher propensity to express CD163 in the absence of exogenous stimuli.

5.13.2 Modulation of cell phenotype by PPARγ

The down-regulation of CD80 expression in response to a PPARγ agonists and enhanced expression of CD80 in response to a PPARγ antagonist has previously been shown in CD14+ monocyte-derived dendritic cells (Szatmari et al., 2007) and served as a useful control for the change of the monocyte-derived macrophage phenotype in response to PPARγ activation status. PPARγ activation initiates a cascade of gene transcription, which can govern the function of a cell. Here, it was demonstrated that activation of PPARγ resulted in a change in phenotype of the macrophage population, as shown by the loss of CD80 expression. Activation of PPARγ with troglitazone and investigation of PPARγ expression and localisation at the day 11 time point showed predominantly cytoplasmic localisation. As described in the introduction to this chapter, upon activation PPARγ translocates to the nucleus to initiate or suppress transcription of target gene. Absence of PPARγ in the nuclei of cells at day 11 coupled with the observed loss of CD80 at this time point indicates initial PPARγ activation can govern macrophage phenotype at later time point. Inhibition of PPARγ with T0070907 dramatically changed the morphology of the cells from a mixed population of macrophages that had 'fried egg'-like morphology or elongated morphology to a predominantly elongated or spindle-like morphology. This spindle-like morphology of *in vitro* human monocyte-derived macrophages has previously been associated with 'M2'-type macrophages generated with M-CSF (Verreck et al., 2006), however inhibition of PPARγ in this study was associated with an inflammatory macrophage phenotype. This discrepancy cannot currently be explained. Many groups have used different stimulation periods with different PPARγ agonists, ranging from hours (Jiang et al., 1998; Szatmari et al., 2007; Szanto et al., 2010) to days (Nencioni et al., 2002) before harvesting the cells, but all investigations maintained the monocyte-derived cells in culture in the presence of the PPARγ agonist. The activation of PPARγ through treatment with the PPARγ agonist, troglitazone for 48 hours followed by culture in control medium for a further nine days has not previously been described. In addition, this study showed a role for PPARγ activation in the expression of the macrophage scavenger receptor CD163.

5.13.2.1 Regulation of CD163 by PPARγ

Bouhlel et al investigated the association between PPARγ activation and CD163 expression by investigating the priming of alternate 'M2' macrophages from human monocytes. Interleukin 4 was used to differentiate primary human monocytes towards an 'M2' anti-inflammatory lineage and the expression of M2 associated genes was then compared to

'resting' macrophages (Bouhlel et al., 2007). CD163 mRNA expression was down-regulated in response to IL-4 (Bouhlel et al., 2007). Activation of PPARγ in 'resting' macrophages by either GW1929 or rosiglitazone showed no significant change in CD163 gene expression. In addition, stimulation of PPARγ in primed 'M2' macrophages with GW1929 showed a significant reduction in CD163 mRNA expression compared to the IL-4 primed 'M2' macrophages alone, indicating that PPARγ stimulation enhanced the IL-4 dependent down-regulation of CD163. The group did not however, explore the effects of PPARγ inhibition on the expression of CD163 in 'resting' macrophages (Bouhlel et al., 2007). In this study, inhibition of PPARγ with T0070907 determined that PPARγ activation is required to maintain the sub-population of CD163+ human monocyte-derived macrophages. Further more, PPARγ function is required for the glucocorticoid receptor dependent up-regulation of CD163. Interestingly, the activation of PPARγ with the agonist, troglitazone only showed a change in CD163 expression by a proportion of the population of monocyte-derived macrophages at day 11, in contrast to the change in CD80 expression by monocyte-derived macrophages following PPARγ activation. This indicated that PPARγ has the potential to work by multiple mechanisms either by; a) increasing the existing CD163+ population through increased capacity of monocyte-derived macrophages to express CD163 by regulating known drivers of CD163; or b) the potential expansion of a monocyte-derived macrophage sub-population. Both mechanisms will briefly be discussed here.

5.13.2.2 Cross-talk between PPARγ and the glucocorticoid receptor

Emerging evidence of cross talk between PPARγ and the glucocorticoid receptor indicates that the nuclear receptors function in combination to repress pro-inflammatory gene expression. The nuclear glucocorticoid receptor, like PPARγ has been shown to inhibit transcription of pro-inflammatory genes by NF-κB, potentially through an interaction between the p65 subunit of NF-κB and GR (Ray and Prefontaine, 1994). Investigation into the role of PPARγ and the glucocorticoid receptor in gastric ulcer healing in a rodent model showed that in the gastric tissue, nuclear NF-κB was significantly reduced following treatment with the synthetic PPARγ agonist pioglitazone compared to the ulcer control. The group also reported significantly greater nuclear and cytoplasmic glucocorticoid receptor expression in the gastric tissue following pioglitazone treatment compared to the ulcer control. PPARγ was reported to immunoprecipitate with nuclear glucocorticoid receptor following pioglitazone treatment suggesting a physical interaction between the two receptors (Lahiri et al., 2009). In addition, a physical interaction between PPARγ and

the glucocorticoid receptor was also demonstrated by immunoprecipitation in TNFα-stimulated human airway smooth muscle cells following treatment with the PPARγ ligand 15d-PGJ_2 (Nie et al., 2005). Promoter consensus sequence analysis indicated a putative glucocorticoid receptor binding sequence upstream of the *PPARγ* transcription start site, which indicates that the glucocorticoid receptor can regulate PPARγ expression. Further more, stimulation of the glucocorticoid receptor with dexamethasone showed intense cytoplasmic PPARγ expression by monocyte-derived macrophages. Conversely, PPARγ inhibition showed a loss of glucocorticoid receptor expression by monocyte-derived macrophages at day 11 highlighting that PPARγ activation is required to maintain expression of the glucocorticoid receptor, however a putative PPRE was not identified up-stream of the glucocorticoid receptor gene start site. This indicates a potential feedback loop between the two nuclear receptors. PPARγ activation may enhance glucocorticoid receptor expression, which may in turn give monocyte-derived macrophages a greater ability to sense either exogenous or endogenous glucocorticoids and thus a greater ability to drive the expression of CD163. However, this proposal would not explain why the whole population is not CD163 positive and raises questions about a potential source of glucocorticoids within the culture system.

5.13.2.3 PPARγ dependent expression of IL-10

Sulahian and colleagues identified that the 'regulatory' cytokine, IL-10 increased CD163 expression by human mononuclear cells in a dose-dependent manner (Sulahian et al., 2000). Peripheral blood monocyte-derived CD1a-PPARγ+DC-SIGN+ DCs have been identified as having a greater capacity to produce IL-10 compared to CD1a+PPARγ-CD-SIGN+ DCs (Gogolák et al., 2007). In addition, DCs pulsed with the PPARγ agonist, rosiglitazone, were shown to enhance the stimulated production of IL-10 by T-lymphocytes isolated from the murine mesenteric lymph node (Hammad et al., 2004). Further more, rosiglitazone enhanced the production of IL-10 by human peripheral blood monocyte-derived DCs activated with either CD40L or LPS (Thompson et al., 2007). The PPARγ dependent up-regulation of IL-10 identified in monocyte-derived DC suggests the potential for up-regulation of CD163 by the monocyte-derived macrophages in response to PPARγ activation may also be mediated through IL-10 autocrine signalling however, this proposal requires confirmation using an anti-IL-10 neutralising antibody in the presence of troglitazone.

5.13.2.4 Proliferative macrophages

Emerging evidence of *in situ* macrophage proliferation has indicated that murine macrophages are able to repopulate a tissue following inflammation in order to reconstitute and maintain the tissue resident population (Davies et al., 2011). Self-renewal of murine tissue macrophages can be driven by IL-4, indicating that an anti-inflammatory macrophage phenotype has an ability to self-renew and may have implications during wound repair (Jenkins et al., 2011). Although the IL-4-dependent self-renewal of macrophage populations has been well defined in mice, early studies of human alveolar macrophages indicated that these cells can proliferate (Golde et al., 1974; van Maarsseveen et al., 1991). It is intriguing to speculate that the self-renewal of a defined population of macrophages, which have a higher propensity to express CD163, may explain the increase in the CD163 positive population. Ki67+ day 11 monocyte-derived macrophages cultured in complete PBMC medium only were observed by immunofluorescent imaging (Appendix IV-XXIII) however, Ki67+ cell counts following PPARγ activation versus control cells were not performed.

5.13.3 Modulation of macrophage phenotype by decellularised biological scaffolds

Few studies have investigated the *in vitro* macrophage phenotype in response to decellularised matrices. Early studies used the monocytic cell line, U-937 seeded onto decellularised biological scaffolds (Rieder et al., 2005; Ariganello et al., 2009), however, use of cell lines allows for only limited interpretation of the human primary monocyte-derived macrophage response to these scaffolds. Culture of human monocyte-derived macrophages on decellularised bovine pericardium showed decreased esterase and acid phosphatase activity compared to monocyte-derived macrophages cultured on tissue culture plastic (Ariganello et al., 2010). In a follow-up study, Ariganello et al determined that peripheral blood monocyte-derived macrophages seeded onto the decellularised bovine pericardium released higher amounts of IL-6, IL-8 and MCP-1 and decreased amounts of IL-10, IL-1ra, TNFα and MIP-1β compared to monocyte-derived macrophages seeded onto tissue culture plastic (Ariganello et al., 2011). The authors concluded in both studies that the decellularised bovine pericardium did not 'activate' human monocyte-derived macrophages (Ariganello et al., 2010; 2011). To determine if the porcine bladder biological scaffold influenced the expression of function macrophage markers, human monocyte-derived macrophages were seeded onto the porcine bladder scaffold. Investigation of PPARγ expression by human monocyte-derived macrophages cultured on the porcine bladder matrix showed that the receptor was localised to the nucleus

indicating that the receptor pathway was active. A subpopulation of CD163+ monocyte-derived macrophages was observed in cells cultured on the porcine bladder biological scaffold as observed by monocyte-derived macrophages on a glass substrate. A basal level of CD80 expression was observed by human monocyte-derived macrophages cultured on a glass substrate in complete PBMC medium however, CD80 expression was not observed by human monocyte-derived macrophages cultured on the porcine bladder biological scaffold in complete PBMC medium. Activation of PPARγ by human monocyte-derived macrophages seeded on the porcine bladder biological scaffold, may suppress CD80 expression. Further work is required to determine if inhibition of PPARγ activation using T0070907 up-regulates CD80 expression by monocyte-derived macrophages culture on the porcine bladder matrix and if there is a difference between the number of CD163+ cells observed on the porcine bladder biological scaffold compared to macrophages cultured on glass.

5.13.4 The expression pattern of CD163 by *in vitro* monocyte-derived macrophages

The pattern of CD163 expression by human monocyte-derived macrophages in culture is summarised in graphical form in figure 5-32. The majority of peripheral blood monocytes express CD163 however, adherence to a glass substrate showed loss of CD163 expression. CD163 expression re-emerged in a subpopulation of monocyte-derived macrophages. The rate of re-emergence of CD163 expression is not currently understood however, CD163 was observed as early as 48 hours in culture. In addition the expression of CD163 by monocyte-derived macrophages is dependent on the activation PPARγ.

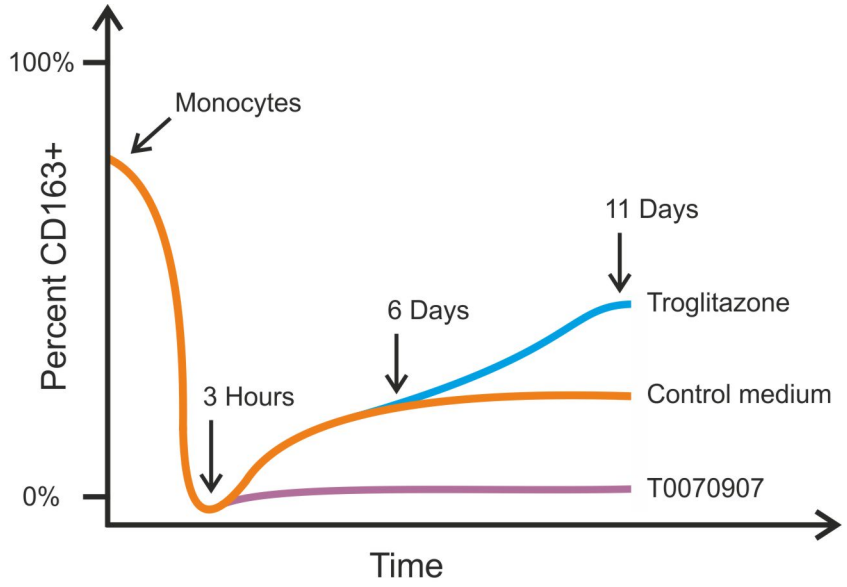

Figure 5-32. Schematic diagram summarising the change in the percentage of CD163+ monocyte-derived macrophages with manipulation of PPARγ activation. Approximately 80% of peripheral blood monocytes express CD163. Upon adherence to a glass substrate, CD163 expression is lost. Over the culture period a subpopulation of $CD163^{hi}$ macrophages emerges. This population can be increased by activating PPARγ (blue line) or eliminated by inhibiting PPARγ activation (purple line).

5.14 Summary

- Eighty percent of CD11b+ peripheral blood monocytes were positive for CD163 expression however, CD163 expression was lost upon adherence to the glass substrate and re-established over an 11-day culture period.
- A subpopulation of CD11b+ monocyte-derived macrophages showed a greater propensity to express CD163 when cultured on a glass substrate.
- Activation of PPARγ reprogrammed human monocyte-derived macrophages, increasing the sub-population size of CD11b+CD163+ macrophages and eliminating CD80 expression.
- Expression of CD163 by the subpopulation of monocyte-derived macrophages was dependent of PPARγ function.
- The glucocorticoid receptor mediated up-regulation of the macrophage CD163 was dependent on PPARγ function.
- Monocyte-derived macrophages express a basal level of CD80 when cultured on a glass substrate but do not express CD80 when cultured on the porcine bladder biological scaffold.

6.0 Final discussion

6.1 Thesis overview

The aim of the research presented in this thesis was to examine an *ex vivo* biomaterial-human tissue interface to explore the potential mechanisms that govern the host tissue response to a biological scaffold which has potential applications in regenerative medicine. A major achievement of the research was the establishment of a novel *ex vivo* biological scaffold-urinary tract tissue interface. Analysis of this interface indicated that mononuclear phagocytes were the first tissue-derived cells to infiltrate the biological scaffold. Comparisons with previous observations from studies of the subcutaneous implantation of biological scaffolds in rodents suggested that the biomaterial-human tissue interface model could be used to interrogate the specific mononuclear phagocyte response to biological scaffolds. The predominant expression of CD163 by macrophages at the biomaterial-tissue interface and in the absence of the inflammatory marker CD80 was indicative of a non-inflammatory macrophage phenotype. The intense nuclear localisation of PPARγ and the glucocorticoid receptor at the interface indicated that these receptor signalling pathways were active. Mechanistic investigations of CD163 expression by human monocyte-derived macrophages demonstrated a previously unrecognised hierarchical role for PPARγ in the glucocorticoid receptor-dependent regulation of CD163 expression. This study also established that CD163 expression by human monocyte-derived macrophages *in vitro* was restricted to a subpopulation of macrophages in the absence of exogenous stimuli, and that expression of CD163 by this subpopulation was dependent on PPARγ function. Activation of PPARγ in monocyte-derived macrophage increased the number of CD163+ cells, whist abating CD80 expression, suggesting that PPARγ activation can modulate the phenotype of human monocyte-derived macrophages. This also indicated that some macrophage populations have a greater propensity towards particular PPARγ-dependent functions. CD163+ macrophages may represent, lineage-determined macrophages that are poised to respond to certain environmental signals. Overall, this study has shown that the *ex vivo* biomaterial-organ culture model has utility for further exploration of the response of macrophages to biomaterials, in particular to test the hypothesis that the macrophage response to biological scaffolds is indicative of inflammation resolution.

6.2 The development of an *ex vivo* biomaterial-tissue interface

This study was initiated by results from studies in which biomaterials were implanted in rodents and that indicated that mononuclear phagocytes were involved in the tissue response to acellular biological scaffolds. Little is known about the factors that can determine the macrophage response following implantation of a biological scaffold. There is a need for the development of better models of human-biomaterial interactions, since rodent biomaterial implantation studies may not necessarily translate to humans. Therefore, in this study an experimental system was developed in which fresh human urinary tract tissue was maintained in close apposition to a decellularised biological scaffold. This enabled the interactions between human tissue and the biological scaffold to be assessed. Use of immunohistological analysis to interrogate the biomaterial-organ culture constructs allowed a range of antigens to be assessed, but meant that the precise dynamics of the cellular infiltration, and importantly, the origin of the mononuclear phagocytes observed at the biomaterial-tissue interface could not be determined except by extrapolation from fixed time points. The limited size of human urinary tract tissue samples resulted in a restricted number of porcine:human biomaterial-organ culture replicates that could be prepared per donor. Future studies would focus on extending the organ culture period to investigate the extent of infiltration by the mononuclear phagocytes, the dynamics of the cell phenotype at the interface and the potential of other cells, such as αSMA+ stromal and CD34+ vascular cells, to infiltrate into the scaffold, as reported to be observed *in vivo*. It is exciting to speculate that adaptation of the culture system, through incorporation of other tissues and validation of *ex vivo* biomaterial-tissue constructs may prove to be valuable tool in initial biocompatibility screening of biomaterials in future studies, thus reducing the number of animal implantation studies performed, of which there were 402 performed in rodents in 2009 (homeoffice.gov.uk/publications/science-research-statistics).

6.2.1 The phenotype of cells at the interface

Cells at the biomaterial-human tissue interface were identified as mononuclear phagocytes based on morphology and expression of CD68 and labelling with MAC387. Cells at the biomaterial-tissue interface and within the central region of the tissue were negative for the pro-inflammatory macrophage marker, CD80. Cells infiltrating the porcine bladder biological scaffold expressed HLA-DR, supporting the evidence that these cells were

'professional' antigen presenting cells. HLA-DR expression showed a qualitative decrease between days two and day 11. A significant temporal increase in CD163 expression was observed at the biomaterial-tissue interface over the 11-day culture period, with little expression of CD163 observed within the central regions of the tissue at any time point. Furthermore, cells infiltrating the porcine bladder biological scaffold were intensely positive for CD163 expression. Dual labelling experiments showed that CD117, arginase 1 and CD36 expression did not co-localise with CD163+ cells migrating into the biological scaffold in agreement with observations in dual labelling experiments made in the human control tissue. Additionally, αSMA, CD34 and CD3 expression was not observed in cells infiltrating the biological scaffold. Further dual labelling experiments using an extended panel of functional markers would refine the characterisation of the cells at the biomaterial-tissue interface.

Proposed models of macrophage activation are dependent on the functional markers assigned to each macrophage phenotype. Emphasis should be made of the importance of understanding the functional significance of each marker expressed and the factors that regulate the expression of the markers, not simply how the macrophage phenotype 'fits' into each model of activation. This approach has not been fully adopted in studies of biological scaffold integration and regenerative medicine, despite the importance of this type approach when studying a novel environment. *In vivo* investigation into the macrophage response to biological scaffolds have been limited to the basic interpretation of macrophage phenotype (Brown et al., 2009; 2012b). Concentration on the M1/M2 macrophage-activation paradigm in *in vivo* biological scaffold implantation studies has resulted in little consideration to the potential signalling mechanism active at the interface between a biological scaffold and a tissue, in particular, with regard to the factors released following tissue injury. Here, a major goal in the development of the biomaterial-organ culture model was to identify potential signalling mechanisms active at the interface and to investigate the contribution of these signalling mechanisms that could govern the macrophage phenotype and response.

6.3 The implications of CD163+ macrophages at a biomaterial-tissue interface

A striking feature of this study was the identification of CD163+ cells, with a macrophage-like morphology, at the interface between the porcine bladder biological scaffold and the urinary tract tissue after 11 days of organ culture. The origins of the CD163+ cells at the *ex*

vivo biomaterial-tissue interface are currently unknown. For example, it is not known whether there is selective recruitment of a particular CD163+ macrophage subset or whether factors present at the interface are responsible for driving CD163 expression by infiltrating cells. CD163 antigen expression has previously been identified on macrophages in inflamed gingival tissue (gingivitis) as well as during the late or 'healing' phase of acute inflammation (Zwadlo et al., 1987). It has therefore been suggested that CD163+ macrophages found in inflamed tissue play a key role in the 'resolution' phase of inflammation (Tippett et al., 2011). The observation that CD163+ macrophages were present at the *in vitro* biomaterial-tissue interface coupled with the identification of CD163+ macrophages during an integrative response to acellular porcine urinary bladder biological scaffold and acellular rat body wall biological scaffold implanted into Sprague-Dawley rats (Brown et al., 2009), indicates that macrophages expressing CD163 may have an important role in cellular integration of a biological scaffold.

Biological scaffolds cannot be implanted into a living recipient without tissue injury. As discussed in the introduction, tissue injury initiates the release of pro-inflammatory factors, such as prostaglandins and leukotrienes, which recruit inflammatory cells to the site of insult to combat microorganisms in the environment and to initiate the wound healing process. This inflammation must then be resolved to restore tissue homeostasis. Factors associated with inflammation resolution have been shown to activate PPARγ. The pro-resolving lipoxins have been reported to signal through a designated G-protein coupled receptor (GPCR) in human (Fiore et al., 1994) and murine (Takano et al., 1997) neutrophils and macrophages (Serhan et al., 2008). However, it has also been reported that 1nM and 10nM lipoxin A_4 was able to significantly enhance the transcriptional activity of PPARγ in the rodent brain (Sobrado et al., 2009). In addition, inhibition of PPARγ using T0070907 significantly reduced the lipoxin A_4-mediated neuroprotective effect in rodent brain indicating that the mediator of resolution, Lipoxin A_4, may be a natural ligand for PPARγ (Sobrado et al., 2009). The observation that PPARγ was localised in the nucleus of cells at the biomaterial-tissue interface and expressed by cells with a mononuclear phagocyte morphology within the biological scaffold, prompted investigation of the 'resolution-associated' signals which may promote a 'resolution-associated' macrophage phenotype. This drove further studies into the mechanisms governing CD163 expression using human peripheral blood monocyte-derived macrophages. The hypothesis that PPARγ activation modulates CD163 expression in human monocyte-derived macrophages was tested.

6.4 The potential for a pre-determined CD163+ macrophage subset?

In vitro culture of monocyte-derived macrophages on a glass substrate for 11 days showed a previously undescribed subpopulation of CD11b+ macrophages, which have a greater propensity towards expression of CD163. This study also defined a previously undescribed role for PPARγ in mediating expression of CD163 by identifying that the expression of CD163 by peripheral blood monocyte-derived macrophages was dependent on PPARγ function. *In vitro*, not all monocyte-derived macrophages expressed CD163 in response to the PPARγ agonist, indicating that only a subpopulation of macrophages had the ability to express CD163, at least in response to this trigger. This response was not the same for the expression of CD80 by monocyte-derived macrophages, where PPARγ activation abated CD80 expression. As illustrated in the introduction of this thesis, macrophage heterogeneity can arise from lineage diversity, which suggests macrophage phenotype is programmed, and/or the ability of the macrophage phenotype to be modulated by the environment (plasticity). This interpretation may be dependent on the functional markers investigated. Investigation of CD80 expression by monocyte-derived macrophages in this study showed a dichotomy of expression, which can be modulated by PPARγ activation, while investigation of CD163 expression indicated that some macrophages *in vitro* have a greater 'propensity' to express CD163. This suggests that macrophages show plasticity with regard to expression of some functional markers and programming with regard to the ability to express others.

The hypothesis can be put forward that *in vitro,* CD163+ macrophages represent a pre-determined subpopulation of macrophages, which are predisposed to express CD163 through a greater ability to receive certain signals and 'interpret' these signals. Studies using human monocyte-derived macrophages have indicated that human macrophage function can be fixed following modulation with exogenous stimuli. For example, investigation using human peripheral blood monocyte-derived macrophages showed that 'M1' macrophages induced with GM-CSF, excreted IL-12p40 and IL-1β in response to LPS and mycobacteria sonicate respectively (Verreck et al., 2006). 'M2' macrophages induced with M-CSF showed up-regulated expression of CD163 however, by contrast, failed to induce the pro-inflammatory cytokine, IL-12p40 in response to LPS, mycobacteria sonicate or zymosan A. Instead these 'M2' macrophages downregulated HLA-DR and the costimulatory molecule, CD86 and induced the regulatory cytokine IL-10, indicating that

the 'M2' macrophage phenotype was fixed following skewing with M-CSF (Verreck et al., 2006).

Evidence contributing to the supposition that, while macrophages display plasticity, some macrophage subsets have a greater propensity towards some functions/phenotypes over others has been highlighted in murine studies. CD11b+ F4/80^{bright} murine resident peritoneal macrophages have been shown to express 12/15-LOX, while the CD11b+ F4/80^{lo} murine resident peritoneal macrophages were shown to be negative for 12/15-LOX expression, as determined by immunofluorescence imaging (Dioszeghy et al., 2008), indicating that some macrophage populations favour the 15-LOX 'anti-inflammatory' pathway. A recent report showed that in resting murine tissue macrophages, PPARγ mRNA expression was restricted to mature splenic and lung macrophages indicating that *in vivo* in the mouse, only a subset of murine macrophages may express PPARγ (Gautier et al., 2012). Furthermore, analysis of Ly6C^{hi} 'inflammatory' murine monocytes and Ly6C^{lo} 'resident' monocytes showed that Ly6C^{lo} monocytes express greater amounts of PPARγ mRNA than Ly6C^{hi} monocytes (Gautier et al., 2012). Treatment of the mice with the PPARγ agonist pioglitazone was shown to enhance the protein expression of CD36 and the PPARγ target gene, fatty acid binding protein (FABP) 4 by Ly6C^{lo} monocytes, but not by Ly6C^{hi} monocytes, suggesting that only the 'resident' monocyte population had the ability to respond to the PPARγ agonist. Use of LysM Cre x PPARγ$^{flox/flox}$ mice indicated that the absence of PPARγ+ macrophages did not impede the ability to mount an inflammatory response in thioglycollate-induced peritonitis however, there were significantly greater numbers of neutrophils and Ly6C^{hi} monocytes in the peritoneal cavity at day five and eight post administration of thioglycollate compared to control mice, indicating that PPARγ+ macrophages are required during the resolution phase of thioglycollate-induced acute inflammation (Gautier et al., 2012). Differential deposition of macrophages from different sources such as myeloid-, lymphoid- or splenic-derived monocytes or yolk sac-derived macrophages highlights potential macrophage heterogeneity, which is dependent on lineage. It is interesting to speculate that resident-type macrophages maybe pre-programmed or poised to receive certain signals from the environment. While these observations were made in mouse (Gautier et al., 2012), the described phenotypic characteristics that murine Ly6C^{hi} and Ly6C^{lo} monocytes share with 'classical' and 'non-classical' human monocytes respectively allows consideration of similar functions in humans. Extensive studies in mice also highlight that further work is required in developing robust human models of mononuclear phagocyte activation and function.

The CD163+ macrophage populations observed both *ex vivo* and *in vitro* may have a defined lineage, which is maintained even in culture. Furthermore, CD163+ human macrophages may represent a particular differentiated lineage of macrophages, which is dependent on PPARγ function and which can be enhanced with PPARγ stimulation in cells poised to receive the signal. Enhancement of the CD163+ macrophage population may be through self-renewal or induced expression of CD163 by cells that, in the absence of agonist, would otherwise be negative for CD163. Preliminary evidence that contributes towards the supposition that a macrophage subset has a predisposition for CD163 expression was found in the observed restoration of CD163+ cells following removal of the PPARγ antagonist, T0070907 (Appendix V-I). However, further work is required to determine the reproducibility and significance of this observation. Immunofluorescence imaging of PPARγ expression indicated that all monocyte-derived macrophages express the nuclear receptor indicating that other factors, such as cross talk with other signalling pathways, such as the glucocorticoid receptor, may be determinant. Future work would aim to separate the *in vitro* monocyte-derived macrophage populations based on CD163 expression either in the presence or absence of PPARγ stimulation and determine differences in the gene expression profile using cell sorting and whole transcriptome array technologies (Figure 6-1).

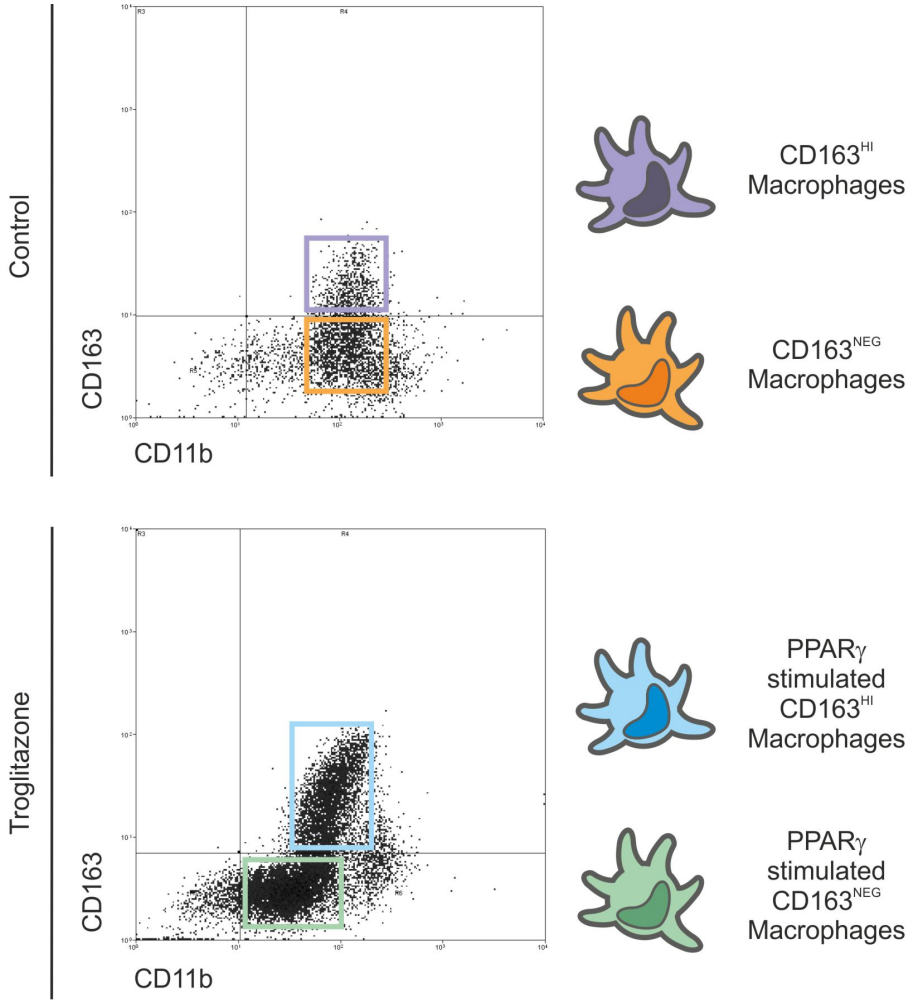

Figure 6-1. Schematic diagram of the experimental strategy for isolation and profiling of CD163^{HI} and CD163^{NEG} human monocyte-derived macrophages. Human peripheral blood-derived macrophages would be isolated using flow cytometry cell sorting based on CD163 and CD11b expression, following culture for 11 days either in control medium or a 'pulse' treatment with troglitazone for two days followed by culture in control medium. Separated cells would then be profiled using transcriptome analysis.

6.5 Resolution signals and regenerative medicine

Currently the factors that govern the macrophage phenotype during biomaterial integration are not completely understood. The observation made at the *ex vivo* biomaterial-tissue interface of the intense nuclear localisation of the glucocorticoid receptor and PPARγ, indicated that these nuclear receptor signalling pathways may be important. Studies in mice have begun to determine the role of 'pro-resolving' signals in the promotion of tissue regeneration, which may be important in the integration of biological scaffolds. There has been little consideration of the process of inflammation resolution in regenerative medicine due to the focus on the fixed M1/M2 paradigm. The importance in the ability of the immune system to resolve polarised macrophage phenotypes and the impact of this on the functional success of implanted biological scaffold is only just being recognised (Brown et al., 2012b). Overall, this has led to a lack of mechanistic understanding of biological scaffold integration by host tissue, despite the large number of studies in animals. Central to the concept of regenerative medicine is the reliance of wound inflammation to resolve and tissue repair to commence; failure to resolve inflammation leads to progression of chronic tissue fibrosis and lack of regeneration. It is interesting that a resolution-associated macrophage phenotype was observed in the biomaterial-organ culture system despite a limited inflammation response due the 'closed' nature of the system. The presence of CD163+ macrophages at the biomaterial-tissue interface may be a pre-programmed macrophage response to tissue injury however, the exact nature of host and scaffold-derived factors present in the *ex vivo* biomaterial-tissue interface environment requires further investigation.

Candidate factors present at the biomaterial-tissue interface include arachidonic acid derivatives and glucocorticoids. Future experimental strategies would aim to investigate the role of these factors as agonists of PPARγ and GCR at the biomaterial-tissue interface and to determine if inhibition of these nuclear receptors in the organ culture constructs affected the mononuclear phagocyte phenotype. Inhibition of PPARγ function in the biomaterial-organ culture system, with T0070907 would determine if the presence of CD163 expression was dependent on PPARγ function in this culture model and if the cells in the culture system have the ability to express markers associated with inflammation, or if the mononuclear phagocyte phenotype was fixed, whatever the stimuli. In line with this proposed study, further work would also aim to examine the human tissue response to the presence of non-decellularised porcine bladder tissue to determine if the presence of a

xenogeneic cellular component in the organotypic culture model can affect a different human tissue response *ex vivo*.

Further work would also investigate the impact that the biological scaffold has on macrophage phenotype, in particular CD80 expression and PPARγ activation. It has been reported that the degradation products of biological scaffolds can stimulated the migration and proliferation of cells *in vitro.* Matrikines are described as derivatives of larger ECM proteins, such as collagen, which possess chemotactic and mitogenic properties (Beattie et al., 2009). MRL blastema cells have shown increased cell proliferation and cell migration in response to porcine urinary bladder ECM degradation products released by pepsin/HCL digestion (Reing et al., 2009), indicating the porcine urinary bladder matrix possesses factors that can be released and which can influence cellular behaviour. Application of the porcine urinary bladder matrix to repair an Achilles tendon defect in C57BL/6 and MRL/MpJ mice produced an ECM scaffold that had been remodelled and degraded *in vivo*. Evaluation of the day seven excised urinary bladder matrix for *in vitro* chemotactic ability showed a significant increase in the migration of MRL/MpJ progenitor cells compared compare to normal tendon tissue and autologous repair tissue (Beattie et al., 2009). Inhibition of PPARγ function in monocyte-derived macrophages seeded onto the porcine bladder biological scaffold with T0070907 would determine if the observed absence of CD80 expression was dependent on PPARγ in this culture system and provide insight into the potential role of the porcine bladder biological scaffold in determining the phenotype of human monocyte-derived macrophages. In addition, quantification of the number of CD163+ monocyte-derived macrophages present when cultured on the porcine bladder biological scaffold compared to donor-matched macrophages cultured on a glass substrate would determine if the nuclear localisation of PPARγ and absence of CD80 expression were coupled with an increased number of CD163+ macrophages.

6.6 Concluding remarks

This thesis aimed to understand the interface between human tissue and a decellularised porcine-derived biological scaffold, through the development of an *ex vivo* biomaterial-organ culture system. This culture system identified the importance of understanding wound healing mechanisms and the potential contribution of nuclear receptor signalling in mononuclear phagocytes in governing the response to biomaterials. This study highlights that further understanding of the nature of inflammation resolving signals in the macrophage response to biological scaffold is required. Utilising 'pro-resolving' signals, such as lipoxin A_4, through incorporation into biomaterials could enhance integration of biomaterials prone to a chronic inflammatory response. Through harnessing lipid mediators of inflammation resolution, these approaches would drive the field of tissue engineering and regenerative medicine forward.

Glossary of terms

Abbreviations

°C – Degrees Celsius

15-LOX - 15-Lipooxygenase

15d-PGJ_2 - 15-deoxy-$\Delta^{12,14}$- PGJ_2

5-LOX – 5-Lipooxygenase

AP – Alkaline phosphatase

AP-1 – Activator protein-1

APC – Allophycocyanin

BSA – Bovine serum albumin

$CaCl_2$ – Calcium chloride

CAM – Cell adhesion molecule

CD – Cluster of differentiation

CDP – Common DC progenitor

cm - Centimeter

cm^2 – Centimeters squared

CO_2 – Carbon dioxide

COX2 – Cyclooxygenase 2

CSA – Catalysed signal amplification

CTL – Cytotoxic

DAB – Diaminobenzidene

DAMPs – Damage-associated molecular patterns

DC – Dendritic cell

DHA – Docoshexaenoic acid

Abbreviations

DMEM – Dulbecco's modified Eagles medium

DMSO – Dimethyl Sulfoxide

Doux – Dual oxidase

DTT – Dithiothreitol

ECM – Extracellular matrix

EDTA - Ethylenediaminetetraacetic acid

FABP – Fatty acid binding protein

FBGC – Foreign body giant cell

FBS – Foetal bovine serum

FC – Flow cytometry

FITC - Fluorescein isothiocyanate

GCR – Glucocorticoid receptor

GPCR – G-protein coupled receptor

GRE – Glucocorticoid response element

H&E – Haematoxylin and eosin

H_2O_2 – Hydrogen peroxide

H33258 – Hoechst 33258

HBSS – Hank's balanced salt solution

HCL – Hydrochloric acid

HEMA – hydroxyethyl methacrylate

HEPA – High efficiency particulate air

HEPES - 4-(2-hydroxyethyl)-1-piperazineethanesulphonic acid

HMGB1 – High mobility group box 1

HRP – Horseradish peroxidase

HRP-IHC – Horseradish peroxidase immunohistochemistry

Abbreviations

HYMS-EMU – Hull York Medical School Experimental Medicine Unit

IF – Immunofluorescence

IFNγ - Interferon gamma

IHC – Immunohistochemistry

IL - interleukin

iNOS – inducible nitric oxide synthetase

IR – Infrared

IκB – inhibitor of NFκB

LAMP – lysosome associated membrane protein

LBD – Ligand binding domain

LDS – Lithium dodecyl sulphate

LPS – Lipopolysaccharide

LTB_4 – Leukotriene B_4

M-CSF – Macrophage colony stimulating factor

Maresin – Macrophage mediator of resolving inflammation

MCP – Mast cell progenitor

$MgCl_2$ – Magnesium chloride

MHC – Major histocompatibility complex

MI – Myocardial infarction

mL – Milliliter

mm - Millimeter

MMPs – Matrix metalloproteases

MPS – Mononuclear phagocyte system

MyD88 – Myeloid differentiation primary response gene 88

NA – Not applicable

ND – Not determined/No data

Abbreviations

NALP3 – NACHT, PRR and PYD domains containing protein 3

NaN_3 – Sodium azide

NCoR – Nuclear receptor co-repressor

NFκB – Nuclear factor kappa B

ng – Nanogram

nm - Nanometers

nM - Nanomolar

NOHA – N^6-hydroxyl-L-arginine

OIR – Oxygen-induced retinopathy

PAA – Peracetic acid

PAMPs – Pathogen-associated molecular pattern

PBS – Phosphate buffered saline

PBSc – PBS plus calcium

PE – Phycoerythrin

PFPE - perfluoropolyether

PGE_2 – Prostaglandins E_2

PIC – Protease inhibitor cocktail

PMA – Phorbol 12-myristate 13-acetate

PMBC – Peripheral blood mononuclear cells

PPARγ - Peroxisome proliferator-activated receptor gamma

PPRE – PPAR response element

PRR – Pattern recognition receptor

PVDF – Polyvinylidene fluoride

ROA – Region of analysis

rpm – Revolutions per minute

RPMI – Roswell Park Memorial Institute

Abbreviations

RXRα - Retinoid X receptor alpha

SDS – Sodium dodecyl sulphate

SIS – Small intestinal submucosa

SR-A – Scavenger receptor A

SRCR – Scavenger receptor cysteine-rich

TBS – Tris buffered saline

TBST - Tween® 20 in TBS

TCR – T-cell receptor

Th – T-helper

TNFα - Tumour necrosis factor alpha

TURP – Transurethral resection of prostate

TWEAK – TNF-like weak inducer of apoptosis

UV – Ultra violet

V – Volts

v/v – Volume/volume

VCAM – vascular cell adhesion molecule

VEGF – Vascular endothelial growth factor

VLA – Very late antigen

W - Watts

w/v – Weight/volume

αSMA – Alpha smooth muscle actin

μL – Microliter

μm - Micrometer

μM - Micromolar

Appendices

Appendices I – Materials and methods

Appendix I-I – List of suppliers

Supplier name	Supplier contact details
3M	www.3m.com
ATCC®	www.lgcstandards-atcc.org
Atlas Antibodies	www.atlasantibodies.com
Autogen Bioclear UK Ltd	Holly Ditch Farm, Mile Elm, Wiltshire, UK
Axis-Shield Plc	www.axis-shield.com
Bayer Healthcare Pharmaceuticals	Healthcare.bayer.com
BD Biosciences	www.bdbiosciences.com
BD Falcon™	www.bdbiosciences.com
Becton, Dickinson and Company	www.bd.com/uk
Bio-Rad	www.bio-rad.com
CA Hendley	Oakwood Hill Industrial Estate, Loughton, Essex, UK
CellPath	www.cellpath.co.uk
Corning Incorporated	www.corning.com
Dako	www.dako.com
Elga LabWater	www.elgalabwater.com
Fisher Scientific	www.fisher.co.uk
Fisons	NA
GlaxoSmithKline	www.gsk.com
GraphPad	www.graphpad.com
Iwaki	www.sterilin.co.uk

Li-Cor Biosciences	www.licor.com
Life technologies Corporation	www.lifetechnologies.com
Medical Air Technology	www.medicalairtechnology
Melford Laboratories	www.melford.co.uk
Millipore	www.millipore.com
Miltenyi Biotec	www.miltenyibiotec.com
Molecular Probes	www.invitrogen.com
National Institute for Health	www.nih.gov
Novocastra	www.leica-microsystems.com
Nunc	www.nuncbrand.com
Olympus	www.olympus.co.uk
ProteinTech	www.ptg.com
R&D Systems	www.rndsystems.com
Rockland	www.rockland-inc.com
Santa Cruz	www.scbt.com
Sarstedt	www.sarstedt.com
Scientific Laboratory Supplies Ltd	www.scientificlabs.co.uk
Sera Laboratories International Ltd	www.seralab.co.uk
AbD Serotec	www.abdserotec
Sigma-Aldrich	www.sigmaaldrich.com
Sterilin	www.sterilin.co.uk
Thermo Electron Corporation	www.thermoscientific.com
Thermo Fisher	www.thermofisher.com
Thermo Scientific	www.thermoscientific.com
Tocris	www.tocris.com
Vector Laboratories	www.vectorlabs.com
Whatman	www.whatman.com

Appendix I-II – General reagents

Phosphate Buffered Saline (PBS)

PBS was prepared using phosphate buffered saline tablets (Sigma P4417).

One tablet was dissolved in 200mL of dH_2O.

Tris Buffered Saline (TBS)

0.05M Tris-HCL pH 7.6

0.15M NaCl

Made up to one litre using dH_2O and pH adjusted to 7.6

Trypsin-Versene

20mL 10x Trypsin (Sigma, catalogue number T4549)

4mL 1% (w/v) EDTA

Made up to 200mL using HBSS -Ca^{2+} -Mg^{2+}

Appendix I-III – Histology reagents

10% (v/v) Formalin

100mL 37% (v/v) Formaldehyde

Made up to one litre using PBS containing 0.5mM $MgCl_2$, and 0.9mM $CaCl_2$.

Zinc salt fixative

0.5% (w/v) Zinc acetate,

0.05% (w/v) Zinc chloride

Made up to one litre using 0.05% (w/v) Calcium acetate in 0.1M Tris in dH_2O at pH 7.4.

Haematoxylin

Solution 1

3g Haematoxylin in 20mL 100% (v/v) ethanol

Solution 2

0.3g Sodium Iodate

1g Citric acid

50g Aluminum Potassium Sulphate

made up to 850mL using dH_2O

Haematoxylin solution 1 was added to haematoxylin solution 2 and mixed well. One hundred and twenty millilitres of glycerol was added to the combined solutions and the final haematoxylin solution stored at ambient temperature in the dark.

Scott's Tap Water

2% (w/v) $MgSO_4$

0.35% (w/v) $NaHCO_3$

Made up to one litre using dH_2O

Appendix I-IV – Immunofluorescence reagents

IF anti-fade mountant

0.1% (w/v) p-PhenylendiaminoDihydrochloride in 90% (w/v) glycerol in PBS.

Adjusted to pH 8.0 using carbonate-bicarbonate buffer at pH9.6

Appendix I-V – Western blot reagents

2x SDS Lysis buffer

20% (v/v) glycerol

2% (w/v) Sodium Dodecyl Sulphate

125mM Tris-HCL (pH 6.8)

0.42g Sodium fluoride (NaF)

18.4mg Sodium orthovanadate (Na_3PO_4)

0.446g tetra-Sodium pyrophosphate

Made up to a total volume of 50mL using dH_2O, aliquoted and stored at -20°C

Protease inhibitor cocktail (PIC) content

104mM AEBSF

80µM Aprotinin

4mM Bestatin

1.4mM E-64

2mM Leupeptin

1.5mM Pepstatin A

1x Transfer buffer

12mM Tris

96mM Glycine

20% (v/v) Methanol

Made up to one litre with dH_2O.

10x Ponceau red

5g Ponceau

10mL glacial acetic acid

Made up to 100mL with dH_2O.

Western blot TBS

10mM Tris

140mM NaCl

Made up to one litre using dH_2O and pH adjusted to 7.4

Western blot TBS-Tween 20

10mM Tris

140mM NaCl

0.1% (w/v) Tween® 20

Made up to one litre using dH_2O and pH adjusted to 7.4

Appendix I-VI – Alkaline phosphatase reagents

Alkaline phosphatase TBS

0.2M Tris-HCL pH 7.6

0.6M NaCl

Made up to one litre using dH_2O and pH adjusted to 8.2-8.3

Appendix I-VII – CSA immunohistochemistry reagents

TBST

0.05M Tris-HCL

0.3M NaCl

0.1% (w/v) Tween® 20

Made up to one litre using dH_2O.

Appendices II – Method development and characterisation

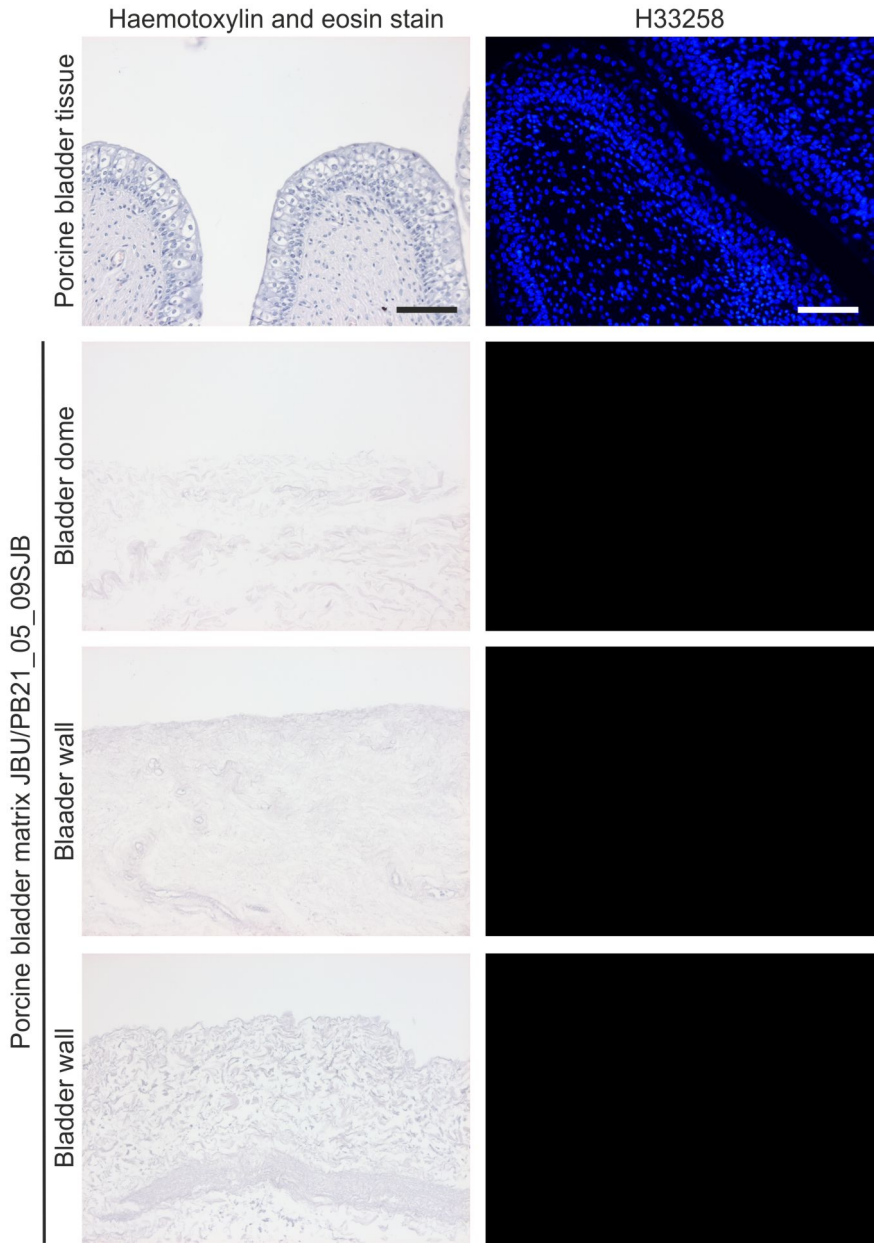

Appendix II-I. Confirmation of porcine bladder decellularisation of batch JBU/PB21_05_09SJB using H&E and H33258 staining. Following the decellularisation process, biopsies of the porcine bladder matrix from three anatomical areas of the bladder were processed into paraffin-wax and sections either stained with H&E or H33258 followed by visualisation with brightfield or fluorescent microscopy. Camera exposures for fluorescent images were set using the porcine bladder tissue stained with Hoechst 33258. Scale bars represent 100 microns.

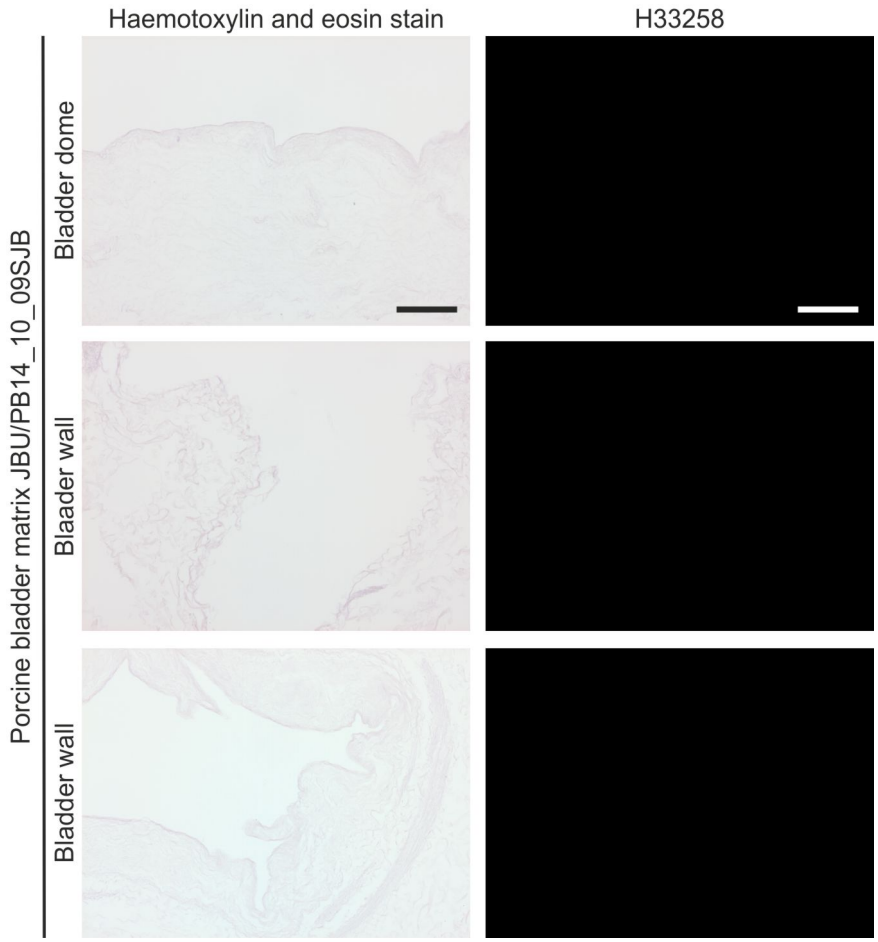

Appendix II-II. Confirmation of porcine bladder decellularisation of batch JBU/PB14_10_09SJB using H&E and H33258 staining. Following the decellularisation process, biopsies of the porcine bladder matrix from three anatomical areas of the bladder were processed into paraffin-wax and sections either stained with H&E or H33258 followed by visualisation with brightfield or fluorescent microscopy. Camera exposures for fluorescent images were set using porcine bladder tissue stained with Hoechst 33258. Scale bars represent 100 microns.

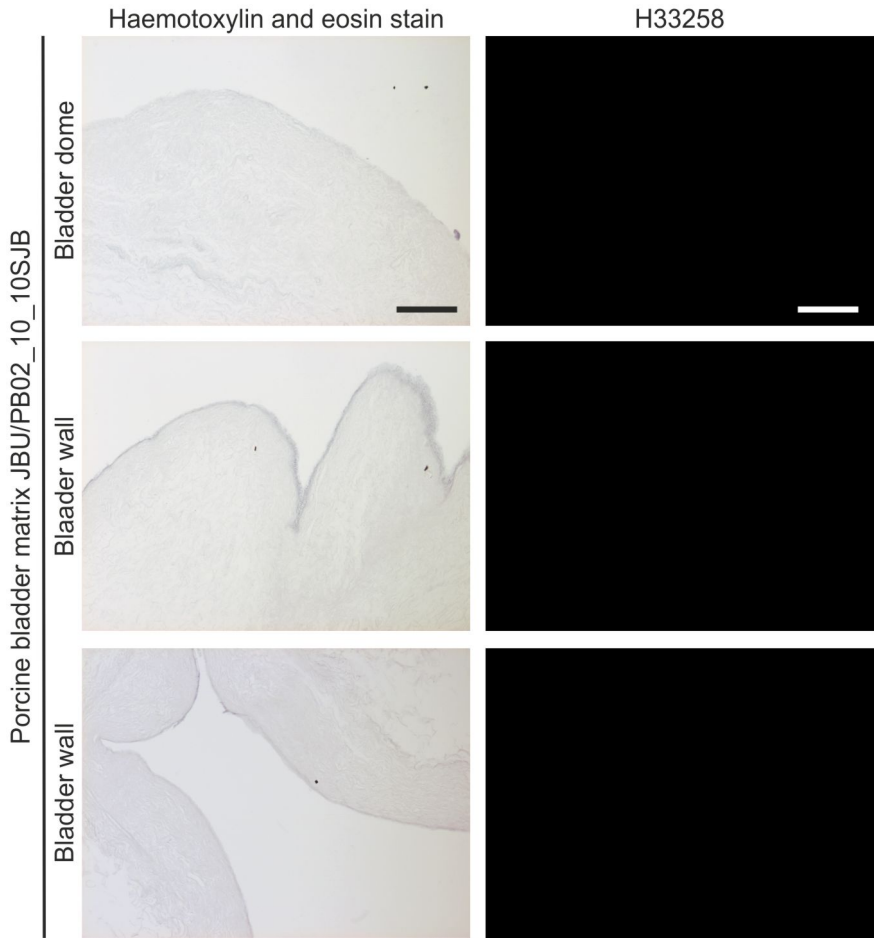

Appendix II-III. Confirmation of porcine bladder decellularisation of batch JBU/PB02_10_10SJB using H&E and H33258 staining. Following the decellularisation process, biopsies of the porcine bladder matrix from three anatomical areas of the bladder were processed into paraffin-wax and sections either stained with H&E or H33258 followed by visualisation with brightfield or fluorescent microscopy. Camera exposures for fluorescent images were set using porcine bladder tissue stained with Hoechst 33258. Scale bars represent 100 microns.

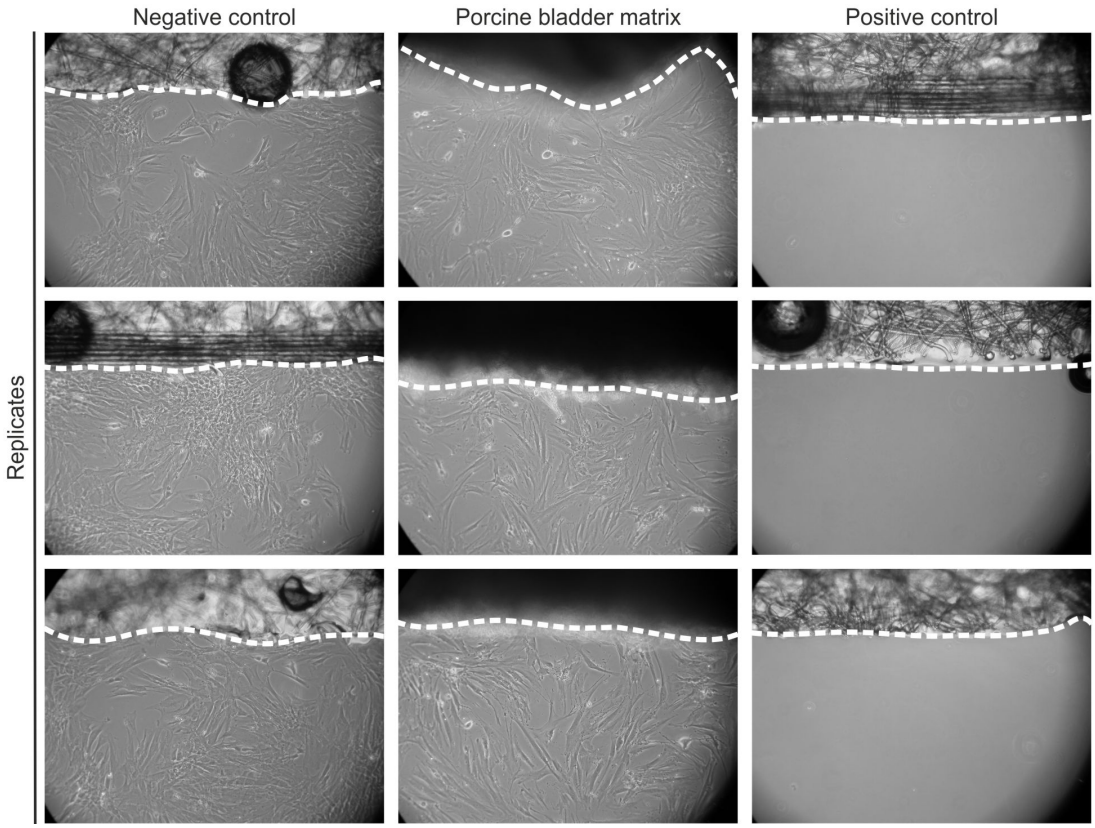

Appendix II-IV. Phase contrast images of the contact cytotoxicity assay of porcine bladder matrix batch JBU/PB02_10_10SJB. Dotted line represents the interface between the Steri-strip™, native porcine bladder matrix or the SDS pre-treated porcine bladder matrix. Human urinary tract stromal cells were cultured for 48 hours before phase contrast images were captured. Images from three intra-assay replicates are shown.

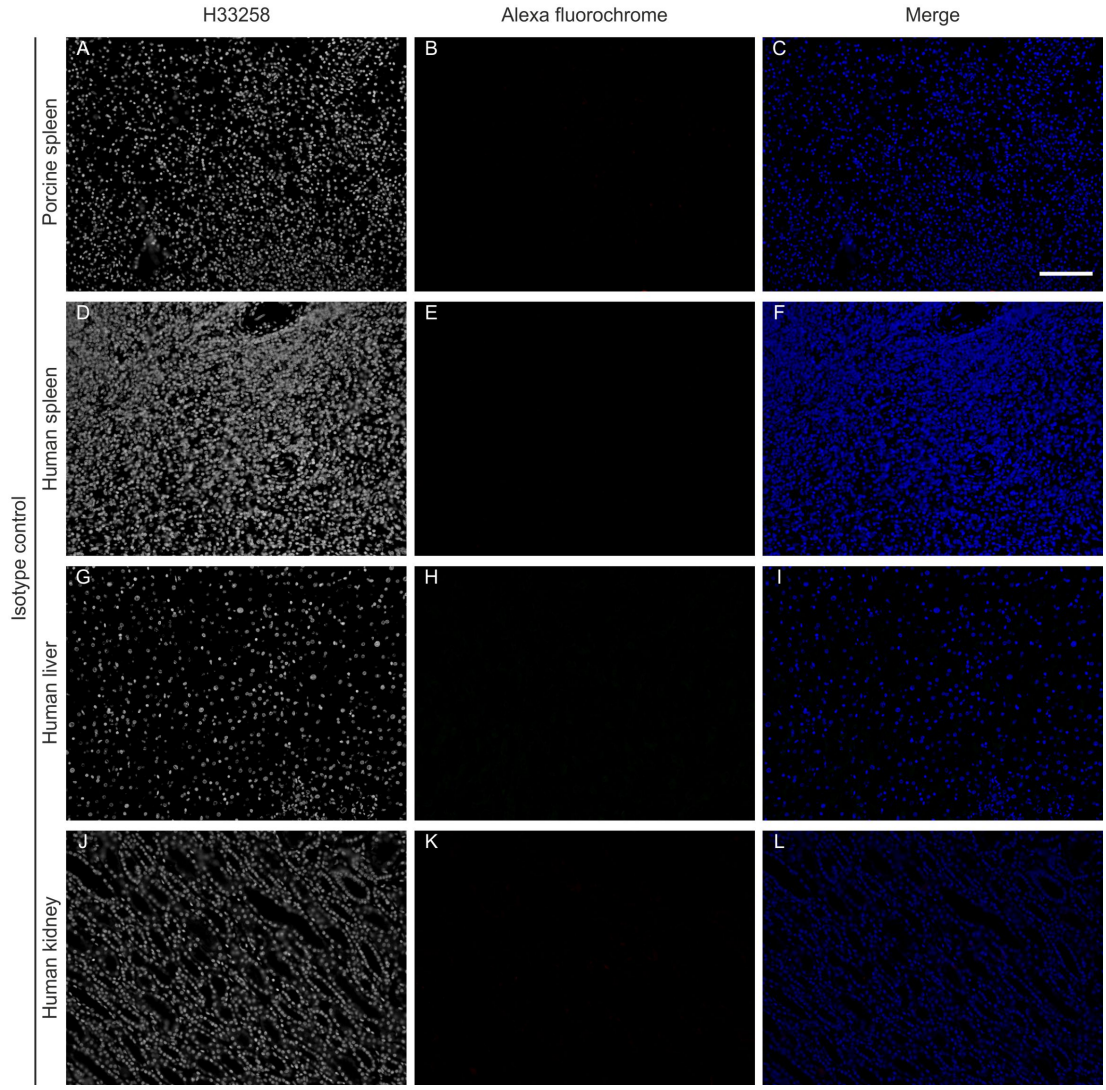

Appendix II-V. Isotype control immunofluorescence labelling of a panel of tissues to confirm the specificity of indirect labelling using a fluorochrome-conjugated secondary antibody. Antigens were retrieved on formalin-fixed, paraffin embedded tissue and tissue sections incubated with in relevant isotype control at a concentration equal to the highest concentration of primary antibody used. Labelling was then determined using a fluorochrome-conjugated secondary antibody. Scale bar represents 100 microns.

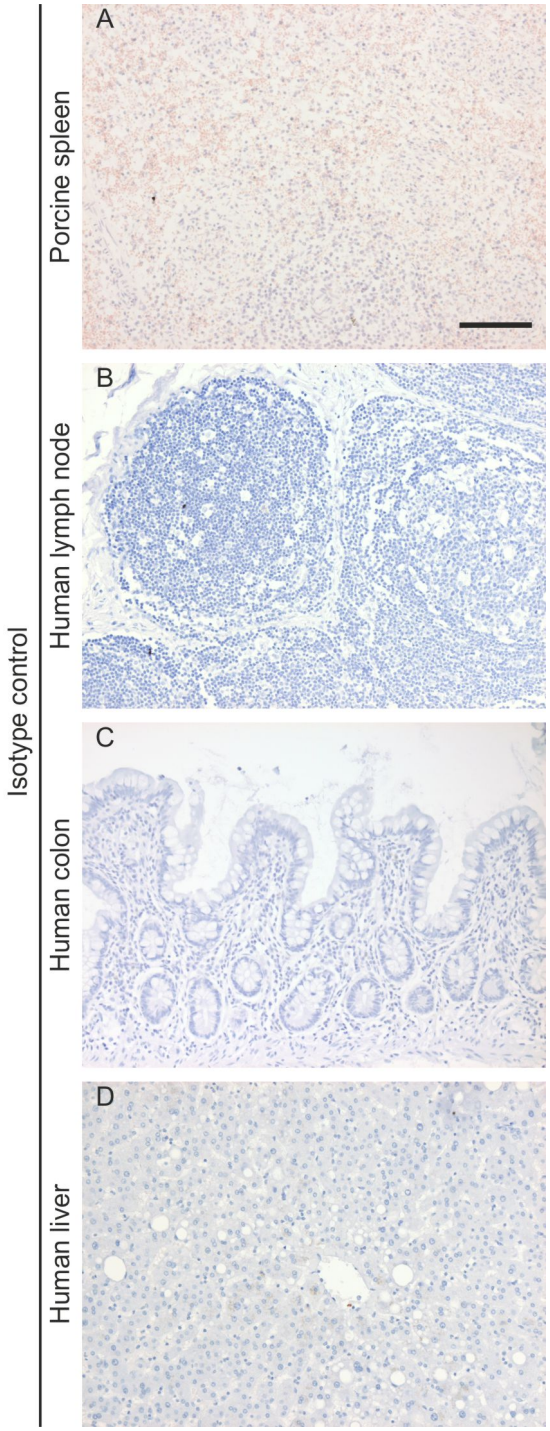

Appendix II-VI. Isotype control immunohistochemical labelling of a panel of tissues to confirm the specificity of indirect labelling using a biotinylated secondary antibody. Antigens were retrieved on formalin-fixed, paraffin wax-embedded tissue and tissue sections incubated with the relevant isotype control at a concentration equal to the highest concentration of primary antibody used. Labelling was then determined using a biotin-conjugated secondary antibody and either alkaline phosphatase (A) or horseradish peroxidase (B-D). Scale bar represents 100 microns.

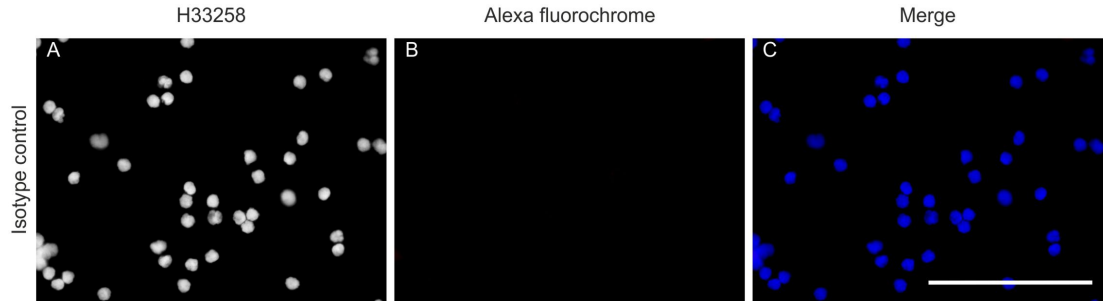

Appendix II-VII. Isotype control immunofluorescent labelling of cytospun preparations of PBMC to determine the specificity of labelling using a fluorochrome-conjugated secondary antibody. Methanol:acetone fixed PBMC were incubated with the isotype control at a concentration equal to the highest concentration of primary antibody used. Labelling was then detected using a fluorochrome-conjugated secondary antibody. Scale bar represents 100 microns.

Appendices III - Development of a biomaterial-organ culture system to interrogate events at a urinary tract-biomaterial interface.

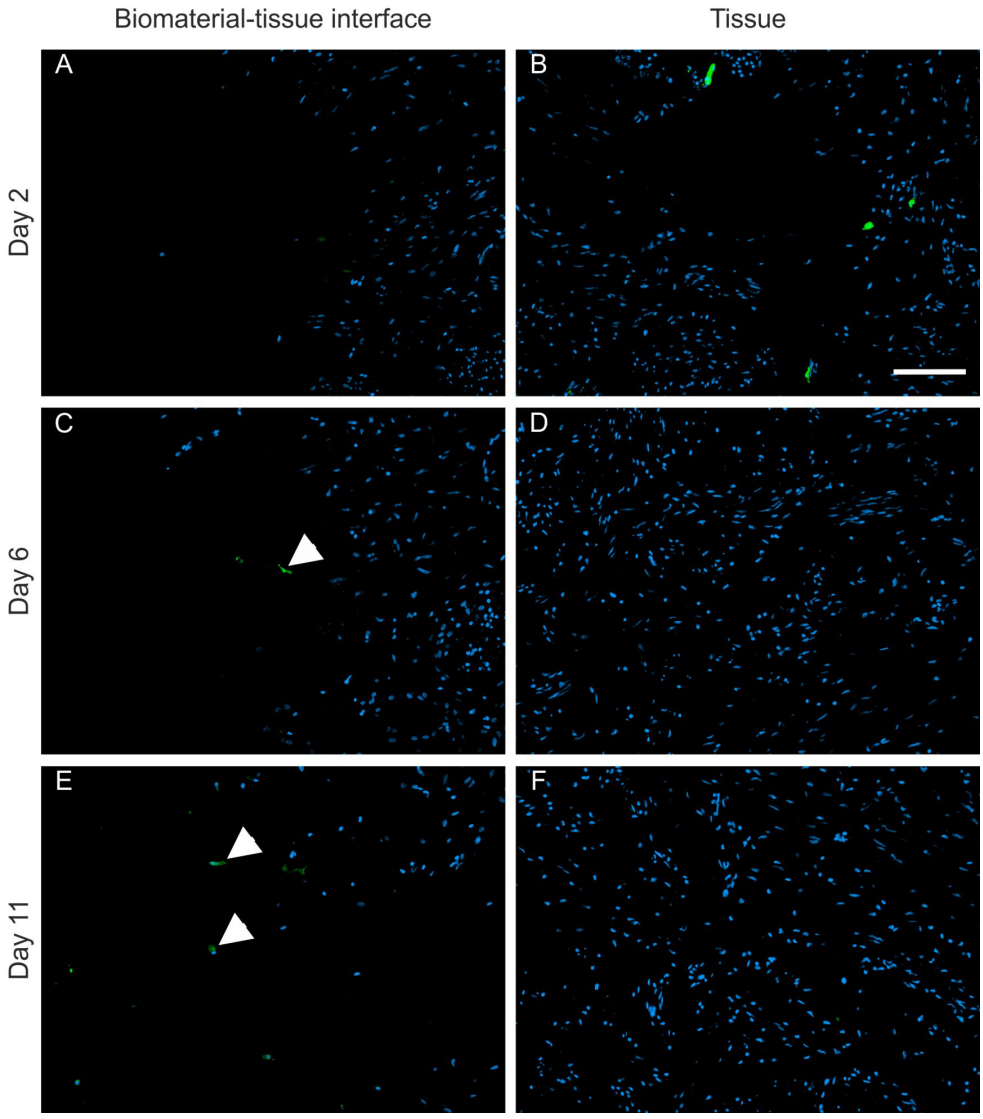

Appendix III-I. Fluorescent immunolabelling of tissue sections from the porcine:human biomaterial-organ culture system using human ureter Y1129 with the antibody MAC387. The biomaterial-tissue interface is shown is micrographs A, C and E and the central regions of the tissue are shown in micrographs B, D and F. Positive labelling with MAC387 (green and arrows) is observed at the biomaterial-tissue interface at day 11. H33258 staining is shown in blue. Scale bars represent 100.

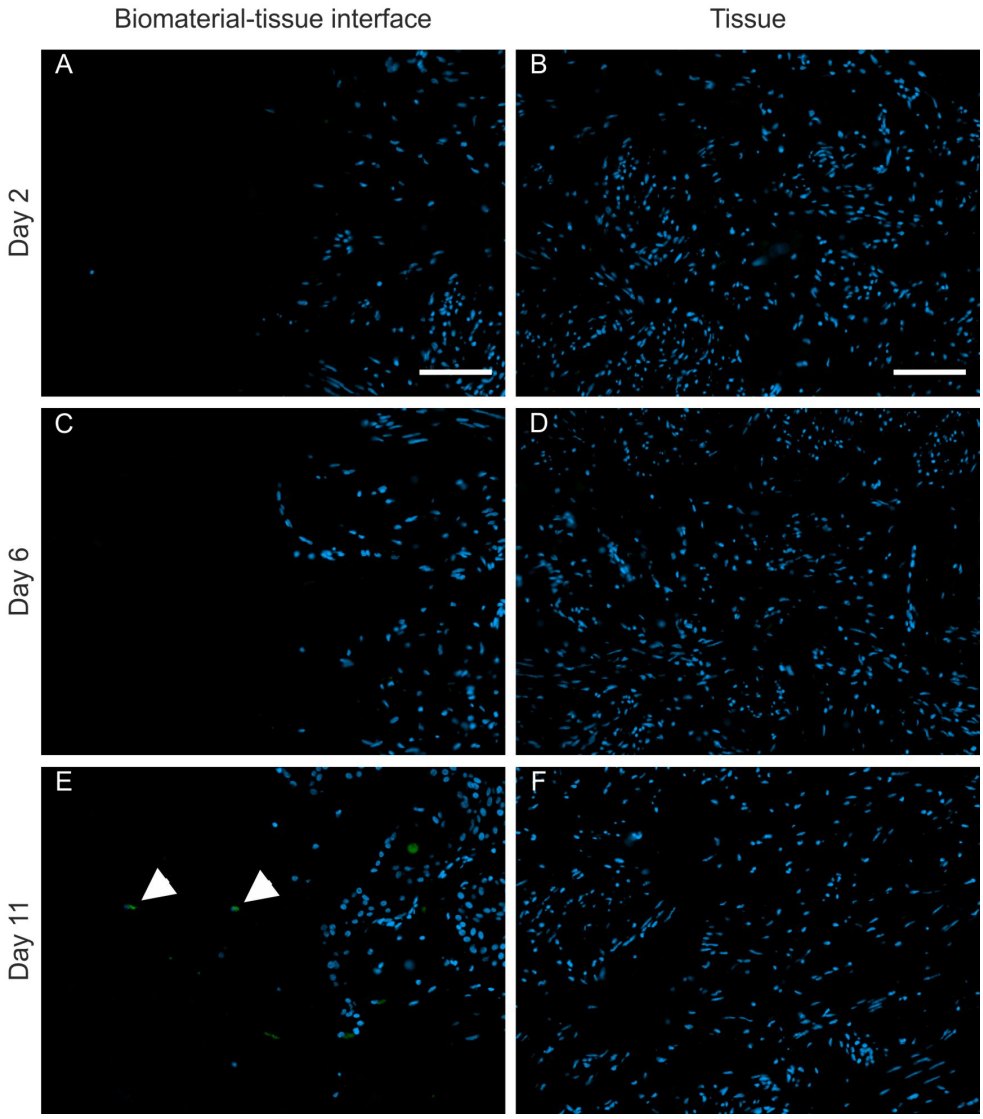

Appendix III-II. Fluorescent immunolabelling for CD68 expression in the porcine:human biomaterial-organ culture system using donor human ureter Y1129. The biomaterial-tissue interface is shown is micrographs A, C and E and the central regions of the tissue are shown in micrographs B, D and F. Positive labelling for CD68 (green and arrows) expression is observed at the biomaterial-tissue interface at days 6 and 11. H33258 staining is shown in blue. Scale bars represent 100 microns.

Appendix III-III. Immunoperoxidase labelling of CD80 expression on histological sections of the biomaterial-organ culture construct Y1132. The biomaterial-tissue interface is shown is micrographs A, B, E, F, I and J the central regions of the tissue are shown in micrographs C, D, G, H, K and L. Cells present in the biological scaffold are negative for CD80 expression (arrows). Positive control labelling was confirmed using human colon tissue as shown on chapter 3. Scale bars represent 100 microns.

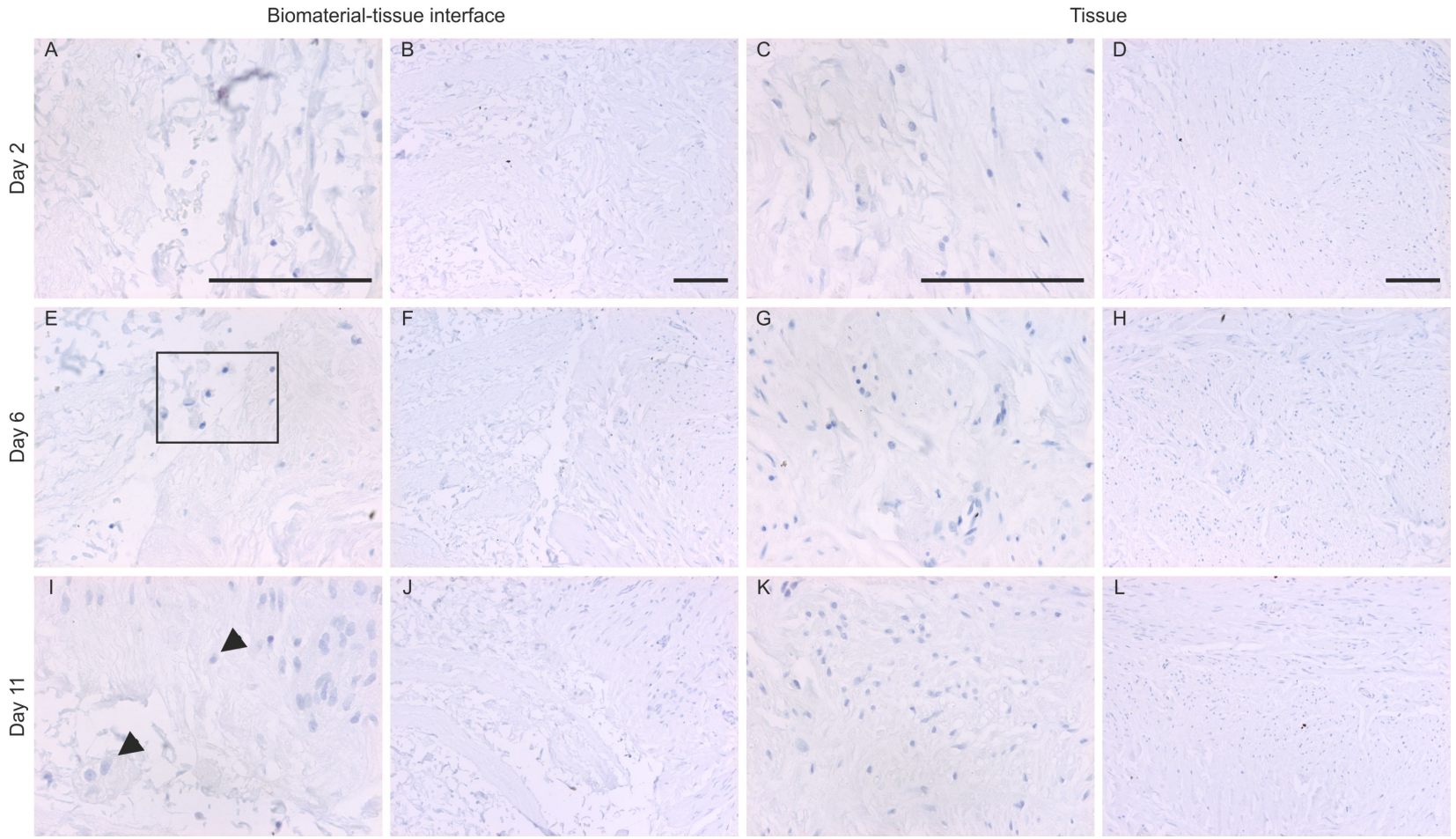
Biomaterial-tissue interface
Tissue
Day 2
Day 6
Day 11
A
B
C
D
E
F
G
H
I
J
K
L

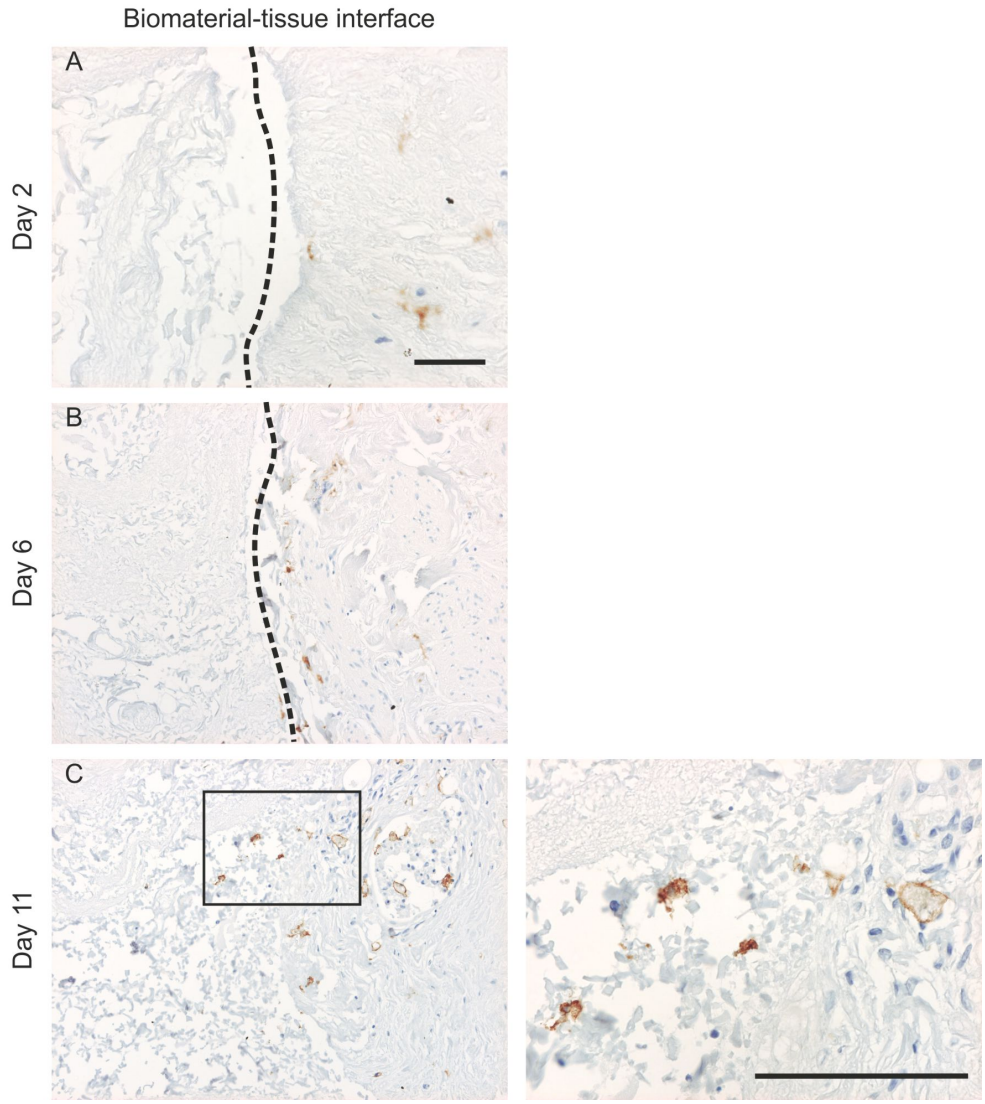

Appendix III-IV. Immunoperoxidase labelling of CD163 in the porcine:human biomaterial-organ culture system Y1129. Photomicrographs show biomaterial-tissue interface over the eleven-day time course (A-C). Dotted line on photomicrographs A and B highlight biomaterial-tissue interface. Black box on day 11 photomicrograph (C) indicates orientation and location of higher magnification image. Scale bars represent 100 microns.

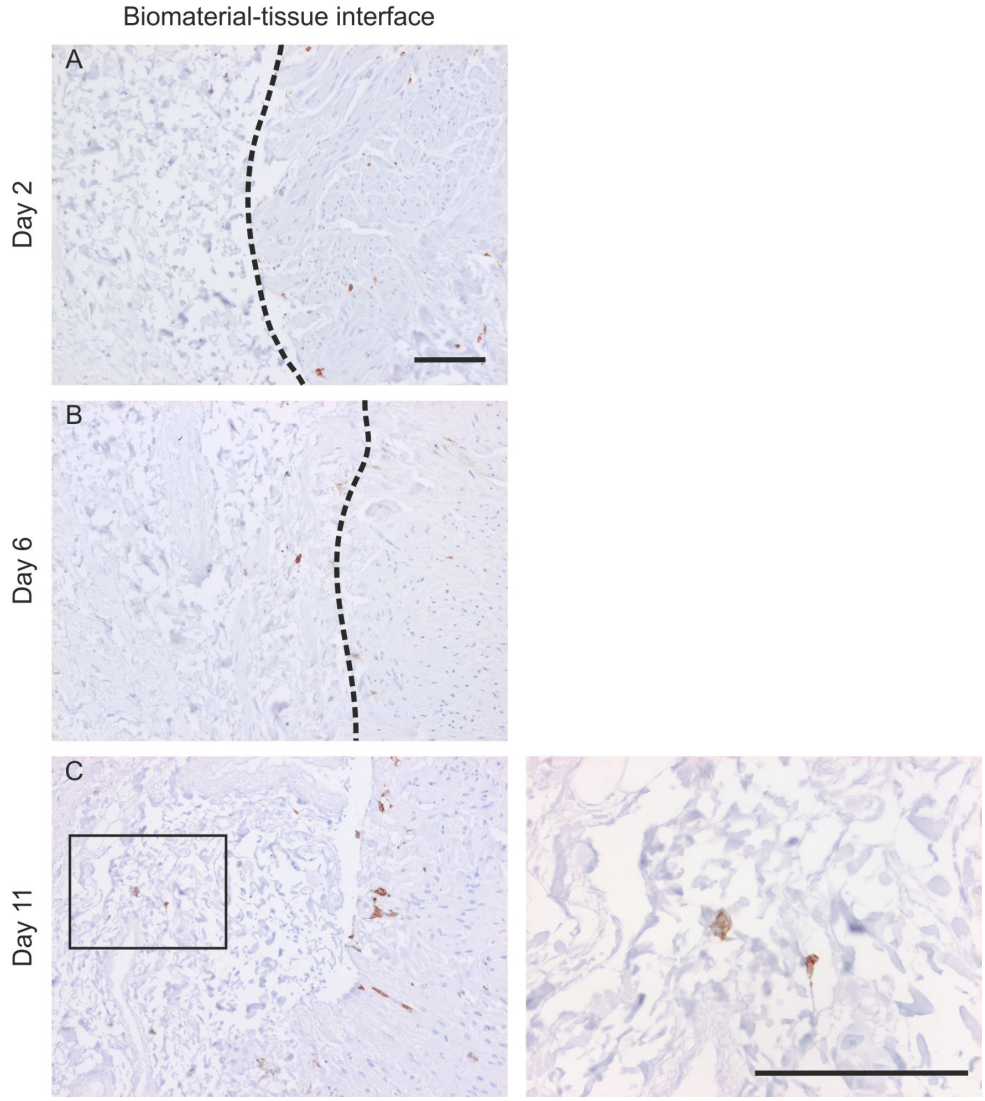

Appendix III-V. Immunoperoxidase labelling of CD163 in the porcine:human biomaterial-organ culture system Y1132. Photomicrographs show biomaterial-tissue interface over the eleven-day time course (A-C). Dotted line on photomicrographs A and B highlight biomaterial-tissue interface. Black box on day 11 photomicrograph (C) indicates orientation and location of higher magnification image. Scale bars represent 100 microns.

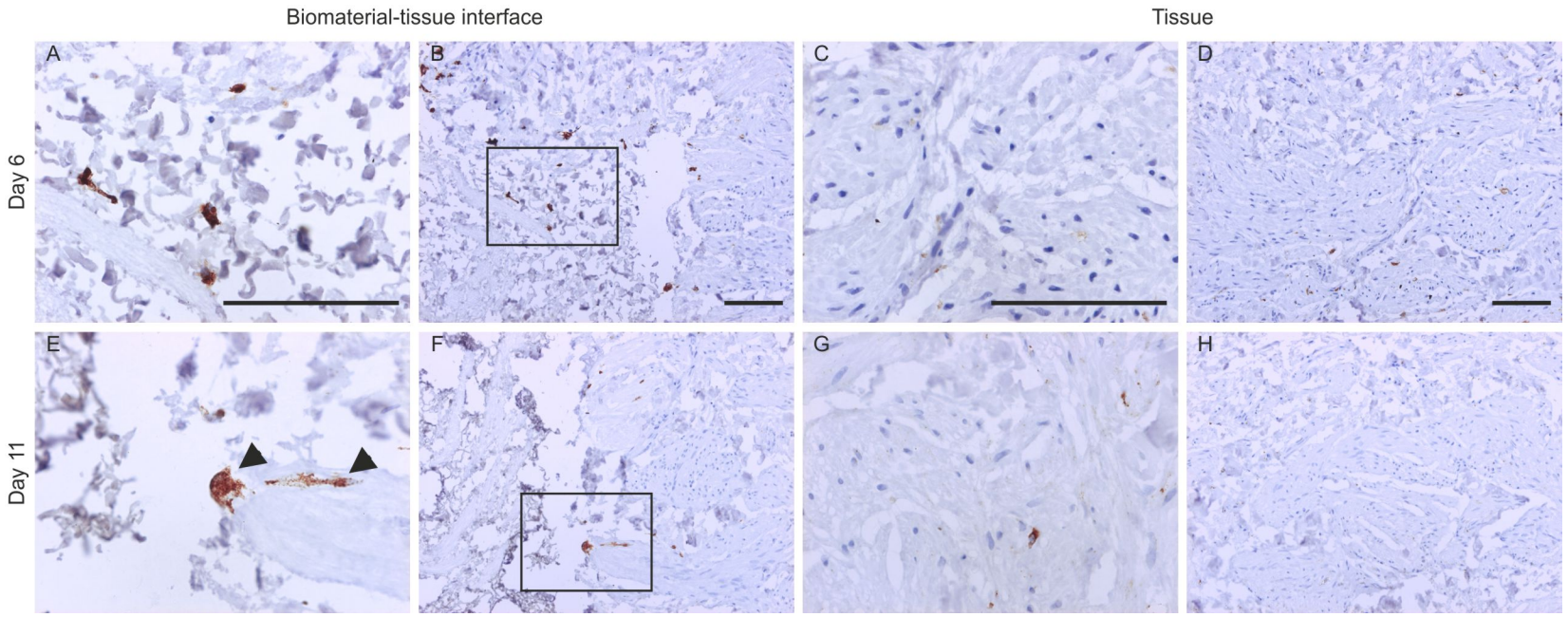

Appendix III-VI. Immunoperoxidase labelling of CD68 on histological sections of porcine:human biomaterial-organ culture using donor tissue Y1193 in the presence of hydrocortisone hemisuccinate harvested at days 6 and 11. The biomaterial-tissue interface is shown is micrographs A, B, E and F the central regions of the tissue are shown in micrographs C, D, G and H. Arrow on image B shows indicated cell in image A. Black box on image F represent area of high magnification image E. Scale bars represent 100 microns.

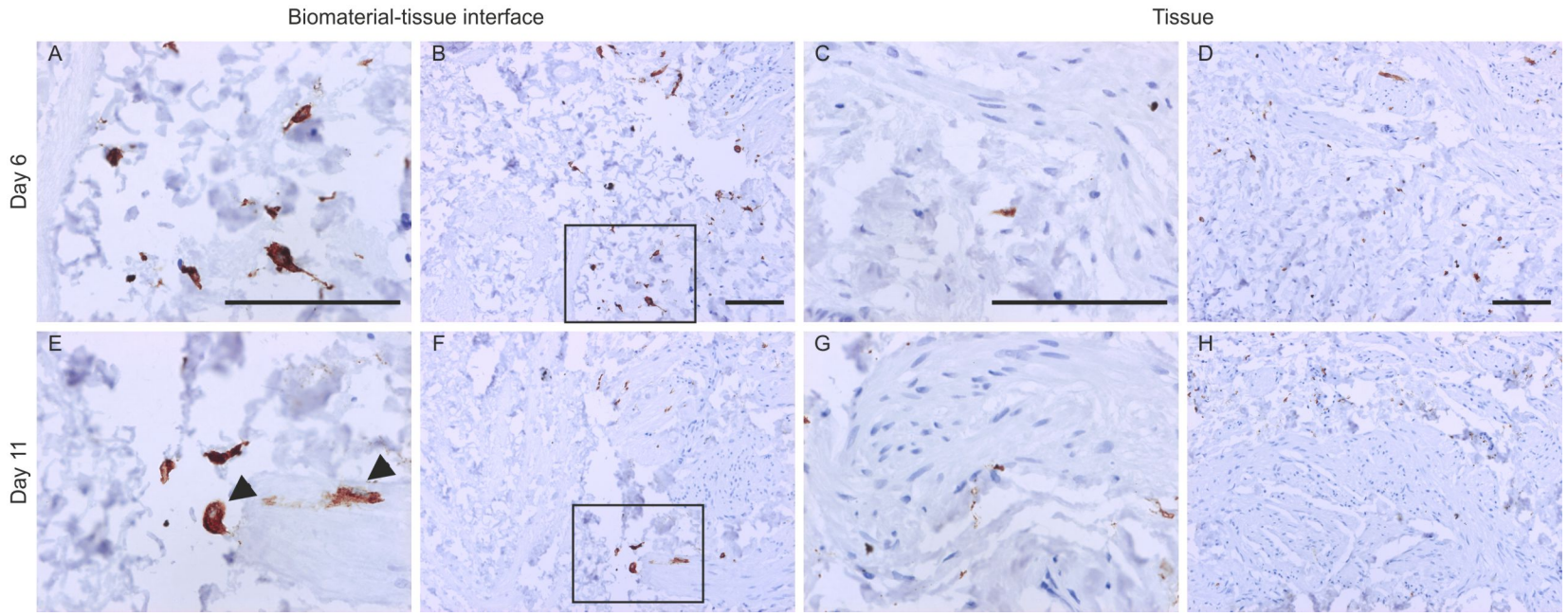

Appendix III-VII. Immunoperoxidase labelling of CD163 on histological sections of porcine:human biomaterial-organ culture using donor tissue Y1193 in the presence of hydrocortisone hemisuccinate harvested at days 6 and 11. The biomaterial-tissue interface is shown is micrographs A, B, E and F the central regions of the tissue are shown in micrographs C, D, G and H. Arrow on image B shows indicated cell in image A. Black box on image F represent area of high magnification image E. Scale bars represent 100 microns.

Appendices IV – Nuclear receptor modulation of CD163 expression

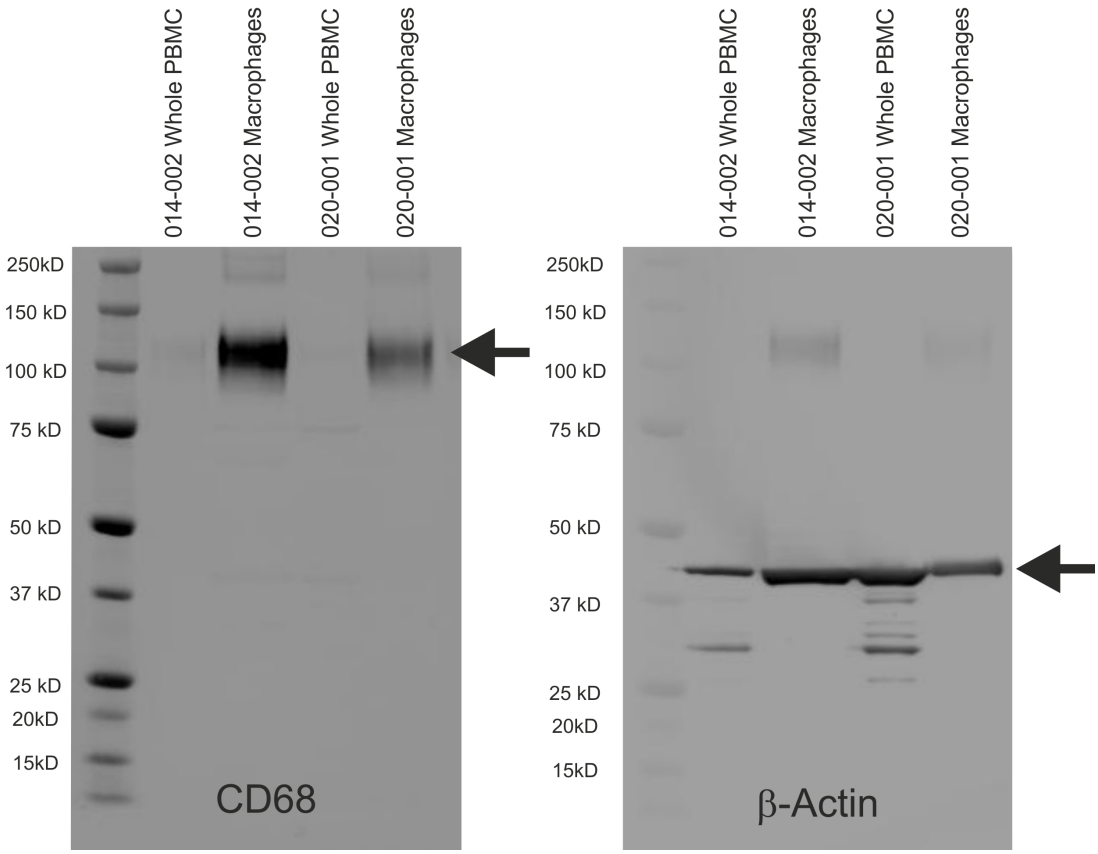

Appendix IV-I. Whole Western blot membrane images of CD68 expression by PBMC and monocyte-derived macrophages. Protein lysates from matched whole PBMC taken directly following isolation from peripheral blood and adherent mononuclear cells seeded onto a glass substrate for 11 days from two independent donors were separated on a 4-12% (w/v) Bis-Tris gel. Lane 1 – Human liver microsomes positive control for CD163. Lane 2 – 014-002 Whole PBMC. Lane 3 – 014-002 Macrophages. Lane 4 – 020-001 Whole PBMC. Lane 5 – 020-001 Macrophages. Labelling of β-Actin was used as a loading control. Antibodies were added sequentially to the PVDF membrane, CD68>β-Actin.

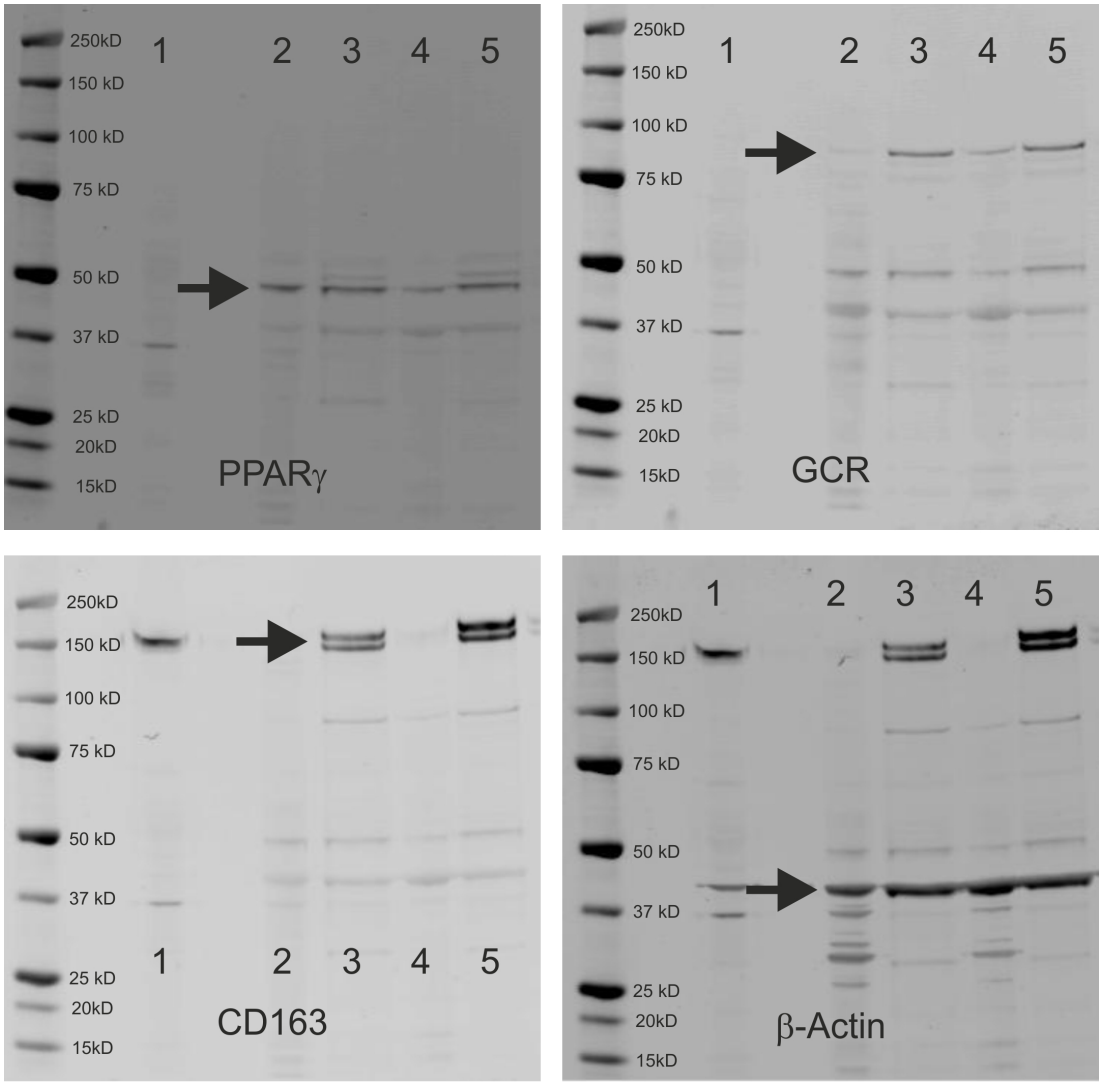

Appendix IV-II. Whole Western blot membrane images of CD163, GCR and PPARγ expression by PBMC and monocyte-derived macrophages. Protein lysates from donor matched whole PBMC taken directly following isolation from peripheral blood and adherent mononuclear cells seeded onto a glass substrate for 11 days were separated on a 4-12% (w/v) Bis-Tris gel. Lane 1 – Human liver microsomes positive control for CD163. Lane 2 – 014-002 Whole PBMC. Lane 3 – 014-002 Macrophages. Lane 4 – 020-001 Whole PBMC. Lane 5 – 020-001 Macrophages. Primary antibodies against PPARγ, CD163, GCR and β-Actin were added sequentially to the PVDF membrane, PPARγ>GCR>CD163>β-Actin and expression detected with an IR-Dye-conjugated secondary antibody. Labelling of β-Actin was used as a loading control.

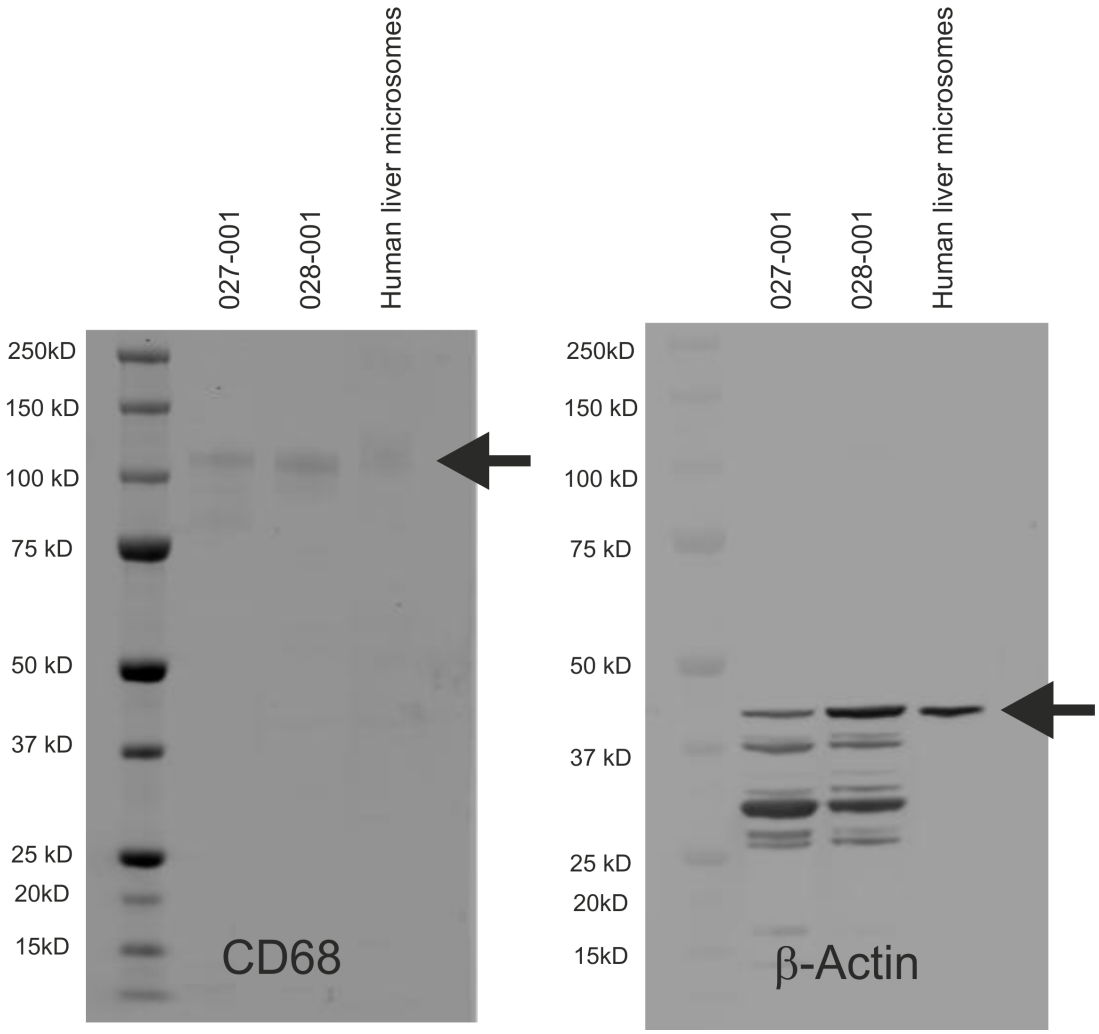

Appendix IV-III. Whole Western blot images of CD68 protein expression by adherent PBMC. Protein lysates from adherent PBMC from two independent donors were extracted from human liver microsomes were separated on a 4-12% (w/v) Bis-Tris gel and CD68 expression was detected by Western blot. Labelling of β-Actin was used as a loading control. Antibodies were added sequentially to the PVDF membrane, CD68>β-Actin.

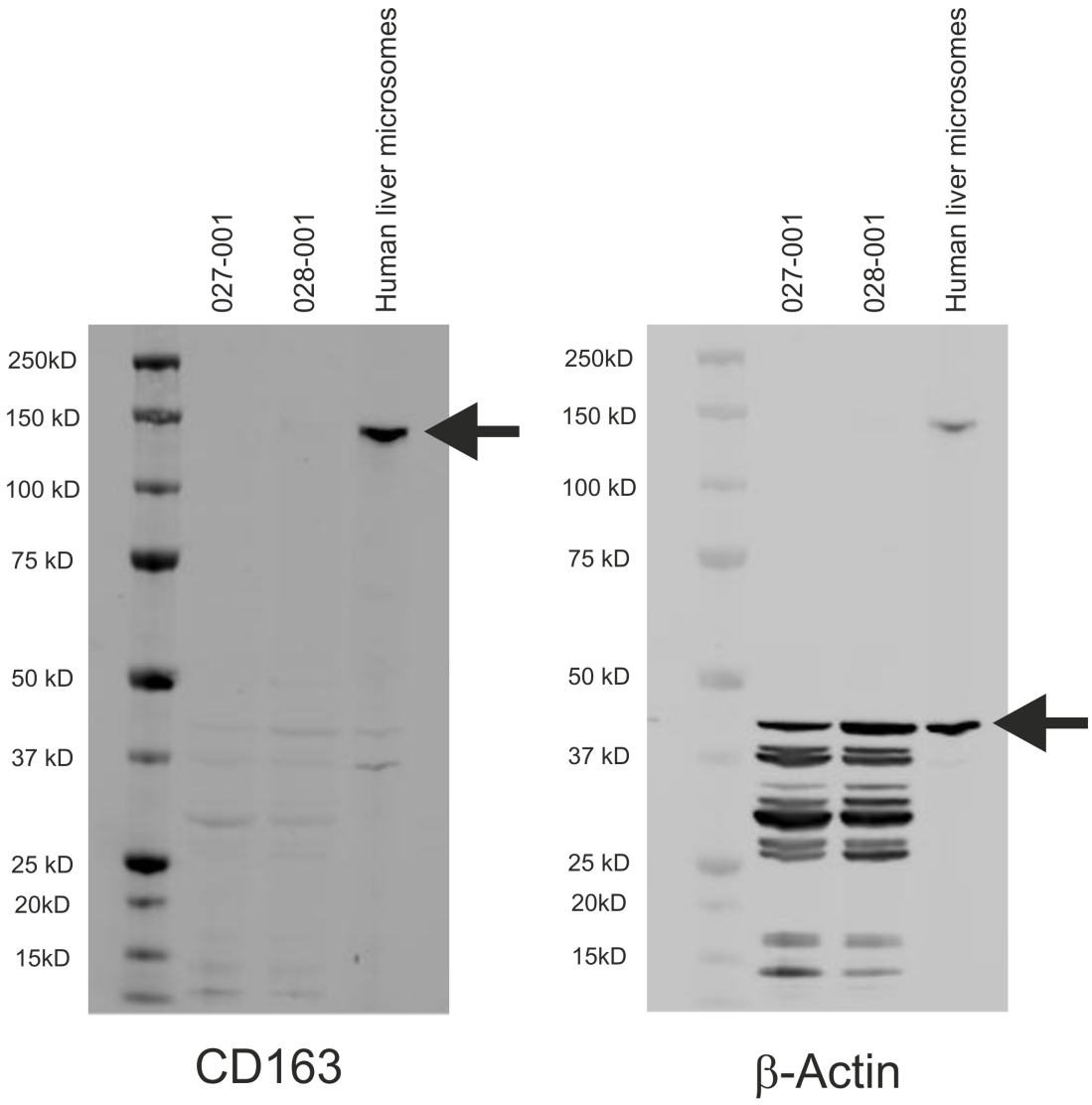

Appendix IV-IV. Whole Western blot membrane images of CD163 protein expression by adherent PBMC. Protein lysates from adherent PBMC from two independent donors and protein extracts from human liver microsomes were separated on a 4-12% (w/v) Bis-Tris gel and CD163 protein expression was detected by Western blot. Labelling of β-Actin was used as a loading control. Antibodies were added sequentially to the PVDF membrane, CD163>β-Actin.

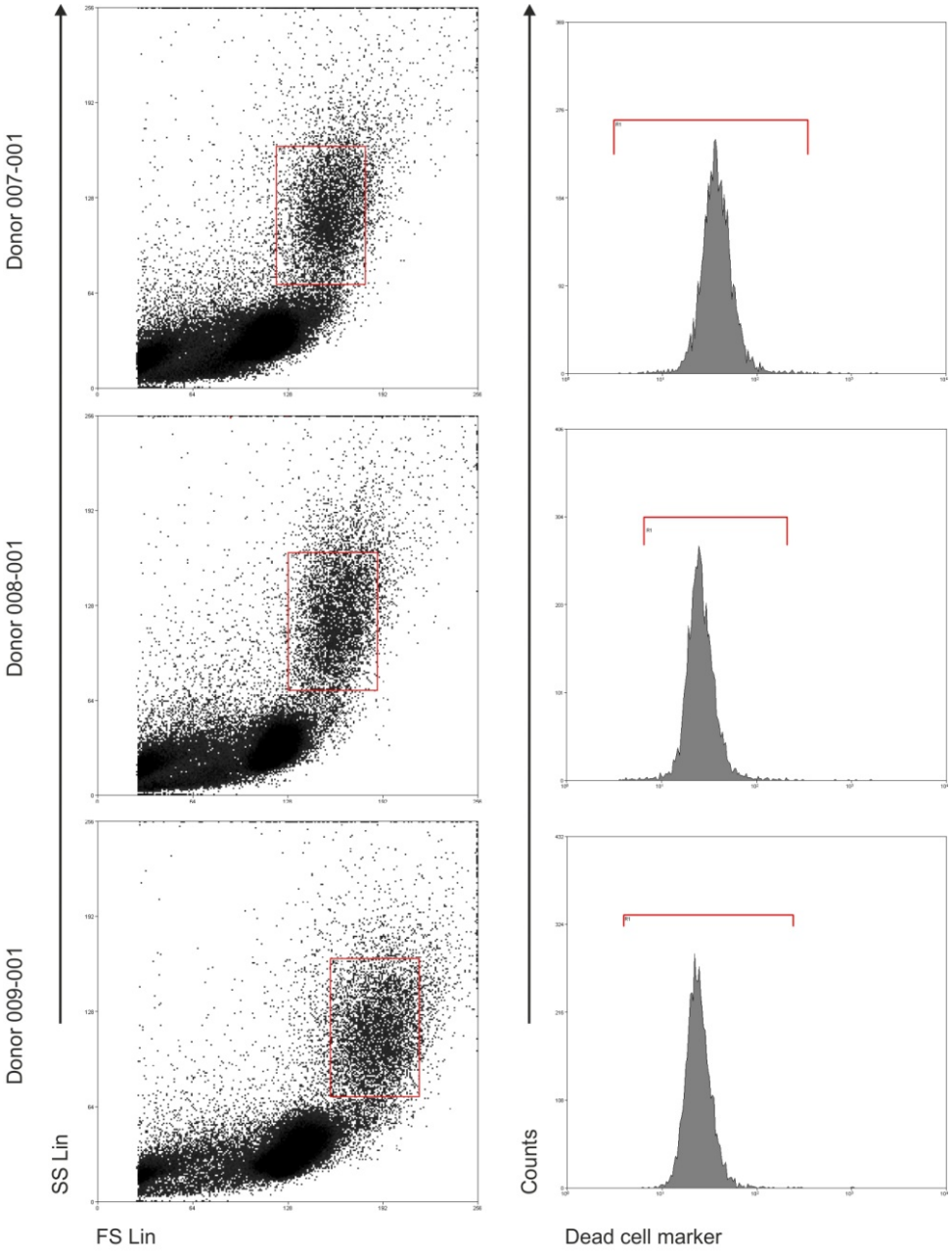

Appendix IV-V. Gating of 'live' peripheral blood monocytes from donors 007-01, 008-001 and 009-001 using FS Lin and SS Lin and a dead cell marker. Peripheral blood monocytes were gated based on the FS Lin and SS Lin properties of the cells as described in chapter three. 'Live' cells were gated using the LIVE/DEAD stain (red bar) as described in chapter three.

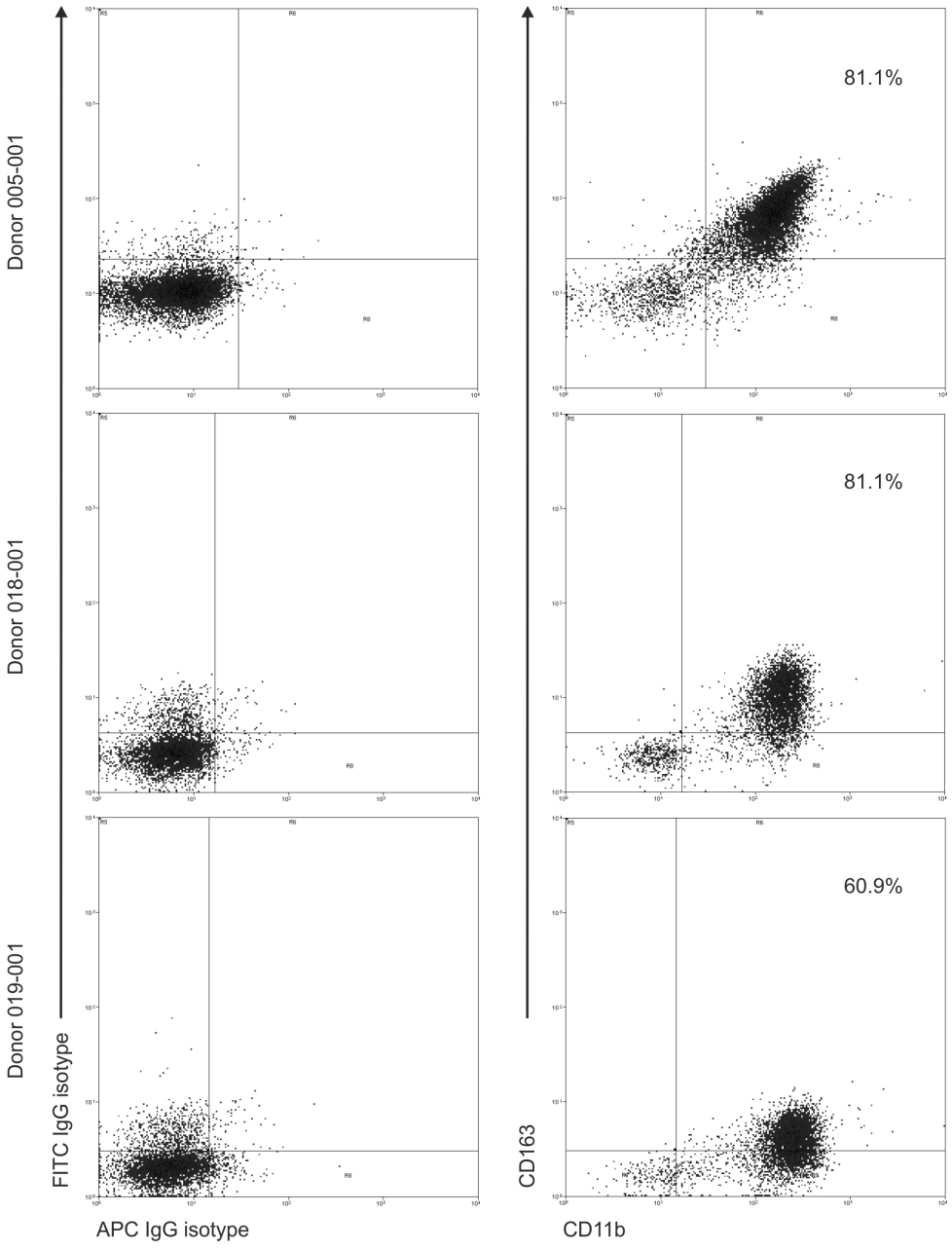

Appendix IV-VI. CD163 expression by CD11b+ peripheral blood monocytes from donors 005-001, 018-001 and 019-001. Isolated peripheral blood mononuclear cells were labelled with APC conjugated anti-CD11b and FITC-conjugated anti-CD163 antibodies. Human peripheral blood monocytes were gated based on FS Lin and SS Lin and dead cells excluded from the analysis (Appendix IV-VII). Analysis regions for CD11b, CD163 labelling were set using the fluorescent profiles of the APC-IgG and FITC-IgG isotype controls for each donor. Percentage of double positive cells shown.

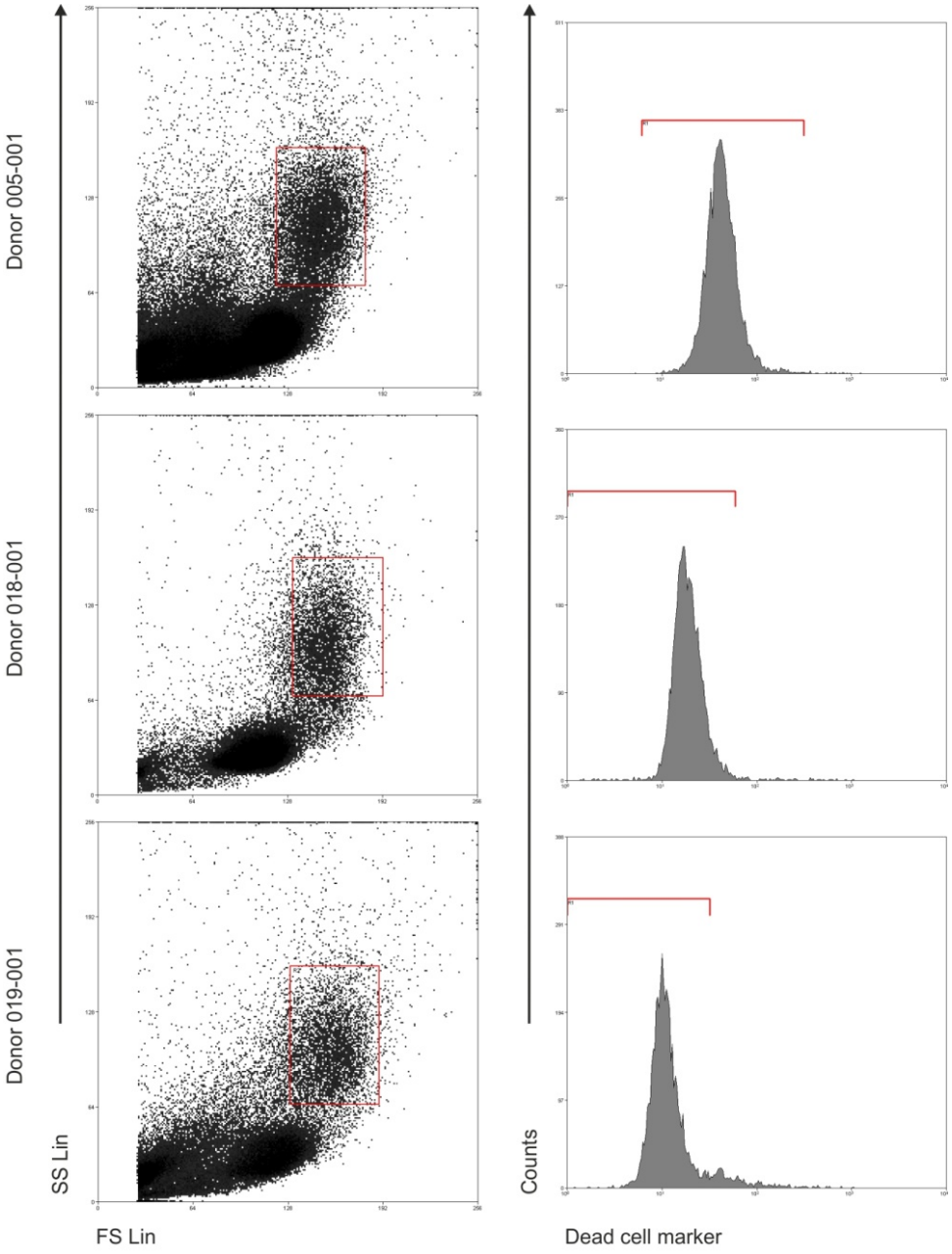

Appendix IV-VII. Gating of 'live' peripheral blood monocytes from donors 005-001, 018-001 and 019-001 using FS Lin and SS Lin and a dead cell marker from donors. Peripheral blood monocytes were gated based on the FS Lin and SS Lin properties of the cells as described in chapter three. 'Live' cells were gated using the LIVE/DEAD stain (red bar) as described in chapter three.

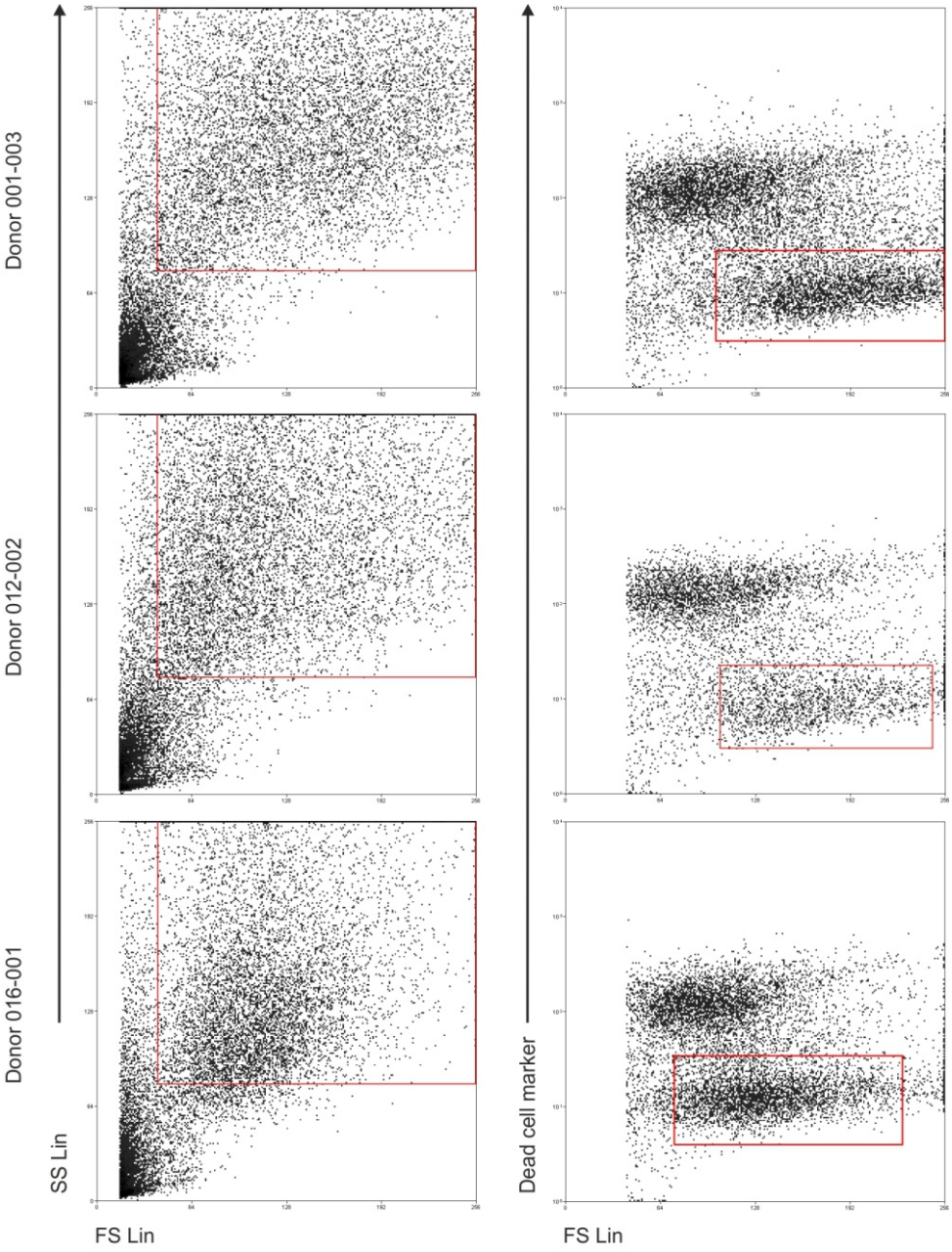

Appendix IV-VIII. Gating of 'live' monocyte-derived macrophages from donors 001-003, 012-002 and 016-001 using FS Lin and SS Lin and a dead cell marker. Monocyte-derived macrophages, harvested for flow cytometry following 11 days in culture, were gated based on the FS Lin and SS Lin properties of the cells as described in chapter three. 'Live' cells were gated using the LIVE/DEAD stain (red box) as described in chapter three.

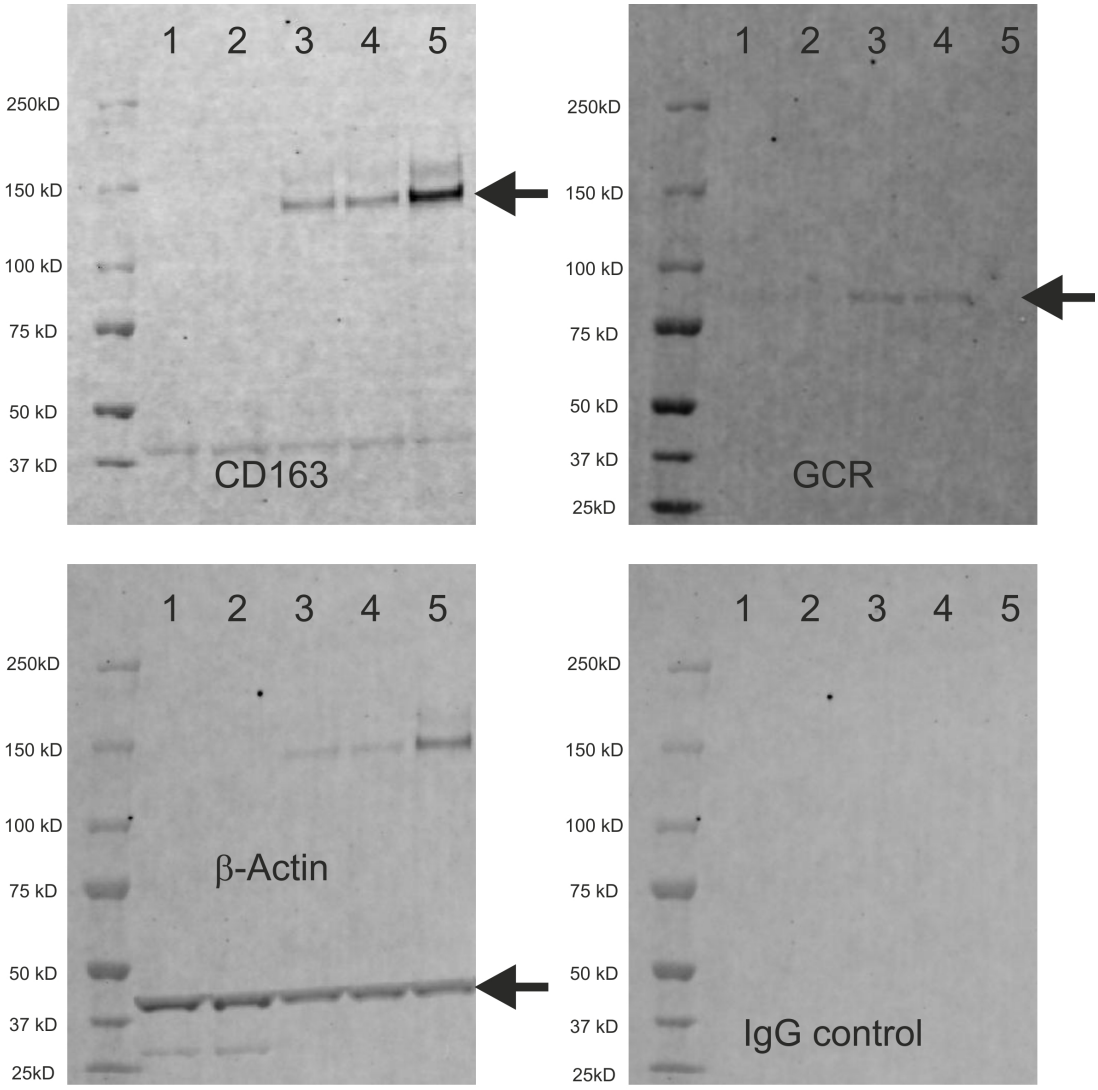

Appendix IV-IX. Whole Western blot membrane images of CD163 or glucocorticoid receptor expression by THP-1 cells. THP-1 cell protein lysates were separated on a 3-8% (w/v) Tris-Acetate gel and CD163 and GCR expression determined by Western blot. Lane 1 – Medium only. Lane 2 – Medium + chloroform. Lane 3 – PMA only. Lane 4 – PMA + Ethanol. Lane 5 – PMA + Dexamethasone. Medium plus chloroform was the vehicle control for the PMA. PMA plus ethanol was the vehicle control for the dexamethasone. Labelling of β-Actin was used as a loading control. IgG control showed that the IR-conjugated secondary antibody did not label the membrane non-specifically.

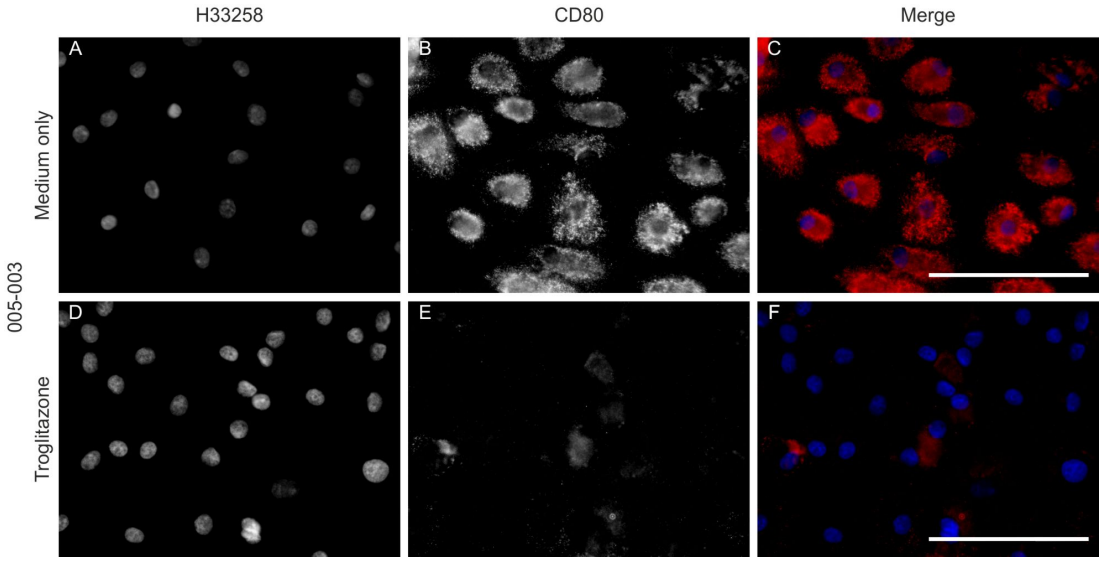

Appendix IV-X. Preliminary data on the effect of PPARγ activation on the expression of CD80 by monocyte-derived macrophages. Day 11 monocyte-derived macrophages from donor 005-003 were either cultured in complete PBMC medium only (A-C) or complete PBMC medium containing troglitazone for 48 hours followed by nine days in complete PBMC medium (D-F). Fixed cells were immunolabelled for CD80 expression. 32-bit greyscale images of H33258 staining and CD80 expression were merged to produce a colour image. Scale bar represent 100 microns.

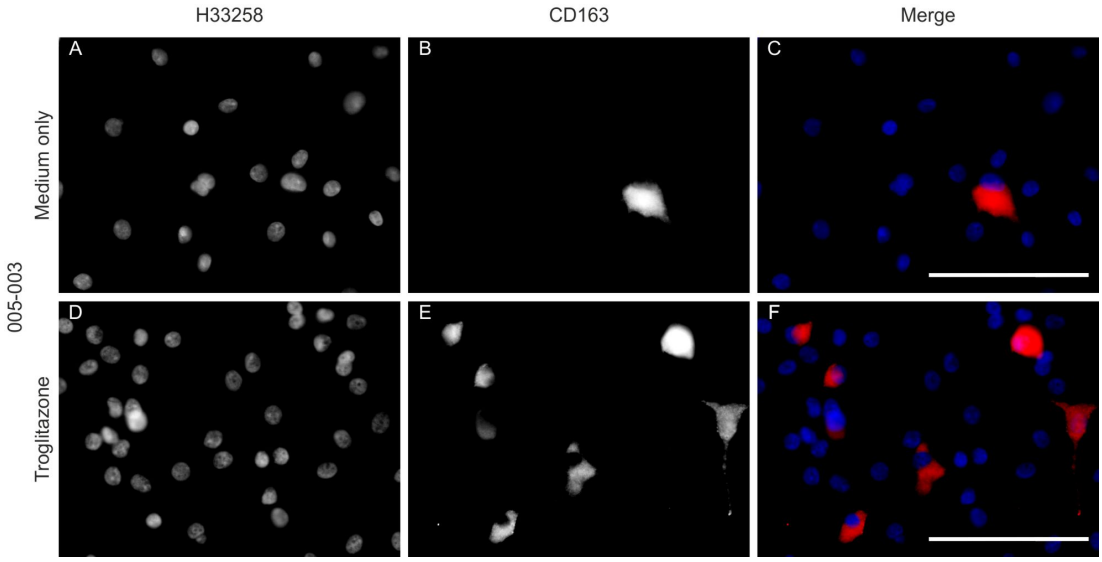

Appendix IV-XI. Preliminary data on the effect of PPARγ activation on the expression of CD163 by monocyte-derived macrophages. Day 11 monocyte-derived macrophages from donor 005-003 were either cultured in complete PBMC medium only (A-C) or complete PBMC medium containing troglitazone for 48 hours followed by nine days in complete PBMC medium (D-F). Fixed cells were immunolabelled for CD163 expression. 32-bit greyscale images of H33258 staining and CD163 expression were merged to produce a colour image. Scale bar represent 100 microns.

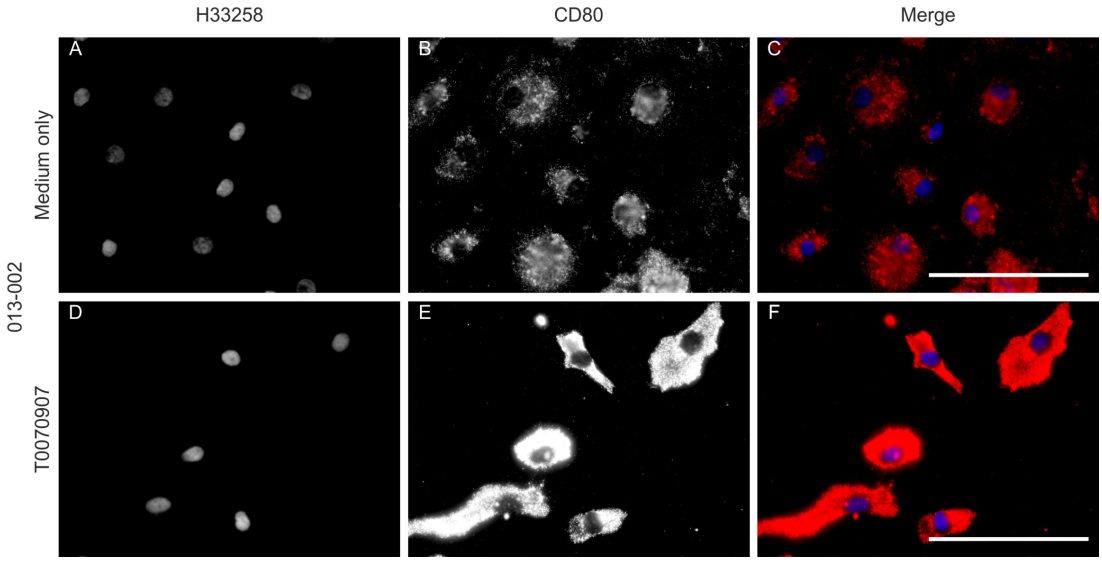

Appendix IV-XII. Preliminary data on the effect of PPARγ inhibition on the expression of CD80 by monocyte-derived macrophages. Day 11 monocyte-derived macrophages from donor 013-002 were either cultured in complete PBMC medium only (A-C) or complete PBMC medium containing T0070907 (D-F). Fixed cells were immunolabelled for CD80 expression. 32-bit greyscale images of H33258 staining and CD80 expression were merged to produce a colour image. Scale bar represent 100 microns.

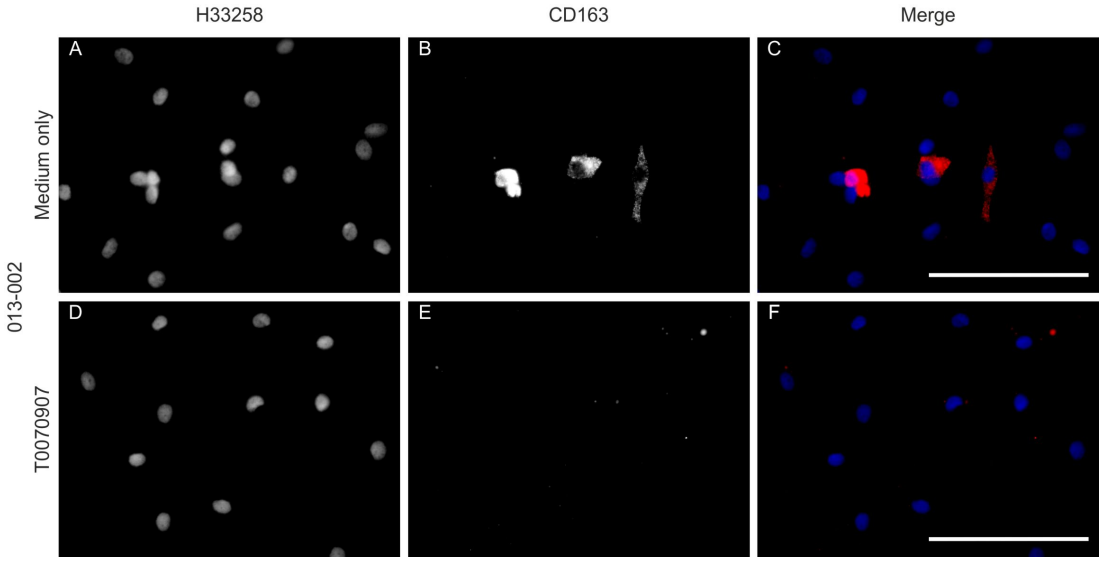

Appendix IV-XIII. Preliminary data on the effect of PPARγ inhibition on the expression of CD163 by monocyte-derived macrophages. Day 11 monocyte-derived macrophages from donor 013-002 were either cultured in complete PBMC medium only (A-C) or complete PBMC medium containing T0070907 (D-F). Fixed cells were immunolabelled for CD163 expression. 32-bit greyscale images of H33258 staining and CD163 expression were merged to produce a colour image. Scale bar represent 100 microns**.**

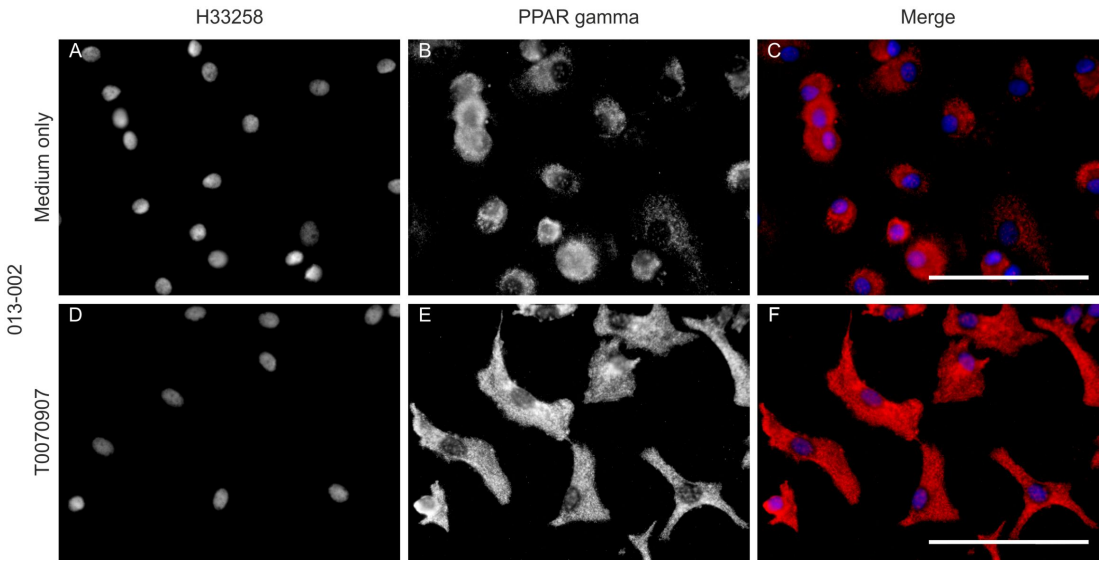

Appendix IV-XIV. Preliminary data on the effect of PPARγ inhibition on the expression of PPARγ by monocyte-derived macrophages. Day 11 monocyte-derived macrophages from donor 013-002 were either cultured in complete PBMC medium only (A-C) or complete PBMC medium containing T0070907 (D-F). Fixed cells were immunolabelled for PPARγ expression. 32-bit greyscale images of H33258 staining and PPARγ expression were merged to produce a colour image. Scale bar represent 100 microns**.**

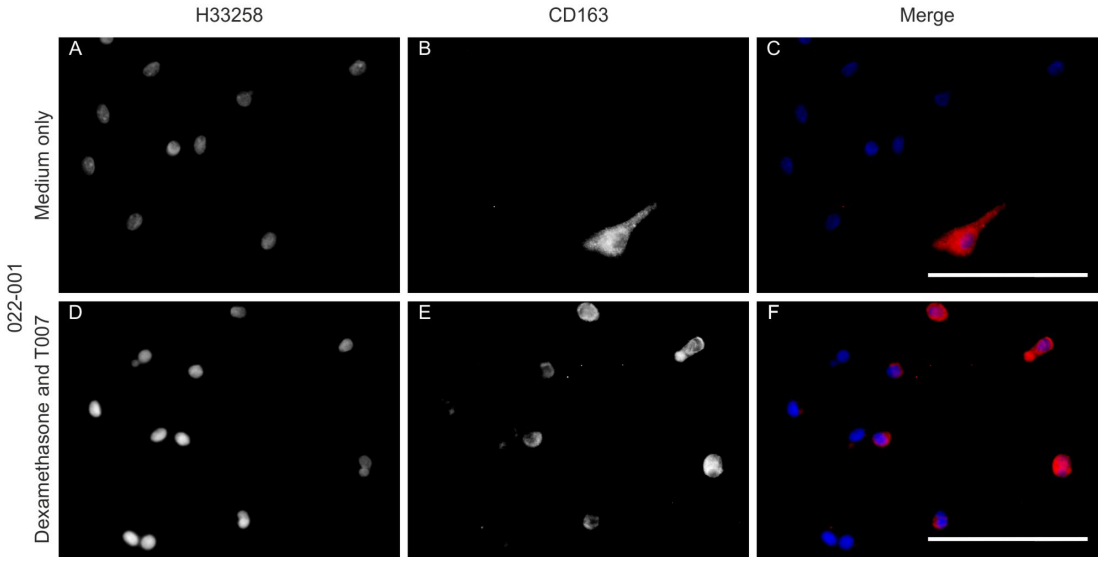

Appendix IV-XV. Preliminary data on the effect of PPARγ inhibition and GCR stimulation on the expression of CD163 by monocyte-derived macrophages. Day 11 monocyte-derived macrophages from donor 022-001 were either cultured in complete PBMC medium only (A-C) or complete PBMC medium containing T0070907 and dexamethasone (D-F). Fixed cells were immunolabelled for CD163 expression. 32-bit greyscale images of H33258 staining and CD163 expression were merged to produce a colour image. Scale bar represent 100 microns.

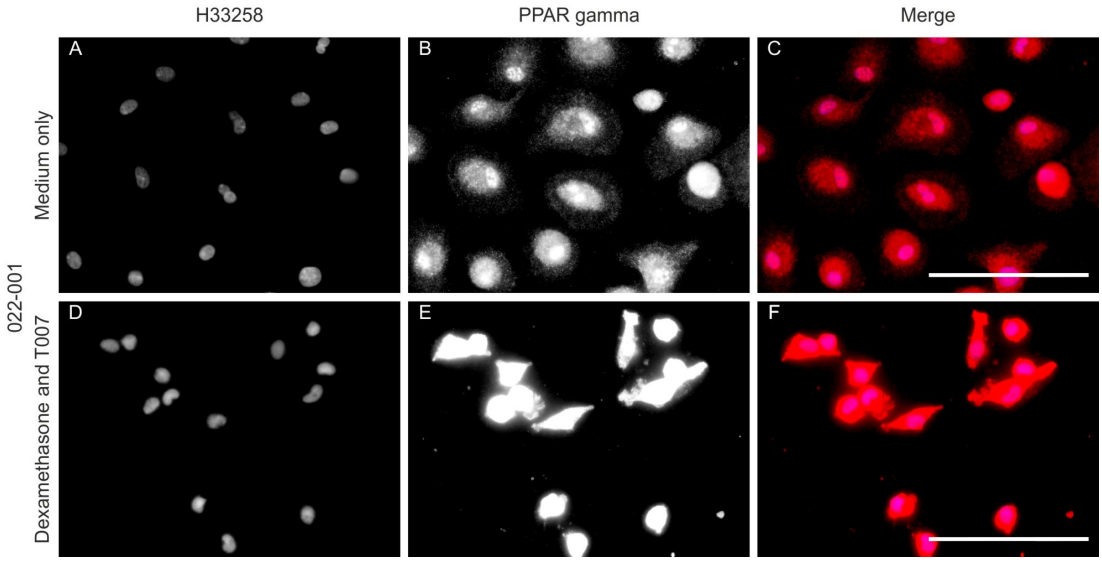

Appendix IV-XVI. Preliminary data on the effect of PPARγ inhibition and GCR stimulation on the expression of PPARγ by monocyte-derived macrophages. Day 11 monocyte-derived macrophages from donor 022-001 were either cultured in complete PBMC medium only (A-C) or complete PBMC medium containing T0070907 and dexamethasone (D-F). Fixed cells were immunolabelled for PPARγ expression. 32-bit greyscale images of H33258 staining and PPARγ expression were merged to produce a colour image. Scale bar represent 100 microns.

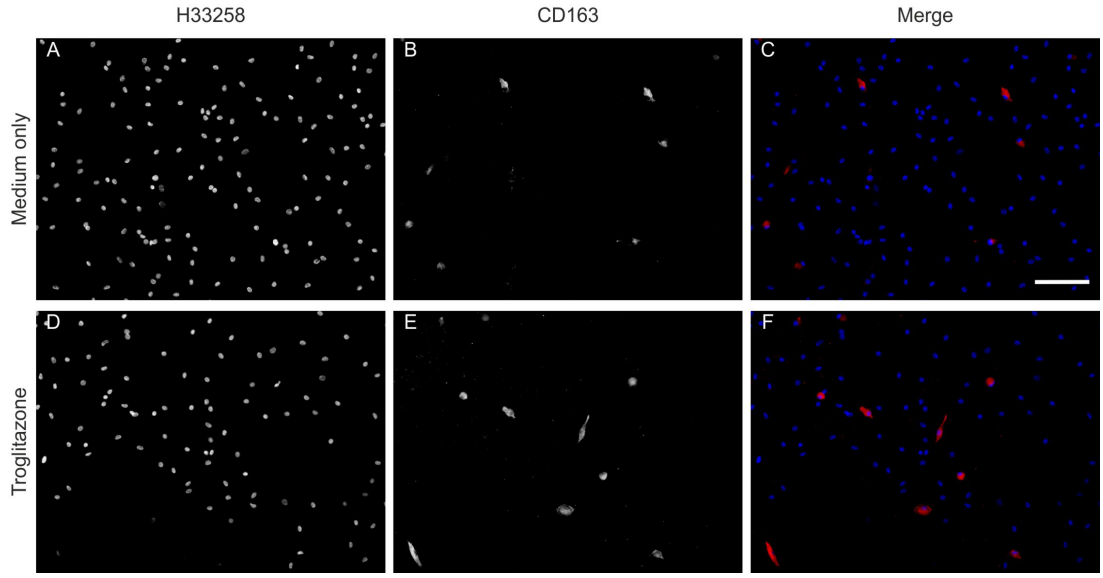

Appendix IV-XVII. Effect of PPARγ activation on the expression of CD163 by monocyte-derived macrophages. Day 11 monocyte-derived macrophages from donor 015-002 were either cultured in complete PBMC medium only (A-C) or complete PBMC medium containing troglitazone for 48 hours followed by nine days in complete PBMC medium (D-F). Fixed cells were immunolabelled for CD163 expression. 32-bit greyscale images of H33258 staining and CD163 expression were merged to produce a colour image. Scale bar represent 100 microns.

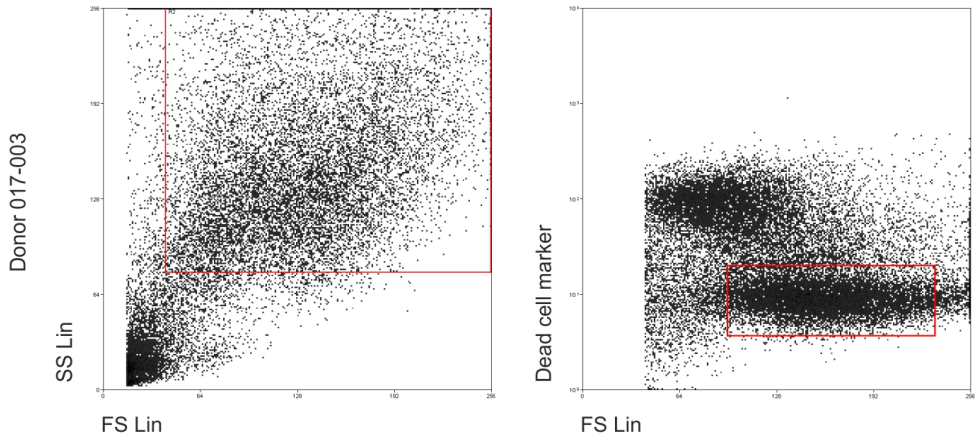

Appendix IV-XVIII. Gating of 'live' monocyte-derived macrophages from donor 017-003 treated with troglitazone using FS Lin and SS Lin and a dead cell marker. Monocyte-derived macrophages treated with troglitazone for 48 hours followed by nine days in DMSO control medium were harvested for flow cytometry following 11 days in culture and gated based on the FS Lin and SS Lin properties of the cells as described in chapter three. 'Live' cells were gated using the LIVE/DEAD stain (red box) as described in chapter three.

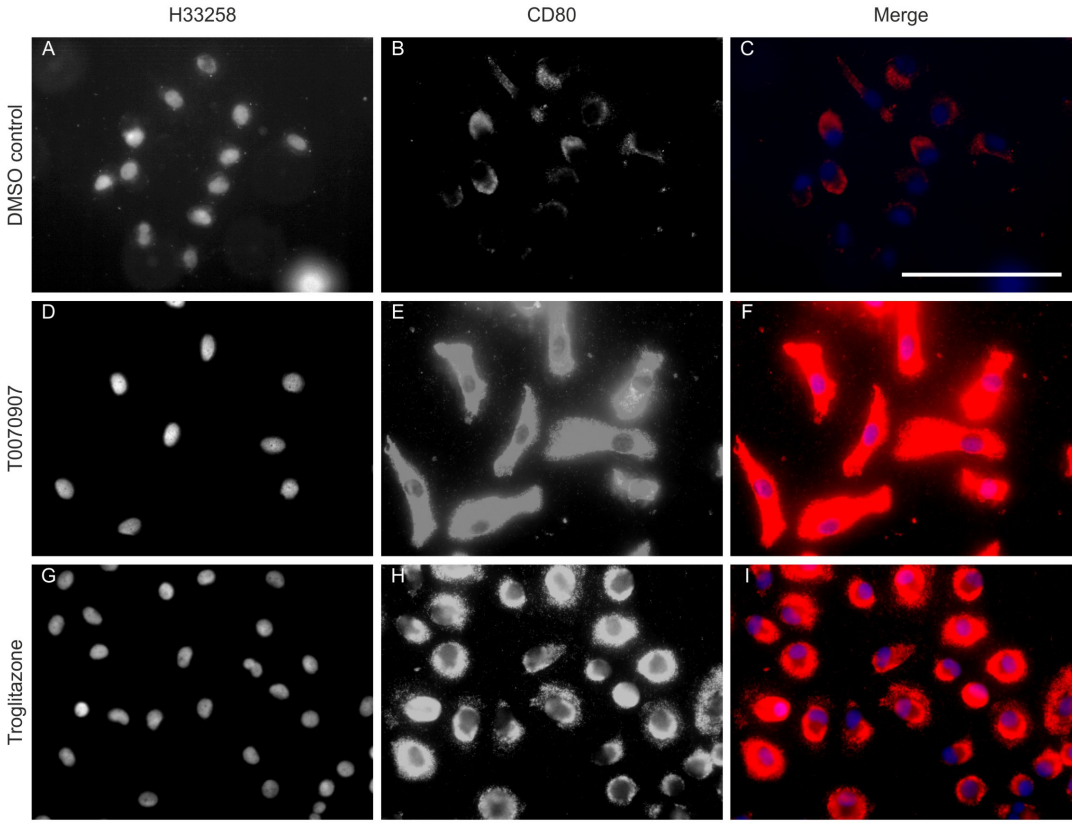

Appendix IV-XIX. Effect of PPARγ activation and inhibition on CD80 expression by monocyte-derived macrophages. Day 6 monocyte-derived macrophages from donor 006-002 were cultured either in DMSO control medium for 6 days (A-C), T0070907 for 6 days (D-F), troglitazone for 48 hours followed by four days in DMSO control medium (G-I). Fixed cells were immunolabelled for CD80 expression and all images captured at the same exposure, initially set using the control cells. 32-bit greyscale images were merged as previously described. Scale bar represents 100 microns.

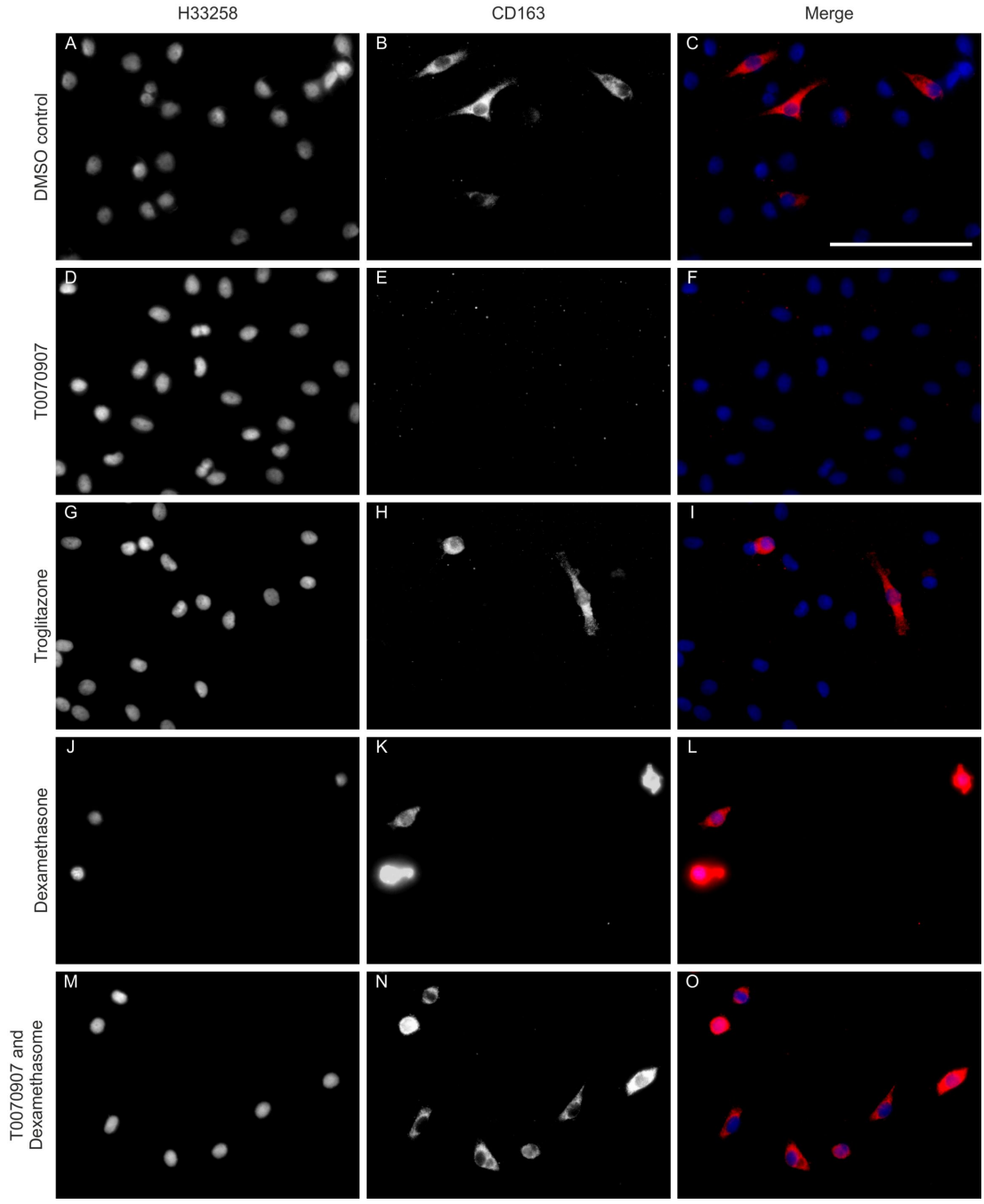

Appendix IV-XX. Effect of PPARγ activation and inhibition and glucocorticoid receptor activation on the expression of CD163 by day 6 monocyte-derived macrophages. Day 6 monocyte-derived macrophages from donor 006-002 were cultured in complete PBMC medium containing either DMSO control for 11 days (A-C), T0070907 for 11 days (D-F), troglitazone for 48 hours followed by nine days in DMSO control medium (G-I), dexamethasone for 11 days (J-L) or dexamethasone in the presence of T0070907 for 11 days (M-O). Fixed cells were immunolabelled for CD163 expression and all images captured at the same exposure, set using the control cells. 32-bit greyscale images were merged to produce colour images. Scale bar represents 100 microns.

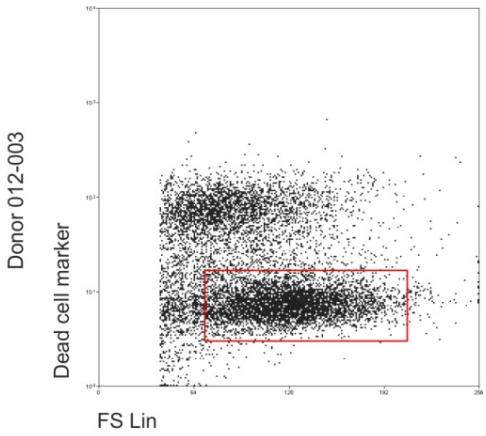

Appendix IV-XXI. Gating of 'live' monocyte-derived macrophages from donor 012-003 using a dead cell marker. Monocyte-derived macrophages cultured in complete PBMC medium were harvested for flow cytometry following 6 days in culture. 'Live' cells were gated using the LIVE/DEAD stain (red box) as described in chapter three.

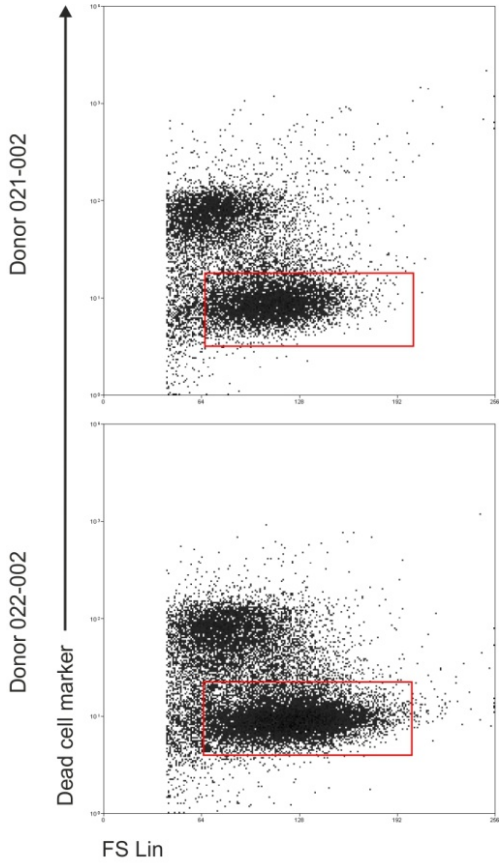

Appendix IV-XXII. Gating of 'live' monocyte-derived macrophages from donors 021-002 and 022-002 using a dead cell marker. Monocyte-derived macrophages cultured in complete PBMC medium containing T0070907 were harvested for flow cytometry following 6 days in culture. 'Live' cells were gated using the LIVE/DEAD stain (red box) as described in chapter three.

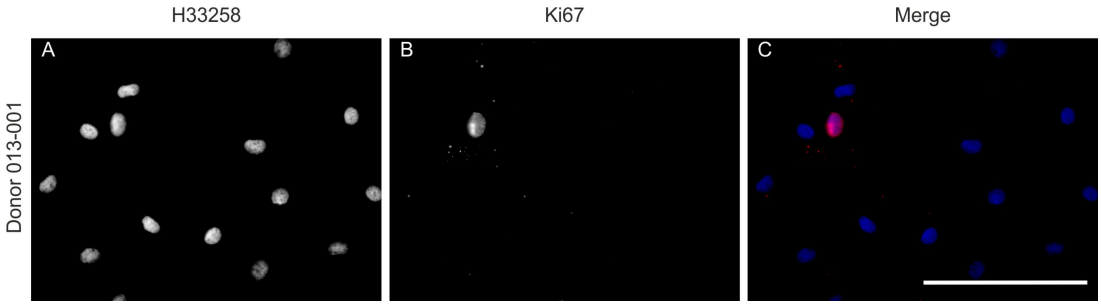

Appendix IV-XXIII. Ki67 expression by monocyte-derived macrophages from donor 013-001. Monocyte-derived macrophages from donor 006-002 were cultured in complete PBMC medium for 11 days before fixing in methanol:acetone. Fixed cells were immunolabelled for Ki67 expression. 32-bit greyscale images were merged as previously described. Scale bar represents 100 microns.

Appendices V – Discussion

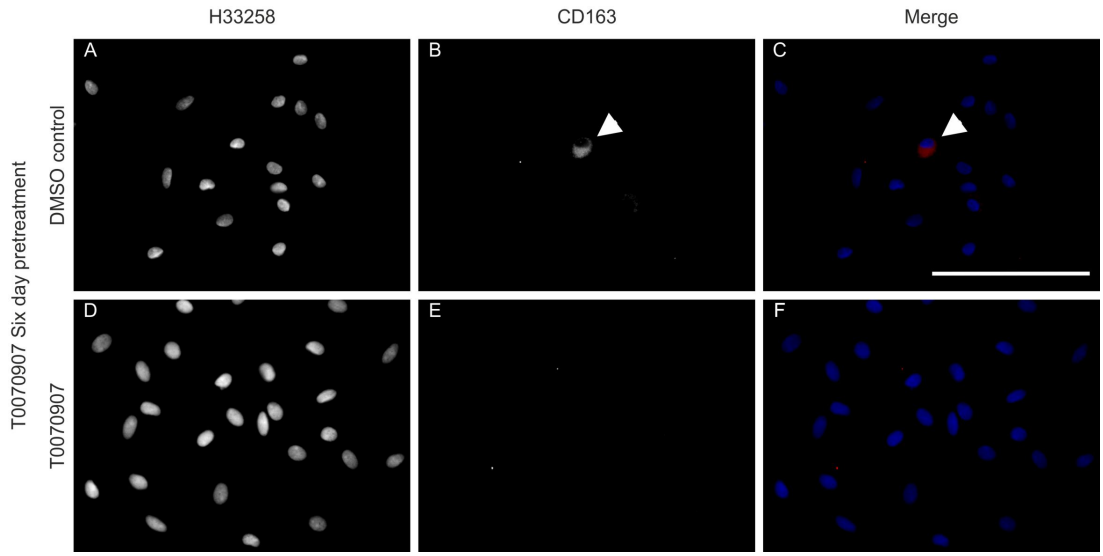

Appendix V-I. The restoration of CD163+ cells following removal of T0070907. Peripheral blood monocyte-derived macrophages from donor 030-001 were culture for six days in the presence of T0070907. The T0070907 was then either replenished or exchanges for DMSO control medium for a further two days before fixation of the cells and detection of CD163 expression by fluorescent immunolabelling. Scale bar represents 100 microns.

References

Aitken, K.J., and D.J. Bägli. 2009. The bladder extracellular matrix. Part II: regenerative applications. *Nat Rev Urol*. 6:612–621.

Ambarus, C.A., S. Krausz, M. van Eijk, J. Hamann, T.R.D.J. Radstake, K.A. Reedquist, P.P. Tak, and D.L.P. Baeten. 2012. Systematic validation of specific phenotypic markers for in vitro polarized human macrophages. *J. Immunol. Methods*. 375:196–206.

Anderson, C.F., and D.M. Mosser. 2002. A novel phenotype for an activated macrophage: the type 2 activated macrophage. *Journal of Leukocyte Biology*. 72:101–106.

Anderson, J.M., A. Rodriguez, and D.T. Chang. 2008. Foreign body reaction to biomaterials. *Semin Immunol*. 20:86–100.

Ariganello, M.B., D.T. Simionescu, R.S. Labow, and J.M. Lee. 2011. Macrophage differentiation and polarization on a decellularized pericardial biomaterial. *Biomaterials*. 32:439–449.

Ariganello, M.B., R.S. Labow, and J.M. Lee. 2009. Response of macrophage-like U937 cells to decellularized tissue heart valve materials. *J. Heart Valve Dis.* 18:187–197.

Ariganello, M.B., R.S. Labow, and J.M. Lee. 2010. In vitro response of monocyte-derived macrophages to a decellularized pericardial biomaterial. *J Biomed Mater Res*. 93:280–288.

Atala, A., S.B. Bauer, S. Soker, J.J. Yoo, and A.B. Retik. 2006. Tissue-engineered autologous bladders for patients needing cystoplasty. *Lancet*. 367:1241–1246.

Auffray, C., D. Fogg, M. Garfa, G. Elain, O. Join-Lambert, S. Kayal, S. Sarnacki, A. Cumano, G. Lauvau, and F. Geissmann. 2007. Monitoring of blood vessels and tissues by a population of monocytes with patrolling behavior. *Science*. 317:666–670.

Auffray, C., D.K. Fogg, E. Narni-Mancinelli, B. Senechal, C. Trouillet, N. Saederup, J. Leemput, K. Bigot, L. Campisi, M. Abitbol, T. Molina, I. Charo, D.A. Hume, A. Cumano, G. Lauvau, and F. Geissmann. 2009a. CX3CR1+ CD115+ CD135+ common macrophage/DC precursors and the role of CX3CR1 in their response to inflammation. *J Exp Med*. 206:595–606.

Auffray, C., M.H. Sieweke, and F. Geissmann. 2009b. Blood monocytes: development, heterogeneity, and relationship with dendritic cells. *Annu. Rev. Immunol.* 27:669–692.

Auphan, N., J.A. DiDonato, C. Rosette, A. Helmberg, and M. Karin. 1995. Immunosuppression by glucocorticoids: inhibition of NF-kappa B activity through induction of I kappa B synthesis. *Science*. 270:286–290.

Ayyildiz, A., K.T. Akgül, E. Huri, B. Nuhoğlu, B. Kiliçoğlu, H. Ustün, M. Gürdal, and C. Germiyanoğlu. 2008. Use of porcine small intestinal submucosa in bladder augmentation in rabbit: long-term histological outcome. *ANZ J Surg*. 78:82–86.

Backé, E., R. Schwarting, J. Gerdes, M. Ernst, and H. Stein. 1991. Ber-MAC3: new monoclonal antibody that defines human monocyte/macrophage differentiation antigen. *J. Clin. Pathol.* 44:936–945.

Badylak, S., S. Meurling, M. Chen, A. Spievack, and A. Simmons-Byrd. 2000. Resorbable bioscaffold for esophageal repair in a dog model. *J. Pediatr. Surg.* 35:1097–1103.

Badylak, S.F. 2002. The extracellular matrix as a scaffold for tissue reconstruction. *Semin Cell Dev Biol*. 13:377–383.

Badylak, S.F. 2004. Xenogeneic extracellular matrix as a scaffold for tissue reconstruction. *Transpl. Immunol.* 12:367–377.

Badylak, S.F. 2007. The extracellular matrix as a biologic scaffold material. *Biomaterials*. 28:3587–3593.

Badylak, S.F., and T.W. Gilbert. 2008. Immune response to biologic scaffold materials. *Semin Immunol*. 20:109–116.

Badylak, S.F., D.O. Freytes, and T.W. Gilbert. 2009. Extracellular matrix as a biological scaffold material: Structure and function. *Acta biomaterialia*. 5:1–13.

Badylak, S.F., G.C. Lantz, A. Coffey, and L.A. Geddes. 1989. Small intestinal submucosa as a large diameter vascular graft in the dog. *J. Surg. Res.* 47:74–80.

Badylak, S.F., J.E. Valentin, A.K. Ravindra, G.P. Mccabe, and A.M. Stewart-Akers. 2008. Macrophage phenotype as a determinant of biologic scaffold remodeling. *Tissue Engineering Part A*. 14:1835–1842.

Badylak, S.F., R. Tullius, K. Kokini, K.D. Shelbourne, T. Klootwyk, S.L. Voytik, M.R. Kraine, and C. Simmons. 1995. The use of xenogeneic small intestinal submucosa as a biomaterial for Achilles tendon repair in a dog model. *J Biomed Mater Res*. 29:977–985.

Baker, S.C., and J. Southgate. 2008. Towards control of smooth muscle cell differentiation in synthetic 3D scaffolds. *Biomaterials*. 29:3357–3366.

Baker, S.C., G. Rohman, J. Hinley, J. Stahlschmidt, N.R. Cameron, and J. Southgate. 2011. Cellular integration and vascularisation promoted by a resorbable, particulate-leached, cross-linked poly(ε-caprolactone) scaffold. *Macromol Biosci*. 11:618–627.

Bannenberg, G., M. Arita, and C.N. Serhan. 2007. Endogenous receptor agonists: resolving inflammation. *ScientificWorldJournal*. 7:1440–1462.

Bannenberg, G.L., N. Chiang, A. Ariel, M. Arita, E. Tjonahen, K.H. Gotlinger, S. Hong, and C.N. Serhan. 2005. Molecular circuits of resolution: formation and actions of resolvins and protectins. *J Immunol*. 174:4345–4355.

Beattie, A.J., T.W. Gilbert, J.P. Guyot, A.J. Yates, and S.F. Badylak. 2009. Chemoattraction of progenitor cells by remodeling extracellular matrix scaffolds. *Tissue Engineering Part A*. 15:1119–1125.

Beckstead, B.L., J.C. Tung, K.J. Liang, Z. Tavakkol, M.L. Usui, J.E. Olerud, and C.M. Giachelli. 2009. Methods to promote Notch signaling at the biomaterial interface and evaluation in a rafted organ culture model. *J Biomed Mater Res*. 91:436–446.

Bedoni, M., C. Sforza, C. Dolci, and E. Donetti. 2007. Proliferation and differentiation biomarkers in normal human breast skin organotypic cultures. *J. Dermatol. Sci.* 46:139–142.

Bernard, A., and L. Boumsell. 1984. Les antigènes de différenciation leucocytaire humains [Human leukocyte differentiation antigens]. *Presse Med*. 13:2311–2316.

Birkedal-Hansen, H. 1995. Proteolytic remodeling of extracellular matrix. *Curr. Opin. Cell Biol.* 7:728–735.

Biswas, S.K., and A. Mantovani. 2010. Macrophage plasticity and interaction with lymphocyte subsets: cancer as a paradigm. *Nat. Immunol.* 11:889–896.

Blom, B., S. Ho, S. Antonenko, and Y.J. Liu. 2000. Generation of interferon alpha-producing predendritic cell (Pre-DC)2 from human CD34(+) hematopoietic stem cells. *J Exp Med*. 192:1785–1796.

Bogdan, C., Y. Vodovotz, J. Paik, Q.W. Xie, and C. Nathan. 1994. Mechanism of suppression of nitric oxide synthase expression by interleukin-4 in primary mouse macrophages. *Journal of Leukocyte Biology*. 55:227–233.

Bolland, F., S. Korossis, S.-P. Wilshaw, E. Ingham, J. Fisher, J.N. Kearney, and J. Southgate. 2007. Development and characterisation of a full-thickness acellular porcine bladder matrix for tissue engineering. *Biomaterials*. 28:1061–1070.

Boruch, A.V., A. Nieponice, I.R. Qureshi, T.W. Gilbert, and S.F. Badylak. 2010. Constructive remodeling of biologic scaffolds is dependent on early exposure to physiologic bladder filling in a canine partial cystectomy model. *J. Surg. Res.* 161:217–225.

Bouhlel, M.A., B. Derudas, E. Rigamonti, R. Dièvart, J. Brozek, S. Haulon, C. Zawadzki, B. Jude, G. Torpier, N. Marx, B. Staels, and G. Chinetti-Gbaguidi. 2007. PPARgamma activation primes human monocytes into alternative M2 macrophages with anti-inflammatory properties. *Cell Metab.* 6:137–143.

Boumsell, L. 1996. The international workshops and conferences on human leukocyte differentiation antigens. Birth, current status and future. *Tissue Antigens*. 48:238–241.

Bover, L.C., M. Cardó-Vila, A. Kuniyasu, J. Sun, R. Rangel, M. Takeya, B.B. Aggarwal, W. Arap, and R. Pasqualini. 2007. A previously unrecognized protein-protein interaction between TWEAK and CD163: potential biological implications. *J Immunol*. 178:8183–8194.

Bro-Rasmussen, F.B., H. S oslash rensen, E. Bredahl, and A. Kelstrup. 1965. The Structure and Function of the Urinary Bladder. *Urol Int*. 19:280–295.

Bronte, V., and P. Zanovello. 2005. Regulation of immune responses by L-arginine metabolism. *Nat Rev Immunol*. 5:641–654.

Brown, A.L., W. Farhat, P.A. Merguerian, G.J. Wilson, A.E. Khoury, and K.A. Woodhouse. 2002. 22 week assessment of bladder acellular matrix as a bladder augmentation material in a porcine model. *Biomaterials*. 23:2179–2190.

Brown, B.N., B.D. Ratner, S.B. Goodman, S. Amar, and S.F. Badylak. 2012a. Macrophage polarization: An opportunity for improved outcomes in biomaterials and regenerative medicine. *Biomaterials*. 33:3792–3802.

Brown, B.N., C.A. Barnes, R.T. Kasick, R. Michel, T.W. Gilbert, D. Beer-Stolz, D.G. Castner, B.D. Ratner, and S.F. Badylak. 2010. Surface characterization of extracellular matrix scaffolds. *Biomaterials*. 31:428–437.

Brown, B.N., J.E. Valentin, A.M. Stewart-Akers, G.P. Mccabe, and S.F. Badylak. 2009. Macrophage phenotype and remodeling outcomes in response to biologic scaffolds with and without a cellular component. *Biomaterials*. 30:1482–1491.

Brown, B.N., R. Londono, S. Tottey, L. Zhang, K.A. Kukla, M.T. Wolf, K.A. Daly, J.E. Reing, and S.F. Badylak. 2012b. Macrophage phenotype as a predictor of constructive remodeling following the implantation of biologically derived surgical mesh materials. *Acta biomaterialia*. 8:978–987.

Buechler, C., M. Ritter, E. Orsó, T. Langmann, J. Klucken, and G. Schmitz. 2000. Regulation of scavenger receptor CD163 expression in human monocytes and macrophages by pro- and antiinflammatory stimuli. *Journal of Leukocyte Biology*. 67:97–103.

Bullido, R., M. Gómez del Moral, F. Alonso, A. Ezquerra, A. Zapata, C. Sánchez, E. Ortuño, B. Alvarez, and J. Domínguez. 1997. Monoclonal antibodies specific for porcine monocytes/macrophages: macrophage heterogeneity in the pig evidenced by the expression of surface antigens. *Tissue Antigens*. 49:403–413.

CALVANO, C.J., M.E. MORAN, A. PAREKH, P.J. DESAI, and L.J. CISEK. 2000. Laparoscopic Augmentation Cystoplasty Using the Novel Biomaterial Surgisis ™: Small-Intestinal Submucosa. *Journal of Endourology*. 14:213–217.

Cannon, G.J., and J.A. Swanson. 1992. The macrophage capacity for phagocytosis. *J. Cell. Sci.* 101:907–913.

Ceredig, R., A.G. Rolink, and G. Brown. 2009. Models of haematopoiesis: seeing the wood for the trees. *Nat Rev Immunol*. 9:293–300.

Chang-Rodriguez, S., W. Hoetzenecker, C. Schwärzler, T. Biedermann, S. Saeland, and A. Elbe-Bürger. 2005. Fetal and neonatal murine skin harbors Langerhans cell precursors. *Journal of Leukocyte Biology*. 77:352–360.

Chawla, A., Y. Barak, L. Nagy, D. Liao, P. Tontonoz, and R.M. Evans. 2001. PPAR-gamma dependent and independent effects on macrophage-gene expression in lipid metabolism and inflammation. *Nat Med*. 7:48–52.

Chen, C.-C., M.A. Grimbaldeston, M. Tsai, I.L. Weissman, and S.J. Galli. 2005. Identification of mast cell progenitors in adult mice. *Proc. Natl. Acad. Sci. U.S.A.* 102:11408–11413.

Chen, F., J.J. Yoo, and A. Atala. 1999. Acellular collagen matrix as a possible “off the shelf” biomaterial for urethral repair. *Urology*. 54:407–410.

Chen, G.Y., and G. Nuñez. 2010. Sterile inflammation: sensing and reacting to damage. *Nat Rev Immunol*. 10:826–837.

Chen, M.K., and S.F. Badylak. 2001. Small bowel tissue engineering using small intestinal submucosa as a scaffold. *J. Surg. Res.* 99:352–358.

Cho, M., T.K. Hunt, and M.Z. Hussain. 2001. Hydrogen peroxide stimulates macrophage vascular endothelial growth factor release. *Am. J. Physiol. Heart Circ. Physiol.* 280:H2357–63.

Chung, S.W., B.Y. Kang, S.H. Kim, Y.K. Pak, D. Cho, G. Trinchieri, and T.S. Kim. 2000. Oxidized low density lipoprotein inhibits interleukin-12 production in lipopolysaccharide-activated mouse macrophages via direct interactions between peroxisome proliferator-activated receptor-gamma and nuclear factor-kappa B. *J Biol Chem*. 275:32681–32687.

Collin, M., V. Bigley, M. Haniffa, and S. Hambleton. 2011. Human dendritic cell deficiency: the missing ID? *Nat Rev Immunol*. 11:575–583.

Connolly, R.J. 2006. Evaluation of a unique bovine collagen matrix for soft tissue repair and reinforcement. *Int Urogynecol J*. 17 Suppl 1:S44–S47.

Cros, J., N. Cagnard, K. Woollard, N. Patey, S.-Y. Zhang, B. Senechal, A. Puel, S.K. Biswas, D. Moshous, C. Picard, J.-P. Jais, D. D'Cruz, J.-L. Casanova, C. Trouillet, and F. Geissmann. 2010. Human CD14dim monocytes patrol and sense nucleic acids and viruses via TLR7 and TLR8 receptors. *Immunity*. 33:375–386.

Dai, X.-M., G.R. Ryan, A.J. Hapel, M.G. Dominguez, R.G. Russell, S. Kapp, V. Sylvestre, and E.R. Stanley. 2002. Targeted disruption of the mouse colony-stimulating factor 1 receptor gene results in osteopetrosis, mononuclear phagocyte deficiency, increased primitive progenitor cell frequencies, and reproductive defects. *Blood*. 99:111–120.

Danon, D., M.A. Kowatch, and G.S. Roth. 1989. Promotion of wound repair in old mice by local injection of macrophages. *Proc. Natl. Acad. Sci. U.S.A.* 86:2018–2020.

Darby, I., O. Skalli, and G. Gabbiani. 1990. Alpha-smooth muscle actin is transiently expressed by myofibroblasts during experimental wound healing. *Lab. Invest.* 63:21–29.

Davies, L.C., M. Rosas, P.J. Smith, D.J. Fraser, S.A. Jones, and P.R. Taylor. 2011. A quantifiable proliferative burst of tissue macrophages restores homeostatic macrophage populations after acute inflammation. *Eur. J. Immunol.* 41:2155–2164.

Dawson, C., and H. Whitfield. 1996. ABC of urology. Urological trauma and bladder reconstruction. *BMJ*. 312:1352–1354.

de Groat, W.C. 1993. Anatomy and physiology of the lower urinary tract. *Urol. Clin. North Am.* 20:383–401.

Dioszeghy, V., M. Rosas, B.H. Maskrey, C. Colmont, N. Topley, P. Chaitidis, H. Kühn, S.A. Jones, P.R. Taylor, and V.B. O'Donnell. 2008. 12/15-Lipoxygenase regulates the inflammatory response to bacterial products in vivo. *J Immunol*. 181:6514–6524.

Domenech, N., M.P. Rodríguez-Carreño, P. Filgueira, B. Alvarez, S. Chamorro, and J. Domínguez. 2003. Identification of porcine macrophages with monoclonal antibodies in formalin-fixed, paraffin-embedded tissues. *Vet Immunol Immunopathol*. 94:77–81.

Doulatov, S., F. Notta, E. Laurenti, and J.E. Dick. 2012. Hematopoiesis: A Human Perspective. *Stem Cell*. 10:120–136.

Doulatov, S., F. Notta, K. Eppert, L.T. Nguyen, P.S. Ohashi, and J.E. Dick. 2010. Revised map of the human progenitor hierarchy shows the origin of macrophages and dendritic cells in early lymphoid development. *Nat. Immunol.* 11:585–593.

Doyle, A.G., G. Herbein, L.J. Montaner, A.J. Minty, D. Caput, P. Ferrara, and S. Gordon. 1994. Interleukin-13 alters the activation state of murine macrophages in vitro: comparison with interleukin-4 and interferon-gamma. *Eur. J. Immunol.* 24:1441–1445.

Ehrchen, J., L. Steinmüller, K. Barczyk, K. Tenbrock, W. Nacken, M. Eisenacher, U. Nordhues, C. Sorg, C. Sunderkötter, and J. Roth. 2007. Glucocorticoids induce differentiation of a specifically activated, anti-inflammatory subtype of human monocytes. *Blood*. 109:1265–1274.

Erwig, L.-P., and P.M. Henson. 2007. Immunological consequences of apoptotic cell phagocytosis. *Am J Pathol*. 171:2–8.

Erwig, L.-P., and P.M. Henson. 2008. Clearance of apoptotic cells by phagocytes. *Cell Death Differ.* 15:243–250.

Evans, M.D.M., G.A. McFarland, R.Z. Xie, S. Taylor, J.S. Wilkie, and H. Chaouk. 2002. The use of corneal organ culture in biocompatibility studies. *Biomaterials*. 23:1359–1367.

Ezquerra, A., C. Revilla, B. Alvarez, C. Pérez, F. Alonso, and J. Domínguez. 2009. Porcine myelomonocytic markers and cell populations. *Dev. Comp. Immunol.* 33:284–298.

Fantin, A., J.M. Vieira, G. Gestri, L. Denti, Q. Schwarz, S. Prykhozhij, F. Peri, S.W. Wilson, and C. Ruhrberg. 2010. Tissue macrophages act as cellular chaperones for vascular anastomosis downstream of VEGF-mediated endothelial tip cell induction. *Blood*. 116:829–840.

Farhat, W.A., J. Chen, J. Haig, R. Antoon, J. Litman, C. Sherman, K. Derwin, and H. Yeger. 2008. Porcine bladder acellular matrix (ACM): protein expression, mechanical properties. *Biomedical materials (Bristol, England)*. 3:025015.

Feige, J.N., L. Gelman, L. Michalik, B. Desvergne, and W. Wahli. 2006. From molecular action to physiological outputs: peroxisome proliferator-activated receptors are nuclear receptors at the crossroads of key cellular functions. *Prog. Lipid Res.* 45:120–159.

Fichtner-Feigl, S., W. Strober, K. Kawakami, R.K. Puri, and A. Kitani. 2006. IL-13 signaling through the IL-13alpha2 receptor is involved in induction of TGF-beta1 production and fibrosis. *Nat Med*. 12:99–106.

Fiore, S., J.F. Maddox, H.D. Perez, and C.N. Serhan. 1994. Identification of a human cDNA encoding a functional high affinity lipoxin A4 receptor. *J Exp Med*. 180:253–260.

Fogg, D.K., C. Sibon, C. Miled, S. Jung, P. Aucouturier, D.R. Littman, A. Cumano, and F. Geissmann. 2006. A clonogenic bone marrow progenitor specific for macrophages and dendritic cells. *Science*. 311:83–87.

Foreman, D.M., S. Pancholi, J. Jarvis-Evans, D. McLeod, and M.E. Boulton. 1996. A simple organ culture model for assessing the effects of growth factors on corneal re-epithelialization. *Exp. Eye Res.* 62:555–564.

Fox, J.M., E. Letellier, C.J. Oliphant, and N. Signoret. 2011. TLR2-dependent pathway of heterologous down-modulation for the CC chemokine receptors 1, 2, and 5 in human blood monocytes. *Blood*. 117:1851–1860.

Fukano, Y., N.G. Knowles, M.L. Usui, R.A. Underwood, K.D. Hauch, A.J. Marshall, B.D. Ratner, C. Giachelli, W.G. Carter, P. Fleckman, and J.E. Olerud. 2006. Characterization of an in vitro model for evaluating the interface between skin and percutaneous biomaterials. *Wound Repair Regen*. 14:484–491.

Galli, S.J., and M. Tsai. 2010. Mast cells in allergy and infection: versatile effector and regulatory cells in innate and adaptive immunity. *Eur. J. Immunol.* 40:1843–1851.

Galli, S.J., N. Borregaard, and T.A. Wynn. 2011. Phenotypic and functional plasticity of cells of innate immunity: macrophages, mast cells and neutrophils. *Nat. Immunol.* 12:1035–1044.

Gautier, E.L., A. Chow, R. Spanbroek, G. Marcelin, M. Greter, C. Jakubzick, M. Bogunovic, M. Leboeuf, N. Van Rooijen, A.J. Habenicht, M. Merad, and G.J. Randolph. 2012. Systemic Analysis of PPARγ in Mouse Macrophage Populations Reveals Marked Diversity in Expression with Critical Roles in Resolution of Inflammation and Airway Immunity. *J Immunol*. 189:2614–2624.

Geissmann, F., M.G. Manz, S. Jung, M.H. Sieweke, M. Merad, and K. Ley. 2010. Development of monocytes, macrophages, and dendritic cells. *Science*. 327:656–661.

Geissmann, F., S. Jung, and D.R. Littman. 2003. Blood monocytes consist of two principal subsets with distinct migratory properties. *Immunity*. 19:71–82.

Glass, C.K., and K. Saijo. 2010. Nuclear receptor transrepression pathways that regulate inflammation in macrophages and T cells. *Nat Rev Immunol*. 10:365–376.

Godson, C., S. Mitchell, K. Harvey, N.A. Petasis, N. Hogg, and H.R. Brady. 2000. Cutting edge: lipoxins rapidly stimulate nonphlogistic phagocytosis of apoptotic neutrophils by monocyte-derived macrophages. *J Immunol*. 164:1663–1667.

Goerdt, S., and C.E. Orfanos. 1999. Other functions, other genes: alternative activation of antigen-presenting cells. *Immunity*. 10:137–142.

Gogolák, P., B. Rethi, I. Szatmari, A. Lanyi, B. Dezso, L. Nagy, and E. Rajnavölgyi. 2007. Differentiation of CD1a- and CD1a+ monocyte-derived dendritic cells is biased by lipid environment and PPARgamma. *Blood*. 109:643–652.

Golde, D.W., L.A. Byers, and T.N. Finley. 1974. Proliferative capacity of human alveolar macrophage. *Nature*. 247:373–375.

Gordon, S. 2003. Alternative activation of macrophages. *Nat Rev Immunol*. 3:23–35.

Gordon, S., and F.O. Martinez. 2010. Alternative activation of macrophages: mechanism and functions. *Immunity*. 32:593–604.

Gordon, S., and P.R. Taylor. 2005. Monocyte and macrophage heterogeneity. *Nat Rev Immunol*. 5:953–964.

Gosset, P., A.S. Charbonnier, P. Delerive, J. Fontaine, B. Staels, J. Pestel, A.B. Tonnel, and F. Trottein. 2001. Peroxisome proliferator-activated receptor gamma activators affect the maturation of human monocyte-derived dendritic cells. *Eur. J. Immunol.* 31:2857–2865.

Gronert, K., N. Maheshwari, N. Khan, I.R. Hassan, M. Dunn, and M. Laniado Schwartzman. 2005. A role for the mouse 12/15-lipoxygenase pathway in promoting epithelial wound healing and host defense. *J Biol Chem*. 280:15267–15278.

Guermonprez, P., J. Valladeau, L. Zitvogel, C. Théry, and S. Amigorena. 2002. Antigen presentation and T cell stimulation by dendritic cells. *Annu. Rev. Immunol.* 20:621–667.

Hammad, H., H.J. de Heer, T. Soullié, V. Angeli, F. Trottein, H.C. Hoogsteden, and B.N. Lambrecht. 2004. Activation of peroxisome proliferator-activated receptor-gamma in dendritic cells inhibits the development of eosinophilic airway inflammation in a mouse model of asthma. *Am J Pathol*. 164:263–271.

Heinäniemi, M., J.O. Uski, T. Degenhardt, and C. Carlberg. 2007. Meta-analysis of primary target genes of peroxisome proliferator-activated receptors. *Genome Biol.* 8:R147.

Hesse, M., M. Modolell, A. La Flamme, M. Schito, J. Fuentes, A. Cheever, E. Pearce, and T. Wynn. 2001. Differential Regulation of Nitric Oxide Synthase-2 and Arginase-1 by Type 1/Type 2 Cytokines In Vivo: Granulomatous Pathology Is Shaped by the Pattern of l-Arginine Metabolism 1. *J Immunol*. 167:6533–6544.

HICKS, R.M. 1975. The mammalian urinary bladder an accommodating organ. *Biological Reviews*. 50:215–246.

Hoeffel, G., Y. Wang, M. Greter, P. See, P. Teo, B. Malleret, M. Leboeuf, D. Low, G. Oller, F. Almeida, S.H.Y. Choy, M. Grisotto, L. Renia, S.J. Conway, E.R. Stanley, J.K.Y. Chan, L.G. Ng, I.M. Samokhvalov, M. Merad, and F. Ginhoux. 2012. Adult Langerhans cells derive predominantly from embryonic fetal liver monocytes with a minor contribution of yolk sac-derived macrophages. *J Exp Med*. 209:1167–1181.

Högger, P., J. Dreier, A. Droste, F. Buck, and C. Sorg. 1998. Identification of the integral membrane protein RM3/1 on human monocytes as a glucocorticoid-inducible member of the scavenger receptor cysteine-rich family (CD163). *J Immunol*. 161:1883–1890.

Hu, W.J., J.W. Eaton, T.P. Ugarova, and L. Tang. 2001. Molecular basis of biomaterial-mediated foreign body reactions. *Blood*. 98:1231–1238.

Hume, D.A. 2008. Macrophages as APC and the dendritic cell myth. *J Immunol*. 181:5829–5835.

Hume, D.A., I.L. Ross, S.R. Himes, R.T. Sasmono, C.A. Wells, and T. Ravasi. 2002. The mononuclear phagocyte system revisited. *Journal of Leukocyte Biology*. 72:621–627.

Hunt, T.K., D.R. Knighton, K.K. Thakral, W.H. Goodson, and W.S. Andrews. 1984. Studies on inflammation and wound healing: angiogenesis and collagen synthesis stimulated in vivo by resident and activated wound macrophages. *Surgery*. 96:48–54.

Ingham, E. 1990. Modulation of the proliferative response of murine thymocytes stimulated by IL-1, and enhancement of IL-1 beta secretion from mononuclear phagocytes by tetracyclines. *J. Antimicrob. Chemother.* 26:61–70.

Jaeschke, H., A. Farhood, and C.W. Smith. 1991. Neutrophil-induced liver cell injury in endotoxin shock is a CD11b/CD18-dependent mechanism. *Am. J. Physiol.* 261:G1051–6.

Janeway, C.A., and R. Medzhitov. 2002. Innate immune recognition. *Annu. Rev. Immunol.* 20:197–216.

Jenkins, S.J., D. Ruckerl, P.C. Cook, L.H. Jones, F.D. Finkelman, N. Van Rooijen, A.S. MacDonald, and J.E. Allen. 2011. Local macrophage proliferation, rather than recruitment from the blood, is a signature of TH2 inflammation. *Science*. 332:1284–1288.

Jiang, C., A.T. Ting, and B. Seed. 1998. PPAR-gamma agonists inhibit production of monocyte inflammatory cytokines. *Nature*. 391:82–86.

Jones, J.A., D.T. Chang, H. Meyerson, E. Colton, I.K. Kwon, T. Matsuda, and J.M. Anderson. 2007. Proteomic analysis and quantification of cytokines and chemokines from biomaterial surface-adherent macrophages and foreign body giant cells. *J Biomed Mater Res*. 83:585–596.

Juge-Aubry, C., A. Pernin, T. Favez, A.G. Burger, W. Wahli, C.A. Meier, and B. Desvergne. 1997. DNA binding properties of peroxisome proliferator-activated receptor subtypes on various natural peroxisome proliferator response elements. Importance of the 5'-flanking region. *J Biol Chem*. 272:25252–25259.

Kapetanovic, R., L. Fairbairn, D. Beraldi, D.P. Sester, A.L. Archibald, C.K. Tuggle, and D.A. Hume. 2012. Pig bone marrow-derived macrophages resemble human macrophages in their response to bacterial lipopolysaccharide. *J Immunol*. 188:3382–3394.

Kapoor, M., F. Kojima, L. Yang, and L.J. Crofford. 2007. Sequential induction of pro- and anti-inflammatory prostaglandins and peroxisome proliferators-activated receptor-gamma during normal wound healing: a time course study. *Prostaglandins Leukot. Essent. Fatty Acids*. 76:103–112.

Karupiah, G., Q.W. Xie, R.M. Buller, C. Nathan, C. Duarte, and J.D. MacMicking. 1993. Inhibition of viral replication by interferon-gamma-induced nitric oxide synthase. *Science*. 261:1445–1448.

Kaufmann, S.H., and U.E. Schaible. 2005. Antigen presentation and recognition in bacterial infections. *Current opinion in immunology*. 17:79–87.

Kim, S.R., K.S. Lee, H.S. Park, S.J. Park, K.H. Min, S.M. Jin, and Y.C. Lee. 2005. Involvement of IL-10 in peroxisome proliferator-activated receptor gamma-mediated anti-inflammatory response in asthma. *Mol. Pharmacol.* 68:1568–1575.

Kimuli, M., I. Eardley, and J. Southgate. 2004. In vitro assessment of decellularized porcine dermis as a matrix for urinary tract reconstruction. *BJU international*. 94:859–866.

Kiriakidis, S., E. Andreakos, C. Monaco, B. Foxwell, M. Feldmann, and E. Paleolog. 2003. VEGF expression in human macrophages is NF-kappaB-dependent: studies using adenoviruses expressing the endogenous NF-kappaB inhibitor IkappaBalpha and a kinase-defective form of the IkappaB kinase 2. *J. Cell. Sci.* 116:665–674.

Koch, R.M., N.S. Roche, W.T. Parks, G.S. Ashcroft, J.J. Letterio, and A.B. Roberts. 2000. Incisional wound healing in transforming growth factor-beta1 null mice. *Wound Repair Regen*. 8:179–191.

Kreft, M.E., M. Sterle, P. Veranic, and K. Jezernik. 2005. Urothelial injuries and the early wound healing response: tight junctions and urothelial cytodifferentiation. *Histochem. Cell Biol.* 123:529–539.

Kristiansen, M., J.H. Graversen, C. Jacobsen, O. Sonne, H.J. Hoffman, S.K. Law, and S.K. Moestrup. 2001. Identification of the haemoglobin scavenger receptor. *Nature*. 409:198–201.

Kropp, B.P., B.L. Eppley, C.D. Prevel, M.K. Rippy, R.C. Harruff, S.F. Badylak, M.C. Adams, R.C. Rink, and M.A. Keating. 1995. Experimental assessment of small intestinal submucosa as a bladder wall substitute. *Urology*. 46:396–400.

Kropp, B.P., M.K. Rippy, S.F. Badylak, M.C. Adams, M.A. Keating, R.C. Rink, and K.B. Thor. 1996. Regenerative urinary bladder augmentation using small intestinal submucosa: urodynamic and histopathologic assessment in long-term canine bladder augmentations. *J Urol*. 155:2098–2104.

Kurihara, T., G. Warr, J. Loy, and R. Bravo. 1997. Defects in macrophage recruitment and host defense in mice lacking the CCR2 chemokine receptor. *J Exp Med*. 186:1757–1762.

Kuziel, W.A., S.J. Morgan, T.C. Dawson, S. Griffin, O. Smithies, K. Ley, and N. Maeda. 1997. Severe reduction in leukocyte adhesion and monocyte extravasation in mice deficient in CC chemokine receptor 2. *Proc. Natl. Acad. Sci. U.S.A.* 94:12053–12058.

Lahiri, S., T. Sen, and G. Palit. 2009. Involvement of glucocorticoid receptor and peroxisome proliferator activated receptor-gamma in pioglitazone mediated chronic gastric ulcer healing in rats. *Eur. J. Pharmacol.* 609:118–125.

Lawrence, T., D.A. Willoughby, and D.W. Gilroy. 2002. Anti-inflammatory lipid mediators and insights into the resolution of inflammation. *Nat Rev Immunol*. 2:787–795.

Le Poole, I.C., R.M. Van den Wijngaard, W. Westerhof, J.A. Dormans, F.M. Van den Berg, R.P. Verkruisen, K.P. Dingemans, and P.K. Das. 1994. Organotypic culture of human skin to study melanocyte migration. *Pigment Cell Res.* 7:33–43.

Leibovich, S.J., and R. Ross. 1975. The role of the macrophage in wound repair. A study with hydrocortisone and antimacrophage serum. *Am J Pathol*. 78:71–100.

Levy, B.D., C.B. Clish, B. Schmidt, K. Gronert, and C.N. Serhan. 2001. Lipid mediator class switching during acute inflammation: signals in resolution. *Nat. Immunol.* 2:612–619.

Ley, K., C. Laudanna, M.I. Cybulsky, and S. Nourshargh. 2007. Getting to the site of inflammation: the leukocyte adhesion cascade updated. *Nat Rev Immunol*. 7:678–689.

Li, M.-D., and X. Yang. 2011. A Retrospective on Nuclear Receptor Regulation of Inflammation: Lessons from GR and PPARs. *PPAR Res*. 2011:1–9.

Liang, H.-C., Y. Chang, C.-K. Hsu, M.-H. Lee, and H.-W. Sung. 2004. Effects of crosslinking degree of an acellular biological tissue on its tissue regeneration pattern. *Biomaterials*. 25:3541–3552.

Lin, P., W.C.W. Chan, S.F. Badylak, and S.N. Bhatia. 2004. Assessing porcine liver-derived biomatrix for hepatic tissue engineering. *Tissue Engineering*. 10:1046–1053.

Loke, P., M.G. Nair, J. Parkinson, D. Guiliano, M. Blaxter, and J.E. Allen. 2002. IL-4 dependent alternatively-activated macrophages have a distinctive in vivo gene expression phenotype. *BMC Immunol*. 3:7.

Ma, J., T. Chen, J. Mandelin, A. Ceponis, N.E. Miller, M. Hukkanen, G.F. Ma, and Y.T. Konttinen. 2003. Regulation of macrophage activation. *Cell. Mol. Life Sci.* 60:2334–2346.

MacLauchlan, S., E.A. Skokos, N. Meznarich, D.H. Zhu, S. Raoof, J.M. Shipley, R.M. Senior, P. Bornstein, and T.R. Kyriakides. 2009. Macrophage fusion, giant cell formation, and the foreign body response require matrix metalloproteinase 9. *Journal of Leukocyte Biology*. 85:617–626.

Maddox, J.F., and C.N. Serhan. 1996. Lipoxin A4 and B4 are potent stimuli for human monocyte migration and adhesion: selective inactivation by dehydrogenation and reduction. *J Exp Med*. 183:137–146.

Maderna, P., and C. Godson. 2009. Lipoxins: resolutionary road. *Br. J. Pharmacol.* 158:947–959.

Madsen, M., H.J. Møller, M.J. Nielsen, C. Jacobsen, J.H. Graversen, T. van den Berg, and S.K. Moestrup. 2004. Molecular characterization of the haptoglobin.hemoglobin receptor CD163. Ligand binding properties of the scavenger receptor cysteine-rich domain region. *J Biol Chem*. 279:51561–51567.

Maniecki, M.B., A. Etzerodt, S.K. Moestrup, H.J. Møller, and J.H. Graversen. 2011. Comparative assessment of the recognition of domain-specific CD163 monoclonal antibodies in human monocytes explains wide discrepancy in reported levels of cellular surface CD163 expression. *Immunobiology*. 216:882–890.

Mantovani, A., A. Sica, S. Sozzani, P. Allavena, A. Vecchi, and M. Locati. 2004. The chemokine system in diverse forms of macrophage activation and polarization. *Trends Immunol*. 25:677–686.

Manz, M.G., D. Traver, T. Miyamoto, I.L. Weissman, and K. Akashi. 2001. Dendritic cell potentials of early lymphoid and myeloid progenitors. *Blood*. 97:3333–3341.

Marchetti, V., O. Yanes, E. Aguilar, M. Wang, D. Friedlander, S. Moreno, K. Storm, M. Zhan, S. Naccache, G. Nemerow, G. Siuzdak, and M. Friedlander. 2011. Differential macrophage polarization promotes tissue remodeling and repair in a model of ischemic retinopathy. *Sci Rep*. 1:76.

Martin, P., and S.J. Leibovich. 2005. Inflammatory cells during wound repair: the good, the bad and the ugly. *Trends Cell Biol.* 15:599–607.

Martin, P., D. D'Souza, J. Martin, R. Grose, L. Cooper, R. Maki, and S.R. McKercher. 2003. Wound healing in the PU.1 null mouse--tissue repair is not dependent on inflammatory cells. *Curr. Biol.* 13:1122–1128.

Martinon, F., V. Pétrilli, A. Mayor, A. Tardivel, and J. Tschopp. 2006. Gout-associated uric acid crystals activate the NALP3 inflammasome. *Nature*. 440:237–241.

Matthews, K.E., S.G. Mueller, C. Woods, and D.N. Bell. 2006. Expression of the hemoglobin-haptoglobin receptor CD163 on hematopoietic progenitors. *Stem Cells Dev.* 15:40–48.

McDonald, J.A. 1988. Extracellular matrix assembly. *Annu. Rev. Cell Biol.* 4:183–207.

McNally, A.K., and J.M. Anderson. 1995. Interleukin-4 induces foreign body giant cells from human monocytes/macrophages. Differential lymphokine regulation of macrophage fusion leads to morphological variants of multinucleated giant cells. *Am J Pathol*. 147:1487–1499.

Merguerian, P.A., P.P. Reddy, D.J. Barrieras, G.J. Wilson, K. Woodhouse, D.J. Bagli, G.A. McLorie, and A.E. Khoury. 2000. Acellular bladder matrix allografts in the regeneration of functional bladders: evaluation of large-segment (> 24 cm) substitution in a porcine model. *BJU international*. 85:894–898.

Michalik, L., and W. Wahli. 2006. Involvement of PPAR nuclear receptors in tissue injury and wound repair. *J. Clin. Invest.* 116:598–606.

Mills, C., K. Kincaid, J. Alt, M. Heilman, and A. Hill. 2000. M-1/M-2 Macrophages and the Th1/Th2 Paradigm 1. *J Immunol*. 164:6166–6173.

Mirsadraee, S., H.E. Wilcox, K.G. Watterson, J.N. Kearney, J. Hunt, J. Fisher, and E. Ingham. 2007. Biocompatibility of acellular human pericardium. *J. Surg. Res.* 143:407–414.

Mirsadraee, S., H.E. Wilcox, S.A. Korossis, J.N. Kearney, K.G. Watterson, J. Fisher, and E. Ingham. 2006. Development and characterization of an acellular human pericardial matrix for tissue engineering. *Tissue Engineering*. 12:763–773.

Mokoena, T., and S. Gordon. 1985. Human macrophage activation. Modulation of mannosyl, fucosyl receptor activity in vitro by lymphokines, gamma and alpha interferons, and dexamethasone. *J. Clin. Invest.* 75:624–631.

Moniuszko, M., K. Kowal, M. Rusak, M. Pietruczuk, M. Dabrowska, and A. Bodzenta-Lukaszyk. 2006. Monocyte CD163 and CD36 expression in human whole blood and isolated mononuclear cell samples: influence of different anticoagulants. *Clin. Vaccine Immunol.* 13:704–707.

Moreno, J.A., B. Muñoz-García, J.L. Martín-Ventura, J. Madrigal-Matute, J. Orbe, J.A. Páramo, L. Ortega, J. Egido, and L.M. Blanco-Colio. 2009. The CD163-expressing macrophages recognize and internalize TWEAK: potential consequences in atherosclerosis. *Atherosclerosis*. 207:103–110.

Mosmann, T.R., H. Cherwinski, M.W. Bond, M.A. Giedlin, and R.L. Coffman. 1986. Two types of murine helper T cell clone. I. Definition according to profiles of lymphokine activities and secreted proteins. *J Immunol*. 136:2348–2357.

Mosser, D.M. 2003. The many faces of macrophage activation. *Journal of Leukocyte Biology*. 73:209–212.

Mosser, D.M., and J.P. Edwards. 2008. Exploring the full spectrum of macrophage activation. *Nat Rev Immunol*. 8:958–969.

Munder, M. 2009. Arginase: an emerging key player in the mammalian immune system. *Br. J. Pharmacol.* 158:638–651.

Munder, M., F. Mollinedo, J. Calafat, J. Canchado, C. Gil-Lamaignere, J.M. Fuentes, C. Luckner, G. Doschko, G. Soler, K. Eichmann, F.-M. Müller, A.D. Ho, M. Goerner, and M. Modolell. 2005. Arginase I is constitutively expressed in human granulocytes and participates in fungicidal activity. *Blood*. 105:2549–2556.

Nahrendorf, M., F.K. Swirski, E. Aikawa, L. Stangenberg, T. Wurdinger, J.-L. Figueiredo, P. Libby, R. Weissleder, and M.J. Pittet. 2007. The healing myocardium sequentially mobilizes two monocyte subsets with divergent and complementary functions. *J Exp Med*. 204:3037–3047.

Naik, S.H., P. Sathe, H.-Y. Park, D. Metcalf, A.I. Proietto, A. Dakic, S. Carotta, M. O'Keeffe, M. Bahlo, A. Papenfuss, J.-Y. Kwak, L. Wu, and K. Shortman. 2007. Development of plasmacytoid and conventional dendritic cell subtypes from single precursor cells derived in vitro and in vivo. *Nat. Immunol.* 8:1217–1226.

Nassar, G.M., J.D. Morrow, L.J. Roberts, F.G. Lakkis, and K.F. Badr. 1994. Induction of 15-lipoxygenase by interleukin-13 in human blood monocytes. *J Biol Chem*. 269:27631–27634.

Nencioni, A., F. Grünebach, A. Zobywlaski, C. Denzlinger, W. Brugger, and P. Brossart. 2002. Dendritic cell immunogenicity is regulated by peroxisome proliferator-activated receptor γ. *J Immunol*. 169:1228–1235.

Nie, M., L. Corbett, A.J. Knox, and L. Pang. 2005. Differential regulation of chemokine expression by peroxisome proliferator-activated receptor gamma agonists: interactions with glucocorticoids and beta2-agonists. *J Biol Chem*. 280:2550–2561.

Niethammer, P., C. Grabher, A.T. Look, and T.J. Mitchison. 2009. A tissue-scale gradient of hydrogen peroxide mediates rapid wound detection in zebrafish. *Nature*. 459:996–999.

Odegaard, J.I., R.R. Ricardo-Gonzalez, M.H. Goforth, C.R. Morel, V. Subramanian, L. Mukundan, A. Red Eagle, D. Vats, F. Brombacher, A.W. Ferrante, and A. Chawla. 2007. Macrophage-specific PPARgamma controls alternative activation and improves insulin resistance. *Nature*. 447:1116–1120.

Ogawa, S., J. Lozach, K. Jepsen, D. Sawka-Verhelle, V. Perissi, R. Sasik, D.W. Rose, R.S. Johnson, M.G. Rosenfeld, and C.K. Glass. 2004. A nuclear receptor corepressor transcriptional checkpoint controlling activator protein 1-dependent gene networks required for macrophage activation. *Proc. Natl. Acad. Sci. U.S.A.* 101:14461–14466.

Pascual, G., A.L. Fong, S. Ogawa, A. Gamliel, A.C. Li, V. Perissi, D.W. Rose, T.M. Willson, M.G. Rosenfeld, and C.K. Glass. 2005. A SUMOylation-dependent pathway mediates transrepression of inflammatory response genes by PPAR-gamma. *Nature*. 437:759–763.

Passlick, B., D. Flieger, and H.W. Ziegler-Heitbrock. 1989. Identification and characterization of a novel monocyte subpopulation in human peripheral blood. *Blood*. 74:2527–2534.

Peiser, L., and S. Gordon. 2001. The function of scavenger receptors expressed by macrophages and their role in the regulation of inflammation. *Microbes Infect.* 3:149–159.

Peiser, L., S. Mukhopadhyay, and S. Gordon. 2002. Scavenger receptors in innate immunity. *Current opinion in immunology*. 14:123–128.

Peramo, A., C.L. Marcelo, S.A. Goldstein, and D.C. Martin. 2009. Novel organotypic cultures of human skin explants with an implant-tissue biomaterial interface. *Ann Biomed Eng*. 37:401–409.

Philippidis, P., J.C. Mason, B.J. Evans, I. Nadra, K.M. Taylor, D.O. Haskard, and R.C. Landis. 2004. Hemoglobin scavenger receptor CD163 mediates interleukin-10 release and heme oxygenase-1 synthesis: antiinflammatory monocyte-macrophage responses in vitro, in resolving skin blisters in vivo, and after cardiopulmonary bypass surgery. *Circ. Res.* 94:119–126.

Piechota, H.J., C.A. Gleason, S.E. Dahms, R. Dahiya, L.S. Nunes, T.F. Lue, and E.A. Tanagho. 1999. Bladder acellular matrix graft: in vivo functional properties of the regenerated rat bladder. *Urol. Res.* 27:206–213.

Piechota, H.J., S.E. Dahms, L.S. Nunes, R. Dahiya, T.F. Lue, and E.A. Tanagho. 1998. In vitro functional properties of the rat bladder regenerated by the bladder acellular matrix graft. *J Urol*. 159:1717–1724.

Polverini, P.J., P.S. Cotran, M.A. Gimbrone, and E.R. Unanue. 1977. Activated macrophages induce vascular proliferation. *Nature*. 269:804–806.

Puissegur, M.-P., G. Lay, M. Gilleron, L. Botella, J. Nigou, H. Marrakchi, B. Mari, J.-L. Duteyrat, Y. Guerardel, L. Kremer, P. Barbry, G. Puzo, and F. Altare. 2007. Mycobacterial lipomannan induces granuloma macrophage fusion via a TLR2-dependent, ADAM9- and beta1 integrin-mediated pathway. *J Immunol*. 178:3161–3169.

Pulford, K., K. Micklem, S. McCarthy, J. Cordell, M. Jones, and D.Y. Mason. 1992. A monocyte/macrophage antigen recognized by the four antibodies GHI/61, Ber-MAC3, Ki-M8 and SM4. *Immunology*. 75:588–595.

Raes, G., P. De Baetselier, W. Noël, A. Beschin, F. Brombacher, and G. Hassanzadeh Gh. 2002a. Differential expression of FIZZ1 and Ym1 in alternatively versus classically activated macrophages. *Journal of Leukocyte Biology*. 71:597–602.

Raes, G., W. Noël, A. Beschin, L. Brys, P. De Baetselier, and G.H.G. Hassanzadeh. 2002b. FIZZ1 and Ym as tools to discriminate between differentially activated macrophages. *Dev. Immunol.* 9:151–159.

Rappolee, D.A., D. Mark, M.J. Banda, and Z. Werb. 1988. Wound macrophages express TGF-alpha and other growth factors in vivo: analysis by mRNA phenotyping. *Science*. 241:708–712.

Ray, A., and K.E. Prefontaine. 1994. Physical association and functional antagonism between the p65 subunit of transcription factor NF-kappa B and the glucocorticoid receptor. *Proc. Natl. Acad. Sci. U.S.A.* 91:752–756.

Record, R.D., D. Hillegonds, C. Simmons, R. Tullius, F.A. Rickey, D. Elmore, and S.F. Badylak. 2001. In vivo degradation of 14C-labeled small intestinal submucosa (SIS) when used for urinary bladder repair. *Biomaterials*. 22:2653–2659.

Recum, von, A.F. 1984. Applications and failure modes of percutaneous devices: a review. *J Biomed Mater Res*. 18:323–336.

Reddy, P.P., D.J. Barrieras, G. Wilson, D.J. Bagli, G.A. McLorie, A.E. Khoury, and P.A. Merguerian. 2000. Regeneration of functional bladder substitutes using large segment acellular matrix allografts in a porcine model. *J Urol*. 164:936–941.

Reing, J.E., L. Zhang, J. Myers-Irvin, K.E. Cordero, D.O. Freytes, E. Heber-Katz, K. Bedelbaeva, D. McIntosh, A. Dewilde, S.J. Braunhut, and S.F. Badylak. 2009. Degradation products of extracellular matrix affect cell migration and proliferation. *Tissue Engineering Part A*. 15:605–614.

Ricote, M., A.C. Li, T.M. Willson, C.J. Kelly, and C.K. Glass. 1998. The peroxisome proliferator-activated receptor-gamma is a negative regulator of macrophage activation. *Nature*. 391:79–82.

Rieder, E., G. Seebacher, M.-T. Kasimir, E. Eichmair, B. Winter, B. Dekan, E. Wolner, P. Simon, and G. Weigel. 2005. Tissue engineering of heart valves: decellularized porcine and human valve scaffolds differ importantly in residual potential to attract monocytic cells. *Circulation*. 111:2792–2797.

Roberts, A.B., M.B. Sporn, R.K. Assoian, J.M. Smith, N.S. Roche, L.M. Wakefield, U.I. Heine, L.A. Liotta, V. Falanga, and J.H. Kehrl. 1986. Transforming growth factor type beta: rapid induction of fibrosis and angiogenesis in vivo and stimulation of collagen formation in vitro. *Proc. Natl. Acad. Sci. U.S.A.* 83:4167–4171.

Ross, R., and G. Odland. 1968. Human wound repair. II. Inflammatory cells, epithelial-mesenchymal interrelations, and fibrogenesis. *J Cell Biol*. 39:152–168.

Samuelsson, B. 1983. Leukotrienes: mediators of immediate hypersensitivity reactions and inflammation. *Science*. 220:568–575.

Sanchis, A., L. Alba, V. Latorre, L.M. Sevilla, and P. Pérez. 2012. Keratinocyte-targeted overexpression of the glucocorticoid receptor delays cutaneous wound healing. *PLoS ONE*. 7:e29701.

Sandeman, S.R., A.W. Lloyd, B.J. Tighe, V. Franklin, J. Li, F. Lydon, C.S.C. Liu, D.J. Mann, S.E. James, and R. Martin. 2003. A model for the preliminary biological screening of potential keratoprosthetic biomaterials. *Biomaterials*. 24:4729–4739.

Schulz, C., E. Gomez Perdiguero, L. Chorro, H. Szabo-Rogers, N. Cagnard, K. Kierdorf, M. Prinz, B. Wu, S.E.W. Jacobsen, J.W. Pollard, J. Frampton, K.J. Liu, and F. Geissmann. 2012. A lineage of myeloid cells independent of Myb and hematopoietic stem cells. *Science*. 336:86–90.

Scriven, S.D., C. Booth, D.F. Thomas, L.K. Trejdosiewicz, and J. Southgate. 1997. Reconstitution of human urothelium from monolayer cultures. *J Urol*. 158:1147–1152.

Serhan, C.N. 2010. Novel lipid mediators and resolution mechanisms in acute inflammation: to resolve or not? *Am J Pathol*. 177:1576–1591.

Serhan, C.N., and J. Savill. 2005. Resolution of inflammation: the beginning programs the end. *Nat. Immunol.* 6:1191–1197.

Serhan, C.N., J. Dalli, S. Karamnov, A. Choi, C.-K. Park, Z.-Z. Xu, R.-R. Ji, M. Zhu, and N.A. Petasis. 2012. Macrophage proresolving mediator maresin 1 stimulates tissue regeneration and controls pain. *FASEB J.* 26:1755–1765.

Serhan, C.N., N. Chiang, and T.E. Van Dyke. 2008. Resolving inflammation: dual anti-inflammatory and pro-resolution lipid mediators. *Nat Rev Immunol*. 8:349–361.

Shabir, S., and J. Southgate. 2008. Calcium signalling in wound-responsive normal human urothelial cell monolayers. *Cell Calcium*. 44:453–464.

Shi, C., and E.G. Pamer. 2011. Monocyte recruitment during infection and inflammation. *Nat Rev Immunol*. 11:762–774.

Shi, Y., J.E. Evans, and K.L. Rock. 2003. Molecular identification of a danger signal that alerts the immune system to dying cells. *Nature*. 425:516–521.

Sica, A., and A. Mantovani. 2012. Macrophage plasticity and polarization: in vivo veritas. *J. Clin. Invest.* 122:787–795.

Smoak, K.A., and J.A. Cidlowski. 2004. Mechanisms of glucocorticoid receptor signaling during inflammation. *Mech Ageing Dev*. 125:697–706.

Sobrado, M., M.P. Pereira, I. Ballesteros, O. Hurtado, D. Fernández-López, J.M. Pradillo, J.R. Caso, J. Vivancos, F. Nombela, J. Serena, I. Lizasoain, and M.A. Moro. 2009. Synthesis of lipoxin A4 by 5-lipoxygenase mediates PPARgamma-dependent, neuroprotective effects of rosiglitazone in experimental stroke. *J. Neurosci.* 29:3875–3884.

Stein, M., S. Keshav, N. Harris, and S. Gordon. 1992. Interleukin 4 potently enhances murine macrophage mannose receptor activity: a marker of alternative immunologic macrophage activation. *J Exp Med*. 176:287–292.

Stramer, B.M., R. Mori, and P. Martin. 2007. The inflammation-fibrosis link? A Jekyll and Hyde role for blood cells during wound repair. *The Journal of investigative dermatology*. 127:1009–1017.

Subramaniam, R., J. Hinley, J. Stahlschmidt, and J. Southgate. 2011. Tissue Engineering Potential of Urothelial Cells From Diseased Bladders. *J Urol*. 186:2014–2020.

Sulahian, T.H., P. Högger, A.E. Wahner, K. Wardwell, N.J. Goulding, C. Sorg, A. Droste, M. Stehling, P.K. Wallace, P.M. Morganelli, and P.M. Guyre. 2000. Human monocytes express CD163, which is upregulated by IL-10 and identical to p155. *Cytokine*. 12:1312–1321.

Sutterwala, F.S., G.J. Noel, P. Salgame, and D.M. Mosser. 1998. Reversal of proinflammatory responses by ligating the macrophage Fcgamma receptor type I. *J Exp Med*. 188:217–222.

Swirski, F.K., M. Nahrendorf, M. Etzrodt, M. Wildgruber, V. Cortez-Retamozo, P. Panizzi, J.-L. Figueiredo, R.H. Kohler, A. Chudnovskiy, P. Waterman, E. Aikawa, T.R. Mempel, P. Libby, R. Weissleder, and M.J. Pittet. 2009. Identification of splenic reservoir monocytes and their deployment to inflammatory sites. *Science*. 325:612–616.

Szanto, A., and L. Nagy. 2008. The many faces of PPARgamma: anti-inflammatory by any means? *Immunobiology*. 213:789–803.

Szanto, A., B.L. Balint, Z.S. Nagy, E. Barta, B. Dezso, A. Pap, L. Széles, S. Poliska, M. Oros, R.M. Evans, Y. Barak, J. Schwabe, and L. Nagy. 2010. STAT6 Transcription Factor Is a Facilitator of the Nuclear Receptor PPARγ-Regulated Gene Expression in Macrophages and Dendritic Cells. *Immunity*. 33:699–712.

Szatmari, I., D. Töröcsik, M. Agostini, T. Nagy, M. Gurnell, E. Barta, K. Chatterjee, and L. Nagy. 2007. PPARgamma regulates the function of human dendritic cells primarily by altering lipid metabolism. *Blood*. 110:3271–3280.

Széles, L., D. Töröcsik, and L. Nagy. 2007. PPARgamma in immunity and inflammation: cell types and diseases. *Biochim. Biophys. Acta*. 1771:1014–1030.

Sztein, M.B., P.S. Steeg, H.M. Johnson, and J.J. Oppenheim. 1984. Regulation of human peripheral blood monocyte DR antigen expression in vitro by lymphokines and recombinant interferons. *J. Clin. Invest.* 73:556–565.

Takano, T., S. Fiore, J.F. Maddox, H.R. Brady, N.A. Petasis, and C.N. Serhan. 1997. Aspirin-triggered 15-epi-lipoxin A4 (LXA4) and LXA4 stable analogues are potent inhibitors of acute inflammation: evidence for anti-inflammatory receptors. *J Exp Med*. 185:1693–1704.

Takeuchi, O., and S. Akira. 2010. Pattern Recognition Receptors and Inflammation. *Cell*. 140:805–820.

Takizawa, H., S. Boettcher, and M.G. Manz. 2012. Demand-adapted regulation of early hematopoiesis in infection and inflammation. *Blood*. 119:2991–3002.

Thoma-Uszynski, S., S. Stenger, O. Takeuchi, M.T. Ochoa, M. Engele, P.A. Sieling, P.F. Barnes, M. Rollinghoff, P.L. Bolcskei, M. Wagner, S. Akira, M.V. Norgard, J.T. Belisle, P.J. Godowski, B.R. Bloom, and R.L. Modlin. 2001. Induction of direct antimicrobial activity through mammalian toll-like receptors. *Science*. 291:1544–1547.

Thompson, P.W., A.I. Bayliffe, A.P. Warren, and J.R. Lamb. 2007. Interleukin-10 is upregulated by nanomolar rosiglitazone treatment of mature dendritic cells and human CD4+ T cells. *Cytokine*. 39:184–191.

Tippett, E., W.-J. Cheng, C. Westhorpe, P.U. Cameron, B.J. Brew, S.R. Lewin, A. Jaworowski, and S.M. Crowe. 2011. Differential expression of CD163 on monocyte subsets in healthy and HIV-1 infected individuals. *PLoS ONE*. 6:e19968.

Tomasek, J.J., G. Gabbiani, B. Hinz, C. Chaponnier, and R.A. Brown. 2002. Myofibroblasts and mechano-regulation of connective tissue remodelling. *Nat. Rev. Mol. Cell Biol.* 3:349–363.

Tontonoz, P., L. Nagy, J.G. Alvarez, V.A. Thomazy, and R.M. Evans. 1998. PPARgamma promotes monocyte/macrophage differentiation and uptake of oxidized LDL. *Cell*. 93:241–252.

Tsan, M.-F., and B. Gao. 2004. Endogenous ligands of Toll-like receptors. *Journal of Leukocyte Biology*. 76:514–519.

Turner, A., R. Subramanian, D.F.M. Thomas, J. Hinley, S.K. Abbas, J. Stahlschmidt, and J. Southgate. 2011. Transplantation of autologous differentiated urothelium in an experimental model of composite cystoplasty. *Eur. Urol.* 59:447–454.

Underhill, D.M., and H.S. Goodridge. 2012. Information processing during phagocytosis. *Nat Rev Immunol*. 12:492–502.

Urakami, S., H. Shiina, H. Enokida, K. Kawamoto, N. Kikuno, T. Fandel, K. Vejdani, L. Nunes, M. Igawa, E.A. Tanagho, and R. Dahiya. 2007. Functional improvement in spinal cord injury-induced neurogenic bladder by bladder augmentation using bladder acellular matrix graft in the rat. *World J Urol*. 25:207–213.

Valentin, J.E., A.M. Stewart-Akers, T.W. Gilbert, and S.F. Badylak. 2009. Macrophage participation in the degradation and remodeling of extracellular matrix scaffolds. *Tissue Engineering Part A*. 15:1687–1694.

Van den Heuvel, M.M., C.P. Tensen, J.H. van As, T.K. Van den Berg, D.M. Fluitsma, C.D. Dijkstra, E.A. Döpp, A. Droste, F.A. Van Gaalen, C. Sorg, P. Högger, and R.H. Beelen. 1999. Regulation of CD 163 on human macrophages: cross-linking of CD163 induces signaling and activation. *Journal of Leukocyte Biology*. 66:858–866.

Van Gorp, H., P.L. Delputte, and H.J. Nauwynck. 2010. Scavenger receptor CD163, a Jack-of-all-trades and potential target for cell-directed therapy. *Mol Immunol*. 47:1650–1660.

van Maarsseveen, T., H. Eckert, J. de Groot, H. Renner, R. Christ, R. Hennig, K. Engelmann, R. Riesner, and E. Laake. 1991. Proliferative capacity of mononuclear cells in the human lung. *J. Immunol. Methods*. 143:95–102.

Varin, A., and S. Gordon. 2009. Alternative activation of macrophages: immune function and cellular biology. *Immunobiology*. 214:630–641.

Varley, C.L., and J. Southgate. 2011. Organotypic and 3D reconstructed cultures of the human bladder and urinary tract. *Methods Mol. Biol.* 695:197–211.

Verreck, F.A.W., T. de Boer, D.M.L. Langenberg, L. van der Zanden, and T.H.M. Ottenhoff. 2006. Phenotypic and functional profiling of human proinflammatory type-1 and anti-inflammatory type-2 macrophages in response to microbial antigens and IFN-gamma- and CD40L-mediated costimulation. *Journal of Leukocyte Biology*. 79:285–293.

Visser, J., A. van Boxel-Dezaire, D. Methorst, T. Brunt, E.R. de Kloet, and L. Nagelkerken. 1998. Differential regulation of interleukin-10 (IL-10) and IL-12 by glucocorticoids in vitro. *Blood*. 91:4255–4264.

Voll, R.E., M. Herrmann, E.A. Roth, C. Stach, J.R. Kalden, and I. Girkontaite. 1997. Immunosuppressive effects of apoptotic cells. *Nature*. 390:350–351.

Vukelic, S., O. Stojadinovic, I. Pastar, C. Vouthounis, A. Krzyzanowska, S. Das, H.H. Samuels, and M. Tomic-Canic. 2010. Farnesyl pyrophosphate inhibits epithelialization and wound healing through the glucocorticoid receptor. *J Biol Chem*. 285:1980–1988.

Vyas, J.M., A.G. Van der Veen, and H.L. Ploegh. 2008. The known unknowns of antigen processing and presentation. *Nat Rev Immunol*. 8:607–618.

Walker, D.C., G. Hill, S.M. Wood, R.H. Smallwood, and J. Southgate. 2004. Agent-based computational modeling of wounded epithelial cell monolayers. *IEEE Trans Nanobioscience*. 3:153–163.

Wang, T., D.M. Kendig, S. Chang, D.M. Trappanese, S. Chacko, and R.S. Moreland. 2012. Bladder Smooth Muscle Organ Culture Preparation Maintains the Contractile Phenotype. *Am. J. Physiol. Renal Physiol.* [Epub ahead of print].

Wasserman, W.W., and A. Sandelin. 2004. Applied bioinformatics for the identification of regulatory elements. *Nat. Rev. Genet.* 5:276–287.

Webster, S.J., M. Daigneault, M.A. Bewley, J.A. Preston, H.M. Marriott, S.R. Walmsley, R.C. Read, M.K.B. Whyte, and D.H. Dockrell. 2010. Distinct cell death programs in monocytes regulate innate responses following challenge with common causes of invasive bacterial disease. *J Immunol*. 185:2968–2979.

Weinberg, J.B., M.A. Misukonis, P.J. Shami, S.N. Mason, D.L. Sauls, W.A. Dittman, E.R. Wood, G.K. Smith, B. McDonald, and K.E. Bachus. 1995. Human mononuclear phagocyte inducible nitric oxide synthase (iNOS): analysis of iNOS mRNA, iNOS protein, biopterin, and nitric oxide production by blood monocytes and peritoneal macrophages. *Blood*. 86:1184–1195.

Wezel, F., J. Southgate, and D.F.M. Thomas. 2011. Regenerative medicine in urology. *BJU international*. 108:1046–1065.

Williams, T.J., and M.J. Peck. 1977. Role of prostaglandin-mediated vasodilatation in inflammation. *Nature*. 270:530–532.

Wilshaw, S.-P., J. Kearney, J. Fisher, and E. Ingham. 2008. Biocompatibility and potential of acellular human amniotic membrane to support the attachment and proliferation of allogeneic cells. *Tissue Engineering Part A*. 14:463–472.

Wilshaw, S.-P., J.N. Kearney, J. Fisher, and E. Ingham. 2006. Production of an acellular amniotic membrane matrix for use in tissue engineering. *Tissue Engineering*. 12:2117–2129.

Windhagen, A., J. Newcombe, F. Dangond, C. Strand, M.N. Woodroofe, M.L. Cuzner, and D.A. Hafler. 1995. Expression of costimulatory molecules B7-1 (CD80), B7-2 (CD86), and interleukin 12 cytokine in multiple sclerosis lesions. *J Exp Med*. 182:1985–1996.

Wood, D., and J. Southgate. 2008. Current status of tissue engineering in urology. *Curr Opin Urol*. 18:564–569.

Wu, W.-K., O.P.C. Llewellyn, D.O. Bates, L.B. Nicholson, and A.D. Dick. 2010. IL-10 regulation of macrophage VEGF production is dependent on macrophage polarisation and hypoxia. *Immunobiology*. 215:796–803.

Xiao, W., M.N. Mindrinos, J. Seok, J. Cuschieri, A.G. Cuenca, H. Gao, D.L. Hayden, L. Hennessy, E.E. Moore, J.P. Minei, P.E. Bankey, J.L. Johnson, J. Sperry, A.B. Nathens, T.R. Billiar, M.A. West, B.H. Brownstein, P.H. Mason, H.V. Baker, C.C. Finnerty, M.G. Jeschke, M.C. López, M.B. Klein, R.L. Gamelli, N.S. Gibran, B. Arnoldo, W. Xu, Y. Zhang, S.E. Calvano, G.P. McDonald-Smith, D.A. Schoenfeld, J.D. Storey, J.P. Cobb, H.S. Warren, L.L. Moldawer, D.N. Herndon, S.F. Lowry, R.V. Maier, R.W. Davis, R.G. Tompkins, Inflammation and Host Response to Injury Large-Scale Collaborative Research Program. 2011. A genomic storm in critically injured humans. *J Exp Med*. 208:2581–2590.

Xie, Q.W., R. Whisnant, and C. Nathan. 1993. Promoter of the mouse gene encoding calcium-independent nitric oxide synthase confers inducibility by interferon gamma and bacterial lipopolysaccharide. *J Exp Med*. 177:1779–1784.

Yang, D., Q. Chen, H. Yang, K.J. Tracey, M. Bustin, and J.J. Oppenheim. 2007. High mobility group box-1 protein induces the migration and activation of human dendritic cells and acts as an alarmin. *Journal of Leukocyte Biology*. 81:59–66.

Yoo, J.J., J. Meng, F. Oberpenning, and A. Atala. 1998. Bladder augmentation using allogenic bladder submucosa seeded with cells. *Urology*. 51:221–225.

Zhang, G., and S. Ghosh. 2001. Toll-like receptor-mediated NF-kappaB activation: a phylogenetically conserved paradigm in innate immunity. *J. Clin. Invest.* 107:13–19.

Zhu, J., and W.E. Paul. 2008. CD4 T cells: fates, functions, and faults. *Blood*. 112:1557–1569.

Zhu, J., and W.E. Paul. 2010. Heterogeneity and plasticity of T helper cells. *Cell Res.* 20:4–12.

Ziegler-Heitbrock, L., P. Ancuta, S. Crowe, M. Dalod, V. Grau, D.N. Hart, P.J.M. Leenen, Y.-J. Liu, G. MacPherson, G.J. Randolph, J. Scherberich, J. Schmitz, K. Shortman, S. Sozzani, H. Strobl, M. Zembala, J.M. Austyn, and M.B. Lutz. 2010. Nomenclature of monocytes and dendritic cells in blood. *Blood*. 116:e74–80.

Zola, H., B. Swart, A. Banham, S. Barry, A. Beare, A. Bensussan, L. Boumsell, C. D Buckley, H.-J. Bühring, G. Clark, P. Engel, D. Fox, B.-Q. Jin, P.J. Macardle, F. Malavasi, D. Mason, H. Stockinger, and X. Yang. 2007. CD molecules 2006--human cell differentiation molecules. *J. Immunol. Methods*. 319:1–5.

Zwadlo, G., R. Voegeli, K. Schulze Osthoff, and C. Sorg. 1987. A monoclonal antibody to a novel differentiation antigen on human macrophages associated with the down-regulatory phase of the inflammatory process. *Exp. Cell Biol.* 55:295–304.